THE UNIVERSITY OF MICHIGAN
OCT 31 1960
ENGINEERING

# JOURNAL OF FLUID MECHANICS

VOLUME 9 PART 2

OCTOBER 1960

PUBLISHED BY

CAMBRIDGE UNIVERSITY PRESS

BENTLEY HOUSE, 200 EUSTON ROAD, LONDON, N.W. 1

AMERICAN BRANCH: 32 EAST 57TH STREET, NEW YORK 22, N.Y.

*Price* 30*s.* (*U.S.A.* $5.00)

The JOURNAL OF FLUID MECHANICS exists for the publication of theoretical and experimental investigations of all aspects of the mechanics of fluids, and is issued in four parts per volume.

EDITOR

DR G. K. BATCHELOR

*Department of Applied Mathematics and Theoretical Physics, University of Cambridge, Free School Lane, Cambridge, England*

ASSISTANT EDITORS

DR T. B. BENJAMIN, DR I. PROUDMAN

*Department of Applied Mathematics and Theoretical Physics, University of Cambridge, Free School Lane, Cambridge, England*

ASSOCIATE EDITORS

PROF. G. F. CARRIER

*Pierce Hall, Harvard University, Cambridge* 38, *Massachusetts, U.S.A.*

DR W. C. GRIFFITH

*Research and Development Laboratory, Missile Systems Division, Lockheed Aircraft Corporation, Palo Alto, California, U.S.A.*

M. J. LIGHTHILL

*Royal Aircraft Establishment, Farnborough, Hampshire, England*

PROF. R. R. LONG

*School of Engineering, The Johns Hopkins University, Baltimore* 18, *Maryland, U.S.A.*

DR P. G. SAFFMAN

*Department of Mathematics, King's College, London, W.C.* 2, *England*

Authors wishing to have papers published in the JOURNAL should communicate them to any one of the persons named above, choosing one in their own country where possible.

Authors are urged to ensure that their papers are written clearly and attractively, in order that their work will be readily accessible to readers.

Manuscripts should be typed in double spacing on one side of the paper only, with references listed at the end in alphabetical order of authors. Drawings should be done on a large scale in Indian ink on tracing cloth or drawing paper, the lettering being shown clearly in pencil for reproduction by the printer; the list of captions should be typed at the end of the manuscript. Proofs of papers from overseas will usually be despatched to authors by airmail. There is no charge for publication. Authors are entitled to receive 50 offprints of a paper in the JOURNAL free of charge, and additional offprints can be purchased if ordered in advance.

## SUBSCRIPTIONS

The subscription price for a volume of four parts is £5. 10*s*. net, post free, payable in advance; separate parts 30*s*. net, plus postage. Subscriptions may be sent to any bookseller, or to the Cambridge University Press, Bentley House, 200 Euston Road, London, N.W.1.

Subscribers in the United States should send their orders to the Cambridge University Press, American Branch, 32 East 57th Street, New York 22, N.Y. The subscription price per volume is $18.50, post free, payable in advance; separate parts $5.00, plus postage.

Quotations for available back volumes and parts may be obtained on application to the Cambridge University Press.

# Exact solutions for steady two-dimensional flow of a stratified fluid

By CHIA-SHUN YIH
Department of Engineering Mechanics, University of Michigan†

(Received 15 February 1960)

Three classes of exact solutions for steady two-dimensional flows of a stratified fluid are found. The flows which correspond to these solutions have arbitrary amplitude (however defined). Two of the three classes of solutions have close bearings on the lee-wave problem in meteorology. It is also shown that the amplitudes of the lee-wave components (if there is more than one component) depend not on the details of the shape of the barrier, but only on certain simple integral properties of the function for the singularity distribution generating the barrier.

## 1. The equation governing steady two-dimensional flow of a stratified fluid

This study is restricted to steady two-dimensional flows of a stratified fluid, assumed incompressible, inviscid, and non-diffusive. For such flows the Euler equations are

$$\rho\left(u\frac{\partial}{\partial x}+w\frac{\partial}{\partial z}\right)(u,w)=-\left(\frac{\partial}{\partial x},\frac{\partial}{\partial y}\right)p-(0,g\rho), \tag{1}$$

in which $p$ and $\rho$ are the pressure and the density, $g$ is the gravitational acceleration, $x$ and $z$ are Cartesian co-ordinates, with $z$ measured in the direction opposite to that of gravity, and $u$ and $w$ are the velocity components in the directions of increasing $x$ and $z$, respectively. Since the fluid is incompressible and non-diffusive and the flow is steady,

$$\left(u\frac{\partial}{\partial x}+w\frac{\partial}{\partial z}\right)\rho=0. \tag{2}$$

This permits the equation of continuity to be written in the form

$$\frac{\partial u'}{\partial x}+\frac{\partial w'}{\partial z}=0, \tag{3}$$

and the equations of motion to be written as

$$\rho_0\left(u'\frac{\partial}{\partial x}+w'\frac{\partial}{\partial z}\right)(u',w')=-\left(\frac{\partial}{\partial x},\frac{\partial}{\partial z}\right)p-(0,g\rho), \tag{4}$$

in which

$$u'=u(\rho/\rho_0)^{\frac{1}{2}},\quad w'=w(\rho/\rho_0)^{\frac{1}{2}}, \tag{5}$$

† At Department of Applied Mathematics and Theoretical Physics, University of Cambridge, during 1959–60.

and $\rho_0$ is a reference density. With the pseudo-vorticity $\omega'$ defined by

$$\omega' = \frac{\partial w'}{\partial x} - \frac{\partial u'}{\partial z},$$

and $\psi'$ the pseudo stream function, so that

$$u' = \frac{\partial \psi'}{\partial z}, \quad w' = -\frac{\partial \psi'}{\partial x}, \tag{6}$$

the equations of motion can be further simplified to

$$-\rho_0 \omega' \frac{\partial \psi'}{\partial x} = \frac{\partial}{\partial x}[p + \tfrac{1}{2}\rho_0(u'^2 + w'^2)], \tag{7}$$

$$-\rho_0 \omega' \frac{\partial \psi'}{\partial z} = \frac{\partial}{\partial z}[p + \tfrac{1}{2}\rho_0(u'^2 + w'^2)] + g\rho. \tag{8}$$

If (7) is multiplied by $dx$ and (8) by $dz$, and the results added,

$$-\rho_0 \omega' d\psi = d[p + \tfrac{1}{2}\rho(u^2 + w^2)] + g\rho dz = dH - gz d\rho, \tag{9}$$

in which $$H = p + \tfrac{1}{2}\rho(u^2 + w^2) + g\rho z$$

is the Bernoulli constant, which is constant along a streamline but may vary from streamline to streamline, and is hence a function of $\psi'$ alone. Since for steady flows streamlines are path-lines, and for an incompressible and non-diffusive fluid $\rho$ is constant along a path-line, $\rho$ is also a function of $\psi'$ alone. Thus (9) can be written as

$$\rho_0 \nabla^2 \psi' + gz \frac{d\rho}{d\psi'} = \frac{dH(\psi')}{d\psi'} = h(\psi'), \tag{10}$$

with $\nabla^2 \psi'$ replacing $-\omega'$. Equation (10) is the governing equation sought, and is a modified form of an equation due to Long (1953), who did not relate the arbitrary function of $\psi'$ on the right-hand side of his equation to the Bernoulli constant.

## 2. Types of exact solutions

To discover exact solutions of (10), it is natural to consider circumstances in which the equation becomes linear in $\psi$. To this end, one may adopt two different approaches. Since the function $h(\psi')$ is related to the upstream condition, one may either try different upstream conditions and see whether these will make the equation linear, or assume the equation to be linear to start with and inquire what the corresponding upstream condition must be. The second approach is evidently both exhaustive and more economical. Adopting the first approach, Long said in his impressive paper (Long 1953) of the case in which $\rho u^2$ is constant far upstream where the flow is parallel: 'This is the only case I have been able to discover for which the differential equation governing the motion of a stratified fluid is exactly linear.' This is hardly surprising, because the equation originally discovered by Long is in the form

$$\nabla^2 \psi + \frac{1}{\rho}\frac{d\rho}{d\psi}\left(\frac{\psi_x^2 + \psi_y^2}{2} + gz\right) = f(\psi), \tag{10a}$$

in which $\psi$ is the usual stream function and subscripts indicate partial differentiation, and in this form it is quite unsuitable for discovering all the cases in which (10$a$) is exactly linear. The transformation (6) takes care of the inertia effect of density variation once and for all, removes the troublesome terms (representing the inertia effect) in Long's equation, and produces (10), which, while equivalent to Long's equation, is so much simpler that the second approach can now be applied. It will be shown by the second approach that there are three essentially distinct classes of flows for which (10) is exactly linear, each consisting of infinitely many flows. One of these three classes contains Long's case as a special (but very important) case. Thus the simple transformation (6) proves to be a very fruitful one.

For (10) to be linear in $\psi$, $d\rho/d\psi'$ and $h(\psi')$ must be linear in $\psi'$. The linear equation therefore has the general form

$$\nabla^2\psi' + gz(C + C_1\psi') = C_2 + C_3\psi'. \tag{11}$$

If $C_1 = C_3 = 0$, this equation has the form

$$\nabla^2\psi' + Cgz = C_2. \tag{11a}$$

If $C_1 = 0$ but $C_3 \neq 0$, $\psi'$ can be changed by a constant, and (11) becomes

$$\nabla^2\psi' + Cgz = C_3\psi'. \tag{11b}$$

The class of flows governed by this equation includes Long's case as a special case. If $C_1 \neq 0$ but $C_3 = 0$, (11) becomes, after $\psi'$ has been changed by a constant,

$$\nabla^2\psi' + C_1 gz\psi' = C_2. \tag{11c}$$

If $C_1$ and $C_3$ are both different from zero, the origin of $z$ can be shifted so that the resulting equation is

$$\nabla^2\psi' + gz(C + C_1\psi') = C_0,$$

which, on changing $\psi'$ by a constant, becomes identical in form with (11$c$).

If now the dimensionless parameters

$$\xi = x/d, \quad \eta = z/d, \quad \Psi = \psi'/Vd$$

are introduced, in which $d$ is a reference length and $V$ a reference velocity, (11$a$) to (11$c$) assume the form

$$\nabla^2\Psi + A\eta = B, \tag{12a}$$

$$\nabla^2\Psi + A\eta = B\Psi, \tag{12b}$$

$$\nabla^2\Psi + A\eta\Psi = B, \tag{12c}$$

in which $A$ and $B$ are dimensionless constants, and, now and henceforth,

$$\nabla^2 \equiv \frac{\partial^2}{\partial\xi^2} + \frac{\partial^2}{\partial\eta^2}.$$

## 3. Class ($a$): pseudo-potential flows

For class ($a$), the general solution is of the form

$$\Psi = \Psi_h - A\eta\begin{Bmatrix}\frac{1}{6}\eta^2\\ \frac{1}{2}\xi^2\end{Bmatrix} + \tfrac{1}{2}B\begin{Bmatrix}\eta^2\\ \xi^2\end{Bmatrix} + C\xi\eta + D\begin{Bmatrix}\eta\\ \xi\end{Bmatrix}, \tag{13}$$

in which a fifth constant has been suppressed because $\Psi$ can be changed by an arbitrary constant. Either member of the brackets in (13) can be used, or a linear combination of both members, except that for the first two brackets the linear combinations must be such that (12*a*) is satisfied. The first member on the right-hand side of (13) is a harmonic function satisfying the Laplace equation

$$\nabla^2\Psi_h = 0. \tag{14}$$

A re-examination of (10), (11*a*) and (12*a*) reveals that

$$A = \frac{1}{\rho_0}\frac{d\rho}{d\Psi}\frac{gd}{V^2}, \tag{15}$$

so that, once $\Psi$ is determined,

$$\rho = \frac{A\rho_0 V^2}{gd}\Psi + \text{constant} \tag{16}$$

is also known up to an additive constant. Furthermore, if $\rho$ decreases with increasing $\eta$ (stable stratification), and the flow is from left to right, $d\rho/d\Psi$ is negative, and the expression for $A$ suggests that it is really the negative of the reciprocal of the square of a Froude number:

$$A = -F^{-2}. \tag{17}$$

A first example is furnished by a stratified flow between two horizontal boundaries, at $z = 0$ and $z = d$, into a line sink whose trace is situated at the origin. Since the flow is symmetric with respect to the $z$-axis, it is convenient to consider the flow to be separated by a plane vertical wall at $x = 0$ into two mirror images. The left one of these will be considered. If the flow at $x = -\infty$ is parallel and with the parabolic distribution for the velocity (as weighted by the factor $(\rho/\rho_0)^{\frac{1}{2}}$)

$$U(\eta) = 6U_m\eta(1-\eta), \tag{18}$$

in which $U_m$ is the mean of $U$, then with $U_m$ as the representative velocity $V$,

$$A = 12, \quad B = 6, \quad C = D = 0$$

in (13), and

$$\Psi = \Psi_h - 2\eta^3 + 3\eta^2. \tag{19}$$

The boundary conditions are $\Psi = 0$ at $\eta = 0$, $\Psi = 1$ at $\eta = 1$, and at $\xi = 0$ $(0 < \eta \leqslant 1)$; $\Psi = 3\eta^2 - 2\eta^3$ at $\xi = -\infty$. In terms of $\Psi_h$, these are

$$\Psi_h = 0 \quad \text{at} \quad \eta = 0 \quad \text{and} \quad \eta = 1, \tag{20}$$

$$\Psi_h = 1 + 2\eta^3 - 3\eta^2 \quad \text{at} \quad \xi = 0 \quad (0 < \eta \leqslant 1), \tag{21}$$

$$\Psi_h = 0 \quad \text{at} \quad \xi = -\infty. \tag{22}$$

By the method of separation of variables the solution of (13) to (16) is found to be

$$\Psi_h = \Sigma A_n e^{n\pi\xi}\sin n\pi\eta, \tag{23}$$

in which

$$A_1 = \frac{2}{\pi}, \quad A_2 = \frac{1}{\pi}\left(1 + \frac{3}{\pi^2}\right), \quad A_3 = \frac{2}{3\pi}, \quad A_4 = \frac{1}{\pi}\left(\frac{1}{2} + \frac{3}{8\pi^2}\right), \quad A_5 = \frac{2}{5\pi}, \quad \text{etc.}$$

The final solution is

$$\psi' = U_m d(\Psi + 3\eta^2 - 2\eta^3), \tag{24}$$

and the density variation at infinity is

$$\rho = \rho_0 + (\rho_0 - \rho_1)(\Psi + 3\eta^2 - 2\eta^3), \tag{25}$$

in which $\rho_0$ is the density at the bottom plate and $\rho_1$ that at the top plate. The flow pattern can be expected to have an eddy at the corner bounded by the upper boundary and the vertical wall, extending to infinity.

For another example consider the case of stratified flow with $\Psi = -\frac{1}{6}A\eta^3$ at $\infty$. The lower boundary consists of a semicircle ($r = r_0$, $0 \leqslant \theta \leqslant \pi$) and the lines ($\theta = 0$, $\theta = \pi$, $r \geqslant r_0$). No upper boundary is imposed. After the solution is obtained, any streamline (and in particular the one on which $\rho$ is zero) can be taken to be the upper boundary. Here $C = 0$ in (13), and the upper members in the brackets of (13) can be taken. For illustration, $B$ and $D$ will be taken to be zero. The general case in which $B$ and $D$ are not equal to zero can be solved similarly. The reference length is now the radius of the cylinder, $r_0$. For con-

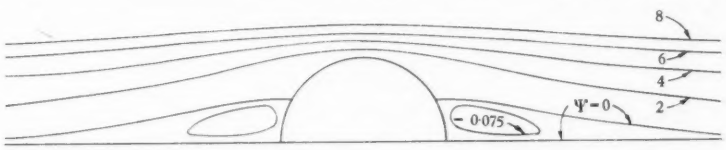


FIGURE 1. Pattern of a pseudo-potential flow of a stratified fluid over a semicircle.

$$\Psi = -\frac{24\psi'}{Cgr_0^3}, \quad C = \frac{1}{\rho_0}\frac{d\rho}{d\psi'}, \quad r_0 = \text{radius of semi-circle}, \quad r_1 = r/r_0.$$

venience, let $r/r_0$ be denoted by $r_1$. The boundary conditions are (for $\Psi = -\frac{1}{6}A\eta^3$ at infinity): $\Psi_h = 0$ at $\eta = 0$ (at least for $r \geqslant 1$), $\Psi_h = 0$ at $r_1 = \infty$, $\Psi_h = \frac{1}{6}A\eta^3$ for $r_1 = 1$ ($\eta \geqslant 0$). The solution is

$$\begin{aligned}\psi' &= \frac{Ar_0^3}{24}\left(\frac{3\sin\theta}{r_1} - \frac{\sin 3\theta}{r_1^3} - 4r_1^3\sin^3\theta\right) \\ &= \frac{Ar_0^3}{24}\left[3\left(\frac{1}{r_1} - r_1^3\right)\sin\theta - \left(\frac{1}{r_1^3} - r_1^3\right)\sin 3\theta\right].\end{aligned} \tag{26}$$

The flow pattern is shown in figure 1. As can be readily calculated from (20), the stagnation points are the points:

$$(r, \theta) = (\infty, 0),\ (\infty, \pi),\ (r_0, 0),\ (r_0, \pi),\ (r_0, \tfrac{1}{6}\pi),\ (r_0, \tfrac{5}{6}\pi).$$

These form the corners of two roughly triangular eddies, symmetrically located over the horizontal boundary, as shown in the figure.

## 4. Class (*b*): waves of arbitrary amplitude, with application to flow over a barrier

The class of flows governed by (12*b*) can be applied to the atmosphere. If the flow is parallel, the corresponding stream function is governed by the equation

$$\frac{d^2\Psi_1}{d\eta^2} + A\eta = B\Psi_1, \tag{27}$$

which has the solution

$$\Psi_1 = \frac{A}{B}\eta + C\sinh\sqrt{B}\,\eta + D\cosh\sqrt{B}\,\eta. \tag{28}$$

If the solution of (12*b*) is written as the sum of two parts, i.e.

$$\Psi = \Psi_1 + \Psi_2, \tag{29}$$

then $\Psi_2$ satisfies

$$\nabla^2\Psi_2 - B\Psi_2 = 0, \tag{30}$$

the solution of which satisfying the boundary conditions† $\Psi_2 = 0$ at $\eta = 0$ and $\eta = 1$ is of the form

$$\Psi_2 = \sum_{n=1}^{\infty} A_n \exp \pm (B + n^2\pi^2)^{\frac{1}{2}}\,\xi \sin n\pi\eta. \tag{31}$$

The special case $C = D = 0$ has been considered by Long (1953). In this case, if $\Psi$ and $\Psi_1$ are expressed in terms of $Ud$, with $U$ denoting the *uniform* velocity (weighted by the factor $(\rho/\rho_0)^{\frac{1}{2}}$) far upstream, $\Psi = \Psi_1 = \eta$ far upstream, and $A = B$. Thus (17), (28), (29) and (31) produce the solution

$$\Psi = \eta + \sum_{n=1}^{\infty} A_n \exp\{\pm (n^2\pi^2 - F^{-2})^{\frac{1}{2}}\,\xi\} \sin n\pi\eta. \tag{32}$$

The solution by Long (1955) for stratified flow over barriers and the solution by Yih (1958) for stratified flow into a sink are of the form (32). These solutions can now be generalized to apply to the infinitely many upstream conditions described by (28). This gain in generality has been possible because (10) is substantially simpler than (10*a*). The actual modification of the solutions of Long and of Yih for application to the generalized upstream condition is straightforward and will not be presented here. Suffice it to say that (28) possesses so much latitude that an actual upstream wind condition can be much better approximated by (28) than by $\Psi_1 = \eta$, by appropriate choice of the constants $A$, $B$, $C$ and $D$. Thus the meteorological significance of (27) is somewhat enhanced. Care must be taken, however, to ensure that $\Psi$ (or $\Psi_1$, since $\Psi_2$ is assumed to vanish far upstream) be monotone in $\eta$, for otherwise (since $d\rho/d\Psi_1$ is constant) an unstable density distribution would be present in a part of the fluid in parallel flow.

If $B$ is negative and greater in numerical value than $(N\pi)^2$ but less than $(N+1)^2\pi^2$, $\Psi_2$ in (31) will contain $N$ terms periodic in $\xi$, representing wave motion. It is commonly assumed (and the assumption has been experimentally verified) that upstream waves do not occur. But if we do not inquire how the waves are made and only ask whether a periodic condition can be consistent with (27), we see immediately that the answer is in the affirmative, because

$$\Psi = \Psi_1 + \sum_{n=1}^{N} (B_n \cos |B + n^2\pi^2|^{\frac{1}{2}}\,\xi + C_n \sin |B + n^2\pi^2|^{\frac{1}{2}}\,\xi) \sin n\pi\eta \tag{33}$$

† The condition $\Psi_2 = 0$ at $\eta = 0$ is imposed to make $\eta = 0$ a streamline. This is desirable if the ground surface is flat or at least flat as $\xi \to \infty$ (since lee-waves, if they exist, will not die out as $\xi \to \infty$). If there is a barrier on the surface of which we demand $\Psi = 0$, then the streamline $\Psi = 0$ consists of the ground surface *and* the line $\eta = 0$ (which may constitute part of the ground surface), if the condition $\Psi_1(0) = 0$ is imposed. The boundary condition $\Psi_2 = 0$ at $\eta = 1$ follows from the requirement $\Psi =$ constant at $\eta = 1$. A discussion of the realism of this requirement when the theory is applied to the atmosphere will be given later in this paper.

is a solution of (27), with $\Psi_1$ given in (28). The corresponding density distribution given by

$$\frac{d\rho}{d\Psi} = \text{constant} \tag{34}$$

is not necessarily unstable, even though in certain regions the density increases upwards, because of the presence of acceleration toward the centre of curvature. The wave motion represented by (33) can have arbitrary amplitudes. For the particular case of $A = B$, $C = D = 0$,

$$\Psi = \eta + \sum_{n=1}^{N} (B_n \cos |F^{-2} - n^2\pi^2|^{\frac{1}{2}} \xi + C_n \sin |F^{-2} - n^2\pi^2|^{\frac{1}{2}} \xi) \sin n\pi\eta, \tag{35}$$

with

$$N\pi < F^{-1} < (N+1)\pi, \tag{36}$$

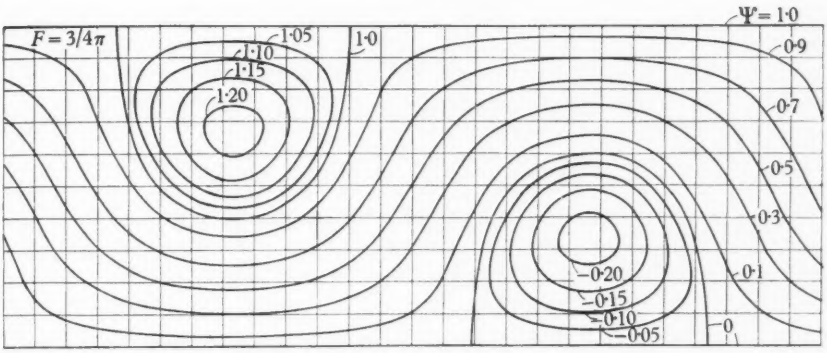


FIGURE 2. Stationary waves of arbitrary amplitude.

$$F = \frac{3}{4\pi}, \quad \Psi = -\frac{\psi'}{F^2 d^3 g C}, \quad C = \frac{1}{\rho_0}\frac{d\rho}{d\psi'}.$$

represents a period motion with $N$ wave components. In spite of what Long himself said (as quoted in § 2), the waves represented by (35)—but not those represented by (33)—can be considered to have been discovered by him, because they are identical with the lee-waves he studied. The flow pattern for

$$\Psi = \eta + \frac{2}{\pi} \cos (F^{-2} - \pi^2)^{\frac{1}{2}} \xi \sin n\pi\eta, \tag{37}$$

with $F = 3/4\pi$, is shown in figure 2. The term $\eta$ in (35) and (37) represents only a pseudo-uniform velocity field, because $\Psi$ is a stream function for the flow field $(u', w')$, and not for the flow $(u, w)$. Therefore the parallel flow represented by $\eta$ does not correspond to an actually uniform velocity, and it is not possible by a shifting of co-ordinate axes to remove the parallel flow altogether. However, if drift is allowed, the discharge relative to a moving frame of reference can be made to be zero. The speed $c$ with which the frame moves is exactly the phase velocity of the wave pattern relative to the moving frame, which is quite different from the stationary wave pattern. This speed can be calculated readily, and will not be given explicitly here.

*Use of vorticity distributions for generating stratified flows over a barrier*

For the case $A = B$, $C = D = 0$, Long (1955) gave a method for generating the solution for flow over a barrier which is approximately the same as one with a prescribed form. We shall now give an alternate method, for generating solutions of (12*b*) for flow over a barrier of unspecified (except implicitly) form. This method has three advantages over Long's method. First, it is simpler. Secondly, the determination of the coefficients is exact, and does not involve the solution of infinitely many equations containing infinitely many unknowns. Thirdly, by means of it we can prove the very important fact† that the amplitudes of the various lee-wave components depend not on the *details* of the shape of the barrier, but only on certain integral properties of the singularities generating the barrier. On the other hand, the shape of the barrier is directly though only approximately accounted for by Long's method, whereas the alternative method to be presented is entirely an inverse method which does not attempt to generate a solution for a *prescribed* barrier even approximately, except indirectly.

The method will now be described. When

$$(N\pi)^2 < -B < (N+1)^2\pi^2,$$

the solution of (12*b*) can be put in the form

$$\left.\begin{aligned} \Psi_- &= \Psi_1 + \sum_{N+1}^{\infty} A_n e^{a_n\xi} \sin n\pi\eta \quad (\text{for } \xi \leqslant 0), \\ \Psi_+ &= \Psi_1 + \sum_{n=1}^{N} (B_n \cos a_n\xi + C_n \sin a_n\xi) \sin n\pi\eta \\ &\quad + \sum_{N+1}^{\infty} D_n e^{-a_n\xi} \sin n\pi\eta \quad (\text{for } \xi \geqslant 0), \end{aligned}\right\} \tag{38}$$

in which $\Psi_1$ is given by (28) and

$$a_n = |B + n^2\pi^2|^{\frac{1}{2}}.$$

The coefficients $A_n$, $B_n$, $C_n$ and $D_n$ are determined by demanding

$$\Psi_- = \Psi_+ \quad \text{at} \quad \xi = 0, \tag{39}$$

$$\frac{\partial\Psi_-}{\partial\xi} - \frac{\partial\Psi_+}{\partial\xi} = f(\eta) \quad \text{at} \quad \xi = 0, \tag{40}$$

in which

$$f(\eta) = 0 \quad \text{for} \quad \eta \geqslant a \quad \text{and} \quad \eta = 0, \tag{41}$$

and is arbitrary elsewhere. Since $\Psi_-$ and $\Psi_+$ satisfy (12*b*), (39) and (40) ensure that $\Psi_+$ is the analytic continuation of $\Psi_-$. There are no singularities in the domain outside of the barrier (which is determined *a posteriori*), and there are no upstream waves. The function $f(\eta)$ corresponds to a sheet of distributed vortices (with horizontal axes) of variable strength at $\xi = 0$, extending from $\eta = 0$ to $\eta = a$. It determines implicitly the shape of the barrier.

† The author is indebted to Dr G. K. Batchelor for pointing out the possibility of this fact.

It will now be seen that $B_n$ and $C_n$ depend not on the details of the function $f(\eta)$ but only on certain of its integral properties, or, more precisely, on certain of its Fourier coefficients associated with the functions $\sin n\pi\eta$. Indeed, (39) demands that

$$A_n = D_n \quad (n > N), \tag{42}$$

$$B_n = 0 \quad (n \leqslant N), \tag{43}$$

and (40) demands

$$a_n(A_n + D_n) = 2\int_0^1 f(\eta)\sin n\pi\eta\, d\eta \quad (n > N), \tag{44}$$

$$a_n C_n = -2\int_0^1 f(\eta)\sin n\pi\eta\, d\eta \quad (n \leqslant N). \tag{45}$$

Thus $A_n$ and $D_n$ are determined from (42) and (44), and $C_n$ from (45).† But (45) is most significant. It states that the amplitudes of the $N$ wave components are equal to the first $N$ Fourier coefficients of the function divided by $a_n$ (which depends only on $B$ and $n$, and is quite independent of $f(\eta)$). Certainly there are infinitely many functions which satisfy (41), have the same first $N$ Fourier coefficients, and yet are different. The barriers corresponding to all these different generating functions have lee-waves with the same wavelengths and the same amplitudes, provided $B$ is the same for the upstream flow. The situation is even independent of the coefficients $A$, $C$, and $D$ in (28), though the shapes of the resulting barriers are dependent upon them. Near the barrier, the flow depends also on $A_n$ and $D_n$, and hence also on the rest of the Fourier components. In other words, near the barrier the flow depends on all the Fourier coefficients of or on the full details of $f(\eta)$, as is to be expected. Thus we have arrived at a sort of St Venant's principle in stratified flow.

Now that the alternative method has proved fruitful, it is desirable to improve the method, in order to obtain some flexibility for dealing with barriers of specified forms. The method outlined above is good for constructing flows over rather bluff barriers, and is not adequate if the barrier is elongated. To remedy this situation, the obvious thing to do is to achieve a freedom for displacing the vortices (represented by $f(\eta)$) in the $x$-direction. This can be done simply by using two or more vertical vortex sheets at different values of $x$ or $\xi$. If (38) is rewritten as

$$\Psi = \Psi_1 + \Psi_2,$$

in which the expressions for $\Psi_2$ are different for $\xi > 0$ and for $\xi < 0$, we see that $\Psi_2$ is the stream function which owes its existence to the presence of the barrier or of the singularities generating this barrier. If an additional line of singularities is situated at $\xi = b$, with distribution function $f_1(\eta)$, and still another situated at $\xi = c$, with distribution function $f_2(\eta)$, the solution is of the form

$$\Psi = \Psi_1 + \Psi_2 + \Psi_3 + \Psi_4,$$

in which $\Psi_3$ and $\Psi_4$ are similar to $\Psi_2$ given in (38), except that the $\xi$ in $\Psi_2$ should be changed to $\xi - b$ and $\xi - c$ for $\Psi_3$ and $\Psi_4$, respectively, and the coefficients are now determined from $f_1(\eta)$ for $\Psi_3$, and from $f_2(\eta)$ for $\Psi_4$. Generalization to

† If $B = -N^2\pi^2$, $a_N = 0$, and in order for the method to work the $N$th Fourier coefficient of $f(\eta)$ must be zero.

the case of more than three vortex sheets is obvious. If it is desirable to use isolated vortices, we can simply take $f(\eta)$ to be a Dirac delta-function located somewhere above $\eta = 0$.

*Use of sources, sinks, and doublets for generating stratified flows over a barrier*

Instead of demanding (39) and (40), we can demand

$$\Psi_- - \Psi_+ = f(\eta) \quad \text{at} \quad \xi = 0,$$

$$\frac{\partial \Psi_-}{\partial \xi} - \frac{\partial \Psi_+}{\partial \xi} = 0 \quad \text{at} \quad \xi = 0,$$

with $$f(\eta) = 0 \quad \text{for} \quad \eta \geqslant a \quad \text{and} \quad \eta = 0,$$

and $f(\eta)$ arbitrary elsewhere. The function $f(\eta)$ now corresponds to a source distribution along a line element at $\xi = 0$. The solution is again in the form of (38), but the formulas for the coefficients are now

$$A_n = -D_n \quad (n > N), \quad C_n = 0 \quad (n \leqslant N),$$

$$A_n - D_n = 2\int_0^1 f(\eta) \sin n\pi\eta \, d\eta \quad (n > N),$$

$$B_n = -2\int_0^1 f(\eta) \sin n\pi\eta \, d\eta \quad (n \leqslant N).$$

If there is more than one line source, the generalization is the same as given in the last paragraph. The total algebraic sum of the sources must be zero in order that the barrier be closed.

Again, by taking $f(\eta)$ to be a Dirac delta-function, the solution corresponding to an isolated source or sink can be obtained. It can be readily shown that if a source is located at $\xi = -b$ and a sink of equal strength ($m$) is located at $\xi = b$ and at the same height $h_s$ (dimensionless), the $n$th ($n \leqslant N$) lee-wave is represented by

$$-4m \sin n\pi h_s \sin a_n b \sin a_n \xi \sin n\pi\eta.$$

If $b$ is small, the amplitudes of the lee-waves are proportional to $2mb$, which is the negative of the moment of the source and sink. Thus, for a doublet of strength $\mu$ (equivalent to $-2mb$), the amplitude of the $n$th lee-wave is

$$2\mu a_n \sin n\pi h_s,$$

and, for a doublet distribution from $\eta = 0$ to $\eta = a$, the amplitude of the $n$th lee-wave is

$$2a_n \int_0^a \mu(\eta) \sin n\pi\eta \, d\eta.$$

If the doublet (isolated or distributed vertically) is not located at $\xi = 0$, *only* the *phase* of the pertaining lee-waves will be changed (by an amount equal to the $\xi$-coordinate of the doublet or doublet distribution).

*An example, and a discussion of the effect of the upper boundary*

Figure 3 shows a stratified flow (case (*b*)) over a barrier, with waves in the lee. The velocity distribution far upstream is given indirectly by (28), with $C = D = 0$ and $A = B = -9/16\pi^2$, so that $u'$ is constant far upstream. The flow is analytically given by (38) and (42) to (45), with

$$\begin{aligned} -f(\eta) &= 10 \sin 5\pi\eta \quad \text{for} \quad 0 \leqslant \eta \leqslant 0{\cdot}2, \\ &= 0 \qquad\qquad\ \ \text{for} \quad 0{\cdot}2 < \eta \leqslant 1. \end{aligned}$$

There is a single lee-wave component, with wavelength $(6/\sqrt{7})d$, $d$ being the depth from the (flat) upper boundary to the flat part of the lower boundary.

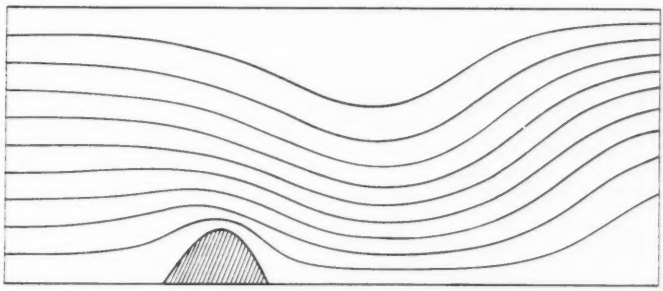

FIGURE 3. A stratified flow over a barrier, with waves in the lee.

Since the wave numbers of the lee-waves are $a_n$ (for those $n$'s that make $B + n^2\pi^2$ negative), the wavelengths must depend on $B$. In the example just given, $B = -F^{-2}$, with

$$F^2 = \frac{\rho_0 U'^2}{gd^2(d\rho/dz)},$$

$U'$ being the (constant) velocity $u'$ at $x = -\infty$, where $d\rho/dz$ is taken. Thus for a given $U'$ and density distribution, the wavelengths depend on $d$. Consequently, the location of the upper boundary has in this case, as indeed it does in general, a profound influence on the flow pattern. This is not surprising, for as the depth increases the wave numbers for those lee-waves just able to stay stationary (i.e. to withstand the sweeping action of the parallel flow) must also increase, and vice versa, because the wave velocities increase with $d$ and decrease with the wave-numbers (Yih 1960). However, the importance of the location of the imaginary upper boundary does raise the question of where to impose it in any given situation, and the question of the error committed by imposing it.

A partial answer to these questions can be obtained by considering two superposed layers of fluids. The lower layer has depth $d$, and is bounded below by a rigid plane boundary (the ground). The upper layer has depth $d_u$ and is bounded above by an auxiliary rigid plane. This auxiliary boundary (not the one the effect of which is under discussion) is imposed only for convenience, and is not necessary, for the same conclusions can be reached on the assumption that the

depth of the upper layer is infinite. The interface of the two layers is the place where the artificial rigid boundary under discussion is supposed to be imposed in the preceding analysis, and it is proposed to see under what conditions the presence of this boundary introduces only small errors. Let the density gradients in the two layers be constant but different, and the density be continuous at the interface. At $x = -\infty$, $u'$ is supposed to be the same for both layers, and is denoted by $U'$. The equations governing fluid motion in the two layers are

$$\nabla^2\Psi - F^{-2}\eta = -F^{-2}\Psi, \quad \nabla^2\Psi_u - F_u^{-2}\eta = -F_u^2\Psi,$$

in which

$$F = -\frac{\rho_0 U'^2}{gd^2(d\rho/dz)}, \quad F_u = -\frac{\rho_0 U'^2}{gd^2(d\rho/dz)_u},$$

the density gradients being taken in the absence of waves. The parallel flow corresponds to

$$\Psi_1 = (\Psi_u)_1 = \eta,$$

and the wave motion is governed by (with the subscript 2 on the stream functions dropped for convenience)

$$\nabla^2\Psi = -F^{-2}\Psi, \quad \nabla^2\Psi_u = -F_u^{-2}\Psi_u.$$

These equations are to be solved with the boundary conditions

(i) $\Psi = 0$ at $\eta = 0$;

(ii) $\Psi_u = 0$ at $\eta = d_u/d$;

(iii) that the displacement be the same for both layers at the interface;

(iv) that the pressure (or, equivalently, the velocity) be continuous at the interface.

The solution of the eigenvalue problem so defined on the basis of a linearized analysis yields the secular equation

$$(F^{-2}-m^2)^{\frac{1}{2}}\cot(F^{-2}-m^2)^{\frac{1}{2}} = -(F_u^{-2}-m^2)^{\frac{1}{2}}\cot(F_u^{-2}-m^2)^{\frac{1}{2}}\left(\frac{d_u}{d}-1\right)$$

for the determination of the eigenvalues for the wave-number $m$ in the factor $\sin m\xi$ contained in $\Psi$ and $\Psi_u$. Since in the atmosphere the gradient of the potential density in the stratosphere is greater than that in the troposphere,

$$F_u^{-2} = \alpha F^{-2} \quad (\alpha > 1).$$

Hence

$$\frac{F_u^{-2}-m^2}{F^{-2}-m^2} = \frac{(\alpha-1)F^{-2}}{F^{-2}-m^2}+1.$$

In the atmosphere, if $d$ is taken to be the depth of the troposphere, $F^2 \ll 1$. Consequently, if $m$ is large enough to make $F^{-2}-m^2$ much smaller than $F^{-2}$, the secular equation can be replaced by

$$\tan(F^{-2}-m^2)^{\frac{1}{2}}\cot(F_u^{-2}-m^2)^{\frac{1}{2}}\left(\frac{d_u}{d}-1\right) = 0.$$

One set of solutions of this equation is

$$m = (F^{-2}-n^2\pi^2)^{\frac{1}{2}} = a_n,$$

so long as $n$ is not so large an integer as to make $m$ small. Another set of solutions is obtained by setting the other factor (in the approximate secular equation) equal

to zero. The wave-numbers obtained are for waves in the upper layer when the interface is replaced by a rigid boundary. Thus, if we take $d$ to be the depth of the troposphere and apply the analysis to meteorological problems, the situation is as follows:

(1) The exponential terms in (38), corresponding to local disturbances only, are least affected by the replacement of the tropopause by a rigid boundary, and, since $d$ is rather large compared with the vertical dimension of a barrier, are practically independent of $d$.

(2) For small values of $F$, the shorter lee-waves predicted by the theory will exist in the atmosphere. The error committed by imposing the upper rigid boundary is small in connexion with the shorter lee-waves.

(3) For the longer lee-waves, the error may be large.

(4) The theory will furnish no information at all on lee-waves extending to the stratosphere.

Because of the situation stated in (3) and (4), further work is necessary to determine more accurately the effect of the upper boundary. In the absence of better information, $d$ should be taken to be the depth of the troposphere when applying the theory presented here (which does have the advantage that the amplitude of the motion treated does not have to be small).

## 5. Class (*c*): another class of waves of arbitrary amplitude, with possible application to atmospheric flows

For convenience, the coefficient $A$ in (12*c*) will be denoted by $\alpha^2$, so that $\alpha$ is imaginary if $A$ is negative. The solution of (12*c*) is of the form

$$\Psi = \Psi_1(\eta) + \Psi_2(\xi, \eta), \tag{46}$$

in which $\Psi_1$ satisfies the equation

$$\frac{d^2\Psi_1}{d\eta^2} + \alpha^2\eta\Psi_1 = B, \tag{47}$$

and $\Psi_2$ satisfies the equation

$$\nabla^2\Psi_2 + \alpha^2\eta\Psi_2 = 0. \tag{48}$$

The density variation now satisfies the equation $d\rho/d\Psi \propto \Psi$.

For $B = 0$ the solution of (47) is, aside from a constant factor,

$$\Psi_1(\eta) = \eta^{\frac{1}{2}}\{J_{\frac{1}{3}}(\tfrac{2}{3}\alpha\eta^{\frac{3}{2}}) + CN_{\frac{1}{3}}(\tfrac{2}{3}\alpha\eta^{\frac{3}{2}})\} \equiv f(\eta). \tag{49}$$

For $B \neq 0$ the substitution

$$\Psi_1 = f(\eta)\,\phi(\eta) + K_1 \tag{50}$$

leads to

$$\Psi_1 = f\left[\int_0^\eta \frac{B\int_0^\eta f\,d\eta - \alpha^2 K_1\int_0^\eta \eta f\,d\eta}{f^2}\,d\eta + K'\right] + K_1. \tag{51}$$

Since $f(0) = 0$, $\Psi_1 = K_1$ at $\eta = 0$. (It is no longer always permissible to take $\Psi = 0$ at $\eta = 0$, because in reaching (11*c*) $\Psi$ is already assumed to have been modified by an additive constant if necessary.) The constant $K'$ in (51) ensures that $\Psi_1$ can be adjusted to take any value $K_2$ at $\eta = 1$ provided $J_{\frac{1}{3}}(\frac{2}{3}\alpha) \neq 0$.

The solution of (48) is of the form

$$\Psi_2 = \sum_{n=1}^{\infty} A_n \exp[\pm(a_n\xi)\beta(\alpha, b_n, \eta)], \tag{52}$$

in which $b = -a^2/\alpha^{\frac{7}{3}}$, and

$$\beta(\alpha, b, \eta) = (\eta - b)^{\frac{1}{2}}\{N_{\frac{1}{3}}[\tfrac{2}{3}\alpha(-b)^{\frac{3}{2}}]J_{\frac{1}{3}}[\tfrac{2}{3}\alpha(\eta-b)^{\frac{3}{2}}] - J_{\frac{1}{3}}[\tfrac{2}{3}\alpha(-b)^{\frac{3}{2}}]N_{\frac{1}{3}}[\tfrac{2}{3}\alpha(\eta-b)^{\frac{3}{2}}]\}, \tag{53}$$

and $b_n$ are the eigenvalues satisfying

$$\beta(\alpha, b, 1) = 0. \tag{54}$$

If $a_n^2$ is negative, (52) corresponds to a wave motion with periodic components.

Solutions $\Psi_1$ and $\Psi_2$, given in (51) and (52), can be used for application of Long's method or the alternative method proposed in § 4, in dealing with flow over a barrier. In fact, the entire development in § 4 can be repeated in a strictly similar manner for the new forms of $\Psi_1$ and $\Psi_2$, and the problem of flow into a sink treated by Yih (1958) can again be solved if the upstream condition is described by (51) and $|A|$ is sufficiently small. We shall not work out the details, which are tedious but straightforward, and shall content ourselves by pointing out that (51) again represents infinitely many upstream conditions, corresponding to the infinitely many sets of values for $A$, $B$, $K'$, and $K_1$, one of which may sometimes be a better approximation to the actual wind distribution than one represented by (28).

This work has been done during the tenure of a Senior Post-Doctoral Fellowship of the National Science Foundation at the University of Cambridge, and the author wishes to express his appreciation to the Foundation for the opportunity to pursue uninterrupted research. The author is indebted to Dr G. K. Batchelor, F.R.S., for stimulation, criticism, and several useful discussions. It is also a pleasure to acknowledge the support of fundamental research on stratified flows by the Office of Ordnance Research in the past several years, without which the present work would have taken much longer to accomplish.

*Note added in proof.* While this paper was in the proof stage, its contents were presented at a seminar of the Institute of Meteorology of the University of Stockholm. At that time Prof. G. Benton kindly informed the author that some of the results presented had already been published by Prof. R. R. Long in a brief note ('Tractable models of steady-state stratified flow with shear', *Quart. J. Roy. Met. Soc.* **84**, 1958, pp. 159–61). Upon examining that note, I found that equation (28) and the upstream condition corresponding to equation (12*c*) had already been obtained by Long by an entirely different approach.

## REFERENCES

Long, R. R. 1953 Some aspects of the flow of stratified fluids. I. A theoretical investigation. *Tellus*, **5**, 42–57.

Long, R. R. 1955 Some aspects of the flow of stratified fluids. III. Continuous density gradients. *Tellus*, **7**, 342–57.

Yih, C.-S. 1958 On the flow of a stratified fluid. *Proc. Third U.S. Nat. Congr. Appl. Mech.* pp. 857–61.

Yih, C.-S. 1960 Gravity waves in a stratified fluid. *J. Fluid Mech.* **8**, 481–508.

# On the disintegration of water drops in an air stream

By K. N. DODD
Royal Aircraft Establishment, Farnborough

(Received 1 March 1960)

A theory is developed, based on the very limited available experimental evidence, to predict the distortion and disintegration of a water drop when it is exposed to a stream of air with continuously increasing relative velocity. The theory is applied to water drops situated in the path of a solid sphere moving through the air.

## 1. Introduction

In the absence of aerodynamic forces, a drop of water will take up a spherical shape under the influence of surface tension. But when the drop moves through the air, aerodynamic forces are also applied to its surface and these will distort the drop from its spherical form. The distortion is of two types. For very high velocities of relative motion, such as occur near explosions, the outer surface is stripped off the drop while the central portion remains momentarily at rest. In this note, however, we shall only be concerned with the second type of distortion which only occurs at lower relative velocities.

The stages in this second type of distortion are shown in figure 1. As the relative velocity is increased from zero, the originally spherical drop (*a*), has its leading surface flattened (*b*), then the flattened surface becomes concave. The hollow increases in depth until it almost protrudes through the back of the drop. After this a spherical bubble in the shape of a bag begins to develop (*c*) and the bubble expands rapidly from the annular ring of water on which it is formed (*d*). The thin sheet of water forming the bubble eventually becomes unstable and disintegrates into tiny droplets (*e*). Soon after this the annular ring also becomes unstable and breaks up into somewhat larger droplets.

## 2. The experimental evidence

The experimental evidence on this subject appears to be limited to some unpublished work by Lane & Edwards (1948) in which photographs of drops in the various stages of bursting outlined above are given. This work is mainly an account of some experiments in which drops of water were dropped under gravity into a vertical wind tunnel. This apparatus consisted of a vertical tube as shown in figure 2, with a flared entry. Air was sucked in through the top and out through an exhausting fan $F$. Water drops $D$ of known size were allowed to fall from a pipette down the centre line of the tube and the air velocity was adjusted until disintegration was obtained in the tube. For our purposes, the main result in this paper was a graph showing the position of a 2·38 mm diameter drop in the

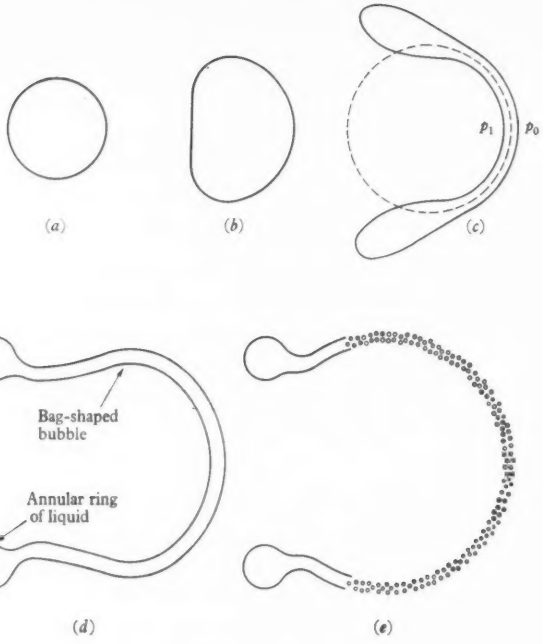


FIGURE 1 (*a–e*). Stages of break-up of a water drop.

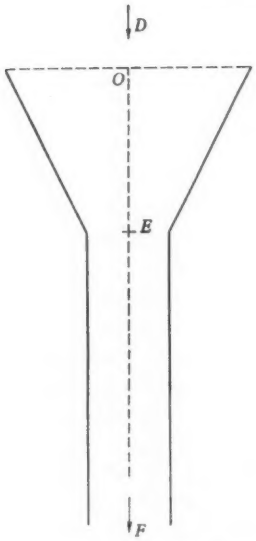


FIGURE 2

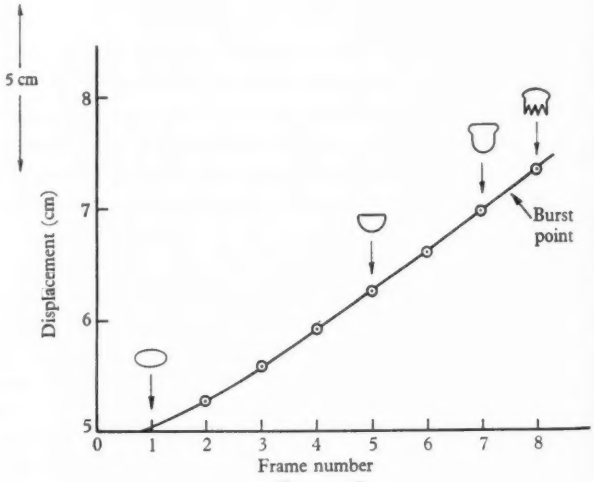


FIGURE 3

FIGURE 2. Cross-section of wind tunnel for experiment.

FIGURE 3. Motion of a water drop in the wind tunnel. Original diameter of the water drop, 2·38 mm. Air velocity, 23·2 m/sec.

tube at intervals of time of about $\frac{1}{2}$ ms. On the graph was also indicated the stage of disintegration reached by the drop at some of the time intervals. This graph is reproduced in figure 3. The displacement is the distance the drop has moved past the point $O$ in figure 2. A good series of photographs like figure 1 was also obtained for a 2·2 mm diameter drop (see also Lane & Green 1956).

We shall also require, for our investigations, the pressure distribution on a solid sphere exposed to a stream of air. This distribution was found from experiment by Hinze (1948) to be

$$\begin{aligned} p &= \rho_a(V-u)^2(9\cos^2\theta - 5)/8 \quad \text{for} \quad 0 \leqslant \theta \leqslant \tfrac{1}{3}\pi, \\ &= -11\rho_a(V-u)^2/32 \qquad\quad \text{for} \quad \tfrac{1}{3}\pi \leqslant \theta \leqslant \pi, \end{aligned}$$

where $\rho_a$ is the density of air, $V$ is the air speed, $u$ is the drop speed and $\theta$ is the angular distance from the point on the sphere facing the oncoming air stream. These formulae appear to be confirmed approximately by other investigations, for example, Fage (1937).

## 3. The condition for disintegration

The main theoretical discussion of the results of experiments on water drops has centred on ascertaining the conditions under which break-up will occur. Lane & Edwards thought that the break-up would occur roughly when the force due to the variation of aerodynamic pressure over the drop exceeds that due to surface tension. They wrote

$$4T/d = k\rho_a(V-u)^2,$$

where $T$ is the surface tension of the liquid, $d$ is the diameter of the drop and $k$ is a constant. From this it follows that

$$d(V-u)^2 = \text{constant},$$

and Lane & Edwards showed from their experiments that this relation holds approximately.

Prandtl (1952, p. 325) discusses the phenomenon and arrives at a similar result. He also mentions some experiments very similar to those of Lane & Edwards which were performed by Hochschwender at Heidelberg as early as 1919. On the other hand, Hinze showed from a theoretical consideration of the break-up of freely falling drops that the condition of break-up is not an explicit equation but depends on the history of the relative velocity $(V-u)$.

Our view is that the Hinze theory is not applicable to Lane & Edwards's experiments.

To propound our theory on the matter, we must refer again to figure 1. As the relative velocity is increased, the drop takes on the form shown in (*c*) in which the bubble is just beginning to form. Let us draw a dotted sphere through this bubble. Then we contend that the critical velocity for bursting is the velocity which makes the radius of this circle a minimum. Let $p_1$ be the pressure just inside the bubble and $p_0$ the pressure just outside and let

$$p_1 - p_0 = \mu\rho_a(V-u)^2,$$

this equation defining $\mu$ which we shall regard as a constant. This equation is assumed to hold for all stages of the bubble formation. Let $r$ be the radius of the bubble, then

$$p_1 - p_0 = 4T/r$$

and taking these equations together we get

$$r(V-u)^2 = 4T/\mu\rho_a$$

which holds for all stages of the bubble formation. Let $r_m$ be the minimum radius of the bubble. Substituting in this equation, we obtain the following expression giving the critical velocity

$$r_m(V-u)^2_{\text{crit.}} = 4T/\mu\rho_a. \tag{1}$$

It appears from what few photographs are available that this minimum radius is about twice the radius of the original spherical drop. Hence we get essentially the same form of condition for break-up as that postulated by Lane & Edwards.

The constant $\mu$ is at this stage unknown but we can get a very rough approximation from the distribution of pressure over a solid sphere. In the distribution given above, the pressure is positive for $\theta$ from 0° to about 43° and is negative and of almost constant value over the rest of the sphere. If we take $p_0$ as this constant value and $p_1$ as the averaged pressure over the positive region of the sphere, we obtain $\mu = 0{\cdot}238 - (-0{\cdot}344) = 0{\cdot}582$.

## 4. The dynamics of the burst

In general the relative velocity $V-u$ is not given. Usually, $V$ is given as a function of position $s$; the drop velocity $u$ being determined by an equation of motion for the drop, which depends on $V$ through the aerodynamic drag. The relative velocity will normally increase up to the critical velocity given by (1) after which there will be a rapid increase in the size of the drop (i.e. bubble) followed by bursting. The critical velocity conveniently divides the motion into two phases. We shall consider phase II first as it is the more interesting both theoretically and for the purpose of our applications.

For phase II we propose to idealize the problem by replacing the bubble by a hollow sphere. Let $m$ be the mass of the original drop of water. We shall suppose a fraction $f$ of this mass is contained in the hollow sphere and that the remaining mass is travelling along with the sphere but is not expanding. Lane & Edwards estimated that a fraction 0·3 of the mass of the original sphere is in the bubble but at present we shall not commit ourselves to this figure. Then the equations of motion for the sphere as a whole moving in a straight line are

$$\frac{ds}{dt} = u, \tag{2}$$

$$m\frac{du}{dt} = mg + \tfrac{1}{2}C_D\pi r^2\rho_a(V-u)^2, \tag{3}$$

where $t$ is time, $r$ is the radius of the hollow sphere and $C_D$ is the drag coefficient. The gravity term has been put in as appropriate for comparison with the Lane & Edwards's experiments. The positive directions of $s$, $u$ and $V$ are all downwards.

To obtain the equation for the expansion of a thin spherical shell, consider a small area $A$ on the shell. Let the thickness of the shell be $\delta r$. The mass of this area of shell is $A\,\delta r$, taking the density of water to be unity; its acceleration is $d^2r/dt^2$. The relation between acceleration and the force acting is thus

$$A\,\delta r \times \frac{d^2r}{dt^2} = A\left[p_1 - p_0 - \frac{4T}{r}\right]$$
$$= A\left[\mu\rho_a(V-u)^2 - \frac{4T}{r}\right].$$

But the total volume of the shell is

$$4\pi r^2 \delta r = f_m, \tag{4}$$

which gives us the value of $\delta r$. Hence we obtain

$$\frac{d^2r}{dt^2} = \frac{4\pi r^2}{f_m}\left[\mu\rho_a(V-u)^2 - \frac{4T}{r}\right]. \tag{5}$$

Equations (2), (3) and (5) govern the behaviour of the drop after the critical velocity has been passed.

For phase I of the motion, the drop is idealized to a sphere of fixed radius but with a larger (but fixed) drag coefficient than that for the original spherical drop. Thus in this phase, equations (4) and (5) do not apply. This is the weakest part of the theory because the drag coefficient will obviously differ greatly for the stages (*a*), (*b*) and (*c*) in figure 1.

Having established the theory of the motion, out next task is to compare it with the Lane & Edwards experiment in the one case for which there was adequate information supplied. The funnel-shaped top of the wind tunnel, figure 2, was three times as wide at the top as at the bottom and its height was 5 cm. Measuring $s$ from the point $O$, the air velocity is given by

$$V(s) = \frac{v}{(3-0{\cdot}4s)^2} \quad \text{for} \quad 0 \leqslant s \leqslant 5,$$
$$= v \quad \text{for} \quad 5 \leqslant s, \tag{6}$$

where $v$ is the air velocity in the tube. The case given by Lane & Edwards was that of a drop of original diameter 0·238 cm. The graph (figure 3) shows the times at which the drop reaches a number of points down the tube. At $s = 7{\cdot}2$ cm, the radius of the bubble is about 0·47 cm and the bubble is on the point of bursting. The position $s = 7{\cdot}2$ cm is reached about 4 ms after passing $s = 5$ cm. $v$ was measured to be 23·2 m/sec. Now from the initial gradient of the $(s, t)$ graph, it appeared that the drop was moving at a velocity $u$ of about 4·8 m/sec at the critical point (assumed to be pretty near $s = 5$ cm). At the critical point we also have $dr/dt = 0$ and $r = r_m = 0{\cdot}238$ cm (assuming that $r_m$ is twice the radius of the original spherical drop). It remains to find the value of $s$ at the critical point. This is done by finding $V$ from equation (1) (using $u = 4{\cdot}8$ m/sec) and hence $s$ from equation (6). From the values of the variables at the critical point, the equations were integrated on an electronic computer to find the conditions at $s = 7{\cdot}2$ cm. To do this, however, three parameters had to be chosen, namely, $\mu$,

$C_D$ and $f$. A value 0·3 was chosen for $f$. With this fixed, numerous integrations had to be performed with different combinations of $\mu$ and $C_D$ in order to get an exact fit to the experimental results. It was found that $\mu$ mainly affected the rate of expansion of the bubble while $C_D$ mainly affected the rectilinear acceleration of the drop but there was some interconnection between the two effects. A solution was eventually found with

$$f = 0{\cdot}3, \quad \mu = 0{\cdot}29, \quad C_D = 0{\cdot}5, \quad s_{\text{crit.}} = 4{\cdot}98\,\text{cm}.$$

To test the effect of changing $f$, a solution was also obtained with

$$f = 0{\cdot}6, \quad \mu = 0{\cdot}30, \quad C_D = 0{\cdot}5, \quad s_{\text{crit.}} = 4{\cdot}96\,\text{cm}.$$

The value of $C_D$ is about what would be expected for a sphere and the values of $\mu$, although somewhat smaller than that calculated from the solid sphere, seem quite plausible. So with these parameters, we felt justified in proceeding to consider other applications of the equations.

During the course of the integration trials, it was found that if $\mu$ was taken too small the bubble did not expand at all. But there was a small critical range of $\mu$ such that the bubble began to expand and then contracted again. We think that this may explain the phenomenon shown in some of Lane & Edwards's photographs in which the tip of the bubble collapses back through the annular ring.

The calculations for phase I of the motion presented less trouble as $C_D$ is the only parameter. It was found that the motion from the pipette down to $s = 0$ was not sensibly different from a free fall under gravity, giving a velocity of $u = 2\,\text{m/sec}$. The acceleration to 4·8 m/sec required a value of about $C_D = 15$ in equation (3), using the radius of the original spherical drop for $r$ in this equation.

## 5. Drops in the path of moving objects

Our main interest in the theory is to apply it to drops situated in the path of objects moving through the air to see whether these drops will be shattered or whether they will collide with the object.

The equations need no modification except (3), which need no longer contain the gravity term if the object is moving horizontally.

We consider the case of a sphere of radius $a$ moving horizontally through the air with speed $v$. It is found convenient to consider the sphere to be at rest and the air to be moving. We placed the origin of co-ordinates at the point on the sphere facing the oncoming air stream and let the $s$-axis point in the direction in which the air was flowing. Drops are then considered as they approach the sphere along the negative $s$-axis.

We use parameters $f = 0{\cdot}6, \mu = 0{\cdot}3$ and $C_D = 0{\cdot}5$. The value chosen for $f$ causes a slower expansion of the bubble than $f = 0{\cdot}3$ and so the probability of bursting is not overestimated. The expression for $V$ is

$$V(s) = v - v\left(\frac{a}{a-s}\right)^3.$$

This expression is obtained from the flow of an ideal fluid round a sphere, but experimental work has shown that the expression is very nearly true for air at subsonic speeds.

Our approach to the problem consists in assuming as a first approximation that the drop travels with speed $v$ up to the critical point. The value of $s$ at the critical point is then given by

$$v\left(\frac{a}{a-s}\right)^3 = \left(\frac{2T}{r\mu\rho_a}\right)^{\frac{1}{2}}.$$

This is equation (1) with the appropriate values of $V$ and $u$ substituted and with $r_m = 2r$, where $r$ is the radius of the originally spherical drop. From the critical point onwards the equations were integrated as previously described to see if the bubble would burst before colliding with the sphere. From the experimental evidence given by Lane & Edwards, the bursting point is taken to be the position at which the radius of the bubble is $2r_m$. But the expansion of the bubble at this point is very rapid and so the calculations are not sensitive to the choice of radius at burst. If the collision occurs before the burst then that is the end of the matter. If the burst occurs first, it is then necessary to test the validity of our assumption that the drop speed is $v$ at the critical point. Of course, it will be slightly less than $v$ but we must estimate by how much. From equation (3), the drag force on the drop is $F = \frac{1}{2}C_D\pi r^2\rho_a(V-u)^2$. The work done by this force up to the critical point is

$$\int_{-\infty}^{s_{\text{crit.}}} F\,ds,$$

and this is equal to the change in kinetic energy of the drop, i.e. $\frac{1}{2}m(v^2-\bar{v}^2)$ where $\bar{v}$ is the true velocity of the drop at the critical point. We can overestimate the value of the integral by putting $u = v$, in which case we get

$$1-\left(\frac{\bar{v}}{v}\right)^2 = 3\rho_a\frac{a}{r}\left[\frac{a}{a-s_{\text{crit.}}}\right]^5,$$

on using $m = \frac{4}{3}\pi r^3$ and putting $C_D = 20$ as an upper estimate. The value of $\bar{v}$ was calculated from this expression. If it differed greatly from $v$ then the fate of the bubble became uncertain. If $\bar{v}$ turned out close to $v$, the bursting conclusion could be regarded as valid and a slight correction could be applied to the positions of the critical and bursting points.

We considered a range of values of $r$, $a$ and $v$ and the results are tabulated in table 1. $B$ denotes that the drop bursts before hitting the sphere, whereas $C$ denotes that the drop collides with the sphere. In all the $B$ cases, $\bar{v}$ was within 5 % of $v$. There were two uncertain cases and these are indicated by a question mark.

It will be noted that a larger drop may collide while a smaller drop bursts for given $a$ and $v$. This is in spite of the fact that a higher critical relative speed is required for the smaller drop. The explanation is that the smaller drop is more easily blown up once the critical point is past due to the smaller thickness of its bubble.

Finally, it is of interest to compare the gradients of relative velocities (at the critical points) in the above cases with the gradients in the Lane & Edwards experiments for similar drop sizes. The table below gives these gradients, the units being m/sec per cm. The values given under the heading 'sphere' are the

maximum gradients for the cases we have considered in table 1 (i.e. the gradients for $a = 5$, $v = 50$):

| $r$ | Sphere | Lane & Edwards |
|---|---|---|
| 0·2 | 5·33 | 14 |
| 0·1 | 8·46 | 20 |
| 0·05 | 13·43 | 31 |

It will be seen that gradients for the sphere are all less than the corresponding Lane & Edwards's gradients so we can be confident in applying the low-velocity theory in these cases.

$r = 0{\cdot}2$ cm

| $v$ \ $a$ | 5 | 10 | 20 | 40 |
|---|---|---|---|---|
| 200 | *C* | *C* | *C* | *B* |
| 100 | *C* | *C* | *C* | *B* |
| 50 | *C* | *C* | *C* | *B* |

$r = 0{\cdot}1$ cm

| $v$ \ $a$ | 5 | 10 | 20 | 40 |
|---|---|---|---|---|
| 200 | *C* | *C* | *B* | *B* |
| 100 | *C* | *C* | *B* | *B* |
| 50 | *C* | *C* | *C* | ? |

$r = 0{\cdot}05$ cm

| $v$ \ $a$ | 5 | 10 | 20 | 40 |
|---|---|---|---|---|
| 200 | *C* | *B* | *B* | *B* |
| 100 | *C* | *B* | *B* | *B* |
| 50 | *C* | *C* | *C* | ? |

TABLE 1. $v$ is in m/sec, and $a$ in cm.

## 6. Conclusion

In conclusion, it should be emphasized that the theory of bursting which has been put forward is not intended to be final. Indeed, considering the paucity of experimental evidence, it would be surprising if the theory does not need to be modified when further experimental results became available. It seems, however, that the basis of the theory is substantially correct and future work will need to be concentrated on determining the degree to which the 'constants' in our equations must be varied for differing drop sizes.

REFERENCES

FAGE, A. 1937 *A.R.C. Technical Report*, R. & M. No. 1766.

HINZE, J. O. 1948 *Appl. Sci. Res., Hague*, A, **1**, 273.

LANE, W. R. & EDWARDS, J. 1948 Unpublished Ministry of Supply Report.

LANE, W. R. & GREEN, H. L. 1956 The mechanics of drops and bubbles. Article in *Surveys in Mechanics* (Ed. G. K. Batchelor & R. M. Davies). Cambridge University Press.

PRANDTL, L. 1952 *The Essentials of Fluid Dynamics*. London: Blackie.

# Rayleigh instability of a thermal boundary layer in flow through a porous medium

By R. A. WOODING
Emmanuel College, Cambridge†

(Received 31 March 1960)

It is supposed that a heated liquid is rising very slowly through a semi-infinite porous medium towards the permeable horizontal surface, where it mixes with a layer of cool overlying fluid. In the steady state a thermal boundary layer of exponential form exists in the medium. It is shown that the layer is stable provided that the Rayleigh number for the system does not exceed a critical positive value, and that the wave-number of the critical neutral disturbance is finite. The stability properties of the layer are explained qualitatively from physical considerations.

## 1. Introduction

In the geothermal region of Wairakei, New Zealand, it is known that the sub-surface ground water possesses a general upward convective drift, due to buoyancy induced by the high underground temperature. Since the rising ground water is cooled as it approaches the surface, where heat is removed by evaporation, radiation and movement in surface streams, an unstable state may be induced, and complicated convective motions appear in the layers near the surface. It is the purpose of this paper to investigate the conditions for instability to occur.

In an idealized case, one considers a dynamically incompressible fluid, which rises at a constant, uniform rate through a semi-infinite homogeneous porous medium, and passes through the surface to mix with a layer of fluid at constant temperature. When a steady state has been established, a thermal boundary layer of exponential form then exists below the surface.

*The basic equations.* Suppose that a homogeneous isotropic porous medium of porosity $\epsilon$ and permeability $k$ is saturated with a liquid incompressible to pressure changes, the density $\rho$ being a function of temperature $T$ only. To allow for the dilatation and contraction of the fluid with temperature variations, it is convenient to introduce a vector $\mathbf{q}_m$ proportional to the rate of mass flow, and related to the usual volume flow vector $\mathbf{q}$ by

$$\mathbf{q}_m = \frac{1}{\rho_0}\rho\mathbf{q}, \tag{1}$$

where $\rho_0$ is a reference density, corresponding to a temperature $T_0$. Then the

† Present address: D.S.I.R., Box 8018, Wellington, N.Z.

equations of continuity, motion and heat transport for the liquid in the porous medium are

$$\frac{\epsilon}{\rho_0}\frac{\partial \rho}{\partial t} + \operatorname{div} \mathbf{q}_m = 0, \tag{2}$$

$$\frac{1}{\rho_0}\operatorname{grad} P - \mathbf{g}\rho/\rho_0 + \frac{1}{k}\nu \mathbf{q}_m = 0, \tag{3}$$

$$E\frac{\partial T}{\partial t} + \mathbf{q}_m . \operatorname{grad} T = \operatorname{div}(\kappa \operatorname{grad} T). \tag{4}$$

In equation (3), $P$ is the pressure, $\nu \equiv \nu(\rho) = \mu/\rho$ is the kinematic viscosity ($\mu \equiv \mu(\rho)$ being the dynamic viscosity) and $\mathbf{g}$ is the acceleration due to gravity. Inertial terms do not appear in this equation, which is usually called Darcy's law. The conditions for the validity of equation (3) are that the Reynolds number based upon the flow through the pores should not exceed $O(1)$, and that the time scale of unsteady macroscopic motions should be very much greater than $k/\nu$—the time scale of transient motions in a single pore.

In equation (4),

$$c\rho_0 E(\rho) = (1-\epsilon)\, c_s \rho_s + \epsilon c \rho \tag{5}$$

is the heat capacity per unit volume of saturated porous material, $c$ being the specific heat of the liquid, and $c_s$ and $\rho_s$ the specific heat and the density of the solid material. Throughout this paper, the Boussinesq approximation that a linear relationship exists between the density $\rho$ and the temperature $T$ will be assumed, so that $T$ can be replaced by $\rho$ in equation (4). The diffusivity $\kappa = K/c\rho_0$, where $K$ is the thermal conductivity of the saturated porous material, i.e. the heat flux crossing unit area in the presence of a unit temperature gradient. When mechanical dispersion is also present, $\kappa$ must be replaced by a tensor quantity.

## 2. Formulation of the stability problem

Let the horizontal boundary of the porous medium be at $Z = 0$, the axis $OZ$ being directed vertically upwards, and let the porous medium occupy the region $-\infty < Z \leqslant 0$. The surface is assumed to be covered by static liquid of constant temperature, which gives the boundary conditions $\rho = \rho_1 =$ constant and $P =$ constant at $Z = 0$. It will be assumed also that, at $Z = -\infty$, the medium is saturated with a liquid of density $\rho_0$, which is rising vertically at a steady uniform mass flow rate $\rho W = \rho_0 W_m$ (cf. equation (1)). The liquid passes through the permeable boundary at $Z = 0$ and mixes with the layer of standing fluid. When this primary flow is very slow, thermal diffusion from the surface $Z = 0$ into the medium becomes important, and a thermal boundary layer appears. If the thermal diffusivity $\kappa$ taken in the $Z$-direction can be assumed constant, the steady-state primary density distribution is, from equations (2) and (4),

$$\rho = \rho_0 + (\rho_1 - \rho_0)\, e^{W_m Z/\kappa} \tag{6}$$

since $W_m$ is a constant.

Mechanical dispersion is negligible, since it can be shown that the Péclet number of the flow through the pores is of the same order of magnitude as the ratio of a typical pore diameter to the thickness $\kappa/W_m$ of the thermal boundary layer. This ratio will be vanishingly small. It follows that the thermal diffusivity

can be taken to be isotropic, since the medium is isotropic, so that $\kappa$ is a scalar constant in equation (4).

To examine the stability of the given primary flow, one considers the effect of superimposing small perturbations $p$, $\mathbf{q}'_m$ and $\theta$ (say) upon the given primary values of pressure, velocity and density, respectively. The perturbed values are substituted into equations (2), (3) and (4) and, after linearizing in the usual manner, one obtains the perturbation equations

$$\frac{\epsilon}{\rho_0}\frac{\partial\theta}{\partial t}+\operatorname{div}\mathbf{q}'_m=0, \tag{7}$$

$$\frac{1}{\rho_0}\operatorname{grad}p+\mathbf{k}\left(\frac{1}{\rho_0}g+\frac{1}{k}\frac{d\nu}{d\rho}W_m\right)\theta+\frac{1}{k}\nu\mathbf{q}'_m=0, \tag{8}$$

$$E\frac{\partial\theta}{\partial t}+W_m\frac{\partial\theta}{\partial Z}+\frac{\partial\rho}{dZ}w_m=\kappa\nabla^2\theta, \tag{9}$$

where $\mathbf{k}$ is the unit vector in the upward ($Z$-) direction, and $w_m$ is the $Z$-component of $\mathbf{q}'_m$. In these equations, the quantity $d\nu/d\rho$ is assumed known from the properties of the given liquid, while $d\rho/dZ$ is given by (6). The pressure perturbation $p$ and the horizontal components of $\mathbf{q}'_m$ can be eliminated by taking the divergence of (8), using (7), to give

$$\operatorname{div}(\nu\operatorname{grad}w_m)+\frac{\epsilon}{\rho_0}\frac{\partial}{\partial Z}\left(\nu\frac{\partial\theta}{\partial t}\right)+\left(\frac{gk}{\rho_0}+\frac{d\nu}{d\rho}W_m\right)\nabla_1^2\theta=0, \tag{10}$$

where $\nabla_1^2\equiv\nabla^2-\partial^2/\partial Z^2$. When $w_m$ has been eliminated between (10) and (9), one obtains the linearized equation obeyed by the small density perturbation $\theta$

$$\operatorname{div}\left[\nu\operatorname{grad}\left\{\left(\frac{d\rho}{dZ}\right)^{-1}\left(\kappa\nabla^2\theta-W_m\frac{\partial\theta}{\partial Z}-E\frac{\partial\theta}{\partial t}\right)\right\}\right]+\frac{\epsilon}{\rho_0}\frac{\partial}{\partial Z}\left(\nu\frac{\partial\theta}{\partial t}\right)+\left(\frac{gk}{\rho_0}+W_m\frac{d\nu}{d\rho}\right)\nabla_1^2\theta=0. \tag{11}$$

The boundary conditions upon $\theta$ are as follows. At $Z=0$, $\theta=0$ and, using equations (2) and (3), one finds that the boundary condition $p=0$ is equivalent to $\partial w_m/\partial Z=0$ (Lapwood 1948). In terms of $\theta$,

$$\frac{\partial}{\partial Z}\left\{\left(\frac{d\rho}{dZ}\right)^{-1}\left(\kappa\nabla^2\theta-W_m\frac{\partial\theta}{\partial Z}-E\frac{\partial\theta}{\partial t}\right)\right\}=0$$

on $Z=0$. When $Z\to-\infty$, it is necessary that $\theta$ and the derivatives of $\theta$ should tend to zero more rapidly than $\exp(W_mZ/\kappa)$.

It will be convenient to define the natural length unit of the system by the boundary-layer thickness $\kappa/W_m$, taking a new dimensionless variable $z=W_mZ/\kappa$. The same scale unit will be used to define dimensionless variables in the horizontal co-ordinates. Also, let $\sigma=\nu/\nu_0$, where $\nu_0$ is the kinematic viscosity of the liquid when $\rho=\rho_0$.

From the form of the perturbation equation (11), it appears that separable solutions for the density disturbance possess the well-known cellular form of Rayleigh instability (Pellew & Southwell 1940). Let

$$\theta=F(z)\Phi_1e^{\omega t}, \tag{12}$$

where $\Phi_1$ is a solution of the equation $(\nabla_1^2 + a^2)\Phi_1 = 0$ such that the normal gradient of $\Phi_1$ vanishes on a vertical cell boundary. The wave-number $a$ is characteristic of the variations of $\theta$ in the horizontal plane, and is dimensionless since the length $\kappa/W_m$ has been taken as the unit in the horizontal co-ordinates. The operator $\nabla_1^2$ is expressed in terms of these non-dimensional variables.

The eigenvalue equation governing $F(z)$ follows when (12) is substituted into (11). There results

$$\{D(\sigma D) - a^2\sigma\} e^{-z}(D^2 - D - a^2 - E\Omega) F + \Delta_\rho \Omega D(\sigma F) = a^2 \lambda F, \tag{13}$$

where $$D \equiv d/dz, \quad \Delta_\rho = \epsilon(\rho_1 - \rho_0)/\rho_0, \quad \Omega = \kappa\omega/W_m^2,$$

and $$\lambda = \frac{\rho_1 - \rho_0}{\nu_0 W_m}\left(\frac{gk}{\rho_0} + W_m \frac{d\nu}{d\rho}\right).$$

In the derivation leading to equation (13), it has been assumed that the isotropic thermal diffusivity $\kappa$ is a constant, independent of temperature. Further assumptions are necesary in order to simplify the eigenvalue problem represented by (13) together with the boundary conditions upon $\theta$. Suppose that the total density difference $\rho_1 - \rho_0$ is small compared with $\rho_0$, so that the ratio $\Delta_\rho/E$ is small. In (13), if the term involving $\Delta_\rho$ is neglected, the approximation is equivalent to discarding the first term in the equation of continuity (7). Also, replacing $E$ by the constant $E_0 = E(\rho_0)$ introduces an approximation of the same order. A further consequence of the assumption that $(\rho_1 - \rho_0)/\rho_0$ is small compared with unity is that the quantity $d\nu/d\rho$ can be taken constant, equal to $(d\nu/d\rho)_0$ say, which is the value when $\rho = \rho_0$. Then $\lambda$ is a constant, and will be defined as the Rayleigh number for the system.

If $\nu$ is replaced by $\mu/\rho$ in the expression for $\lambda$, there results

$$\lambda = \frac{\rho_1 - \rho_0}{\mu_0 W_m}\left\{gk + W_m\left(\frac{d\mu}{d\rho}\right)_0 - W_m \frac{\mu_0}{\rho_0}\right\}, \tag{14}$$

where $\mu_0$ is the dynamic viscosity when $\rho = \rho_0$.

Evidently, three physical phenomena affect the stability of the system. The first is gravitational instability of the well-known Rayleigh type. The second effect was noted by Saffman & Taylor (1958) in connexion with the instability of an interface between two immiscible liquids, moving normal to itself through a porous medium. These authors showed that, when the forcing liquid has the lower viscosity, there is a tendency for instability to appear at the interface. In the corresponding case here, the sign of the second term in the last line of (14) is positive (tending to produce instability) whenever the viscosity increases in the direction of the primary flow. It is found that no analogue exists for the third term of (14) in the problem discussed by Saffman & Taylor. In the present problem the fluid is in motion with a constant rate of mass flow proportional to $W_m$. However, in the presence of a stationary gradient of density in the flow direction, the fluid must dilate or contract as it moves, and the magnitude of the volume flow rate $W$ is not a constant. Since the fluid experiences a non-uniform body force proportional to $-\mu W = -\mu W_m \rho_0/\rho$ which opposes the flow, the stability of the system is increased when the density increases in the flow direction.

Using the approximate form of equation (13), it is easy to show that small disturbances vary with time in an aperiodic manner. Suppose that $F$ and $\overline{F}$ are complex conjugate solutions of (13) which satisfy the given boundary conditions, with associated parameters $(\Omega, a, \lambda)$ and $(\overline{\Omega}, a, \lambda)$, respectively. (A method of Pellew & Southwell (1940) can be used to show that the wave-number $a$ is always real.) Then, from (13), it is found that

$$(\Omega - \overline{\Omega}) \int_{-\infty}^{0} e^{-z} |F|^2 dz = 0;$$

that is, the exponent $\Omega$ in the time factor is always real. A criterion for neutral stability can be specified by putting $\Omega = 0$ in (13), when the particular disturbance being considered becomes neutral everywhere. Although this result is approximate, it would appear that, in the exact criterion for neutral stability, $\Omega$ will differ from zero by $O(\Delta_\rho)$ at most, and the error in a calculated eigenfunction solution will be of the same order. The error in calculating a criterion for neutral stability will be $O(\Delta_\rho^2)$.

For later convenience, the functions

$$G = e^{-z}(D^2 - D - a^2) F \quad \text{and} \quad H = \{D(\sigma D) - a^2\sigma\} G \tag{15}$$

are introduced. In the neutral case, $G$ is proportional to the $z$-dependence of $w_m$, the perturbation to the vertical component of the disturbance motion, and $H$ is proportional to $F$. Then equations (15) and the approximate form of (13) give

$$(D^2 - D - a^2) H = a^2 \lambda e^z G, \quad (\Omega = 0). \tag{16}$$

## 3. Solution of the problem

*Series solution.* Consider the case of neutral stability, and neglect viscosity variations for the present except where these occur in the Rayleigh number (14). Then $\Omega = 0$ and $\sigma = 1$ in (13). An appropriate series solution is

$$\begin{aligned} F &= \sum_{n=0}^{\infty} \lambda^n (A_n \exp c_1 z + B_n \exp c_2 z)\, e^{nz} \\ &= A_0 F_1 + B_0 F_2 \text{ say}, \end{aligned} \tag{17}$$

in which $A_0$ and $B_0$ are the two constants which are arbitrary. The coefficients $A_{n+1}$ $(n \geqslant 0)$ are given by the recurrence relation

$$\frac{A_{n+1}}{A_n} = \frac{a^2}{\{(c_1+n)^2 - a^2\}\{(c_1+n)(c_1+n+1) - a^2\}},$$

where $c_1 = 1 + a$. For the relation giving $B_{n+1}/B_n$ $(n \geqslant 0)$, it is necessary to replace $c_1$ by $c_2 = \frac{1}{2} + (\frac{1}{4} + a^2)^{\frac{1}{2}}$.

When the boundary conditions $F = DG = 0$ at $z = 0$ are applied to (17), the constants $A_0$ and $B_0$ are found to be non-zero only if the characteristic equation

$$\Delta(z) \equiv \begin{vmatrix} F_1 & F_2 \\ DG_1 & DG_2 \end{vmatrix} = 0 \tag{18}$$

is satisfied at $z = 0$, where use is made of the notation of (15). The solution of (18) gives a relation connecting $\lambda$ and $a$. For a given value of $a$, there exists an infinity of distinct eigenvalues satisfying the problem, the lowest value of the set having the greatest physical significance.

A convenient method of solving (18) consists in forming the differential equation obeyed by $\Delta(z)$, solving the equation in series and then equating the appropriate series solution to zero for $z = 0$ (see for example, Nicholson (1917)). After $F_1$ and $F_2$ have been eliminated, it is found that $\Delta$ obeys the differential equation

$$(D-2)(D-1)\{D^2(D-1)^2-a^2(2D-1)^2\}\Delta+2a^2\lambda e^z(D+1)(2D-1)\Delta=0. \quad (19)$$

Only one of the six solutions of (19) is relevant to the present problem, and is of the form

$$\sum_{n=0}^{\infty} C_n \lambda^n e^{(k+n)z}.$$

The recurrence relation governing the coefficients can be written

$$\frac{C_{n+1}}{C_n} = \frac{-2a^2(k+1+n)(2k-1+2n)}{(1+n)(k-1+n)(k+n)(2k+n)(2k-2a+n)(2a+1+n)},$$

where $k = a+\frac{1}{2}+(\frac{1}{4}+a^2)^{\frac{1}{2}}$ (the appropriate solution of the indicial equation) is determined by comparing the exponent of the leading term in the $C_n$-series with the corresponding exponent in (18). Putting $z = 0$ in the chosen solution of (19), one obtains an expansion of the characteristic equation

$$\Delta = \sum_{n=0}^{\infty} C_n \lambda^n = C_0\left(1+\frac{C_1}{C_0}\lambda\left(1+\frac{C_2}{C_1}\lambda\left(1+\ldots.\right.\right.\right.$$
$$= 0, \quad (20)$$

where the constant $C_0$ is non-zero. If $a$ is given, (20) becomes an equation of infinite order in $\lambda$. Fortunately, the series converges rapidly for the lowest eigenvalue, and (20) may be solved by iteration.

| $a$ | $\lambda$ |
|---|---|
| 0·42669 | $6{\cdot}95400_1$ |
| 0·42723 | $6{\cdot}95396_3$ |
| 0·42850 | $6{\cdot}95394_8$ |
| 0·42971 | $6{\cdot}95396_3$ |
| 0·43032 | $6{\cdot}95403_5$ |

TABLE 1. Values of the lowest root $\lambda$ for values of $a$ near the point of maximum instability.

Table 1 gives the values of the lowest root of equation (20) for five different values of $a$, using the first five terms of the series. When $a = 0{\cdot}4285$, $\lambda$ passes through a minimum value of 6·9539—the critical point for neutral stability.

The forms of the functions $F$ and $G$ for a neutral disturbance, calculated from equations (17) and (15), are shown in figure 1 (*b*) and (*c*). A significant feature of these functions is that the velocity disturbance penetrates farther into the porous medium than does the density disturbance.

### *Solution by Chandrasekhar's method*

A calculation of the form of the neutral curve for the lowest eigenvalue will now be given, using the well-known approximate method of Chandrasekhar (1954).

The relevant differential equations are given by (16) and the second equation in (15). These reduce to a suitable form after the transformations

$$K = e^{-\frac{1}{2}z} H \quad \text{and} \quad \zeta = -cz \quad (c = (4a^2+1)^{\frac{1}{2}})$$

have been carried out. Then

$$(D^2 - \tfrac{1}{4}) K = b^2 \lambda e^{-\zeta/2c} G \tag{21}$$

and

$$\{D(\sigma D) - b^2 \sigma\} G = \frac{1}{c^2} e^{-\zeta/2c} K, \tag{22}$$

where $D \equiv d/d\zeta$ in this case and $b = a/c$.

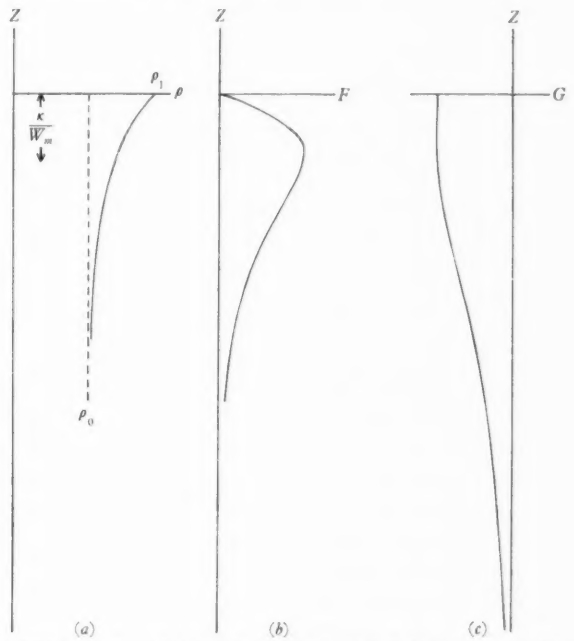


FIGURE 1. Instability of a liquid rising through a semi-infinite porous medium. (*a*) Primary density distribution; (*b*) dependence upon $Z$ of the density perturbation at neutral stability; (*c*) dependence upon $Z$ of the perturbation to the vertical mass flow at neutral stability.

In the right-hand side of (22), one can substitute for $K$ the expansion in orthogonal functions

$$K(\zeta) = \zeta e^{-\frac{1}{2}\zeta} \sum_{n=0}^{\infty} A_n L_n^1(\zeta), \tag{23}$$

where the $A_n$ are constants and the

$$L_n^1(\zeta) \equiv \frac{e^{\zeta}}{n!\,\zeta} D^n(\zeta^{n+1} e^{-\zeta})$$

are Laguerre polynomials (Morse & Feshbach 1953, p. 784). The set of Laguerre polynomials $L_n^1(\zeta)$ ($n = 0, 1, 2, \ldots$) is complete, and the expansion (23) satisfies the boundary conditions $K = 0$ at $\zeta = 0$ and $K \to 0$ exponentially as $\zeta \to +\infty$.

Assuming for the present that $\sigma = 1$ in (22), one solves the equation for $G$, subject to the boundary conditions $DG = 0$ at $\zeta = 0$ and $G \to 0$ exponentially as $\zeta \to +\infty$. This solution and the expansion (23) for $K$ are substituted into (21). Now, if (21) is multiplied through by $\zeta e^{-\frac{1}{2}\zeta} L_m^1(\zeta)$ $(m = 0, 1, 2, \dots)$ and integrated with respect to $\zeta$ over the range $(0, \infty)$, an infinite set of equations results

$$\sum_{n=0}^{\infty} A_n \left\{ I_{mn} - \frac{2c^3}{a\lambda} \delta_{mn}(n+1)^2 \right\} = 0 \quad (m = 0, 1, 2, \dots), \tag{24}$$

where $\delta_{mn}$ is the Kronecker delta, and

$$I_{mn} = \{I_1(Q, P) + I_1(Q, Q) + I_2(Q, P) - I_2(P, Q)\}_{mn},$$

in which

$$(I_1)_{mn}(P, Q) = (m+1)(n+1) \frac{(P-1)^m (Q-1)^n}{P^{m+2} Q^{n+2}}$$

and

$$(I_2)_{mn}(P, Q) = \frac{m+1}{n!} \left[ \frac{d^{n+1}}{du^{n+1}} \frac{(P+Q-u-1)^m (u-1)^n}{(P+Q-u)^{m+2} (u-Q)} \right]_{u=0}.$$

Here $P = (c+1-2a)/2c$ and $Q = (c+1+2a)/2c$, with $c$ defined as before. In the particular case $m = n = 0$, it is found that

$$I_{00} = \frac{1}{Q} \left\{ \frac{1}{Q^3} + \frac{2}{(P+Q)^3} \left( \frac{P}{Q} + 3 \right) \right\}. \tag{25}$$

The characteristic equation obtained from (24) by eliminating the constants $A_n$ must be an infinite determinant. However, satisfactory accuracy can be obtained in the calculation of the lowest eigenvalue $\lambda$ by equating the leading term to zero. The full-line curve of figure 2 has been calculated in this way. The curve is qualitatively similar to a neutral curve of Rayleigh instability in a porous medium, although the minimum occurs at a lower value of $\lambda$ and a lower value of $a$ than would be found for horizontal planes spaced a distance $\kappa/W_m$ apart. When $a = 0{\cdot}4285$, this approximate method gives $\lambda = 6{\cdot}9735$—a result less than $0{\cdot}3\,\%$ higher than the 'exact' value (cf. table 1).

At first, the appearance of a minimum at a finite value of $a$ in the neutral curve for this stability problem would seem to be surprising. By contrast, when a horizontal layer of saturated porous material separates two static liquids which differ in density, it can be shown that the critical Rayleigh number decreases to a minimum value only when the horizontal wave-number of the disturbance tends to zero. A brief heuristic explanation follows. As $z \to -\infty$, a density disturbance of small wave-number $a$ tends to zero approximately as $e^z$, i.e. the disturbance is confined to a boundary layer of constant thickness ($\kappa/W_m$ in dimensional units) in which vertical diffusion effects are important and are independent of $a$. However, the fluid motion associated with the disturbance tends to zero as $e^{az}$, so that, since a roughly similar flow pattern exists for differing small values of $a$, the path length must vary as $1/a$. Consequently, the rate of growth of such a disturbance will be proportional to $a$. It follows that the critical Rayleigh number must tend to infinity as $1/a$ when $a \to 0$, and this is what is actually found.

It is of interest to note that a similar argument, leading to the conclusion that the flow-path length varies as $1/a$, indicates the reason for the linear dependence of $\omega$ upon $a$ found by Saffman & Taylor (1958). Here $\omega$ is the rate of growth of a disturbance (of wave-number $a$) to the interface between two immiscible fluids in a porous medium.

At large values of $a$, the curve of neutral stability in figure 2 becomes parabolic. This occurs because the disturbance is concentrated near the surface of the medium in a region where the density gradient is approximately constant, and

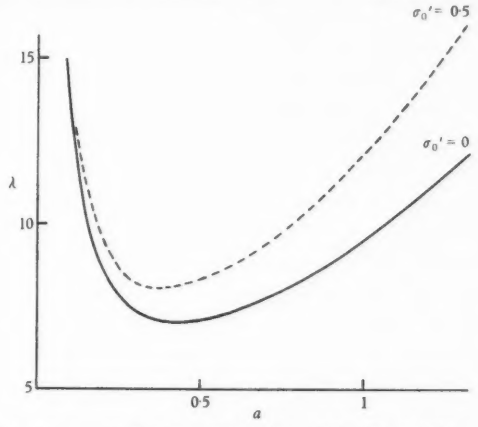


FIGURE 2. Approximate curves showing the value of the Rayleigh number $\lambda$ for neutral stability plotted as a function of the dimensionless wave-number $a$. The kinematic viscosity has the functional form $\nu = \nu_0(1+\sigma_0' e^z)$, where $\sigma_0'$ is assumed constant.

the horizontal dimensions of a typical convection cell are very small compared with the vertical height. Under these conditions, the tendency of the disturbance to grow under the action of vertical forces is independent of the wave-number $a$, but damping takes place by transverse diffusion, which is proportional to $a^2$. Similar considerations apply to the motion of a long convection cell in a vertical tube filled with porous material (Wooding 1959).

An extension of the present method has been used to estimate the effects of variations in kinematic viscosity $\nu$ which have been neglected in the two previous solutions. For example, if $\nu$ is proportional to $\rho$, one has $\sigma = 1+\sigma_0' e^z$, where $\sigma_0' = \nu_0^{-1}(d\nu/d\rho)_0(\rho_1-\rho_0)$. It is then necessary to solve equation (22) approximately. When $\sigma_0' = 0{\cdot}5$ (a positive value, for which the viscosity increases upwards), the curve of neutral stability is modified approximately as shown by the broken-line curve in figure 2. There is an increase in stability, especially at the higher wave-numbers. An increase in the critical value of the Rayleigh number is found, and the corresponding value of the wave-number is decreased. These effects arise because the fluid motion due to a disturbance of high wave-number is restricted to a layer close to the surface of the medium, where $\nu \approx \nu_0(1+\sigma_0')$, whereas the fluid flow due to a disturbance of low wave-number penetrates more deeply into the medium, where $\nu \approx \nu_0$.

The author is indebted to Dr P. G. Saffman for valuable discussions, and to a referee for helpful criticism. The work described in this paper was carried out at the Cavendish Laboratory during the tenure of a National Research Fellowship awarded by the New Zealand Department of Scientific and Industrial Research.

## REFERENCES

CHANDRASEKHAR, S. 1954 *Mathematika*, **1**, 5.

LAPWOOD, E. R. 1948 *Proc. Camb. Phil. Soc.* **44**, 508.

MORSE, P. M. & FESHBACH, H. 1953 *Methods of Theoretical Physics*. New York: McGraw-Hill.

NICHOLSON, J. W. 1917 *Proc. Roy. Soc.* A, **93**, 506.

PELLEW, A. & SOUTHWELL, R. V. 1940 *Proc. Roy. Soc.* A, **176**, 312.

SAFFMAN, P. G. & TAYLOR, Sir GEOFFREY 1958 *Proc. Roy. Soc.* A, **245**, 312.

WOODING, R. A. 1959 *Proc. Roy. Soc.* A, **252**, 120.

# On the dynamics of unsteady gravity waves of finite amplitude

## Part 1. The elementary interactions

By O. M. PHILLIPS

Mechanics Department, The Johns Hopkins University, Baltimore, Maryland

(Received 12 March 1960)

This paper is concerned with the non-linear interactions between pairs of intersecting gravity wave trains of arbitrary wavelength and direction on the surface of water whose depth is large compared with any of the wavelengths involved. An equation is set up to describe the time history of the Fourier components of the surface displacement in which are retained terms whose magnitude is of order (slope)$^2$ relative to the linear (first-order) terms. The second-order terms give rise to Fourier components with wave-numbers and frequencies formed by the sums and differences of those of the primary components, and the amplitudes of these secondary components is always bounded in time and small in magnitude. The phase velocity of the secondary components is always different from the phase velocity of a free infinitesimal wave of the same wave-number. However, the third-order terms can give rise to tertiary components whose phase velocity is equal to the phase velocity of a free infinitesimal wave of the same wave-number, and when this condition is satisfied the amplitude of the tertiary component grows linearly with time in a resonant manner, and there is a continuing flux of potential energy from one wave-number to another. The time scale of the growth of the tertiary component is of order of the $(-2)$-power of the geometric mean of the primary wave slopes times the period of the tertiary wave. The Stokes permanent wave appears as a special case, in which the tertiary wave-number is the same as that of the primary, but its phase is advanced by $\frac{1}{2}\pi$. The energy transfer to the tertiary component in this case is usually interpreted as an increase in the phase velocity of the wave.

The dynamical interactions in water of finite depth are considered briefly, and it is shown that the amplitude of the secondary components becomes large (though bounded in time) as the water depth becomes smaller than the wavelength of the longest primary wave.

## 1. Introduction

In this paper, a start is made towards developing a theory to describe the dynamics of the non-linear interactions of a random field of gravity waves of finite amplitude, such as is generated by wind blowing over the sea. In the initial stages of the development of an ocean wave system under the influence of wind,

it is probable that the resonance theory (Phillips 1957, 1958*b*) provides the dominant mechanism whereby energy is transferred from the wind to the waves. As the waves develop, however, some 'sheltering' mechanism such as that described by Miles (1957, 1959) for infinitesimal waves, becomes increasingly effective. Also there is the certainty that sooner or later the wave amplitudes will be such that non-linear interactions among the wave components begin to modify the rate of growth of a particular Fourier component by interchange of energy from one component to another. We have, at present, no indication whether this will occur before, or after, the sheltering effect has become dominant nor of the interplay between these two mechanisms. Ultimately, however, if the wind duration is sufficiently great, it appears that a saturation value of the spectral amplitude may be attained (Phillips 1958*a*) beyond which any further development results in an instability of the sea surface and a loss of energy from the wave system by the formation of 'white-caps' or 'white horses'.

It is clear that in order to evaluate the relative roles of the various mechanisms during the generation, a statistical theory of the non-linear interactions will have to be set up. But a number of difficulties present themselves. The most feasible method of approach seems to be in terms of a series development rather analogous to the classical finite amplitude approximations (see Lamb 1932, for example). If we form, say, the covariance of the surface elevation, it might be anticipated that our dynamical equation will contain terms involving third, fourth, and all higher order covariances of the surface displacement, and in fact the dynamical equation for the covariance of any order involves all higher orders. (This is reminiscent of the theory of turbulence—see, for example, Batchelor (1953)—but there the equation for the covariance of order $n$ involves only the order $n+1$ in addition.) It seems evident that, in order to make progress, some approximation must be made, either in truncation of the sequences or on the probability distribution of the surface displacement, one possibility being the joint normal distribution hypothesis which enables the fourth covariances to be related to the second. But until we know something of the essential properties of the interaction process, it is difficult to make an intelligent approximation which will retain these properties in our statistical theory.

The purpose of the present paper is therefore to examine in some detail the 'elementary' dynamical interactions between pairs and among triads of wave components with different wavelengths and directions in order to discover the conditions under which a significant and continuing energy transfer can take place. In the following pages are developed a set of series expansions leading to a dynamical equation involving $dB(\mathbf{k}, t)$, the Fourier–Stieltjes transform of the surface displacement, which is the most accessible experimental observable. We have chosen to use the Fourier–Stieltjes component $dB(\mathbf{k})$ rather than the Fourier coefficient $B(\mathbf{k})$ (which would be slightly more convenient for these elementary interactions) in order that the basic equations be directly applicable to the case of a random sea. Terms are retained to the third order, and we investigate in turn the secondary wave components arising from the second-order interactions of two primary waves and the tertiary wave components from the third-order interactions of either a primary wave with a secondary wave or of

three primary waves. We seek the particular types of interaction that are capable of providing a continuing transfer of energy from one component of the wave field to another, so that the latter grows at the expense of the former. With this information there is the possibility of making a meaningful approximation to the statistical problem, fully cognizant of the aspects of the interactions that we neglect and those that we retain.

## 2. Specification of the motion

Let us suppose that the surface displacement $\xi(\mathbf{x}, t)$ is a stationary random function or a periodic function of position $\mathbf{x} = (x, y)$, but not necessarily of time, so that we can use the Fourier–Stieltjes representation

$$\xi(\mathbf{x}, t) = \int_{\mathbf{k}} dB(\mathbf{k}, t)\, e^{i\mathbf{k}\cdot\mathbf{x}}, \tag{2.1}$$

where the integration is over the entire wave-number plane. If $\xi(\mathbf{x}, t)$ is periodic in space, $dB(\mathbf{k}, t)$ degenerates (see Lighthill 1958) to a grid or row of Dirac delta functions multiplied by the element of area in the $\mathbf{k}$-plane. We assume that the water motion is irrotational so that the velocity potential† $\phi(\mathbf{x}, 0, t)$ at the horizontal plane $z = 0$ of the equilibrium free surface is likewise a stationary random (or periodic) function of $\mathbf{x}$. The Fourier–Stieltjes transform $dA(\mathbf{k}, t)$ is given by

$$\phi(\mathbf{x}, 0, t) = \int_{\mathbf{k}} dA(\mathbf{k}, t)\, e^{i\mathbf{k}\cdot\mathbf{x}}. \tag{2.2}$$

Our primary concern is with the case of deep water, so that we seek the solution of

$$\nabla^2\phi(\mathbf{x}, z) = 0, \tag{2.3}$$

with the boundary condition (2.2) at $z = 0$ and

$$\phi \to 0 \quad \text{as} \quad z \to \infty. \tag{2.4}$$

This solution is given by

$$\phi(\mathbf{x}, z, t) = \int dA(\mathbf{k}, t)\, e^{-kz} e^{i\mathbf{k}\cdot\mathbf{x}}, \tag{2.5}$$

where $k = |\mathbf{k}|$ and $z$ is taken vertically downwards.

The immediate problem is to develop a dynamical equation describing the time history of $dB(\mathbf{k}, t)$ from (2.5) and the kinematic and dynamic boundary conditions on the free surface $z = -\xi$.

The Fourier–Stieltjes transform $dB(\mathbf{k}, t)$ is intimately related to the distribution of potential energy per unit area among the components of the wave field. The mean potential energy per unit projected surface area is (Lamb 1932, p. 428)

$$\begin{aligned} V &= \tfrac{1}{2}\rho g\overline{\xi^2} \\ &= \tfrac{1}{2}\rho g \int \Psi(\mathbf{k})\, d\mathbf{k}, \end{aligned} \tag{2.6}$$

† Or its analytic continuation at points $\mathbf{x}$ where the free surface is below $z = 0$.

where the potential energy spectrum $\Psi(\mathbf{k})$ is given from (2.1) by

$$\Psi(\mathbf{k}) = \frac{\overline{dB(\mathbf{k})\,dB^*(\mathbf{k})}}{dk_1\,dk_2}, \tag{2.7}$$

the star denoting a complex conjugate. Non-linear interactions among the components $dB(\mathbf{k})$ can therefore be interpreted in terms of transfer of potential energy from one wave-number to another. The total energy of the motion is, of course, made up of potential and kinetic energy (in equal parts for infinitesimal waves), and there is continuous interchange between the two, but for finite amplitude waves the definition of a meaningful kinetic energy spectrum presents some difficulties. This matter will be taken up in Part II of this paper, since it will not be involved in our present considerations.

## 3. The equation of motion

(1) *The kinematic boundary condition*

At the surface $z = -\xi(\mathbf{x}, t)$,

$$\begin{aligned}\frac{D\xi}{Dt} &= \frac{\partial\xi}{\partial t} + (\nabla\phi)_{-\xi}.\nabla\xi \\ &= -(u_z)_{-\xi} = -(\partial\phi/\partial z)_{-\xi},\end{aligned} \tag{3.1}$$

where $\nabla$ represents the two-dimensional gradient operator $(\partial/\partial x, \partial/\partial y)$ and $u_z$ the downwards vertical velocity component. Thus

$$\frac{\partial\xi}{\partial t} = -\left(\frac{\partial\phi}{\partial z}\right)_{-\xi} - (\nabla\phi)_{-\xi}.\nabla\xi. \tag{3.2}$$

On replacing $\xi$ and $\phi$ by their Fourier–Stieltjes representations, we obtain

$$\begin{aligned}\int_{\mathbf{k}_0} dB'(\mathbf{k}_0, t)\exp(i\mathbf{k}_0.\mathbf{x}) &= \int_{\mathbf{k}_0} dA(\mathbf{k}_0, t)\exp(k_0\xi)\exp(i\mathbf{k}_0.\mathbf{x}) \\ &+ \int_{\mathbf{k}_0}\int_{\mathbf{k}_1} \mathbf{k}_0.\mathbf{k}_1\, dA(\mathbf{k}_0, t)\exp(k_0\xi)\,dB(\mathbf{k}_1, t)\exp[i(\mathbf{k}_0+\mathbf{k}_1).\mathbf{x}],\end{aligned}$$

where the prime denotes a time differentiation. Expanding the factors $\exp(k_0\xi)$ as power series and using (2.1) again, we obtain

$$\begin{aligned}&\int_{\mathbf{k}_0} dB'(\mathbf{k}_0, t)\exp(i\mathbf{k}_0.\mathbf{x}) \\ &= \int_{\mathbf{k}_0} k_0\, dA(\mathbf{k}_0, t)\exp(i\mathbf{k}_0.\mathbf{x}) \\ &\quad + \int_{\mathbf{k}_0}\sum_{n=1}^{\infty}(n!)^{-1}\int_{\mathbf{k}_1}\cdots\int_{\mathbf{k}_n} k_0^{n+1}\,dA(\mathbf{k}_0)\,dB(\mathbf{k}_1)\ldots dB(\mathbf{k}_n) \\ &\qquad\qquad \times\exp[i(\mathbf{k}_0+\mathbf{k}_1+\ldots+\mathbf{k}_n).\mathbf{x}] \\ &\quad + \int_{\mathbf{k}_0}\sum_{n=1}^{\infty}[(n-1)!]^{-1}\int_{\mathbf{k}_1}\cdots\int_{\mathbf{k}_n} \mathbf{k}_0.\mathbf{k}_1\,k_0^{n-1}\,dA(\mathbf{k}_0)\,dB(\mathbf{k}_1)\ldots dB(\mathbf{k}_n) \\ &\qquad\qquad \times\exp[i(\mathbf{k}_0+\mathbf{k}_1+\ldots+\mathbf{k}_n).\mathbf{x}].\end{aligned} \tag{3.3}$$

In the $n$th term of each of the summations make the change of variable

$$\left.\begin{aligned} \mathbf{k} &= \mathbf{k}_0+\mathbf{k}_1+\ldots+\mathbf{k}_n, \\ \mathbf{k}_1 &= \mathbf{k}_1, \\ &\cdots\cdots\cdots\cdots\cdots\cdots \\ \mathbf{k}_n &= \mathbf{k}_n, \end{aligned}\right\} \tag{3.4}$$

and replace $\mathbf{k}_0$ by $\mathbf{k}$ in the single integrals, and it follows that

$$\begin{aligned} dB'(\mathbf{k},t) = k\,dA(\mathbf{k},t) + \sum_{n=1}^{\infty} \int_{\mathbf{k}_1} \ldots \int_{\mathbf{k}_n} \frac{1}{(n-1)!} |\mathbf{k}-\mathbf{k}_1-\ldots-\mathbf{k}_n|^{n-1} \\ \times \left\{ \frac{1}{n} |\mathbf{k}-\mathbf{k}_1-\ldots-\mathbf{k}_n|^2 + \mathbf{k}_1.(\mathbf{k}-\mathbf{k}_1-\ldots-\mathbf{k}_n) \right\} \\ \times dA(\mathbf{k}-\mathbf{k}_1-\ldots-\mathbf{k}_n)\,dB(\mathbf{k}_1)\ldots dB(\mathbf{k}_n), \end{aligned} \tag{3.5}$$

where we assume that the series converges sufficiently rapidly that under at least some conditions (to be specified more precisely later) the first few terms suffice for a good approximation.

The equation (3.5) is the direct Fourier–Stieltjes representation of the kinematic boundary condition (3.2). It will be convenient to express $dA(\mathbf{k},t)$, the Fourier–Stieltjes transform of $\phi(\mathbf{x},0,t)$ in terms of $dB(\mathbf{k},t)$ and its time derivatives. From the first few terms of (3.5),

$$\begin{aligned} k\,dA(\mathbf{k}) = dB'(\mathbf{k}) - \int_{\mathbf{k}_1} \{|\mathbf{k}-\mathbf{k}_1|^2 + \mathbf{k}_1.(\mathbf{k}-\mathbf{k}_1)\}\,dA(\mathbf{k}-\mathbf{k}_1)\,dB(\mathbf{k}_1) \\ - \int_{\mathbf{k}_1}\int_{\mathbf{k}_2} |\mathbf{k}-\mathbf{k}_1-\mathbf{k}_2| \{\tfrac{1}{2}|\mathbf{k}-\mathbf{k}_1-\mathbf{k}_2|^2 + \mathbf{k}_1.(\mathbf{k}-\mathbf{k}_1-\mathbf{k}_2)\} \\ \times dA(\mathbf{k}-\mathbf{k}_1-\mathbf{k}_2)\,dB(\mathbf{k}_1)\,dB(\mathbf{k}_2), \end{aligned}$$

and by successive substitutions for $dA(\mathbf{k}-\mathbf{k}_1)$ and $dA(\mathbf{k}-\mathbf{k}_1-\mathbf{k}_2)$ on the right-hand side, we find that, correct to third-order terms,

$$\begin{aligned} dA(\mathbf{k}) = k^{-1}dB'(\mathbf{k}) - \int_{\mathbf{k}_1} D_1(\mathbf{k},\mathbf{k}_1)\,dB'(\mathbf{k}-\mathbf{k}_1)\,dB(\mathbf{k}_1) \\ - k^{-1}\int_{\mathbf{k}_1}\int_{\mathbf{k}_2} D_2(\mathbf{k},\mathbf{k}_1,\mathbf{k}_2)\,dB'(\mathbf{k}-\mathbf{k}_1-\mathbf{k}_2)\,dB(\mathbf{k}_1)\,dB(\mathbf{k}_2), \end{aligned} \tag{3.6}$$

where

$$\left.\begin{aligned} D_1(\mathbf{k},\mathbf{k}_1) &= \frac{\mathbf{k}.(\mathbf{k}-\mathbf{k}_1)}{\mathbf{k}\,|\mathbf{k}-\mathbf{k}_1|}, \\ D_2(\mathbf{k},\mathbf{k}_1,\mathbf{k}_2) &= \tfrac{1}{2}|\mathbf{k}-\mathbf{k}_1-\mathbf{k}_2|^2 + \mathbf{k}_1.(\mathbf{k}-\mathbf{k}_1-\mathbf{k}_2) \\ &\qquad - \frac{\mathbf{k}.(\mathbf{k}-\mathbf{k}_1)\,(\mathbf{k}-\mathbf{k}_1).(\mathbf{k}-\mathbf{k}_1-\mathbf{k}_2)}{|\mathbf{k}-\mathbf{k}_1|\,|\mathbf{k}-\mathbf{k}_1-\mathbf{k}_2|}. \end{aligned}\right\} \tag{3.7}$$

(ii) *The dynamical boundary condition*

Provided we restrict our attention to wave-numbers less than about $2\,\mathrm{cm}^{-1}$ for which surface tension effects in an air-water system are unimportant, the pressure at the free surface $z=-\xi(\mathbf{x},t)$ is continuous, so that

$$-\frac{p}{\rho} = \left(\frac{\partial\phi}{\partial t}\right)_{-\xi} + \tfrac{1}{2}(\mathbf{u}^2)_{-\xi} + g\xi, \tag{3.8}$$

where $p$ represents the pressure on the surface resulting from the air motion, $\rho$ the water density and $g$ the gravitational acceleration. The Fourier–Stieltjes transform of $p(\mathbf{x}, t)$ can be defined by

$$p(\mathbf{x}, t) = \int d\varpi(\mathbf{k}, t)\, e^{i\mathbf{k}.\mathbf{x}}, \tag{3.9}$$

while the corresponding transform of $\xi(\mathbf{x}, t)$ is $dB(\mathbf{k}, t)$. It remains to develop expansions, correct to third order, of the other two terms of (3.8).

Let

$$\left(\frac{\partial \phi}{\partial t}\right)_{-\xi} = \int dC(\mathbf{k}, t)\, e^{i\mathbf{k}.\mathbf{x}}, \quad \text{say,}$$

$$= \int dA'(\mathbf{k}, t)\, e^{k\xi}\, e^{i\mathbf{k}.\mathbf{x}}, \tag{3.10}$$

from (2.5).† The exponential term in (3.10) is expanded, on the supposition that $k\xi$ is small (in mean square), and after changing the variables of integration as in (3.4), we find that

$$dC(\mathbf{k}, t) = dA'(\mathbf{k}, t) + \int_{\mathbf{k}_1} |\mathbf{k} - \mathbf{k}_1|\, dA'(\mathbf{k} - \mathbf{k}_1)\, dB(\mathbf{k}_1)$$
$$+ \frac{1}{2} \int_{\mathbf{k}_1} \int_{\mathbf{k}_2} |\mathbf{k} - \mathbf{k}_1 - \mathbf{k}_2|^2\, dA'(\mathbf{k} - \mathbf{k}_1 - \mathbf{k}_2)\, dB(\mathbf{k}_1)\, dB(\mathbf{k}_2), \tag{3.11}$$

correct to the third order The expression (3.6) can now be used to eliminate $dA(\mathbf{k})$ from the right-hand side, which becomes, to this order,

$$dC(\mathbf{k}, t) = k^{-1}\, dB''(\mathbf{k}, t) + \int_{\mathbf{k}_1} \{1 - D_1(\mathbf{k}, \mathbf{k}_1)\}\, dB''(\mathbf{k} - \mathbf{k}_1)\, dB(\mathbf{k}_1)$$
$$- \int_{\mathbf{k}_1} D_1(\mathbf{k}, \mathbf{k}_1)\, dB'(\mathbf{k} - \mathbf{k}_1)\, dB'(\mathbf{k}_1)$$
$$- \int_{\mathbf{k}_1} \int_{\mathbf{k}_2} E(\mathbf{k}, \mathbf{k}_1, \mathbf{k}_2)\, dB''(\mathbf{k} - \mathbf{k}_1 - \mathbf{k}_2)\, dB(\mathbf{k}_1)\, dB(\mathbf{k}_2)$$
$$- \int_{\mathbf{k}_1} \int_{\mathbf{k}_2} F(\mathbf{k}, \mathbf{k}_1, \mathbf{k}_2)\, dB'(\mathbf{k} - \mathbf{k}_1 - \mathbf{k}_2)\, dB'(\mathbf{k}_1)\, dB(\mathbf{k}_2), \tag{3.12}$$

where

$$\left.\begin{aligned} E(\mathbf{k}, \mathbf{k}_1, \mathbf{k}_2) &= k^{-1} D_2(\mathbf{k}, \mathbf{k}_1, \mathbf{k}_2) + |\mathbf{k} - \mathbf{k}_1|\, D_1(\mathbf{k} - \mathbf{k}_1, \mathbf{k}_2) - \tfrac{1}{2} |\mathbf{k} - \mathbf{k}_1 - \mathbf{k}_2|, \\ F(\mathbf{k}, \mathbf{k}_1, \mathbf{k}_2) &= k^{-1} [D_2(\mathbf{k}, \mathbf{k}_1, \mathbf{k}_2) + D_2(\mathbf{k}, \mathbf{k}_2, \mathbf{k}_1)] + |\mathbf{k} - \mathbf{k}_2|\, D_1(\mathbf{k} - \mathbf{k}_2, \mathbf{k}_1), \end{aligned}\right\} \tag{3.13}$$

and the functions $D_1$ and $D_2$ are as given previously in (3.7).

Finally, the horizontal velocity components at the surface are given by

$$(u_x, u_y) = \nabla \phi = i \int \mathbf{k}\, dA(\mathbf{k}, t)\, e^{k\xi}\, e^{i\mathbf{k}.\mathbf{x}}, \tag{3.14}$$

where $\nabla = (\partial/\partial x_1, \partial/\partial x_2)$, and the vertical velocity component by

$$u_z = \frac{\partial \phi}{\partial z} = \int k\, dA(\mathbf{k}, t)\, e^{k\xi}\, e^{i\mathbf{k}.\mathbf{x}}, \tag{3.15}$$

† Note that $\left(\dfrac{\partial \phi}{\partial t}\right)_{-\xi} \neq \dfrac{\partial}{\partial t} (\phi)_{-\xi}$ since $\xi = \xi(\mathbf{x}, t)$.

so that

$$\mathbf{u}^2 = \int_{\mathbf{k}_0}\int_{\mathbf{k}_1} [k_0 k_1 - \mathbf{k}_0.\mathbf{k}_1]\, dA(\mathbf{k}_0)\, dA(\mathbf{k}_1) \exp[(k_0+k_1)\xi] \exp[i(\mathbf{k}_0+\mathbf{k}_1).\mathbf{x}]. \tag{3.16}$$

The reduction of this expression to a series of terms involving integrations over $dB(\mathbf{k},t)$ and its time derivatives proceeds along the same lines as before. The three steps are (*a*) expansion of the factor $\exp[(k_0+k_1)\xi]$ (here two terms suffice to given an expression correct to third order), (*b*) a change of the integration variables to the set (3.4), and (*c*) elimination of $dA(\mathbf{k},t)$ from the integrals by using (3.6). The reader who follows the calculation through in detail will notice that he obtains two third-order terms involving integrals over

$$dB'(\mathbf{k}-\mathbf{k}_1)\, dB'(\mathbf{k}_1-\mathbf{k}_2)\, dB(\mathbf{k}_2)$$

and

$$dB'(\mathbf{k}-\mathbf{k}_1-\mathbf{k}_2)\, dB'(\mathbf{k}_1)\, dB(\mathbf{k}_2).$$

The first form can be reduced to the second by an obvious further change of variable. The end result of this calculation is that the Fourier–Stieltjes transform of $(\mathbf{u}^2)_{-\xi}$ is found to be

$$\int_{\mathbf{k}_1} \left\{1 - \frac{\mathbf{k}_1.(\mathbf{k}-\mathbf{k}_1)}{k_1|\mathbf{k}-\mathbf{k}_1|}\right\} dB'(\mathbf{k}-\mathbf{k}_1)\, dB'(\mathbf{k}_1)$$

$$- \int_{\mathbf{k}_1}\int_{\mathbf{k}_2} G(\mathbf{k},\mathbf{k}_1,\mathbf{k}_2)\, dB'(\mathbf{k}-\mathbf{k}_1-\mathbf{k}_2)\, dB'(\mathbf{k}_1)\, dB(\mathbf{k}_2), \tag{3.17}$$

where

$$G(\mathbf{k},\mathbf{k}_1,\mathbf{k}_2) = |\mathbf{k}-\mathbf{k}_1| \left\{1 - \frac{\mathbf{k}_1.(\mathbf{k}-\mathbf{k}_1)}{k_1|\mathbf{k}-\mathbf{k}_1|}\right\} D_1(\mathbf{k}-\mathbf{k}_1,\mathbf{k}_2)$$

$$+ |\mathbf{k}_1+\mathbf{k}_2| \left\{1 - \frac{(\mathbf{k}_1+\mathbf{k}_2).(\mathbf{k}-\mathbf{k}_1-\mathbf{k}_2)}{|\mathbf{k}_1+\mathbf{k}_2|\,|\mathbf{k}-\mathbf{k}_1-\mathbf{k}_2|}\right\} D_1(\mathbf{k}_1+\mathbf{k}_2,\mathbf{k}_2)$$

$$- \{k_1 + |\mathbf{k}-\mathbf{k}_1-\mathbf{k}_2|\} \left\{1 - \frac{\mathbf{k}_1.(\mathbf{k}-\mathbf{k}_1-\mathbf{k}_2)}{k_1|\mathbf{k}-\mathbf{k}_1-\mathbf{k}_2|}\right\}. \tag{3.18}$$

The Fourier–Stieltjes transform of the dynamical boundary condition (3.8) can now be expressed in terms of $d\varpi(\mathbf{k},t)$ and of $dB(\mathbf{k},t)$ and its time derivatives. From (3.12) and (3.17), together with the supplementary conditions (3.13) and (3.18), it is found, after a little algebra that

$$-\rho^{-1} d\varpi(\mathbf{k}) = k^{-1} dB''(\mathbf{k}) + g\, dB(\mathbf{k})$$

$$+ \int_{\mathbf{k}_1} H_1(\mathbf{k},\mathbf{k}_1)\, dB''(\mathbf{k}-\mathbf{k}_1)\, dB(\mathbf{k}_1) + \int_{\mathbf{k}_1} H_2(\mathbf{k},\mathbf{k}_1)\, dB'(\mathbf{k}-\mathbf{k}_1)\, dB'(\mathbf{k}_1)$$

$$- \int_{\mathbf{k}_1}\int_{\mathbf{k}_2} H_3(\mathbf{k},\mathbf{k}_1,\mathbf{k}_2)\, dB''(\mathbf{k}-\mathbf{k}_1-\mathbf{k}_2)\, dB(\mathbf{k}_1)\, dB(\mathbf{k}_2)$$

$$- \int_{\mathbf{k}_1}\int_{\mathbf{k}_2} H_4(\mathbf{k},\mathbf{k}_1,\mathbf{k}_2)\, dB'(\mathbf{k}-\mathbf{k}_1-\mathbf{k}_2)\, dB'(\mathbf{k}_1)\, dB(\mathbf{k}_2), \tag{3.19}$$

where all the transform functions are understood to be functions of time $t$ also, and the primes represent differentiations with respect to $t$. The functions $H_1, \ldots, H_4$ are given by

$$\begin{aligned} H_1(\mathbf{k}, \mathbf{k}_1) &= 1 - \frac{\mathbf{k}.(\mathbf{k}-\mathbf{k}_1)}{k\,|\mathbf{k}-\mathbf{k}_1|} \\ &= 1 - \cos\theta \\ &= H_1(-\mathbf{k}, -\mathbf{k}_1); \end{aligned} \tag{3.20}$$

$$\begin{aligned} H_2(\mathbf{k}, \mathbf{k}_1) &= \frac{1}{2}\left\{1 - \frac{\mathbf{k}_1.(\mathbf{k}-\mathbf{k}_1)}{k_1\,|\mathbf{k}-\mathbf{k}_1|}\right\} - \frac{\mathbf{k}.(\mathbf{k}-\mathbf{k}_1)}{k\,|\mathbf{k}-\mathbf{k}_1|} \\ &= \tfrac{1}{2}(1-\cos\phi) - \cos\theta \\ &= H_2(-\mathbf{k}, -\mathbf{k}_1), \end{aligned} \tag{3.21}$$

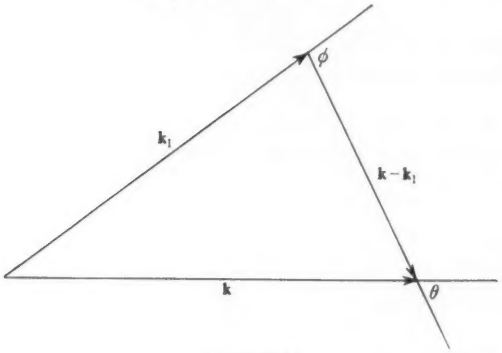


FIGURE 1

the angles $\theta$ and $\phi$ being illustrated in figure 1;

$$\begin{aligned} H_3(\mathbf{k}, \mathbf{k}_1, \mathbf{k}_2) &= (2k)^{-1}\,|\mathbf{k}-\mathbf{k}_1-\mathbf{k}_2|^2 - \tfrac{1}{2}\,|\mathbf{k}-\mathbf{k}_1-\mathbf{k}_2| + k^{-1}\mathbf{k}_1.(\mathbf{k}-\mathbf{k}_1-\mathbf{k}_2) \\ &\quad + |\mathbf{k}-\mathbf{k}_1|\,\frac{(\mathbf{k}-\mathbf{k}_1).(\mathbf{k}-\mathbf{k}_1-\mathbf{k}_2)}{|\mathbf{k}-\mathbf{k}_1|\,|\mathbf{k}-\mathbf{k}_1-\mathbf{k}_2|}\left\{1 - \frac{\mathbf{k}.(\mathbf{k}-\mathbf{k}_1)}{k\,|\mathbf{k}-\mathbf{k}_1|}\right\}, \\ &= H_3(-\mathbf{k}, -\mathbf{k}_1, -\mathbf{k}_2); \end{aligned} \tag{3.22}$$

$$\begin{aligned} H_4(\mathbf{k}, \mathbf{k}_1, \mathbf{k}_2) &= \frac{(\mathbf{k}-\mathbf{k}_1).(\mathbf{k}-\mathbf{k}_1-\mathbf{k}_2)}{2\,|\mathbf{k}-\mathbf{k}_1-\mathbf{k}_2|}\left\{1 - \frac{\mathbf{k}_1.(\mathbf{k}-\mathbf{k}_1)}{k_1\,|\mathbf{k}-\mathbf{k}_1|} - 2\,\frac{\mathbf{k}.(\mathbf{k}-\mathbf{k}_1)}{k\,|\mathbf{k}-\mathbf{k}_1|}\right\} \\ &\quad + \frac{(\mathbf{k}_1+\mathbf{k}_2).\mathbf{k}_1}{2k_1}\left\{1 - \frac{(\mathbf{k}_1+\mathbf{k}_2).(\mathbf{k}-\mathbf{k}_1-\mathbf{k}_2)}{|\mathbf{k}_1+\mathbf{k}_2|\,|\mathbf{k}-\mathbf{k}_1-\mathbf{k}_2|}\right\} \\ &\quad + \frac{(\mathbf{k}-\mathbf{k}_2).(\mathbf{k}-\mathbf{k}_1-\mathbf{k}_2)}{|\mathbf{k}-\mathbf{k}_1-\mathbf{k}_2|}\left\{1 - \frac{\mathbf{k}.(\mathbf{k}-\mathbf{k}_2)}{k\,|\mathbf{k}-\mathbf{k}_2|}\right\} + \frac{\mathbf{k}.(\mathbf{k}-\mathbf{k}_1-\mathbf{k}_2)}{k} \\ &\quad - \tfrac{1}{2}\{k_1 + |\mathbf{k}-\mathbf{k}_1-\mathbf{k}_2|\}\left\{1 - \frac{\mathbf{k}_1.(\mathbf{k}-\mathbf{k}_1-\mathbf{k}_2)}{k_1\,|\mathbf{k}-\mathbf{k}_1-\mathbf{k}_2|}\right\}, \\ &= H_4(-\mathbf{k}, -\mathbf{k}_1, -\mathbf{k}_2). \end{aligned} \tag{3.23}$$

Equation (3.19) describes the motion of the free surface retaining terms to the third order. The terms involving a single integration describe the second-order interactions and those involving a double integration the third-order interactions. It is clear that these interactions are generally rather complicated algebraically; our aim is to discover the types of interaction that are most signi-

ficant and which can be described in simple physical terms. In the present paper, we examine the wave dynamics when the air is undisturbed by wind, so that we can take

$$d\varpi(\mathbf{k}, t) = 0$$

in the following sections. We will first examine the properties of the second-order interactions by neglecting the double integral terms in (3.19) and in § 5 we discuss some general properties of the full equation.

## 4. Secondary wave components

If two primary wave trains of wave-numbers $\boldsymbol{\kappa}_1$ and $\boldsymbol{\kappa}_2$ interact, the second-order terms of (3.19) generate components with wave-numbers $\boldsymbol{\kappa}_1 + \boldsymbol{\kappa}_2$ and $\boldsymbol{\kappa}_1 - \boldsymbol{\kappa}_2$. These products of binary interactions between primary components can conveniently be called 'secondary' waves, and similarly the components arising from the interactions among three primary waves or between a primary and a secondary wave can be called 'tertiary' components.

Solutions to (3.19) from given initial conditions will be sought by the usual perturbation technique. The Fourier component $dB(\mathbf{k}, t)$ of the surface displacement is represented as the sum of primary, secondary, and higher components in a manner analogous to the classical Stokes expansion

$$dB(\mathbf{k}, t) = dB_1(\mathbf{k}, t) + dB_2(\mathbf{k}, t) + dB_3(\mathbf{k}, t) + \ldots, \tag{4.1}$$

where $dB_1(\mathbf{k}, t)$ is the solution to the linear equation

$$k^{-1} dB_1''(\mathbf{k}, t) + g\, dB_1(\mathbf{k}, t) = 0, \tag{4.2}$$

and it is supposed that

$$\overline{|\int dB_1(\mathbf{k}, t)|} \gg \overline{|\int dB_2(\mathbf{k}, t)|} \gg \ldots, \tag{4.3}$$

where the overbar indicates the ensemble average. The next approximation, yielding the secondary wave components is made by substituting

$$dB_1(\mathbf{k}, t) + dB_2(\mathbf{k}, t) \quad \text{for} \quad dB(\mathbf{k}, t)$$

into (3.19) and retaining only the lowest (second)-order terms in the non-linear integrals. In virtue of (4.2), we have

$$\begin{aligned} k^{-1} dB_2''(\mathbf{k}) + g\, dB_2(\mathbf{k}) = &- \int_{\mathbf{k}_1} H_1(\mathbf{k}, \mathbf{k}_1)\, dB_1''(\mathbf{k} - \mathbf{k}_1)\, dB_1(\mathbf{k}_1) \\ &- \int_{\mathbf{k}_1} H_2(\mathbf{k}, \mathbf{k}_1)\, dB_1'(\mathbf{k} - \mathbf{k}_1)\, dB_1'(\mathbf{k}_1). \end{aligned} \tag{4.4}$$

The tertiary components are found, likewise, by including the next term in the expansion, and it is found that

$$\begin{aligned} k^{-1} dB_3''(\mathbf{k}) + g\, dB_3(\mathbf{k}) = &- \int_{\mathbf{k}_1} H_1(\mathbf{k}, \mathbf{k}_1) [dB_1''(\mathbf{k} - \mathbf{k}_1)\, dB_2(\mathbf{k}_1) + dB_2''(\mathbf{k} - \mathbf{k}_1)\, dB_1(\mathbf{k}_1)] \\ &- \int_{\mathbf{k}_1} H_2(\mathbf{k}, \mathbf{k}_1) [dB_1'(\mathbf{k} - \mathbf{k}_1)\, dB_2'(\mathbf{k}_1) + dB_2'(\mathbf{k} - \mathbf{k}_1)\, dB_1'(\mathbf{k}_1)] \\ &+ \int_{\mathbf{k}_1} \int_{\mathbf{k}_2} H_3(\mathbf{k}, \mathbf{k}_1, \mathbf{k}_2)\, dB_1''(\mathbf{k} - \mathbf{k}_1 - \mathbf{k}_2)\, dB_1(\mathbf{k}_1)\, dB_1(\mathbf{k}_2) \\ &+ \int_{\mathbf{k}_1} \int_{\mathbf{k}_2} H_4(\mathbf{k}, \mathbf{k}_1, \mathbf{k}_2)\, dB_1'(\mathbf{k} - \mathbf{k}_1 - \mathbf{k}_2)\, dB_1'(\mathbf{k}_1)\, dB_1(\mathbf{k}_2). \end{aligned} \tag{4.5}$$

Consideration of this last equation is postponed to § 5.

### 4.1. *Single wave train*

The simplest problem is to calculate the secondary components generated by the interaction of an initial sine wave with itself. Although the result is well known the derivation will be discussed in some detail primarily to illustrate a systematic method of selection of the relevant constituents of the interaction. The analysis of more complicated situations follows exactly the same lines, so that much of the detail can be omitted in later sections.

Suppose that

$$dB_1(\mathbf{k},t) = \tfrac{1}{2}\alpha\{\delta(l-l_0)\exp(-in_0t)+\delta(l+l_0)\exp(in_0t)\}\,\delta(m)\,dl\,dm, \quad (4.6)$$

where

$$n_0 = (gl_0)^{\frac{1}{2}}, \quad (4.7)$$

$\delta(l)$ and $\delta(m)$ represent the Dirac delta functions and $\mathbf{k} = (l, m)$. The expression (4.6) satisfies (4.2) and is the Fourier–Stieltjes representation of the primary component

$$\xi_1(x,t) = \alpha\cos(l_0x - n_0t). \quad (4.8)$$

The secondary components are determined by (4.4). When $dB_1(\mathbf{k},t)$ is of the form (4.6), the integral over the wave-numbers $\mathbf{k}_1$ has contributions only when both $\mathbf{k}_1 = (\pm l_0, 0)$ and $\mathbf{k}-\mathbf{k}_1 = (\pm l_0, 0)$, so that the right-hand side is non-zero only near $\mathbf{k} = (\pm 2l_0, 0)$ and $(0,0)$. The formal process of solution is facilitated by integrating the whole equation over a small range containing in turn each of the singular points of the Dirac delta functions, so that the Fourier–Stieltjes transforms degenerate to the coefficients of a Fourier series. If

$$B_2(\mathbf{K},t) = \int_{K_1-\epsilon}^{K_1+\epsilon}\int_{K_2-\epsilon}^{K_2+\epsilon} dB_2(\mathbf{k},t),$$

where $\mathbf{K} = (K_1, K_2) = (\pm 2l_0, 0)$ or $(0,0)$, equation (4.4) becomes

$$B_2''(\mathbf{K},t)+gKB_2(\mathbf{K},t) = -K\int_{\mathbf{k}}\int_{\mathbf{k}_1}\{H_1(\mathbf{k},\mathbf{k}_1)\,dB_1''(\mathbf{k}-\mathbf{k}_1)\,dB_1(\mathbf{k}_1) + H_2(\mathbf{k},\mathbf{k}_1)\,dB_1'(\mathbf{k}-\mathbf{k}_1)\,dB_1'(\mathbf{k}_1)\}, \quad (4.9)$$

where the $\mathbf{k}$-integration is between the limits specified above. Substitution of (4.6) into the right-hand side of (4.9) gives rise to eight terms, and it is a simple matter to pick out the ones relevant to each of the three significant values of $\mathbf{K}$.

When $\mathbf{K} = (2l_0, 0)$, we require $\mathbf{k} = (2l_0, 0)$, $\mathbf{k}_1 = (l_0, 0)$, so that from (4.6) and (4.9),

$$\left\{\frac{d^2}{dt^2}+2l_0g\right\}B_2(2l_0,t) = \tfrac{1}{2}\alpha^2n_0^2l_0\exp(-2in_0t)\{H_1(2l_0,l_0)+H_2(2l_0,l_0)\}, \quad (4.10)$$

where only the $x$-components of the vector arguments are specified explicitly (the components in the $y$-direction are all zero). Similarly, when $\mathbf{K} = (-2l_0, 0)$, $\mathbf{k} = (-2l_0, 0)$ and $\mathbf{k}_1 = (-l_0, 0)$ so that

$$\left\{\frac{d^2}{dt^2}+2l_0g\right\}B_2(-2l_0,t) = \tfrac{1}{2}\alpha^2n_0^2l_0\exp(2in_0t)\{H_1(-2l_0,-l_0)+H_2(-2l_0,-l_0)\}. \quad (4.11)$$

The case $\mathbf{K} = 0$ is trivial, the equation reducing to

$$\frac{d^2}{dt^2} B_2(0,t) = 0.$$

Under the present circumstances, the functions $H_1(\mathbf{k}, \mathbf{k}_1)$ and $H_2(\mathbf{k}, \mathbf{k}_1)$ simplify considerably. Here $\mathbf{k}$ and $\mathbf{k}_1$, are of the forms $(K_0, 0)$ and $(K_1, 0)$ respectively, and from the definitions (3.20) and (3.21),

$$\left.\begin{aligned} H_1(K_0, K_1) = H_1(-K_0, -K_1) &= 0 \quad \text{if} \quad K_0 > K_1, \\ &= 2 \quad \text{if} \quad K_1 > K_0 > 0; \\ H_2(K_0, K_1) = H_2(-K_0, -K_1) &= 0 \quad \text{if} \quad K_0, K_1 \text{ of opposite sign}, \\ &= -1 \quad \text{if} \quad K_0 > K_1 > 0, \\ &= 2 \quad \text{if} \quad K_1 > K_0 > 0. \end{aligned}\right\} \tag{4.12}$$

The equations for the secondary components can thus be combined in the form

$$\left\{\frac{d^2}{dt^2} + 2l_0 g\right\} B_2(\pm 2l_0, t) = -\tfrac{1}{2}\alpha^2 n_0^2 l_0 \exp(\mp 2in_0 t). \tag{4.13}$$

Since the initial wave field was sinusoidal, the initial conditions to be imposed on the component $B_2$ are that

$$B_2 = B_2' = 0 \quad \text{at} \quad t = 0$$

and the solution is readily found to be

$$\begin{aligned} B_2(\pm 2l_0, t) = {} & \tfrac{1}{4} l_0 \alpha^2 \exp(\mp 2in_0 t) + \tfrac{1}{8}(\sqrt{[2]} - 1) l_0 \alpha^2 \exp(\pm i\sqrt{[2]}\, n_0 t) \\ & - \tfrac{1}{8}(\sqrt{[2]} + 1) l_0 \alpha^2 \exp(\mp i\sqrt{[2]}\, n_0 t), \end{aligned} \tag{4.14}$$

where $n_0 = (gl_0)^{\frac{1}{2}}$. In physical space, the secondary wave components are given by

$$\begin{aligned} \xi_2(x,t) &= B_2(2l_0)\exp(2il_0 x) + B_2(-2l_0)\exp(-2il_0 x) \\ &= \tfrac{1}{2} l_0 \alpha^2 \cos(2l_0 x - 2n_0 t) + \tfrac{1}{4}(\sqrt{[2]} - 1) l_0 \alpha^2 \cos(2l_0 x + \sqrt{[2]}\, n_0 t) \\ &\quad - \tfrac{1}{4}(\sqrt{[2]} + 1) l_0 \alpha^2 \cos(2l_0 x - \sqrt{[2]}\, n_0 t), \end{aligned} \tag{4.15}$$

and the solution to the problem, correct to the second order, is

$$\begin{aligned} \xi(x,t) = {} & \alpha\{\cos(l_0 x - n_0 t) + \tfrac{1}{2} l_0 \alpha \cos 2(l_0 x - n_0 t)\} \\ & + \tfrac{1}{4} l_0 \alpha^2 \{(\sqrt{[2]} - 1)\cos(2l_0 x + \sqrt{[2]}\, n_0 t) - (\sqrt{[2]} + 1)\cos(2l_0 x - \sqrt{[2]}\, n_0 t)\}. \end{aligned} \tag{4.16}$$

Certain properties of this solution are of interest in relation to the analysis of more complex situations later. The secondary wave components are of two types. The first is a 'bound secondary' component, given by the first term of (4.15), which has half the wavelength and twice the frequency of the primary component, and so travels at the same phase velocity of the primary. It represents a distortion of the initial sine wave; the first two terms of (4.16) specify a Stokes permanent wave to this order. The remaining terms come from the complementary function in the solution to (4.13), and their amplitude depends on the particular initial conditions chosen for $B_2(\pm 2l_0, t)$. They have half the wave-

length of the primary wave and $\sqrt{2}$ times the frequency, so that their velocity is that of free infinitesimal waves of the same wave-number. These can be called 'free secondary components', and they are dynamically similar to the primary components but their amplitude is smaller by a factor of order $\alpha l_0 \ll 1$.

A point of particular interest is that the amplitudes of the secondary components are *bounded in time*. From the point of view of potential energy transfer, the second-order interactions in this case merely transfer a pulse of energy to the wave-number $2l_0$, but this does not continue. The Stokes permanent wave and the free secondary waves propagate independently (to this order) and do not interact further.

### 4.2. *Two intersecting wave trains*

Suppose that at time $t = 0$, the surface displacement and velocity correspond to two intersecting sinusoidal waves with wave-numbers $\mathbf{K}_0 = (l_0, m_0)$ and $\mathbf{K}_1 = (l_1, m_1)$. The primary wave field is thus

$$\xi_1(\mathbf{x}, t) = \alpha \cos(\mathbf{K}_0 . \mathbf{x} - n_0 t) + \beta \cos(\mathbf{K}_1 . \mathbf{x} - n_1 t), \tag{4.17}$$

whose Fourier–Stieltjes representation is given by

$$\begin{aligned} dB_1(\mathbf{k}, t) = {} & \tfrac{1}{2}\alpha\{\delta(\mathbf{k}-\mathbf{K}_0)\exp(-in_0 t) + \delta(\mathbf{k}+\mathbf{K}_0)\exp(in_0 t)\}\, d\mathbf{k} \\ & + \tfrac{1}{2}\beta\{\delta(\mathbf{k}-\mathbf{K}_1)\exp(-in_1 t) + \delta(\mathbf{k}+\mathbf{K}_1)\exp(in_1 t)\}\, d\mathbf{k}, \end{aligned} \tag{4.18}$$

where $\delta(\mathbf{k}-\mathbf{K}_0) = \delta(l-l_0)\,\delta(m-m_0)$ and $d\mathbf{k} = dl\,dm$. Substitution of (4.18) into the linear equation (4.2) determines the frequencies $n_0$ and $n_1$ of these primary components:

$$\left.\begin{aligned} n_0^2 &= gK_0 = g\{l_0^2 + m_0^2\}^{\frac{1}{2}}, \\ n_1^2 &= gK_1 = g\{l_1^2 + m_1^2\}^{\frac{1}{2}}. \end{aligned}\right\} \tag{4.19}$$

The substitution of (4.18) into the perturbation integrals of (4.4) for the secondary wave components gives rise to a total of 32 terms, not all of which however are of present interest. Four pairs of terms describe the development of wave-numbers $\pm 2\mathbf{K}_0$ and $\pm 2\mathbf{K}_1$, and the generation of the Stokes waves discussed previously. A total of eight terms give the trivial zero wave-number case. The remaining sixteen gives the contributions at wave-numbers $\pm(\mathbf{K}_0 + \mathbf{K}_1)$ and $\pm(\mathbf{K}_0 - \mathbf{K}_1)$, and these are the ones that we wish to select.

When $\mathbf{K} = (\mathbf{K}_0 - \mathbf{K}_1)$, $\mathbf{k} = (\mathbf{K}_0 - \mathbf{K}_1)$ and $\mathbf{k}_1 = \mathbf{K}_0$ or $-\mathbf{K}_1$. Selecting out the relevant terms and integrating over a small range including the Dirac delta functions to reduce the Fourier–Stieltjes transforms to Fourier coefficients, one finds that

$$\begin{aligned} &\left\{\frac{d^2}{dt^2} + g\,|\mathbf{K}_0 - \mathbf{K}_1|\right\} B_2(\mathbf{K}_0 - \mathbf{K}_1, t) \\ &\quad = \tfrac{1}{4}\,|\mathbf{K}_0 - \mathbf{K}_1|\,\alpha\beta \exp\{-i(n_0 - n_1)t\}\{n_1^2 H_1(\mathbf{K}_0 - \mathbf{K}_1, \mathbf{K}_0) + n_0 n_1 H_2(\mathbf{K}_0 - \mathbf{K}_1, \mathbf{K}_0) \\ &\qquad + n_0^2 H_1(\mathbf{K}_0 - \mathbf{K}_1, -\mathbf{K}_1) + n_0 n_1 H_2(\mathbf{K}_0 - \mathbf{K}_1, -\mathbf{K}_1)\} \qquad (4.20) \\ &\quad = \tfrac{1}{4}\,|\mathbf{K}_0 - \mathbf{K}_1|\,\alpha\beta n_0 n_1 \exp\{-i(n_0 - n_1)t\}\,\Gamma(n_0/n_1, \theta, \phi), \qquad (4.21) \end{aligned}$$

say, where

$$\Gamma\left(\frac{n_0}{n_1}, \theta, \phi\right) = \frac{n_1}{n_0} H_1(\mathbf{K}_0 - \mathbf{K}_1, \mathbf{K}_0) + H_2(\mathbf{K}_0 - \mathbf{K}_1, \mathbf{K}_0) + \frac{n_0}{n_1} H_1(\mathbf{K}_0 - \mathbf{K}_1, -\mathbf{K}_1) + H_2(\mathbf{K}_0 - \mathbf{K}_1, -\mathbf{K}_1)$$

$$= \frac{n_1}{n_0} H_1(-\mathbf{K}_0 + \mathbf{K}_1, -\mathbf{K}_0) + H_2(-\mathbf{K}_0 + \mathbf{K}_1, -\mathbf{K}_0) + \frac{n_0}{n_1} H_1(-\mathbf{K}_0 + \mathbf{K}_1, \mathbf{K}_1) + H_2(-\mathbf{K}_0 + \mathbf{K}_1, \mathbf{K}_1), \quad (4.22)$$

in virtue of (3.20) and (3.21).

Similarly, when $\mathbf{K} = -(\mathbf{K}_0 - \mathbf{K}_1)$, $\mathbf{k} = -(\mathbf{K}_0 - \mathbf{K}_1)$ and $\mathbf{k}_1 = -\mathbf{K}_0$ or $\mathbf{K}_1$. Selecting the relevant terms in this case we obtain

$$\left\{\frac{d^2}{dt^2} + g\,|\mathbf{K}_0 - \mathbf{K}_1|\right\} B_2\{-(\mathbf{K}_0 - \mathbf{K}_1), t\}$$

$$= \tfrac{1}{4}\,|\mathbf{K}_0 - \mathbf{K}_1|\,\alpha\beta n_0 n_1 \Gamma\left(\frac{n_0}{n_1}, \theta, \phi\right) \exp\{i(n_0 - n_1)t\}, \quad (4.23)$$

the function $\Gamma$ occurring again by (4.22).

For the other secondary components, when $\mathbf{K} = \pm(\mathbf{K}_0 + \mathbf{K}_1)$, $\mathbf{k} = \pm(\mathbf{K}_0 + \mathbf{K}_1)$ and $\mathbf{k}_1 = \pm\mathbf{K}_0$ or $\pm\mathbf{K}_1$, the selection procedure gives

$$\left\{\frac{d^2}{dt^2} + g\,|\mathbf{K}_0 + \mathbf{K}_1|\right\} B_2\{\pm(\mathbf{K}_0 + \mathbf{K}_1), t\}$$

$$= \tfrac{1}{4}\,|\mathbf{K}_0 + \mathbf{K}_1|\,\alpha\beta n_0 n_1 \Delta\left(\frac{n_0}{n_1}, \theta, \phi\right) \exp\{\mp i(n_0 + n_1)t\}, \quad (4.24)$$

where

$$\Delta\left(\frac{n_0}{n_1}, \theta, \phi\right) = \frac{n_1}{n_0} H_1(\mathbf{K}_0 + \mathbf{K}_1, \mathbf{K}_0) + H_2(\mathbf{K}_0 + \mathbf{K}_1, \mathbf{K}_0) + \frac{n_0}{n_1} H_1(\mathbf{K}_0 + \mathbf{K}_1, \mathbf{K}_1) + H_2(\mathbf{K}_0 + \mathbf{K}_1, \mathbf{K}_1) \quad (4.25)$$

is symmetrical with respect to changes in sign of both the vector arguments or with respect to interchange of $\mathbf{K}_0$ and $\mathbf{K}_1$.

The equations (4.21), (4.23) and (4.24) are all of the form

$$B_2'' + \nu^2 B_2 = A\,e^{i\mu t},$$

and the solutions are of the form

$$\left.\begin{aligned} B_2 &= \frac{A}{\nu^2 - \mu^2} e^{i\mu t} \quad \text{if} \quad \mu^2 \neq \nu^2, \\ \text{or} \qquad B_2 &= -\frac{iA}{2\mu} t\, e^{i\mu t} \quad \text{if} \quad \mu^2 = \nu^2. \end{aligned}\right\} \quad (4.26)$$

The former possibility represents the secondary components of bounded amplitude that we have encountered in the previous section. The latter type of solution, however, would represent a secondary wave component whose amplitude increases with time, or, in terms of the potential energy spectrum, it would represent a *continuing* energy transfer from one component of the wave field to another.

The condition that is required for a continuing transfer of potential energy between different wave-numbers is now clear. It is that the perturbation term for a certain wave-number should have a frequency equal to the frequency of *free infinitesimal* surface waves of the same wave-number. In other words, the non-linear perturbation terms represent a moving disturbance that induces a forced motion of the higher order components. If the frequency of the disturbance term of a certain wave-number is equal to the frequency of a free infinitesimal wave of the same wave-number, then a resonance occurs, and the amplitude of the forced, higher order component grows rapidly. This type of resonance is closely analogous to that which occurs when a turbulent wind blows across the water surface (Phillips 1957), and we should perhaps not be surprised to find a similar mechanism here in view of the nature of the governing equations (4.4) and (4.5).

Is there the possibility of such a resonance within this second approximation? Are there real wave-number vectors $\mathbf{K}_0$ and $\mathbf{K}_1$ such that, as required by equations (4.23) and (4.24),

$$g\,|\mathbf{K}_0 \pm \mathbf{K}_1| = (n_0 \pm n_1)^2\,? \tag{4.27}$$

We have $$n_0 = (gK_0)^{\frac{1}{2}}, \quad n_1 = (gK_1)^{\frac{1}{2}},$$

and let $$\mathbf{K}_0 = (l_0, m_0) = (K_0 \sin\gamma_0,\ K_0 \cos\gamma_0),$$

$$\mathbf{K}_1 = (l_1, m_1) = (K_1 \sin\gamma_1,\ K_1 \cos\gamma_1),$$

so that $\gamma_0 - \gamma_1$ is the angle between the two vectors. Squaring both sides of (4.27), we find that

$$K_0^2 + K_1^2 \pm 2K_0K_1\cos(\gamma_0-\gamma_1) = K_0^2 + K_1^2 + 6K_0K_1 + 4(K_0K_1)^{\frac{1}{2}}(K_0+K_1),$$

or $$\cos(\gamma_0-\gamma_1) = \pm 3 + 4\left\{\frac{\frac{1}{2}(K_0+K_1)}{(K_0K_1)^{\frac{1}{2}}}\right\}. \tag{4.28}$$

But since $K_0 > 0$, $K_1 > 0$,

$$\tfrac{1}{2}(K_0+K_1) > (K_0K_1)^{\frac{1}{2}},$$

except when $K_0 = K_1$. Clearly, then, there are no real solutions to (4.27) and (4.28) except for the difference wave-number when $K_0 = K_1$, $\gamma_0 - \gamma_1 = 0$ that is, the zero wave-number case of the previous section which is trivial, since the coefficient $A$ in (4.26) is zero. We conclude, then, that such solutions cannot occur in the second-order interactions and that these do not give rise to a continuing energy transfer.

The solutions to (4.21), (4.23) and (4.24), being all of the first type of the set (4.26) can now be written down without difficulty. For the difference wave-numbers $\pm(\mathbf{K}_0 - \mathbf{K}_1)$, the Fourier components of the secondary waves are

$$B_2\{\pm(\mathbf{K}_0-\mathbf{K}_1), t\} = \frac{\alpha\beta n_0 n_1 |\mathbf{K}_0-\mathbf{K}_1|\,\Gamma(n_0/n_1, \theta, \phi)}{4\{g\,|\mathbf{K}_0-\mathbf{K}_1| - (n_0-n_1)^2\}} \exp\{\mp i(n_0-n_1)t\}, \tag{4.29}$$

and for $\pm(\mathbf{K}_0+\mathbf{K}_1)$,

$$B_2\{\pm(\mathbf{K}_0+\mathbf{K}_1), t\} = \frac{\alpha\beta n_0 n_1 |\mathbf{K}_0+\mathbf{K}_1|\,\Delta(n_0/n_1, \theta, \phi)}{4\{g\,|\mathbf{K}_0+\mathbf{K}_1| - (n_0+n_1)^2\}} \exp\{\mp i(n_0+n_1)t\}, \tag{4.30}$$

together with, in each case, the *free* secondary components arising from the complementary functions in the equations, whose magnitudes depend on the par-

ticular initial conditions imposed and which propagate, to this order, as free infinitesimal waves. The bound second-order perturbation waves are therefore given by

$$\xi_2(\mathbf{x},t) = \tfrac{1}{2}\alpha\beta(K_0K_1)^{\frac{1}{2}}\{C\cos[(\mathbf{K}_0-\mathbf{K}_1).\mathbf{x}-(n_0-n_1)t] + D\cos[(\mathbf{K}_0+\mathbf{K}_1).\mathbf{x}-(n_0+n_1)t]\}, \tag{4.31}$$

where the amplitude functions $C$ and $D$ are given by

$$\begin{aligned} C &= C(\mathbf{K}_0,\mathbf{K}_1) = \Gamma\left(\frac{n_0}{n_1},\theta,\phi\right)\left\{1-\frac{(n_0-n_1)^2}{g|\mathbf{K}_0-\mathbf{K}_1|}\right\}^{-1}, \\ D &= D(\mathbf{K}_0,\mathbf{K}_1) = \Delta\left(\frac{n_0}{n_1},\theta,\phi\right)\left\{1-\frac{(n_0+n_1)^2}{g|\mathbf{K}_0+\mathbf{K}_1|}\right\}^{-1}. \end{aligned} \tag{4.32}$$

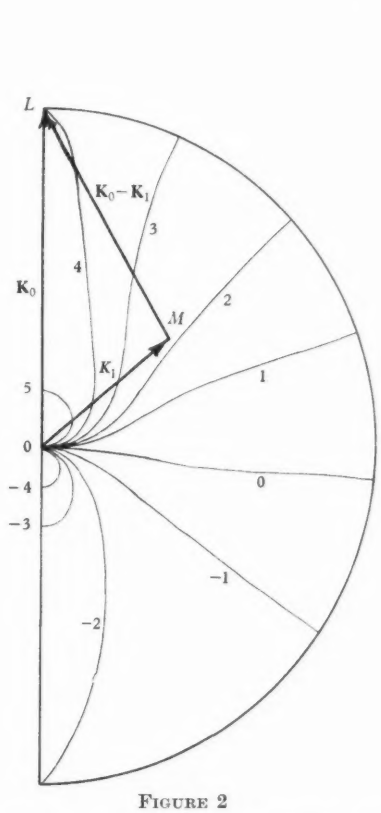


FIGURE 2

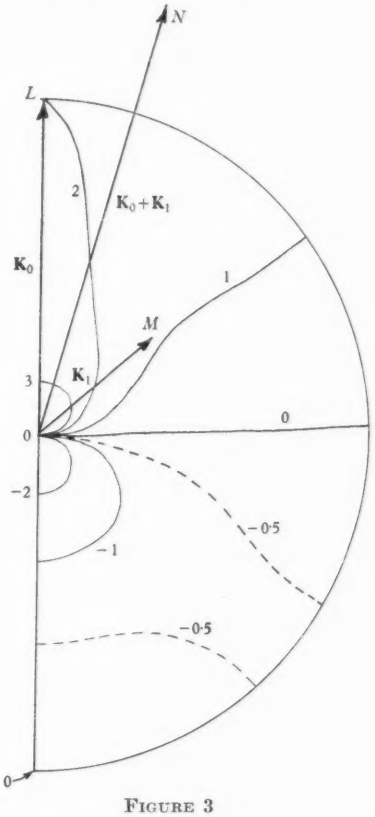


FIGURE 3

FIGURE 2. Contours of the amplitude function $C$ for the difference wave-numbers in second-order interactions. The wave-number $\mathbf{K}_0$, represented by $OL$, interacts with $\mathbf{K}_1$ ($OM$) to give the wave-number $\mathbf{K}_0-\mathbf{K}_1$ ($ML$) whose amplitude is proportional to the value of the function $C$ at the point $M$. The arrows indicate the directions of propagation of the components.

FIGURE 3. Contours of the amplitude function $D$ for the sum wave-number in second-order interactions. The amplitude of the component with wave-number $\mathbf{K}_0+\mathbf{K}_1$ is given by the value of the function at the point $M$.

The numerical values of these functions are illustrated in figure 2 and 3. They are symmetrical about the direction of $\mathbf{K}_0$, and have the same values at reciprocal points inside and outside the circle, so that only the region $K_1 \leqslant K_0$ with angles of intersection between 0 and $\pi$, need be shown. The important property to observe in this context is that, unless $K_1/K_0$ is very small (or very large) the amplitude functions are of order unity. The amplitudes of the secondary wave components are thus always small, of order $(\alpha\beta)^{\frac{1}{2}}(\alpha K_0 \beta K_1)^{\frac{1}{2}}$, that is, of the order of the geometric mean of the primary wave amplitudes times the geometric mean of the maximum primary wave slopes.

When the magnitude of one of the primary wave-numbers is much greater than that of the other, $K_1/K_0$ is very small (or very large), and we are concerned with short waves superimposed on a very much longer wave. The properties of such a system can be derived readily from the expressions given above. This situation has been discussed in detail by Longuet-Higgins & Stewart (1960) who show that the influence of the shorter waves upon the longer can be described in terms of a 'radiation' stress. A number of other special cases are of some interest. When $\mathbf{K}_0 = \mathbf{K}_1$, we have the Stokes permanent wave discussed previously. When $\mathbf{K}_0 = -\mathbf{K}_1$, the second-order approximation to standing waves is obtained. Finally, figures 2 and 3 show that for certain combinations of $\mathbf{K}_0$ and $\mathbf{K}_1$, either $C$ or $D$ is zero, so that the amplitude of the secondary components of either the sum or difference wave-number vanishes.

## 5. Tertiary wave components

It appears that our search for a mechanism of continuing energy transfer will have to be carried to the next approximation. The algebraic complications become much greater, and careful use of our selection procedure is essential if we wish to avoid being buried under an avalanche of terms. Let us consider first the distortion of an initially sinusoidal wave, to this order of approximation.

### 5.1. *Single sinusoidal wave train*

We can ignore here any free secondary components, since they propagate as free infinitesimal waves, and their interactions with the primary wave system is of the same nature as discussed in the previous section, except that the products are smaller by an order of magnitude (i.e. by a factor $\alpha K_0$). The dynamical processes that are new to this situation are the interactions between the primary wave and the bound secondary component, given by the single integral terms on the right-hand side of (4.5), and the triple interactions of the primary wave with itself, given by the double integral terms of that equation. The primary and secondary wave components are given by (4.6) and (4.14), namely

$$\left.\begin{aligned} dB_1(\mathbf{k},t) &= \tfrac{1}{2}\alpha\{\delta(l-l_0)\exp(-in_0t)+\delta(l+l_0)\exp(in_0t)\}\,\delta(m)\,dl\,dm, \\ dB_2(\mathbf{k},t) &= \tfrac{1}{4}l_0\alpha^2\{\delta(l-2l_0)\exp(-2in_0t)+\delta(l+2l_0)\exp(2in_0t)\}\,\delta(m)\,dl\,dm. \end{aligned}\right\} \quad (5.1)$$

The substitution of these expressions into the right-hand side of (4.5), gives rise to contributions when $\mathbf{k} = (\pm l_0, 0)$ and $(\pm 3l_0, 0)$. The various combinations that occur are given in table 1 below, in which the signs associated with an entry

in each column is taken as the upper or lower alternative throughout. Thus, in the primary-secondary interactions, the primary wave-number $l_0$ and the secondary $2l_0$ give rise to the tertiaries $3l_0$ or $-l_0$ (the sum or difference) with the associated time factors $\exp(-3in_0t)$ or $\exp(in_0t)$ respectively. Similarly, in the triple primary interactions, the wave-numbers $l_0$ and $-l_0$ give rise to a tertiary component of wave-number $l_0$ or $-l_0$ (in combination with a third primary of wave-number $l_0$ or $-l_0$) with a time factor of $\exp(-in_0t)$ or $\exp(in_0t)$ respectively.

| Primary wave-number | Secondary wave-number | Tertiary wave-number | Time factor |
|---|---|---|---|
| $\pm l_0$ | $\pm 2l_0$ | $\pm 3l_0$ | $\exp(\mp 3in_0t)$ |
| $\pm l_0$ | $\pm 2l_0$ | $\mp l_0$ | $\exp(\pm in_0t)$ |
| $\pm l_0$ | $\mp 2l_0$ | $\mp l_0$ | $\exp(\pm in_0t)$ |
| $\pm l_0$ | $\mp 2l_0$ | $\pm 3l_0$ | $\exp(\mp 3in_0t)$ |

(*a*) Primary-secondary interactions

| $k_1$ | $k_2$ | Tertiary wave-number $k$ $(k-k_1-k_2=\pm l_0)$ | Time factor |
|---|---|---|---|
| $\pm l_0$ | $\pm l_0$ | $\pm 3l_0$ | $\exp(\mp 3in_0t)$ |
| $\pm l_0$ | $\pm l_0$ | $\pm l_0$ | $\exp(\mp in_0t)$ |
| $\pm l_0$ | $\mp l_0$ | $\pm l_0$ | $\exp(\mp in_0t)$ |
| $\pm l_0$ | $\mp l_0$ | $\mp l_0$ | $\exp(\pm in_0t)$ |

(*b*) Triple primary interactions

TABLE 1. Wave-numbers involved in third-order interactions of an initially sinusoidal wave train.

As before, it is convenient to integrate equation (4.5) over a small range of $\mathbf{k}$ containing the wave-number of interest, to obtain the Fourier *coefficients* for this wave-number. The selection of all the relevant terms can now be made, and it is found, for example, that when $\mathbf{k} = (3l_0, 0)$, the primary-secondary interaction term gives

$$\tfrac{1}{8}l_0\alpha^3n_0^2\exp(-3in_0t)\{H_1(3l_0, 2l_0)+4H_1(3l_0, l_0)+2H_2(3l_0, 2l_0)+2H_2(3l_0, l_0)\}, \quad (5.2)$$

where the numerical coefficients of the $H$ functions arise from the time differentiation of the double frequency secondary components and where only the vectorial components in the $x$-direction are shown in the arguments. The triple primary interaction term yields

$$-\tfrac{1}{8}\alpha^3n_0^2\exp(-3in_0t)\{H_3(3l_0, l_0, l_0)+H_4(3l_0, l_0, l_0)\}. \quad (5.3)$$

The values of $H_1$ and $H_2$ are given, for this simple case, by (4.12), and $H_3$ and $H_4$ are evaluated from the expressions (3.22) and (3.23).

The calculations, though still rather tedious, are quite straightforward, and lead to the following expressions for the combined perturbation terms:

$$\left.\begin{aligned} -\tfrac{3}{8}\alpha^3n_0^2l_0\exp(\mp 3in_0t) \quad &\text{when} \quad \mathbf{k} = (\pm 3l_0, 0), \\ \tfrac{1}{2}\alpha^3n_0^2l_0\exp(\mp in_0t) \quad &\text{when} \quad \mathbf{k} = (\pm l_0, 0). \end{aligned}\right\} \quad (5.4)$$

The dynamical equations for the tertiary components are therefore

$$\left.\begin{aligned}\left(\frac{d^2}{dt^2}+3l_0g\right)B_3(\pm 3l_0,0) &= -\tfrac{9}{8}\alpha^3n_0^2l_0^2\exp(\mp 3in_0t),\\ \left(\frac{d^2}{dt^2}+l_0g\right)B_3(\pm l_0,0) &= \tfrac{1}{2}\alpha^3n_0^2l_0^2\exp(\mp in_0t).\end{aligned}\right\} \tag{5.5}$$

The first of these equations has the bounded amplitude solution of the first type of the set (4.26), namely

$$B_3(\pm 3l_0,0) = \tfrac{3}{16}\alpha^3l_0^2\exp(\mp 3in_0t), \tag{5.6}$$

together with complementary terms representing free tertiary waves. The second equation of the set (5.5), however, is of the second type of (4.26) and its solution represents a sine wave whose amplitude increases linearly with time:

$$B_3(\pm l_0,0) = \pm\tfrac{1}{4}i\alpha^3l_0^2(n_0t)\exp(\mp in_0t). \tag{5.7}$$

The complete bound tertiary wave components are given by

$$\begin{aligned}\xi_3(x,t) &= B_3(l_0,t)\exp(il_0x)+B_3(-l_0,t)\exp(-il_0x)+B_3(3l_0,t)\exp(3il_0x)\\ &\qquad +B_3(-3l_0,t)\exp(-3il_0x)\\ &= \tfrac{1}{2}\alpha^3l_0^2n_0t\sin(l_0x-n_0t)+\tfrac{3}{8}\alpha^3l_0^2\cos 3(l_0x-n_0t),\end{aligned} \tag{5.8}$$

and the surface displacement, to the third approximation is

$$\begin{aligned}\xi(x,t) &= \alpha[\cos(l_0x-n_0t)+\tfrac{1}{2}\alpha^2l_0^2n_0t\sin(l_0x-n_0t)]\\ &\qquad +\tfrac{1}{2}\alpha^2l_0\cos 2(l_0x-n_0t)+\tfrac{3}{8}\alpha^3l_0^2\cos 3(l_0x-n_0t).\end{aligned} \tag{5.9}$$

Here we have our first example of a developing tertiary component in which the frequency of the perturbation term at $\mathbf{k} = (\pm l_0, 0)$ is the same as the frequency of a free infinitesimal surface wave of the same wave-number. This example is, however, rather special in that the wave-number at which the tertiary component grows under this resonance type of interaction is *the same as the primary wave-number*. But the phase of the growing tertiary component is in advance of the phase of the primary wave by $\frac{1}{2}\pi$; this transfer of potential energy to the same wave-number at an earlier phase can be (and usually is) interpreted as an increase in the phase speed of the primary component. As it stands, the solution (5.9) is only valid for $n_0t \ll (\frac{1}{2}\alpha^2l_0^2)^{-1}$, after which the developing tertiary wave has an amplitude comparable with that of the primary wave, but the increase in phase velocity is readily found. For this time interval,

$$\tfrac{1}{2}\alpha^3l_0^2n_0t \doteq \sin(\tfrac{1}{2}\alpha^2l_0^2n_0t),$$

so that

$$\cos(l_0x-n_0t)+\tfrac{1}{2}\alpha^2l_0^2n_0t\sin(l_0x-n_0t) \doteq \cos\{l_0x-(1+\tfrac{1}{2}\alpha^2l_0^2)n_0t\}, \tag{5.10}$$

and the phase velocity $c$ is given by

$$c = c_0(1+\tfrac{1}{2}\alpha^2l_0^2),$$

where $c_0 = n_0/l_0 = (g/l_0)^{\frac{1}{2}}$, in accord with the classical Stokes expression (see Lamb 1932, § 250). Notice that the interaction time, or the time scale of development of the resonant tertiary component is of the order of $(-2)$-power of the maximum primary wave slope times the wave period.

## 5.2. Two intersecting wave trains

Suppose that initially we have two intersecting wave trains with wave-numbers $\mathbf{K}_0 = (l_0, m_0)$ and $\mathbf{K}_1 = (l_1, m_1)$. As in (4.18) the Fourier–Stieltjes components of the primary wave field are given by

$$dB_1(\mathbf{k},t) = \tfrac{1}{2}\alpha\{\delta(\mathbf{k}-\mathbf{K}_0)\exp(-in_0t)+\delta(\mathbf{k}+\mathbf{K}_0)\exp(in_0t)\}\,d\mathbf{k} + \tfrac{1}{2}\beta\{\delta(\mathbf{k}-\mathbf{K}_1)\exp(-in_1t)+\delta(\mathbf{k}+\mathbf{K}_1)\exp(in_1t)\}\,d\mathbf{k}, \quad (5.11)$$

| Primary wave-number | Secondary wave-number | Tertiary wave-numbers | |
|---|---|---|---|
| $\pm\mathbf{K}_0$ | $\pm 2\mathbf{K}_0$ | $\pm 3\mathbf{K}_0$, $\pm\mathbf{K}_0$ | (Stokes wave) |
| $\pm\mathbf{K}_0$ | $\pm 2\mathbf{K}_1$ | $\pm(\mathbf{K}_0 \pm 2\mathbf{K}_1)$ | — |
| $\pm\mathbf{K}_0$ | $\pm(\mathbf{K}_0-\mathbf{K}_1)$ | $\pm(2\mathbf{K}_0-\mathbf{K}_1)$, $\pm\mathbf{K}_1$ | — |
| $\pm\mathbf{K}_0$ | $\pm(\mathbf{K}_0+\mathbf{K}_1)$ | $\pm(2\mathbf{K}_0+\mathbf{K}_1)$, $\pm\mathbf{K}_1$ | — |

(*a*) Primary-secondary interactions

| Primary wave-numbers | | | Tertiary wave-numbers | |
|---|---|---|---|---|
| $\pm\mathbf{K}_0$ | $+\mathbf{K}_0$ | $\pm\mathbf{K}_0$ | $\pm 3\mathbf{K}_0$, $\pm\mathbf{K}_0$ | (Stokes wave) |
| $\pm\mathbf{K}_0$ | $\pm\mathbf{K}_0$ | $\pm\mathbf{K}_1$ | $\pm(2\mathbf{K}_0\pm\mathbf{K}_1)$, $\pm\mathbf{K}_1$ | — |
| $\pm\mathbf{K}_0$ | $\pm\mathbf{K}_1$ | $\pm\mathbf{K}_1$ | $\pm(\mathbf{K}_0\pm 2\mathbf{K}_1)$, $\pm\mathbf{K}_0$ | — |
| $\pm\mathbf{K}_1$ | $\pm\mathbf{K}_1$ | $\pm\mathbf{K}_1$ | $\pm 3\mathbf{K}_1$, $\pm\mathbf{K}_1$ | (Stokes wave) |

(*b*) Triple primary interactions

TABLE 2. Wave-numbers involved in the third-order interactions of two intersecting wave trains. In part (*a*), further possibilities are obtained by interchanging the subscripts.

and the secondary components are, from (4.14), (4.29) and (4.30),

$$\begin{aligned} dB_2(\mathbf{k},t) = {} & \tfrac{1}{4}K_0\alpha^2\{\delta(\mathbf{k}-2\mathbf{K}_0)\exp(-2in_0t)+\delta(\mathbf{k}+2\mathbf{K}_0)\exp(2in_0t)\}\,d\mathbf{k} \\ & + \tfrac{1}{4}K_1\beta^2\{\delta(\mathbf{k}-2\mathbf{K}_1)\exp(-2in_1t)+\delta(\mathbf{k}+2\mathbf{K}_1)\exp(2in_1t)\}\,d\mathbf{k} \\ & + \tfrac{1}{4}\alpha\beta(K_0K_1)^{\frac{1}{2}}C\{\delta(\mathbf{k}-\mathbf{K}_0+\mathbf{K}_1)\exp[-i(n_0-n_1)t] \\ & + \delta(\mathbf{k}+\mathbf{K}_0-\mathbf{K}_1)\exp[i(n_0-n_1)t]\}\,d\mathbf{k} \\ & + \tfrac{1}{4}\alpha\beta(K_0K_1)^{\frac{1}{2}}D\{\delta(\mathbf{k}-\mathbf{K}_0-\mathbf{K}_1)\exp[-i(n_0+n_1)t] \\ & + \delta(\mathbf{k}+\mathbf{K}_0+\mathbf{K}_1)\exp[i(n_0+n_1)t]\}\,d\mathbf{k}, \end{aligned} \quad (5.12)$$

where the functions $C$ and $D$ are as given in (4.32). These expressions, if substituted into the right-hand side of (4.5), would give a total of 256 terms, all of which, fortunately, are not of present interest. The various types of interactions can be classified according to table 2 above. The exponential time factors are not indicated, but in every case the exponent has the same structure as the wave-number vector except that the signs are changed. For example, associated with the contribution at wave-number $2\mathbf{K}_0-\mathbf{K}_1$ is the factor

$$\exp\{-i(2n_0-n_1)t\}.$$

The components of particular interest are those with wave-numbers $\pm(2\mathbf{K}_0\pm\mathbf{K}_1)$ (or the symmetrical type $\pm(\mathbf{K}_0\pm 2\mathbf{K}_1)$). We will first investigate

whether the resonance interaction is possible apart from the special case discussed in the previous section, which requires the existence of real solutions to the equation

$$g\,|2\mathbf{K}_0 \pm \mathbf{K}_1| = (2n_0 \pm n_1)^2, \tag{5.13}$$

where $n_0 = (gK_0)^{\frac{1}{2}}$, $n_1 = (gK_1)^{\frac{1}{2}}$. Making as before, the substitutions

$$\mathbf{K}_0 = (K_0 \sin\gamma_0,\ K_0 \cos\gamma_0),$$
$$\mathbf{K}_1 = (K_1 \sin\gamma_1,\ K_1 \cos\gamma_1),$$

it is found that (5.13) leads to

$$\cos(\gamma_0 - \gamma_1) = \frac{8[\frac{1}{2}(4K_0 + K_1)]}{(4K_0K_1)^{\frac{1}{2}}} \pm \left(\frac{3K_0}{K_1} + 6\right). \tag{5.14}$$

Since, for $K_0 > 0$, $K_1 > 0$,

$$\tfrac{1}{2}(4K_0 + K_1) > (4K_0K_1)^{\frac{1}{2}},$$

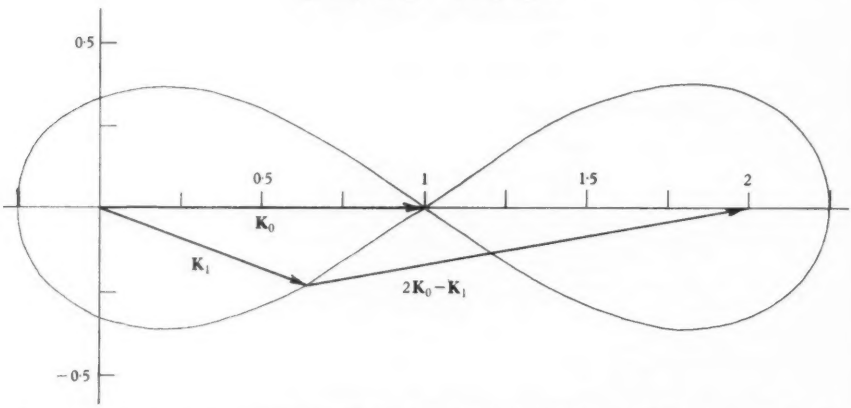


FIGURE 4. The resonance loop for third-order binary interactions. The wave-number $\mathbf{K}_1$ interacts with the bound secondary component associated with $\mathbf{K}_0$ to produce a developing component of wave-number $2\mathbf{K}_0 - \mathbf{K}_1$. The arrows represent the directions of propagation.

it appears that resonant interactions *are* possible, but only for certain pairs of the *difference* wave-numbers $\pm(2\mathbf{K}_0 - \mathbf{K}_1)$ (or for $\pm(\mathbf{K}_0 - 2\mathbf{K}_1)$) for which the negative sign in (5.14) is relevant. Figure 4 represents the function

$$\cos(\gamma_0 - \gamma_1) = \frac{2(\eta + 4)}{\sqrt{\eta}} - \frac{3}{\eta} - 6, \tag{5.15}$$

where $\eta = K_1/K_0$, and illustrates the primary wave-numbers $\mathbf{K}_1$ which can produce a resonant interaction with the secondary component of given wave-number $2\mathbf{K}_0$, resulting in a continuing energy transfer to the wave-number $\pm(2\mathbf{K}_0 - \mathbf{K}_1)$. It can readily be confirmed that these resonant tertiary wave-numbers do not coincide with any of the secondary wave-numbers generated, for this would require

$$2\mathbf{K}_0 - \mathbf{K}_1 = \pm 2\mathbf{K}_0,\ \pm 2\mathbf{K}_1,\ \pm(\mathbf{K}_0 + \mathbf{K}_1) \quad \text{or} \quad \pm(\mathbf{K}_0 - \mathbf{K}_1),$$

or equivalently $\mathbf{K}_1 = -2\mathbf{K}_0,\ 0,\ \frac{1}{2}\mathbf{K}_0,\ \frac{2}{3}\mathbf{K}_0,\ \frac{3}{2}\mathbf{K}_0,\ 4\mathbf{K}_0$ or $\infty$,

none of which lie on the resonance loop of figure 4. The physical reasons for this type of energy transfer have been described in § 4.2. Although it was not possible within the second approximation, it appears that, within the third approximation it is.

Having established the existence of the resonant type of continuing potential energy transfer, it only remains for us to estimate the order of magnitude of the coefficient $A$ in the second equation of the set (4.26) to provide an estimate of the characteristic interaction time, or the development time of the growing tertiary component. Selecting out the relevant contributions as before, it is found that the Fourier coefficient at the wave-number $2\mathbf{K}_0-\mathbf{K}_1$ is given by the solution of

$$\left\{\frac{d^2}{dt^2}+|2\mathbf{K}_0-\mathbf{K}_1|\,g\right\}B_2(2\mathbf{K}_0-\mathbf{K}_1,t)$$
$$=\tfrac{1}{8}\,|2\mathbf{K}_0-\mathbf{K}_1|\,(K_0K_1)^{\frac{1}{2}}\,n_0n_1\alpha^2\beta f(\eta,\gamma)\exp\{-i(2n_0-n_1)t\}, \quad (5.16)$$

where $\eta = K_1/K_0$ and $\gamma$ is the angle between the two interacting wave-numbers. The function $f(\eta,\gamma)$ is given by

$$\begin{aligned}
f(\eta,\gamma) = {} & (K_0/K_1)^{\frac{1}{2}}\{C(\mathbf{K}_0,\mathbf{K}_1)\,[H_1(2\mathbf{K}_0-\mathbf{K}_1,\mathbf{K}_0-\mathbf{K}_1)+H_2(2\mathbf{K}_0-\mathbf{K}_1,\mathbf{K}_0-\mathbf{K}_1)\\
& +H_1(2\mathbf{K}_0-\mathbf{K}_1,\mathbf{K}_0)+H_2(2\mathbf{K}_0-\mathbf{K}_1,\mathbf{K}_0)]+4(K_0/K_1)^{\frac{1}{2}}\,H_1(2\mathbf{K}_0-\mathbf{K}_1,-\mathbf{K}_1)\\
& -(K_0K_1)^{-\frac{1}{2}}\,[H_3(2\mathbf{K}_0-\mathbf{K}_1,-\mathbf{K}_1,\mathbf{K}_0)+H_3(2\mathbf{K}_0-\mathbf{K}_1,\mathbf{K}_0,-\mathbf{K}_1)\\
& +H_4(2\mathbf{K}_0-\mathbf{K}_1,\mathbf{K}_0,-\mathbf{K}_1)]\}\\
& +2(K_0/K_1)^{\frac{1}{2}}\,[H_2(2\mathbf{K}_0-\mathbf{K}_1,2\mathbf{K}_0)+H_2(2\mathbf{K}_0-\mathbf{K}_1,-\mathbf{K}_1)]\\
& -C(\mathbf{K}_0,\mathbf{K}_1)\,[2H_1(2\mathbf{K}_0-\mathbf{K}_1,\mathbf{K}_0)+H_2(2\mathbf{K}_0-\mathbf{K}_1,\mathbf{K}_0-\mathbf{K}_1)\\
& +H_2(2\mathbf{K}_0-\mathbf{K}_1,\mathbf{K}_0)]\\
& -(K_0K_1)^{-\frac{1}{2}}\,[H_4(2\mathbf{K}_0-\mathbf{K}_1,\mathbf{K}_0,\mathbf{K}_0)+H_4(2\mathbf{K}_0-\mathbf{K}_1,-\mathbf{K}_1,\mathbf{K}_0)]\\
& +(K_1/K_0)^{\frac{1}{2}}\{(K_0/K_1)^{\frac{1}{2}}\,H_1(2\mathbf{K}_0-\mathbf{K}_1,2\mathbf{K}_0)+C(\mathbf{K}_0,\mathbf{K}_1)\,H_1(2\mathbf{K}_0-\mathbf{K}_1,\mathbf{K}_0)\\
& -(K_0K_1)^{-\frac{1}{2}}\,H_3(2\mathbf{K}_0-\mathbf{K}_1,\mathbf{K}_0,\mathbf{K}_0)\}, \qquad (5.17)
\end{aligned}$$

where the function $C$ is as given in (4.32), and the $H$ functions are specified by (3.20) to (3.23). The equation for the wave-number $-(2\mathbf{K}_0-\mathbf{K}_1)$ is similar (since all the terms in $f(\eta,\gamma)$ are invariant with respect to changes in the signs of all wave-numbers) except that the exponential factor is $\exp\{i(2n_0-n_1)t\}$. When

$$g\,|2\mathbf{K}_0-\mathbf{K}_1| = (2n_0-n_1)^2, \qquad (5.18)$$

the solution to equation (5.16) is

$$B_3\{\pm(2\mathbf{K}_0-\mathbf{K}_1),t\} = \mp\tfrac{1}{16}i\alpha(K_0\alpha)\,(K_1\beta)\,(2n_0-n_1)\,t\,.\,f(\eta,\gamma)\exp\{\mp i(2n_0-n_1)t\}, \qquad (5.19)$$

so that the growing tertiary component is

$$\xi_3(\mathbf{x},t) = \tfrac{1}{8}\alpha f(\eta,\gamma)\,(K_0\alpha)\,(K_1\beta)\,(2n_0-n_1)\,t\,.\sin\{(2\mathbf{K}_0-\mathbf{K}_1).\mathbf{x}-(2n_0-n_1)t\}. \qquad (5.20)$$

The numerical value of the function $f(\eta,\gamma)$ for wave-numbers such that (5.18) is satisfied could be computed from (5.17), but this would be an extremely tedious operation. It is sufficient for our purpose to know its order of magnitude only. We do already know (either by comparison with the first term on the right-hand side of (5.8), or by direct calculation from (5.17)) that when $\mathbf{K}_0=\mathbf{K}_1, f(\eta,\gamma)=2$.

Since, on inspection of the forms of the functions $H_1, \ldots, H_4$, it is evident that $f(\eta, \gamma)$ has no singularities, it is safe to assume that this function is of order unity for all wave-number pairs given by the crossed loop of figure 4.

We can therefore conclude that the characteristic development time of the resonant tertiary interactions, or the time for the amplitude to become comparable with that of the primary, is of order

$$T = (K_0 \alpha)^{-1} (K_1 \beta)^{-1} (2n_0 - n_1)^{-1}, \tag{5.21}$$

that is, of order of the wave period of the tertiary component divided by the product of the maximum slopes of the primary waves. As the tertiary component develops, the primary components of course begin to subside as the energy is transferred to the tertiary components. This decay is described by the presence of tertiary terms of wave-number $\pm \mathbf{K}_0$ and $\pm \mathbf{K}_1$ in the last two rows of table 2*a*, and the middle two rows of table 2*b*, and can be calculated in a manner analogous to that above.

In the light of this analysis, the exceptional nature of the Stokes permanent wave is perhaps more evident. Figure 4 shows that this is the *only* situation in which the resonant tertiary wave-number is equal to that of the primary wave, and so provides the only case in which the tertiary interactions can be interpreted as a change in phase velocity of the primary wave. In all other binary interactions, the wave-number of the resonant tertiary component is different from that of either primary, so that a *new* Fourier component of the wave field develops in time.

Finally, it might be remarked that the triple interactions among three different primary waves can also give rise to a developing tertiary component with a new wave-number. The situation discussed above is clearly a special case of this, when two of the primary wave-numbers coalesce. The analysis of the more general case is, however, complicated and little of conceptual value is to be gained from it.

## 6. Secondary interactions in water at finite depth

We have found that, in water of infinite depth, if the wave-number and frequency of the interaction term correspond to the wave-number and frequency of a *free* infinitesimal wave, then we have a resonant situation in which the amplitude of the interaction wave increases linearly with time. The interaction wave-number is the vector sum or difference of the primary wave-numbers, and the frequency is the sum or difference of the primary frequencies. The simplicity of this criterion and of its physical interpretation makes it possible to anticipate the qualitative nature of the interactions when the water depth is not necessarily large compared with any of the wavelengths involved.

The detailed analysis of this case is very complicated, but the form of the basic equations is not changed. Two primary wave-components of wave-number $\mathbf{K}_0$ and $\mathbf{K}_1$ give rise to an interaction term with wave-numbers $\pm(\mathbf{K}_0 + \mathbf{K}_1)$, $\pm(\mathbf{K}_0 - \mathbf{K}_1)$ and frequencies $n_0 + n_1$ and $n_0 - n_1$, where

$$\left.\begin{aligned} n_0 &= \{gK_0 \tanh K_0 d\}^{\frac{1}{2}}, \\ n_1 &= \{gK_1 \tanh K_1 d\}^{\frac{1}{2}}, \end{aligned}\right\} \tag{6.1}$$

where $d$ is the mean water depth. If

$$(n_0 \pm n_1)^2 = g\,|\mathbf{K}_0 \pm \mathbf{K}_1| \tanh\,[|\mathbf{K}_0 \pm \mathbf{K}_1|\,d], \tag{6.2}$$

then resonant interactions can occur for the secondary components. The question of the existence or otherwise of real solutions to (6.2) can be most easily established by the following geometrical argument.

In figure 5, the curved line represents the function

$$\left(\frac{d}{g}\right)^{\frac{1}{2}} n = \{Kd \tanh Kd\}^{\frac{1}{2}},$$

specifying the frequency of free infinitesimal surface waves in water of mean depth $d$ as a function of wave-number $K$. The slope of this curve decreases monotonically with increasing $K$, except when $Kd \ll 1$, when it is constant. Suppose we

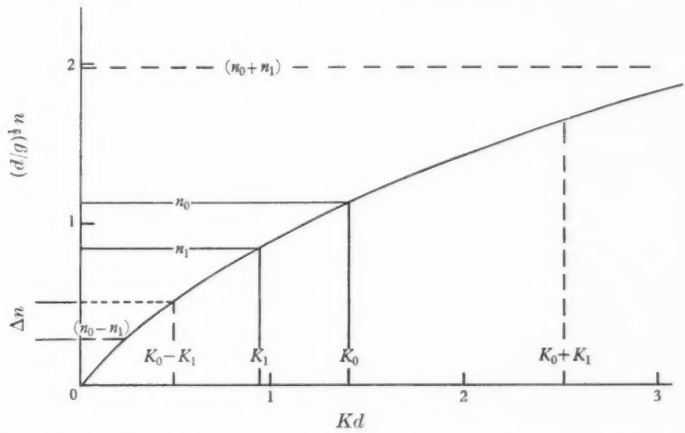


FIGURE 5. Second-order wave-numbers and frequencies in water of finite depth.

have two primary components of wave-numbers $\mathbf{K}_0$ and $\mathbf{K}_1$ and frequencies $n_0$ and $n_1$. The interaction frequencies are therefore $n_0+n_1$ and $n_0-n_1$ and the magnitudes of the interaction wave-numbers lie within the limits $|K_0+K_1|$ and $|K_0-K_1|$, whatever the angle of intersection of the primary waves. If the frequencies $n_0+n_1$ or $n_0-n_1$ correspond to wave-numbers lying within that range, then a resonance is possible. It is clear from figure 5, however, that in general this is not so, since the curve is concave downwards and the difference frequency corresponds to a wave-number less than $|K_0-K_1|$ and the sum frequency to a wave-number greater than $|K_0+K_1|$. A trivial exception is given when $\mathbf{K}_0 = \mathbf{K}_1$; the difference terms give the zero frequency, zero wave-number case discussed above.

More interesting is the case when for all wave-numbers $\mathbf{K}$ concerned, $Kd \ll 1$. In this shallow water case,† the phase velocity of an infinitesimal wave is in-

† Caution must be exercised lest the small amplitude approximation be pressed too far in shallow water. Stokes (1847) showed that this approximation is valid only when $\alpha K \ll (Kd)^3$, so that when $Kd$ is small, $\alpha K$ is required to be very small indeed.

dependent of the wave-number so that the dispersive nature of the waves is lost and the frequency curve reduces to a straight line (figure 6). It is evident that the sum and difference frequencies correspond to sum and difference wave-numbers at the ends of the permissible range, which are attained when $\mathbf{K}_0$ and $\mathbf{K}_1$ are parallel. Thus, in very shallow water, any pair of parallel wave-numbers will produce resonant interactions in the sense described above. This may also be deduced directly from (6.2), since

$$\tanh\left[|\mathbf{K}_0 \pm \mathbf{K}_1|\, d\right] \simeq |\mathbf{K}_0 + \mathbf{K}_1|\, d$$

under these circumstances.

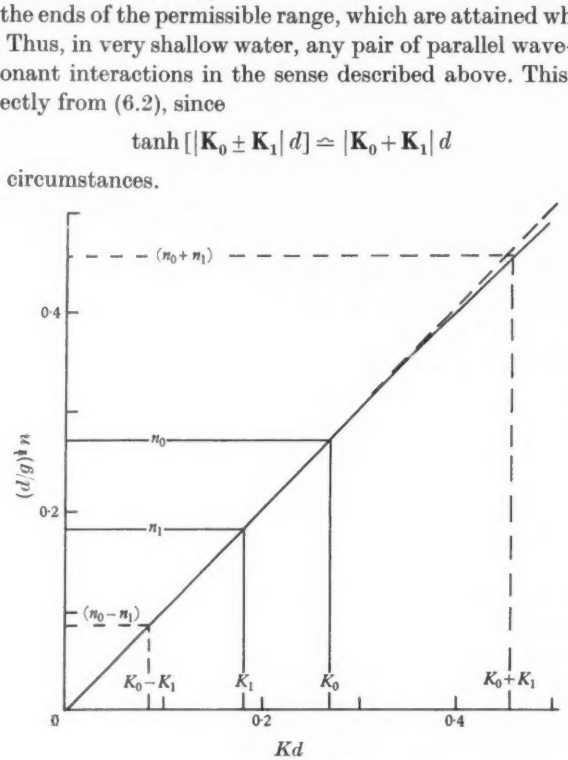


FIGURE 6. Second-order wave-numbers and frequencies in very shallow water.

It may also be interesting to notice that if the difference frequency (say) is only slightly smaller than the frequency of a free surface wave of the difference wave-number, then there is no resonance but, for the first equation of the set (4.26), the amplitude of the bound secondary component is inversely proportional to this frequency difference (shown as $\Delta n$ in figure 5). If $|\mathbf{K}_0 - \mathbf{K}_1|\, d$ is of order unity or a little less, $\Delta n$ may be small, so that the amplitude of the secondary waves, though bounded in time, may be large and the second-order interactions may assume considerable dynamical significance. The tendency for waves to break over shoals, indicating appreciable non-linear interaction, is consistent with this general conclusion.

## 7. Conclusions

The principal result of this analysis is the demonstration that, although the tertiary interactions among wave components are given by a perturbation term that is algebraically smaller than that representing the secondary interactions,

their cumulative dynamical effect is much more profound because of the existence of resonant wave-numbers whose amplitude grows with time. This implies that, in the development of a dynamical theory to describe a finite amplitude random gravity wave field, the tertiary interactions are essential, and any theory in which they are neglected will ignore the dominant mechanism of energy transfer among the wave components.

The results, however, do have immediate relevance to the question of the interaction between a swell and a local storm. Suppose that swell with wave-number $\mathbf{K}_0$ (figure 4) is generated by a distant disturbance on the ocean and passes through a storm area. If the wave-numbers $\mathbf{K}_1$ of the locally generated waves lie along the crossed loop of figure 4, then appreciable components with wave-number $2\mathbf{K}_0 - \mathbf{K}_1$ may be generated by the resonant interaction, and would appear as a 'ghost' to an observation station. The wave-number and direction of this ghost component may be very different from the dominant contributions to the storm or the swell, and should be readily distinguishable from components of the swell scattered by the turbulence in the water near the storm centre (Phillips 1959).

This work was supported by the Office of Naval Research under Contract Nonr 248 (56).

## REFERENCES

Batchelor, G. K. 1953 *The Theory of Homogeneous Turbulence.* Cambridge University Press.

Lamb, H. 1932 *Hydrodynamics.* Cambridge University Press.

Lighthill, M. J. 1958 *Fourier Analysis and Generalised Functions.* Cambridge University Press.

Longuet-Higgins, M. S. & Stewart, R. W. 1960 *J. Fluid Mech.* **8**, 565.

Miles, J. W. 1957 *J. Fluid Mech.* **3**, 185–204.

Miles, J. W. 1959 *J. Fluid Mech.* **6**, 568–82.

Phillips, O. M. 1957 *J. Fluid Mech.* **2**, 417–45.

Phillips, O. M. 1958*a* *J. Fluid Mech.* **4**, 426–33.

Phillips, O. M. 1958*b* *Proc. 3rd U.S. Congr. Appl. Mech.* pp. 785–9.

Phillips, O. M. 1959 *J. Fluid Mech.* **5**, 177–92.

Stokes, G. G. 1847 *Trans. Camb. Phil. Soc.* **8**, 441.

# Deposition of a viscous fluid on a plane surface

By G. I. TAYLOR
Cavendish Laboratory, Cambridge

(Received 28 April 1960)

Two mechanisms by which a viscous fluid can be deposited on a plane surface are described. Measurement of the thickness of the deposit are compared with calculated values. It is found that the two agree within rather wide limits of experimental error provided the effect of surface tension can be neglected, and the conditions under which this is legitimate are discussed.

## The paint brush

There are many ways in which a viscous fluid can be deposited on a plane surface. Perhaps the best known is by means of a paint brush. This consists of a number of flexible cylinders or hairs between which the fluid lies. As these hairs are dragged over the surface they lie with their axes parallel to the direction of motion and the paint is dragged through between them by tangential stress. The fluid dragged out by tangential stress acting at one side of the brush on the fluid surrounding the outermost layer of hairs must be replaced by fluid flowing transversely from the interstices between hairs further from the outer layer. This process can be understood qualitatively but to describe it mathematically is difficult. For this reason it seemed worthwhile to describe an ideal structure which would deliver fluid at a calculable rate even though it has no practical use in the art of painting.

The simplest is a plate sliding at height $h_0$ over a fixed parallel plane. If fluid is supplied at atmospheric pressure between the leading edge of the moving plate and the fixed plane, and if the length of the plane is great compared with $h_0$, the pressure in the fluid will be constant and a film of depth $\frac{1}{2}h_0$ will be left behind on the fixed plane.

If the moving plate is replaced by a portion of a cylindrical surface of any cross-section moving parallel to the generators it is possible to calculate the volume of fluid left behind. Two examples will be given.

### *Parallel plates*

An arrangement by which plates spaced at distance $2d$ apart could be made to slide on their edges over a horizontal plane is shown in figure 1. Taking an origin in the surface of the horizontal plane midway between two vertical plates, the co-ordinate $x$ is in the direction of motion, i.e. parallel to the plates and $z$ is vertical. The velocity $u$ is parallel to the direction of motion at all points and satisfies

$$\frac{\partial^2 u}{\partial y^2}+\frac{\partial^2 u}{\partial z^2}=0. \tag{1}$$

It is convenient to take $u$ as the velocity relative to the moving plates, so that the boundary conditions are

$$u = 0 \quad \text{at} \quad y = \pm d \quad \text{and} \quad u = U \quad \text{at} \quad z = 0.$$

The solution of (1) which satisfies these conditions is

$$u = \frac{4U}{\pi} \sum_0^\infty \frac{(-1)^n}{2n+1} \cos \frac{(2n+1)\pi y}{d} e^{-(2n+1)\pi z/2d}. \tag{2}$$

The total volume deposited on the horizontal plane per second from the fluid contained between each pair of plates is

$$Q = \int_{-d}^{+d} \int_0^\infty u \, dz \, dy = \frac{32Ud^2}{\pi^3} \sum_0^\infty \frac{1}{(2n+1)^3} = 1{\cdot}085Ud^2. \tag{3}$$

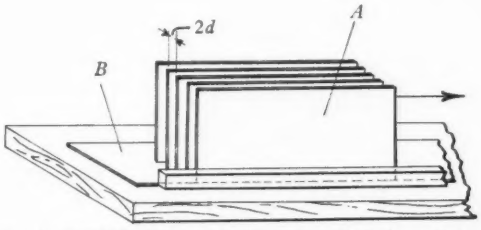


FIGURE 1. *A*, parallel plates; *B*, sheet on which deposit is collected.

*Semicircular grooves*

In the above example the way in which the fluid emerges from the spaces between the parallel plates was not considered nor was the manner in which the fluid entered them. The effect of gravity and of possible vertical motion between the plates was also assumed to be negligible. To avoid these uncertainties a 'mathematical paint brush' was designed in which the supply of fluid occurred only at the forward end of the channels which regulated the flow. A number of semicircular grooves were cut in the plane base of a Perspex block. These grooves ended at the supply end in a chamber large enough to ensure that the fluid was supplied at atmospheric pressure. There were 5 grooves each of radius 0·1 cm and they extend from the rear end of the block through a length of 6·1 cm to a cavity from which the fluid was supplied. The method of experiment is indicated in figure 2. The block *A* was placed on a strip of very thin metal foil *B* which had been pressed on to a steel surface plate. The block was charged with a viscous fluid, usually glycerine, through the hole *C* which led into the supply chamber. No fluid could escape except through the grooves. The block rested against a guide so that it could move parallel to the grooves while depositing fluid on the foil. The foil was then peeled off the surface plate and a section cut from the middle using a photographic trimming knife. This section was then weighed with its deposit. After removing the deposit it was weighed again.

In a series of such experiments made with glycerine the weights deposited per cm of foil varied from 0·0422 to 0·0467 g. The mean of six runs was 0·0437 g and the corresponding volume was 0·0347 c.c. Thus the experimental value of

the volume deposited per cm from each of the five grooves was 0·00694 c.c. The calculation of the volume deposited from a semicircular groove of radius $a$ was made in the same way as for the parallel plates, giving the result that the volume deposited per unit length of run was $2a^2/\pi$.* When $a = 0{\cdot}1$ cm, we have $2a^2/\pi = 0{\cdot}00638$. This is 8 % smaller than the observed value 0·00694. The discrepancy may well be due to small errors in the shaping of the grooves or to slight undetected variations in the flatness of the surface of the foil. The neglect in the calculation of the small pressure gradient along the grooves may give rise to a small error. This error, however, could be calculated and it was much less than the 8 % discrepancy, though its contribution was to increase the deposit above the calculated value $2a^2/\pi$.

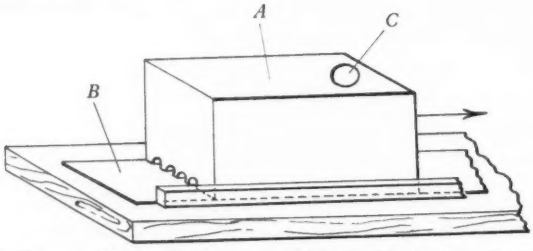


FIGURE 2. *A*, Perspex block; *B*, sheet on which fluid is deposited; *C*, filling hole.

## Porous rollers

Another way in which a viscous fluid can be deposited on a plane surface under conditions for which the flow can be described mathematically is by the use of a porous roller. This method is used by printers and sometimes by house-painters. The flow of fluid in this case has been discussed mathematically by Taylor & Miller (1956) though the connexion between the thickness of the layer deposited and the hydraulic resistance of the porous cylinder is not contained explicitly in their paper. They express their results in non-dimensional co-ordinates $x_1$ and $y$ but here $p_1$ is substituted for their $y$ as a symbol whose meaning is more obvious and

$$x_1 = x(96\kappa R^3)^{-\frac{1}{4}}, \quad p_1 = -\frac{p\kappa R}{\mu U}(96\kappa R^3)^{-\frac{1}{4}}. \tag{4}$$

Here $R$ is the radius of the cylinder, $p$ is the pressure in the fluid at distance $x$ from the point of contact, $U$ is the velocity of the roller, $\mu$ is the viscosity of the fluid and $\kappa$ is a coefficient of the dimensions of a length which occurs when Darcy's law connecting the rate of flow through a porous sheet, $W$, with $p$, is expressed in the form

$$W = \kappa p/\mu. \tag{5}$$

* Later Dr F. Ursell pointed out that the calculation could have been much simplified, because the solution of $\nabla^2 u = 0$ which satisfies $u = 0$ on the circumference and $u = U$ on the diameter is

$$u = U\left(\frac{2\theta}{\pi} - 1\right),$$

where $\theta$ is the angle subtended at the point where the velocity is $u$ by the two ends of the diameter.

Thus $\kappa$ is not the same as that which would be suitable for use with a porous medium, for the latter would be of dimensions (length)$^2$. The total rate of flow through unit length of the porous cylinder is

$$Q = \int_0^\infty W\,dx, \tag{6}$$

and on substituting from (4) and (5) we find

$$Q = (96\kappa R)^{\frac{1}{2}}\,U \int_0^\infty p_1\,dx_1. \tag{7}$$

The computed relationship between $p_1$ and $x_1$, is given in the form of a curve (figure 3, p. 134 of Taylor & Miller 1956). By graphical integration over the main part of the curve and the use of the asymptotic expression for $p_1$ at large values of $x_1$, $\int_0^\infty p_1\,dx_1$ was found to be 0·302 so that

$$Q = 2{\cdot}96U(\kappa R)^{\frac{1}{2}}. \tag{8}$$

This value for $Q$ is the value which would apply if the whole space between the porous cylinder and the plane on which it rolls were filled with fluid. In fact the fluid only passes through the porous cylindrical surface when there is suction and, at a certain point which my analysis could not determine, the flow separates at a meniscus, some fluid remaining on the flat plate and some adhering to the cylinder. Beyond this meniscus there is no further suction. In the absence of further evidence it seems that the meniscus is likely to divide the fluid equally into two streams as it would if the cylindrical surface had not been porous. Assuming this to be the case the thickness $t$ of the layer deposited would be

$$t = \frac{1}{2}\frac{Q}{U} = 1{\cdot}48(\kappa R)^{\frac{1}{2}}. \tag{9}$$

### *Measurements*

A perforated cylinder 21 cm long and 13·5 cm in diameter was made by wrapping a perforated sheet round some circular disks. These disks had central holes to permit the entry of the fluid to the inner surface of the cylinder. Two layers of flannel were wrapped round the cylinder and the seam pulled tight. The fabric was bent over the ends of the cylinder, sewn through the end perforations and sealed on the inner side to prevent fluid from escaping without passing through the flannel.

Two methods were used to measure $t$. The first was to roll the cylinder on a sheet of plate glass and then blot up the deposit with weighed sheets of blotting paper which were then rapidly enclosed in a container to prevent evaporation and weighed again with the absorbed fluid. The second, indicated in figure 3, was to use the technique employed in the experiments with the 'idealized' paint brushes described earlier, but since the thickness of the film deposited was much less than before, larger pieces of foil had to be used. Even so the blotting-paper technique proved to be more satisfactory because it was difficult to prevent the foil from being pulled off the plate on which it had been pressed as the roller

passed over it. The porous roller was constructed in the manner described in order to make possible a comparison with the theoretical calculation, but even so the range of fluids for which that comparison could be made was limited.

When water was used the thickness left on the plate was sometimes very small and it was concluded that on these occasions one of the conditions assumed in the theory, that the fluid filled the space between plate and roller, was not valid and cavitation occurred. More consistent results were obtained when more viscous fluids were used, but when fluids as viscous as pure glycerine were used the suction was so great at any but very low speeds that there was danger that the flannel would leave the perforated surface on which it was stretched and thus upset the geometry of the flow.

Some of the measurements are given in table 1.

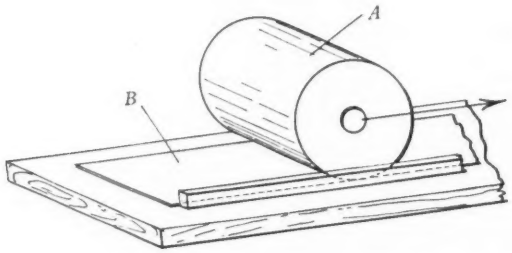


FIGURE 3. $A$, porous roller; $B$, sheet on which fluid is deposited.

| Liquid | $\mu$ (g cm$^{-1}$ sec$^{-1}$) | Film thickness ($10^{-3}$ cm) | Mean |
|---|---|---|---|
| 50 % glycerine | 0·085 | 2·39, 2·12, 1·86, 2·6, 2·44 | 2·28 |
| 30 % glycerine | 0·030 | 2·25, 1·67, 1·95, 1·77 | 1·91 |
| Water | 0·011 | 0·89, 1·28, 0·64, 1·21, 0·73 | 0·95 |

TABLE 1. Measurements of thickness of film deposited by roller.

*Measurements of $\kappa$*

It seemed desirable to measure $\kappa$ with the flannel stretched on the perforated cylinder. The cylinder was therefore set with its axis vertical in a cylinderical vessel from which the outflow could be measured. The height $H_2$ of the fluid outside the cylinder, as well as the difference in height $H_1$ between the fluid inside and outside the porous surface, was measured. Water was used in this experiment. The volume $Q'$ flowing through the porous cylinder per second was taken as being given by

$$Q' = \frac{2\pi R\kappa}{\mu} H_1(H_2 + \tfrac{1}{2}H_1). \tag{10}$$

It was found that when the measured values of $H_1$, $H_2$, and $Q'$ were inserted in (10) the values of $\kappa$ so found ranged from $1{\cdot}5 \times 10^{-7}$ to $3{\cdot}5 \times 10^{-7}$ cm. It seems from this large variation in $\kappa$ that flannel is not a very suitable porous material for this kind of experiment. It may be that the flow affects the geometry of the fibre structure of the flannel.

*Comparison with theory*

The theoretical values for the thickness of the deposited layer found by inserting these limiting values $1{\cdot}5 \times 10^{-7}$ and $3{\cdot}5 \times 10^{-7}$ for $\kappa$ in (9) are $1{\cdot}5 \times 10^{-3}$ and $2{\cdot}3 \times 10^{-3}$ cm. Comparison of these with the observed values given in table 1 shows that except in the case of water the agreement with the theoretical analysis is within the limit of experimental error. A possible explanation of the discrepancy in the case of water is given later.

## Effect of surface tension at the air-fluid interface

In the cases which have so far been discussed it has been tacitly assumed that the surface tension produces negligible effects. This is justifiable if the pressures due to the curvature of the free surface are small compared with those which would produce an appreciable change in the flow. In the case of the 'idealized paint brush', since the curvature of the free surface must be of the order $1/a$ (or $1/d$) for the two cases considered the pressure change on passing through the meniscus is of order $T/a$, where $T$ is the surface tension. The viscous stresses are of order $\mu U/a$. It might therefore be thought that the analysis is only realistic when $T/\mu U$ is small. This is not the case however. Taking the case illustrated in figure 2, the change in $Q$ due to change in pressure $\delta p$ between the ends of the grooves is of order $a^4 \delta p/\mu L$, where $L$ is the length of the grooves. $Q$ is of order $a^2 U$, so that the condition that a change $\delta p$ will make a negligible change in $Q$ is that $a^2 \delta p/\mu U L$ shall be small. If $\delta p$ is of order $T/a$, this condition is that $Ta/\mu U L$ shall be small.

When the measurements were made with the apparatus shown in figure 2, the influence of the surface tension was not fully appreciated so that accurate measurements of $U$ were not made. They were, however, of order $U = 4$ cm/s. At this speed, and with glycerine, for which $\mu = 9\,\mathrm{g\,cm^{-1}\,sec^{-1}}$ and $T = 63\,\mathrm{g\,sec^{-2}}$, $T/\mu U = 1{\cdot}7$. This is not small, but the length of the grooves was 6 cm while the radius was 0·1 cm, so that $Ta/\mu U L = 0{\cdot}03$ and thus was sufficiently small to warrant an expectation that the calculated value of $Q$ (namely, $2a^2/\pi$) might be realized. When water was used instead of glycerine, much thinner layers were deposited.

Similar considerations apply to the porous roller. The calculations (Taylor & Miller 1956) were made assuming that the whole field of flow was flooded. In fact a meniscus or interface formed itself and divided the fluid into two streams one of which remains on the plane surface and the other is carried round on the outer surface of the roller. The meniscus is not likely to affect the distribution of suction between plane and roller unless it establishes itself within the range where the suction is appreciable. A suitable criterion for estimating whether the meniscus will have appreciable effect is to imagine that the meniscus establishes itself at the point where the calculated suction is equal to the pressure rise on passing through the meniscus due to surface tension. If this point is in the range where the suction is small compared with its maximum value, then it would not be expected to make an appreciable change in the value of $Q$.

The suction at a distance $x$ from the point of contact of roller and plane is given (Taylor & Miller 1956, p. 135) by the equation (4) and the relationship between the non-dimensional quantities $p_1$ and $x_1$ is shown in figure 3 of that paper. If the radius of curvature of the meniscus is taken as half of the distance between plane and roller at distance $x$, the meniscus will establish itself near the point where

$$\frac{4TR}{x^2} = -p. \tag{11}$$

Substitution for $x$ and $p$ from (4) and (11) gives

$$p_1 x_1^2 = \frac{T}{\mu U}(96)^{-\frac{1}{3}}\left(\frac{\kappa}{R}\right)^{\frac{1}{3}}. \tag{12}$$

When $x_1 > 1$ the asymptotic form of Taylor & Miller's expression may be used. This is

$$p_1 x_1^3 \sim \tfrac{1}{6}. \tag{13}$$

Dividing (13) by (12), an approximate value for the position of the meniscus is

$$x_1 \sim 5{\cdot}1\left(\frac{\mu U}{T}\right)\left(\frac{R}{\kappa}\right)^{\frac{1}{3}}, \tag{14}$$

where 5·1 is the approximate value of $(96)^{\frac{1}{3}}(\frac{1}{6})$.

When therefore the value of $x_1$ calculated from (14) is larger than unity, so that the corresponding value of $p_1$ is small compared with its maximum value 0·38, agreement may be expected between Taylor & Miller's calculation and the measured thickness of the deposited film of fluid. If the value calculated using (14) is less than unity the boundary condition used by Taylor & Miller in their calculation is not valid, so that agreement would not be expected. Taking values appropriate to the apparatus described, namely, $R = 6{\cdot}9$ cm and $\kappa = 2{\cdot}5 \times 10^{-7}$ cm, the value of $x_1$ at the meniscus was, according to (13),

$$x_1 \sim 3{\cdot}7 \times 10^2(\mu U/T). \tag{15}$$

In the experiments $U$ was about 3 cm/sec and $T = 62\,\mathrm{g\,sec^{-2}}$. When 50% glycerine for which $\mu = 0{\cdot}085$ was used, $\mu U/T = 4{\cdot}1 \times 10^{-3}$ so that the value of $x_1$ at the meniscus was $(3{\cdot}7 \times 10^2)(4{\cdot}1 \times 10^{-3}) = 1{\cdot}5$. The corresponding value of $p_1$, namely, $(1{\cdot}5)^3/6$, was 0·056. This is well below the maximum value 0·378 which occurs at $x_1 = 0{\cdot}43$ (Taylor & Miller 1956) so that little difference would be expected between the amount deposited when the suction region was curtailed by a meniscus and the amount which would pass through the porous roller if the space between it and the plane were flooded.

When the working fluid is water, for which $\mu = 0{\cdot}011$ and $T = 73$ in c.g.s. units, the corresponding value of $x_1$ according to (15) would be 0·17, which is even below the value $x_1 = 0{\cdot}43$ which corresponds with the maximum value of $p_1$. Under these conditions where the suction at the meniscus is not small compared with the maximum suction, the boundary condition used by Taylor & Miller is not even approximately valid, so that the lack of agreement between the measured and calculated thickness of the deposit is understandable.

## REFERENCE

Taylor, G. I. & Miller, J. C. P. 1956 *Quart. J. Mech. Appl. Math.* **9**, 129.

# Experiments on the effect of suction on the flow due to a rotating disk

By N. GREGORY AND W. S. WALKER
Aerodynamics Division, National Physical Laboratory, Teddington

(Received 8 April 1960)

The stability and transition Reynolds numbers for the flow due to a disk rotating in still air were increased by low rates of suction through either a woven wire-cloth or a slitted surface. Observations on the slitted disk at rotational speeds between 550 and 1250 r.p.m. showed that the critical value of the Reynolds number $r^2\omega/\nu$ for instability increased from about 135,000 without suction to nearly 250,000 for a value of the suction parameter $a$ of 0·4. The corresponding values for transition increased from about 275,000 to about 400,000. A given increase in stability Reynolds number required about 75% more suction than that theoretically predicted for uniform distributed suction, a satisfactory result in view of the limitations of the apparatus.

At higher rates of suction ($0{\cdot}4 < a < 1{\cdot}6$), the reduction in secondary flow allowed transverse turbulent contamination to spread inwards from the rim. Consequently the vortices associated with secondary-flow instability were not found, though disturbances of larger wavelength appeared. Intermittent turbulent flow was spread over a much larger region of the disk and no laminar flow could be obtained above a Reynolds number of 400,000. Owing to this feature of the flow, it was not possible to extend laminar flow to values of the unit Reynolds number (ratio of stream velocity to kinematic viscosity) corresponding to flight conditions on a swept-back wing. It is concluded that the rotating disk is not a satisfactory tool for the investigation of the effects of suction on secondary-flow instabilities such as arise in the case of a swept-back wing, or for the testing of suction surfaces.

## 1. Introduction

Transition to turbulence in the flow over a smooth disk rotating in still air results from the instability of a secondary-flow profile, as in the flow over a swept-back wing. This instability has been discussed by Gregory, Stuart & Walker (1955).

In the case of a swept-back wing, boundary-layer control by suction should extend the laminar flow range by reducing the magnitude of the secondary-flow velocity, by decreasing the thickness of the boundary layer and by altering the secondary-flow profile to one that is inherently more stable. In the case of a rotating disk, however, this last alleviation would not be expected to occur, as Stuart (1954) has shown theoretically that there is little change in the shape of the velocity profiles with uniform distributed suction.

Attempts to increase the extent of laminar flow on a disk by suction through a woven wire-cloth surface have previously been described by the authors in detail (1953). The present paper briefly refers to this work and reports additional tests with a slitted surface. It was hoped that the tests would prove of value in connexion with the application of a similar surface to a laminar flow swept-back wing, but the difficulties met with earlier in extending laminar flow on a rotating disk were again encountered. This time, however, the difficulties are shown to be fundamental to the disk flow and not to be due to the nature of the porous surface.

## 2. Apparatus

The basic disk consisted of a slab of dural 3 ft. in diameter, perforated with a large number of $\frac{1}{2}$ in. diameter holes arranged in concentric circles. On one side of the disk a series of concentric narrow protruding lands, machined from the solid, separated each row of holes and held the test skin away from the surface, thus allowing suction everywhere except over the area of the lands.

The porous surface used by Gregory & Walker (1953) was formed by a rolled piece of monel metal woven wire-cloth which was dry-mounted on to a sheet of aluminium perforated with thirty $\frac{1}{8}$ in. diameter holes per square inch and screwed and glued to the lands. As there was little diffusion of the flow through the wire-cloth, which provided the whole resistance to the suction, the distribution of suction corresponded to the holes in the perforated backing sheet. The porosity of the wire-cloth was not particularly uniform, local suction flow variations of the order of $\pm 30\,\%$ being found, whilst surface waviness up to $\pm 0{\cdot}006$ in. was present over part of the disk.

The disk was mounted flush with, and in the middle of, one of the large faces of a fixed suction box of dimensions 7 ft. $\times$ 7 ft. 6 in. $\times$ 1 ft. The possibility of any static pressure variation over the rear face of the disk arising from its rotation was thus avoided, and uniform suction was obtained by lowering the pressure in the box and metering the flow, due allowance being made for the leakage flow which was measured at the same pressure differential when the surface of the disk was sealed with a sheet of cellophane.

For the experiment with slits, the wire-cloth surface was replaced by a dural skin $\frac{1}{16}$ in. thick. This skin was slitted between the 3 and 14 in. radius circles by seventy-two straight slits, 0·004 in. wide, disposed evenly round the disk and all tangential to the 2 in. diameter circle. In addition, seventy-two short slits, alternating with the long slits, were cut between the 11 and 14 in. radius circles. The flow was controlled partly by strips of Perflec gauze applied as backing, with 0·004 in. apertures very carefully aligned with the slits, and partly by covering all the $\frac{1}{2}$ in. diameter holes in the basic disk by thin film drilled with graded throttle holes so that the velocity into the slits increased linearly with radius except outboard of the 11 in. radius where the velocity was halved. This ensured uniform suction per unit area of disk. The circumferential lands were recessed locally to allow clearance for the backing strips behind the slits and were reduced in their radial thickness so as to offer as little obstruction

as possible to the continuity of flow through the slits. Nevertheless, measurements made when the disk was stationary suggested that the velocity into the slits dropped practically to zero where each slit crossed a land. In addition, the velocity distribution along the length of the slits cannot have been very uniform when the disk was rotating, owing to the radial pressure gradients

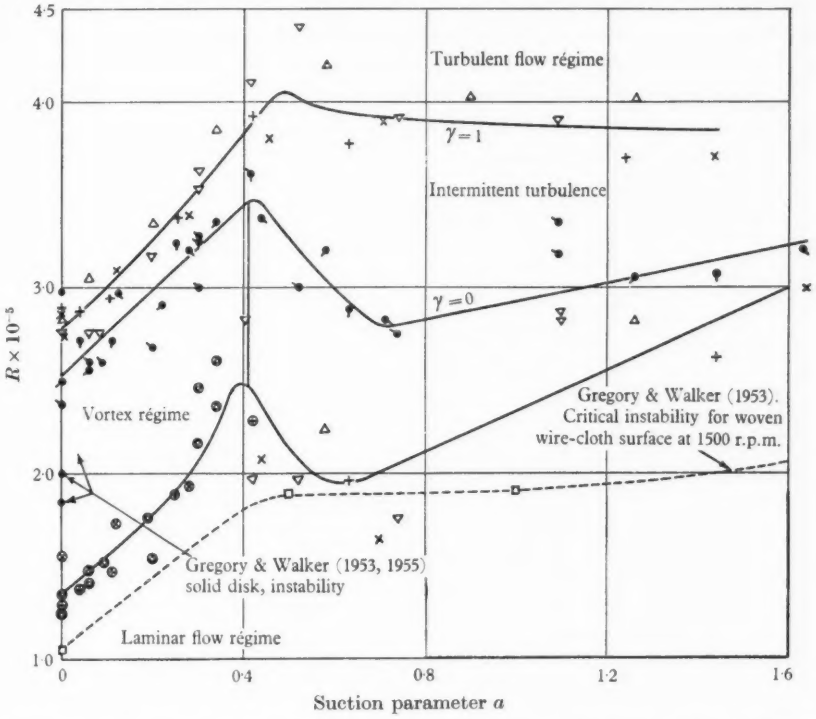


FIGURE 1. Observation of the effect of suction on the state of flow over a slitted rotating disk. $\gamma$ is the turbulent intermittency factor.

| | Disk r.p.m. | | | |
|---|---|---|---|---|
| | 550 | 750 | 980 | 1250 |
| First signs of disturbance | × | + | Δ | ▽ |
| (Ringed symbols indicate onset of vortex regime) | | | | |
| $\gamma = 0$, first bursts of turbulence | ● | ● | ● | ● |
| $\gamma = 1$, fully turbulent | × | + | Δ | ▽ |

between successive lands which arose from the use of small throttle holes on the rear face of the disk. None of the difficulties encountered during the tests, however, could be attributed directly to the poor suction distribution.

Steps due to lack of perfect alignment between adjacent sectors of the skin were kept less than $\pm 0{\cdot}0005$ in., though over the circumference, waves of $\pm 0{\cdot}004$ in. were present. The reading of an anemometer probe held close to the rotating surface was therefore by no means steady.

## 3. Measurements

### 3.1. *State of flow over woven wire-cloth surface*

The state of the boundary layer on the woven wire-cloth surface of the earlier experiment was determined from the display on an oscilloscope of the signal from a probe microphone connected to a total head tube which was held in the flow close to the moving surface. As the probe was sensitive to noise and to the effects of disk vibration and surface waviness, as well as to the turbulence

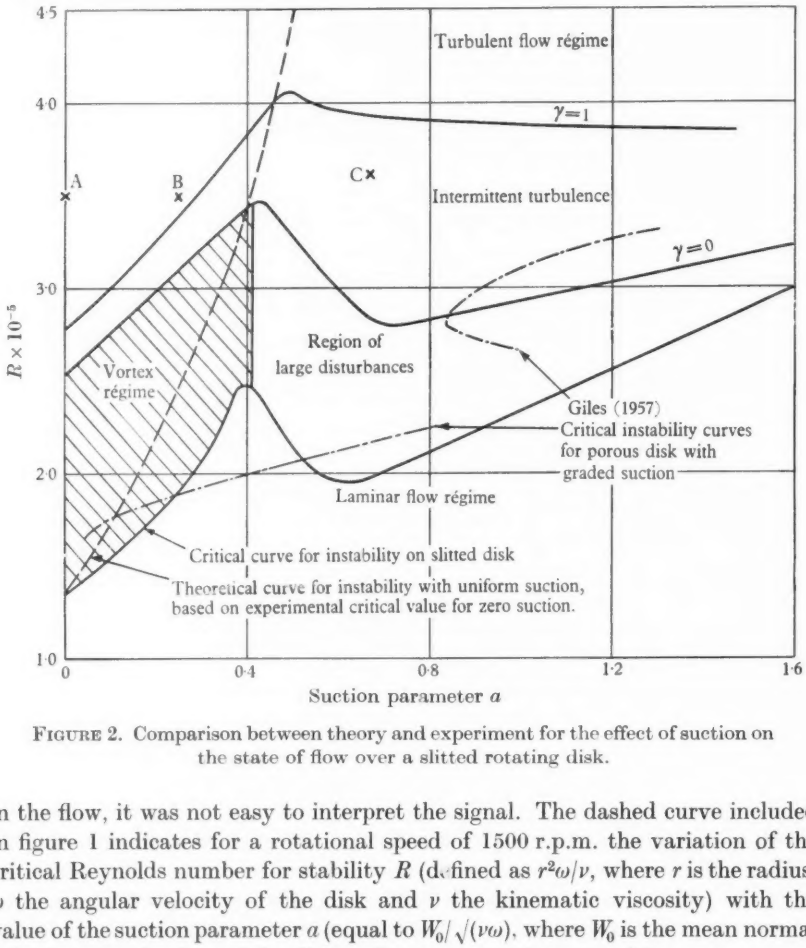


FIGURE 2. Comparison between theory and experiment for the effect of suction on the state of flow over a slitted rotating disk.

in the flow, it was not easy to interpret the signal. The dashed curve included in figure 1 indicates for a rotational speed of 1500 r.p.m. the variation of the critical Reynolds number for stability $R$ (defined as $r^2\omega/\nu$, where $r$ is the radius, $\omega$ the angular velocity of the disk and $\nu$ the kinematic viscosity) with the value of the suction parameter $a$ (equal to $W_0/\sqrt{(\nu\omega)}$, where $W_0$ is the mean normal velocity over the face of the disk as far out as suction extends).

The critical Reynolds number was sensitive to rotational speed (or unit Reynolds number at the critical position) owing to the roughness of the disk, and although a value of 190,000 is indicated in figure 1 for a value of $a$ of 1, the value actually varied between 240,000 at 700 r.p.m. and 156,000 at 2000 r.p.m.

at the same rate of suction. For very high values of the suction parameter, the critical Reynolds number *appeared* to be much larger, increasing to 640,000 for $a = 5$ at 1500 r.p.m. Certainly, at Reynolds numbers 100,000 to 200,000 above this suggested critical value, the flow was undoubtedly turbulent, but it could not definitely be said to be stable below this critical Reynolds number as the signal was by no means disturbance-free and some mean velocity profiles that were measured were not at all close to the theoretical laminar form. As the typical frequencies of the vortices arising from cross-flow instability could not be detected when an analysis was made of the noise, it was concluded that transition with high suction quantities was not caused by instability of the cross flow. This is not surprising in view of the small increase with suction in the observed transition Reynolds number compared with the great theoretical stabilizing effect of suction shown by the dashed curve in figure 2. These results, described fully by Gregory & Walker (1953), were confirmed by the additional investigation with the slitted skin during which the cause of the difficulty was elucidated.

### 3.2. *State of flow over slitted surface*

In the tests with the slitted skin, the velocity fluctuations were observed using a 'Lintronic' hot-film anemometer probe held about 0·01 in. away from the surface. At given disk rotational speeds and suction quantities, the probe was traversed radially and the positions noted at which the state of the flow appeared to change. The observed Reynolds numbers and values of the suction parameter at which the changes occurred are all plotted in figure 1, and as the observations were not so sensitive to rotational speed as on the woven wire-cloth surface, single curves have been drawn through the points. At low suction quantities, a critical boundary can be drawn for the onset of the vortex pattern associated with instability of the secondary flow: at greater Reynolds numbers, transition sets in rapidly. At suction rates above a value of $a$ of 0·4 the vortex pattern does not appear, but with increasing Reynolds number the laminar flow is disturbed by the presence of a wave of much lower frequency and the eventual transition to turbulent flow is spread over a much wider range of Reynolds number. Oscillograms showing typical traces to be found in the various regions are shown in figure 3.

It was not possible to increase the suction flow above a value of $a$ of 1·6 owing to the high resistance of the slits and a limitation on the suction pressure. Although in the case of the woven wire-cloth surface further increases in suction had apparently extended the region of laminar flow, the performance of the slitted disk at a value of $a$ of 1·6 fell a long way short of that suggested by calculation in figure 2, and it was clear that simple instability of the secondary flow was not the prime cause of transition.

### 3.3. *Demonstration of the role of transverse contamination*

The explanation which appeared after further investigation was that at high rates of suction transition on the disk was due to a novel self-contamination effect peculiar to the three-dimensional nature of the flow. For two-dimensional

boundary-layer flow over a flat plate, it had been shown by Schubauer & Klebanoff (1955) that, provided the boundary-layer Reynolds number was not so low that finite disturbances were damped, a wedge of turbulent flow spread laterally, having a fully turbulent core subtending a half angle of 6·4° and an

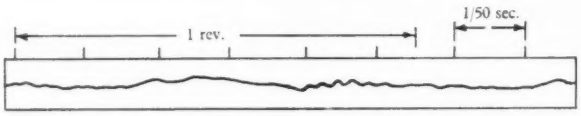


(*a*) Start of vortex region. Zero suction. $R$ = 173,000, 540 r.p.m.

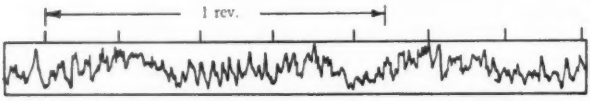


(*b*) Vortices breakdown to turbulence. Zero suction. $R$ = 269,000, 700 r.p.m.

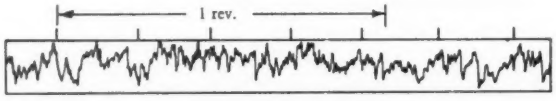


(*c*) Turbulent flow. Zero suction. $R$ = 290,000, 700 r.p.m.

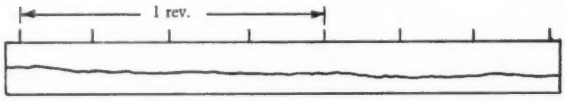


(*d*) Laminar flow with suction. $a$ = 0·42, $R$ = 229,000, 750 r.p.m.

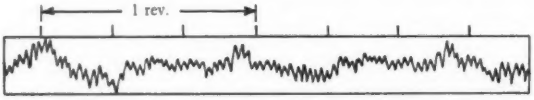


(*e*) Vortex region with suction. $a$ = 0·23, $R$ = 316,000, 1000 r.p.m.

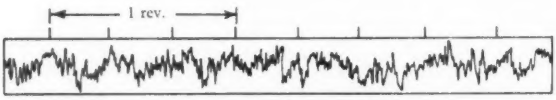


(*f*) Turbulent flow with suction. $a$ = 0·34, $R$ = 360,000, 980 r.p.m.

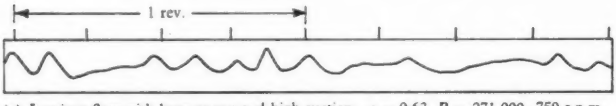


(*g*) Laminar flow with large waves and high suction. $a$ = 0·63, $R$ = 271,000, 750 r.p.m.

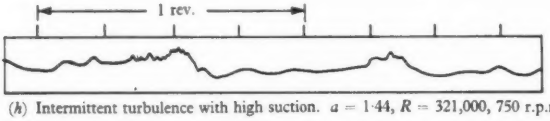


(*h*) Intermittent turbulence with high suction. $a$ = 1·44, $R$ = 321,000, 750 r.p.m.

FIGURE 3. Oscillograms showing the state of flow over slitted disk.

intermittent region with wedge half angle of about $10\frac{1}{2}°$. On a solid disk, the flow in the stationary disturbances generated by instability of the secondary flow travelled downstream and outwards relative to the disk along spiral paths which made an angle of about 14° with the tangential direction (Gregory & Walker 1953; Gregory *et al.* 1955). It was noticed that the centre line of a wedge of turbulence arising from a surface excrescence on a disk lay on a similar

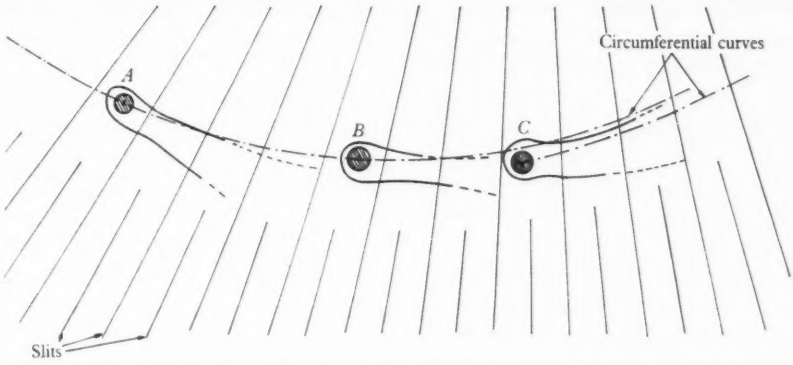


FIGURE 4. Records showing the effect of suction on the spread of the wake of a surface excrescence in turbulent flow, indicated by the sublimation of naphthalene (the position of the three cases in relation to critical conditions is shown in figure 2). *A*: $n$, 750 r.p.m.; $r$, 10 in.; $R$, 350,000; $a$, 0. *B*: $n$, 750 r.p.m.; $r$, 10 in.; $R$, 350,000; $a$, 0·25. *C*: $n$, 750 r.p.m.; $r$, 10·2 in.; $R$, 363,000; $a$, 0·67.

spiral so that the inner edge of the wedge moved outwards along a spiral that eventually made an angle of only a few degrees to the tangential direction when the full spread of the wedge was achieved. As the effect of suction is to reduce the radial outflow it was thought possible that the inner edge of a turbulent wake might lie on a path that would be inclined towards the centre on an inward rather than on an outward moving spiral. This conjecture could not be proved on the disk in a region where suction maintained the flow laminar, since such a region existed only near the centre of the disk at low Reynolds numbers where the postulated flow was not present, presumably because the turbulence was damped out and would not spread laterally at such a large angle. The point was made, however, by experiments in which the naphthalene sublimation technique was used to visualize the wedge of turbulent flow behind a surface excrescence in a *turbulent* boundary layer. Owing to the increased mixing in the wake of the excrescence, a region of increased shearing stress was found extending 2 to 3 in. downstream of the excrescence, and figure 4 shows that at high suction rates the inner boundary to this region becomes parallel to the tangential direction and the disk is therefore self-contaminating.

## 4. Discussion

### 4.1 *Discussion on rotating-disk flow*

It appears that at low suction rates ($a < 0{\cdot}4$) the critical Reynolds number observed experimentally (figures 1 and 2) corresponds to the minimum critical Reynolds number for neutral disturbances of the linearized theory. In view of

the large departure of the suction arrangements from that of uniform distributed suction, the stabilization of the flow to a given Reynolds number by means of a suction rate 75% greater than that predicted with uniform suction is a not unsatisfactory result. Note also that if the velocity profile on the disk is the theoretical one, the observed critical value of the Reynolds number $r^2\omega/\nu$ of 135,000 without suction corresponds to a cross-flow Reynolds number $\chi\,(= v_{\max}\delta/\nu$, where $v_{\max}$ is the maximum value of the cross-flow velocity and $\delta$ is the boundary-layer thickness) of about 340. With the suction parameter $a$ equal to 0·4, the observed critical Reynolds number of 225,000 would correspond to a value of $\chi$ of 270 if the profiles were those appropriate to uniformly distributed suction, although with suction through discrete slits, the values of $\chi$ upstream and downstream of a slit presumably lie above and below this mean value. As expected, there is no stabilization of the cross-flow profile by suction, and the critical value of $\chi$ has not been raised.

At high suction rates, the transverse inward spread of the disturbances enables them to reach regions of lower Reynolds number upstream of those at which linear theory would indicate infinitesimal disturbances to be first amplified. There is presumably a balance between the transverse transfer of energy to a disturbance, the energy dissipated by the disturbance and that given to the mean flow. The oscillograms of figure 3 in the order *f*, *h*, *g* (although not taken with a constant value of the suction parameter) show the more rapid decay of the high compared with the low-frequency turbulence as the Reynolds number is reduced. The observed minimum critical Reynolds number clearly has a value which in the linear theory would be appropriate to some degree of damping. Above this minimum, the oscillograms show that finite disturbances of considerable amplitude are present, so that any attempt to calculate the state of the flow would have to be based on the non-linear mechanics of hydrodynamic stability as discussed by Stuart (1958), with the added complications of both boundary-layer growth and transverse energy transfer. At the moment such calculations do not appear to be feasible.

A significant feature in view of the above considerations is that at low suction rates, turbulence finally develops in the disturbed flow very rapidly with increase in Reynolds number, whilst at the higher suction rates where the undistorted flow is stable to infinitesimal disturbances, turbulence develops but slowly in the direction of increasing Reynolds number. This may also be due to the fact that some energy is now spreading inwards instead of all being convected downstream with the disturbances.

Tests with distributed suction on a wholly porous sintered steel disk have also been reported by Giles (1957). In this experiment, the suction chamber rotated with the disk so that the centrifugal pressure gradient led to a graded suction distribution with inflow at the centre and outflow near the rim, even when there was no net flow through the disk. The stabilization achieved is shown in figure 2, the lower curve representing conditions with no net flow, the upper one with a net flow. The suction parameter represents the mean value of suction out to the instability point; variations in the value were obtained by altering the rotational speed. It can be seen that at small rates of suction ($a < 0{\cdot}4$), the rate of in-

crease in stability with suction is less marked than with the slitted disk, although better than that obtained with the woven wire-cloth surface. Limitations imposed by waviness were again present. At high rates of suction there is a slight improvement over the present results, although the increase in stability Reynolds number is nowhere near that suggested by the linear theory. This improvement is due to two effects. With a wholly porous surface, the rate of spread of a wedge of turbulent flow is slightly reduced by suction so that the self-contaminating effect is postponed to larger rates of suction. Such a reduction in wedge angle due to distributed suction has recently been noted in two-dimensional flow, thus confirming earlier experiments by the present authors (Gregory, Walker & Devereux 1948) which suggested this effect and showed that the wedge was completely suppressed by suction quantities of the order of five times those used in the slitted disk experiments, but this suction rate had the additional effect of reducing $R_{\delta^*}$ to an extremely small value. The second possible reason for improved results with the porous disk used by Giles (1957) may lie in the fact that the suction rate decreased with distance away from the axis of rotation. The effects of inward transverse transfer of energy would thus be greater nearer the centre where the boundary layer $R_{\delta^*}$ is low and disturbances well damped, and less farther out where the boundary layer is more sensitive to the effect. To obtain the maximum extent of laminar flow on a rotating disk it may thus be advantageous to reduce or terminate the suction outboard of the radius at which instability occurs.

Although distributed suction slightly reduces the lateral spread of a wedge of turbulent flow, it is also the most effective way of reducing the outflow on a rotating disk. Calculation shows that the limiting angle at the surface which the flow relative to the disk makes with the tangential direction decreases from 39° 36′ without suction to about 7° at a value of the suction parameter $a$ of 2. Similarly, the angle at a distance from the surface where stationary disturbances generated by instability of the secondary flow are expected decreases from 13° 18′ without suction to about $2\frac{1}{2}$° for $a$ equal to 2. Thus can be seen how the flow over the disk rapidly becomes a self-contaminating 'closed' flow with large suction rates, and extensive laminar motion at high Reynolds numbers is unlikely.

### 4.2. *Relevance to problem of maintaining laminar flow over swept-back wings with slitted surfaces*

Considering now the case of flow over a swept-back wing, similar difficulties arising from the transverse spread of turbulence are only likely to be encountered right on the leading edge where the main flow is in a spanwise direction, and if a turbulent wedge is present, the whole of the flow outboard of the originating excrescence could be turbulent. Wind-tunnel demonstrations of this possibility are reported by Gregory *et al.* (1955), Gregory (1960), whilst Gray of the R.A.E. had observed the phenomenon in flight tests. It is thus possible that it may be necessary to suck somewhat more in the leading-edge region than would be suggested by considerations of the linear stability theory. Further downstream the difficulty could not arise.

As the hoped-for stabilization with suction was not achieved on the rotating disk, it was not possible to test the effectiveness of the slit arrangement at high Reynolds numbers. At the highest critical instability Reynolds number of 240,000 obtained with a value of $a$ of 0·4, calculation suggests that if the boundary layer is taken to be roughly that appropriate to uniform suction then $R_{\delta^*}$ is only 530 and $R_\delta$ is only 2120 for the tangential main flow, which with $H$ roughly equal to 2 is in a very stable state. (The critical value of $R_{\delta^*}$ for $H = 2$ is about 42,000.) The slit Reynolds number was only about 17 under these conditions, and at 1250 r.p.m., the velocity of the disk at the instability point was only 70 ft./sec. All that can be concluded, therefore, is that at this relatively small Reynolds number and value of $U/\nu$, no evidence was found for any effects due to slit contour, due to slit sweep (which could be altered by changing the direction of rotation), due to rapid variations or breaks in continuity of the inflow along the length of the slit, or due to the ends of the additional rows of slits at 11 in. radius. It is possible that the flow was affected by these features but that the indications were masked by the disturbances due to flow turbulence and to waviness and discontinuities in the surface.

The rotating disk can thus no longer be regarded as a satisfactory tool for investigation of the effects of suction on secondary-flow instabilities such as arise on swept-back wings, or for testing suction surfaces.

Acknowledgements are due to Dr G. V. Lachmann for his interest in this work and for arranging for the slitted skin to be manufactured by Messrs Handley Page, Ltd., and to Mr A. Silverleaf of Ship Division, N.P.L., for the loan of the 'Lintronic' hot-film anemometer probe and equipment. The work described above has been carried out as part of the research programme of the National Physical Laboratory, and this paper is published by permission of the Director of the Laboratory.

## REFERENCES

Giles, W. B. 1957 *General Electric Co. America, Tech. Inf. Series, Rep.* no. R57AT.76.

Gregory, N. 1960 *J. Roy. Aero. Soc.* **64**, 562.

Gregory, N., Stuart, J. T. & Walker, W. S. 1955 *Phil. Trans.* A, **248**, 155. Also *Proc. N.P.L. Symp. Boundary-layer Effects in Aerodynamics.* H.M.S.O.

Gregory, N. & Walker, W. S. 1953 *Rep. aero. Res. Coun., Lond.*, no. 16,152. (Unpublished.)

Gregory, N., Walker, W. S. & Devereux, A. N. 1948 *Rep. Memor. aero. Res. Coun., Lond.*, no. 2647.

Schubauer, G. B. & Klebanoff, P. S. 1955 *Rep. nat. adv. Comm. Aero., Wash.*, no. 1289. Also *Proc. N.P.L. Symp. Boundary-layer Effects in Aerodynamics.* H.M.S.O.

Stuart, J. T. 1954 *Quart. J. Mech. appl. Math.* **7**, 446.

Stuart, J. T. 1958 *J. Fluid Mech.* **4**, 1.

# An experimental investigation of turbulent spots and breakdown to turbulence

By J. W. ELDER
Geophysics Division, D.S.I.R., Wellington, New Zealand

(Received 17 February 1960)

The theory of hydrodynamic stability and the impact on it of recent work with turbulent spots is discussed. Emmons's (1951) assumptions about the growth and interaction of turbulent spots are found experimentally to be substantially correct. In particular it is shown that the region of turbulent flow on a flat plate is simply the sum of the areas that would be obtained if all spots grew independently.

An investigation of the conditions required for breakdown to turbulence near a wall, that is, to initiate a turbulent spot, suggests that regardless of how disturbances are generated in a laminar boundary layer and independent of both the Reynolds number and the spatial extent of the disturbances, breakdown to turbulence occurs by the initiation of a turbulent spot at all points at which the velocity fluctuation exceeds a critical intensity. Over most of the layer this intensity is about 0·2 times the free-stream velocity. The Reynolds number is important merely in respect of the growth of disturbances prior to breakdown.

## 1. Introduction

Ever since Reynolds classical experiments, considerable attention has been paid to the problem of the origin of turbulence. Nevertheless, it is only in recent years that a partial understanding of the physical processes involved has been achieved. Throughout this paper we consider only the transition to turbulence on a semi-infinite flat plate lying in the Cartesian plane $y = 0$ with its leading edge along $x = 0$ in a uniform stream of velocity $U_1$ in the $x$-direction. Even under the most carefully controlled conditions the free stream will also contain small velocity fluctuations of order $0{\cdot}001\,U_1$, and indeed it is an immediate consequence of the linear stability theory that without such fluctuations the layer which grows on the plate will remain laminar. In other words a laminar boundary layer cannot spontaneously, without the further action of an external disturbance, become turbulent.

### *The hydrodynamic stability approach*

The early work considered only the initial growth of infinitesimal disturbances superimposed on the laminar undisturbed flow (Schlichting 1955). In 1948 Schubauer & Skramstad brilliantly confirmed the existence of the linear waves postulated by this linear theory of the instability of the boundary layer on a flat plate. A more exact verification of the details of the theory has been given by Shen

(1954). When a small disturbance is applied to a laminar flow for which the Reynolds number exceeds a critical value, initially the disturbance grows exponentially with time. While the disturbance is small the Reynolds stress generated by the disturbance is negligibly small, but as the disturbance amplitude increases the finite velocity fluctuations transport appreciable momentum, and the associated Reynolds stress modifies the mean flow so that the transport of energy from the mean flow to the disturbance is modified and the disturbance growth rate is affected. Recently attempts have been made, notably by Stuart (1958), to extend the wave instability theory to the non-linear case of finite disturbances, but so far only flows for which the local Reynolds number is independent of position in the flow have been considered. Nevertheless, in spite of the success of this work on the growth of two-dimensional waves of infinite streamwise extent, the stability theory contains no feature typical of turbulence and can at best describe the early stages of the flow before the onset of turbulence. In fact, while the suggestion (Landau 1944) that a complex non-linear superposition of two-dimensional waves of various wavelengths and various wave directions is turbulence is plausible for, say, convection between parallel planes, this is certainly not the case for turbulence on a flat plate which originates in very small regions as 'turbulence spots' (Emmons 1951). While turbulent spots can be initiated from high-amplitude portions of a superposition of boundary-layer waves, they can also be initiated by isolated velocity pulses produced say by a spark.

Further, the linear theory shows that below a critical Reynolds number all waves are damped, and this has been verified in detail by experiment. Consideration of the non-linear equations for a flow with varying Reynolds number (Stuart 1956, 1958) has not yet produced a definite conclusion as to whether or not a finite two-dimensional wave is also damped below the critical Reynolds number. Nevertheless, it will be shown below that for a wide class of finite disturbances it is possible to initiate turbulent spots at Reynolds numbers well below the critical value (provided the amplitude exceeds a certain value). In other words, below the critical Reynolds number the flow is stable to small disturbances but unstable to large disturbances. This is a common stability situation. For example, consider a ball resting inside a bowl. After a small disturbance the ball performs a damped oscillation and returns to its original position, but a sufficiently large impulse will make the ball reach the rim and leave the bowl. It is clear that a desirable next step would be a theoretical consideration of the growth in a laminar boundary layer of an isolated velocity pulse.

### *Emmons theory of a transition zone*

A second effect of the modification of the rate of transfer of energy to a disturbance by the Reynolds stresses is the extremely rapid increase in disturbance energy which initiates a turbulent spot. In 1951 Emmons reported the existence of turbulent spots and gave a probability calculation of their interaction in a transition zone. Subsequent work by Dhawan & Narasimha (1958) has established a remarkably good phenomenological theory of a transition zone.

Emmons's theory relies on four assumptions: (1) point-like breakdown, (2) a sharp boundary between the turbulent fluid of a spot and the surrounding laminar

flow, (3) a uniform rate of spot growth and (4) no interaction between spots. These ideas were experimentally investigated in detail by Schubauer & Klebanoff (1955). In practice point-like breakdown means that the turbulent spots originate from a region of extent less than the boundary-layer thickness. If a hot-wire anemometer is placed close to the beginning of a transition zone, the observed turbulent spots will be found to be of small extent. Further, under suitable conditions, an artificial disturbance will initiate a turbulent spot even though the disturbance is of small extent. This can be very clearly demonstrated by the dye method described below in connexion with figure 2 (plate 1). (Nevertheless, the smallest volume of disturbed fluid which will initiate a turbulent spot is not yet known.) Schubauer & Klebanoff (1955) have also verified the assumptions of a sharp boundary and uniform growth but did not give detailed consideration to the interaction assumption, although they indicated that they made qualitative observations in an experiment similar to that below. It will be one of the objects of this paper to give, in §3, experimental evidence for Emmons's fourth assumption that the area of a flat plate covered with turbulent fluid is simply the combined area of the turbulent spots present assuming each spot grows independently of all the others. Thus, in view of the detailed validity of Emmons's assumptions, it is not surprising that the consequent theory of a transition zone is in excellent agreement with experiment.

### *Breakdown*

We have considered the fluid behaviour subsequent to breakdown, but the word breakdown correctly implies that the spots originate from a very small volume and suggests the importance of the disturbance present immediately before breakdown occurs. It is important to note that this does not imply that the character of the flow far upstream of the breakdown point is unimportant, but rather that the role of the upstream flow is to produce and amplify disturbances of which those that satisfy certain local conditions will break down to turbulence. Indeed, the conclusion that breakdown is determined by local conditions is the principal result of this paper.

It has already been noted that spots can be initiated by an isolated velocity pulse established in the laminar boundary layer. Although to specify a pulse in general it would be necessary to give the velocity fluctuation as a function of position and time, an approximate specification is obtained from the longitudinal extent (from zero to zero) in the flow direction $X$, the lateral extent $Z$, and the maximum value of the velocity fluctuation in the flow direction $u_m(y)$ as the pulse passes over the observation point. This specification ignores the other velocity components and the fluid acceleration, but it will appear below that a more detailed specification within the experimental accuracy is not required. Let such a pulse pass over a point at $(x, y)$, where the undisturbed velocity profile is $U(y)$ and the boundary-layer thickness is $\delta$ ($U = 0{\cdot}99U_1$ at $y = \delta$). The subsequent behaviour of the pulse is determined by the seven quantities $x, y, U_1$, or $U(y)$, $X$, $Z$, $u_m$, and either kinematic viscosity $\nu$ or $\delta\,(= 5\sqrt{(\nu x/U_1)})$; from these are obtained the convenient dimensionless parameters the Reynolds number $R = U_1 x/\nu$, $y/\delta$, $u_m/U$, $X/\delta$ and $Z/\delta$. The purpose of the experiment described in §4 is to

investigate the relation between these five parameters for pulses on the verge of breakdown. It will be shown that breakdown occurs for all pulses for which $u_m/U \geqslant u^*$, where $u^*$ is a function only of $y/\delta$ whatever the Reynolds number or the spatial extent of the pulse. This surprisingly simple result confirms the suggestion that breakdown is determined only by local conditions.

Considerable evidence has already been presented by Klebanoff & Tidstrom (1959) to support the result that breakdown depends critically on $u^*$. They produced a boundary-layer wave downstream of a vibrating ribbon and found that breakdown was first noticed in the high amplitude portions of the wave. From measurements restricted to $y/\delta \doteqdot 0{\cdot}2$ and over a small Reynolds number range, they found that this occurred when $u'/U = 0{\cdot}22$, where $u'$ is the root-mean-square $x$-velocity fluctuation. Unfortunately, from Klebanoff & Tidstrom's data it is difficult to relate $u_m$ and $u'$, but just before breakdown was noticed the wave shape was composed of long rather rectangular pulses so that $0{\cdot}7 < u_m/u' < 1$ and $u^* \doteqdot 0{\cdot}25$. That this is somewhat in excess of the value 0·18 to be given here is to be expected. While Klebanoff & Tidstrom find the value of $u'/U$ at which breakdown is first observed at $y/\delta = 0{\cdot}2$ it is clear, as they point out, that this is not necessarily the point at which breakdown first occurs. In fact from their data we find the maximum value of $u'/U$ just prior to breakdown is near $y/\delta = 0{\cdot}3$. Near breakdown there is a very rapid increase in $u'/U$ to a maximum value about twice the breakdown value, so that a small error in locating the position at which breakdown first occurs at all in the layer leads to a large overestimate of the critical value of $u'/U$. Nevertheless, considering that the possible systematic error in determining $u/U$ or $u'/U$ by means of a hot-wire is rather large (10–20 %), it is doubtful if there is any significant difference between Klebanoff & Tidstrom's estimate of $u^*$ and the values given here. Finally, it should be noted that although in the preliminary investigation of this problem a number of different hot-wires were used, all the data presented here was obtained with a single hot-wire which maintained its calibration throughout the experiment, so that although the absolute value of $u^*$ may be somewhat in doubt it was clearly shown that breakdown occurred at a critical value of $u^*$.

## 2. The role of the Reynolds number

*Behaviour of a disturbance generator*

It has been suggested that the Reynolds number is important only in the growth of disturbances prior to breakdown, and in fact it is the dominance of the Reynolds number in this growth that is responsible for the belief that the Reynolds number is also important for breakdown. Those investigations, such as that of Webb & Harrington (1956), which report the Reynolds number of transition as a function of the amplitude of a disturbance generator refer to the operation of the generator rather than to the origin of turbulence. Such investigations do, however, make clear the obvious but important point that at low Reynolds numbers very much larger amplitudes of the disturbance generator are required to produce a given $u/U$. In fact any such device is completely inhibited for $U_1$ sufficiently small.

Consider in detail a particular case (Schlichting 1959), that of transition behind a circular cylinder of diameter $k$ laid normal to the stream at $x$ on a flat plate where the undisturbed boundary-layer thickness is $\delta$. The location of the beginning of the transition zone $x_t$ will be a function of $k, x, \delta$ or $\nu$, $U_1$ or $U(k)$, and some measure of the free-stream disturbances such as $u'$ the root-mean-square $x$-velocity fluctuation. Suitable dimensionless parameters are $R_t = U_1 x_t/\nu$, $R_k = U(k)\,k/\nu$, $k/\delta$ or $x/k$, $u'/U_1$. The experimental data, given by Dryden (1953), is reproduced

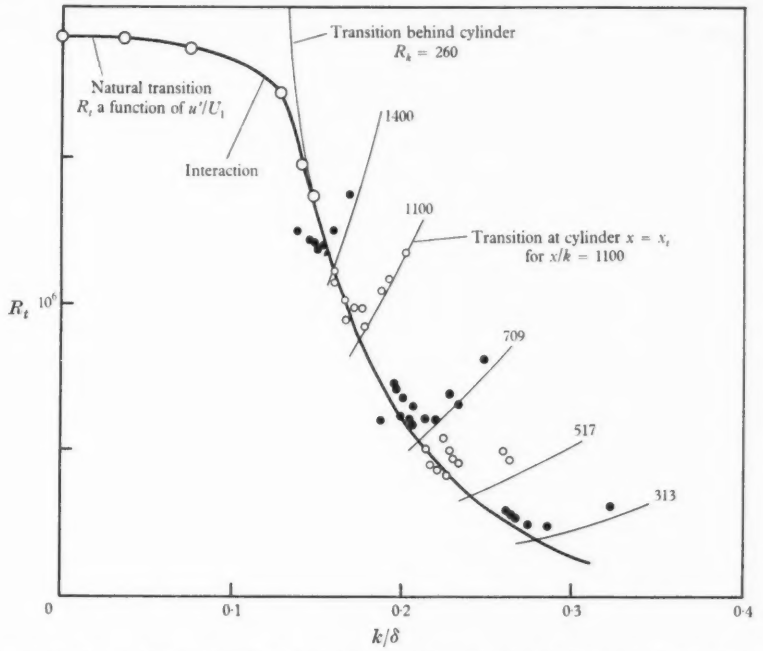


FIGURE 1. Reynolds number of transition behind a cylinder of diameter $k$ placed normal to the stream on a flat plate. Data given by Dryden (1953). Below the heavy curve the flow cannot be turbulent. ○, $k$ varied; ○, ●, $\delta$ varied.

in figure 1 as a relation between $R_t$ and $k/\delta$. Low values of $k/\delta$ were obtained by varying $k$ with fixed $x$, $\delta$, but the higher values of $k/\delta$ were obtained with fixed $x/k$ by varying $\delta$. For $k/\delta$ very small the flow is unaffected by the presence of the roughness element. Here $R_k < 10$ so that the boundary layer does not separate from the cylinder, no vortices are shed and $R_t$ is determined by $u'/U_1$ as in natural transition. Schubauer & Skramstad (1948) have investigated this relation and found that $R_t$ decreases as $u'/U_1$ increases. It is worth noting that in most wind tunnels $u'/U_1$ is a function of $U_1 M/\nu$, where $M$ is a length characteristic of the upstream section of the tunnel (say the gauze spacing). The relation between $R_t$ and $k/\delta$ for $k/\delta < 0{\cdot}15$ is consistent with the result of the present paper and is expressed implicitly by $u_m/U = u^*$, where $u_m$ is the maximum value of $u$ at a given point. The result of the present paper is not applicable in any other region of the flow problem under discussion.

As $k$ increases beyond $R_k \doteqdot 100$ the boundary layer separates at the cylinder and vortices are shed. These vortices interact with the free-stream disturbances, so that the transition point is moved towards the cylinder until for $k$ sufficiently large transition occurs in the shear layer of the separation zone. Transition in the separated shear layer will be determined by $U(k)$, $k$, $\nu$; that is by $R_k$. The curve $R_k = 260$ gives the best fit of Dryden's data. This value is reasonable but a little lower than the value $R_k = 300$ at which visual inspection of the flow in a water channel showed the first signs of disturbances in the separated shear layer. Further increase in $k$ cannot move the transition point past the cylinder position $x$. This is seen in figure 1 where the points taken at constant $x/k$ follow the curves $R_t = U_1 x/\nu$ for larger values of $k/\delta$. The points will begin to approach the curves $R_t = U_1 x/\nu$ when transition first occurs in the separated shear layer.

*Natural transition*

In natural transition on a flat plate six zones can be distinguished in practice. First, there is a laminar zone in which the disturbance amplitude is less than that in the free stream. Secondly, an oscillatory zone commences at

$$R = R_c = 1{\cdot}12 \times 10^5.$$

In this zone the fluctuating motion is largely a rapidly growing two-dimensional boundary-layer wave. With care this zone can be made to extend at least to $R = 3 \times 10^6$ (Schubauer & Skramsted 1948). The third zone is entered when the boundary-layer wave begins to interact with the free-stream disturbances. It can be shown that a vortex line moving near the wall in a boundary layer is unstable to small disturbances along its length. Even the most careful attempt to reduce the free-stream disturbances does not prevent the wave front becoming rapidly distorted (Hama, Long & Hegarty 1956). The behaviour of the first three zones is dominated by the Reynolds number. Generally by this stage the disturbance intensity is approaching $u^*$ and the fluid passes into a fourth zone in which breakdown occurs at the high intensity points of the wave front where the intensity reaches $u^*$. This breakdown zone is narrow (Dhawan & Narasimha 1958) because the rate of growth of the velocity fluctuations is rapid in the third zone. In the fifth zone, the so-called transition zone, the spots grow linearly—evidence that they are only weakly affected by the Reynolds number—until they merge into the sixth zone of full turbulence which is again dominated by the Reynolds number. It is perhaps not entirely surprising that the two regions, laminar and turbulent, each differently dependent on the Reynolds number should be separated by a breakdown region independent of the Reynolds number.

## 3. Turbulent spots, experimental results

*Form and growth*

Turbulent spots can be conveniently visualized by placing a flat plate in a water channel and injecting dye through a slit parallel to the plate leading edge, or more simply by sprinkling dye particles onto the plate so that dye spreads downstream in a thin layer which remains close to the plate wall. If now a localized

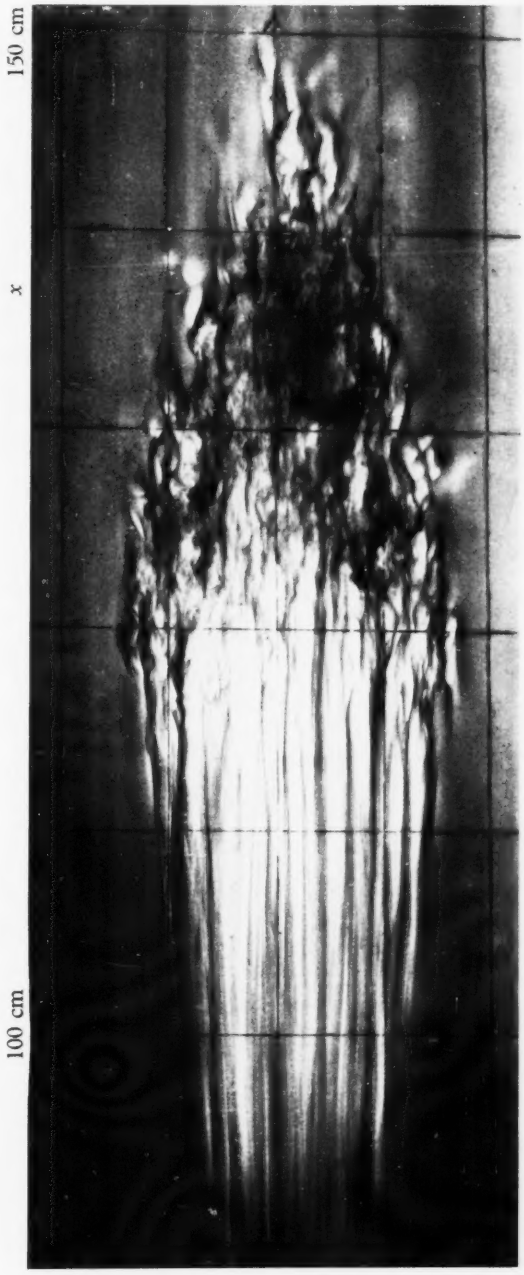


FIGURE 2. Photograph of a turbulent spot 3·9 sec after a 0·1 sec disturbance at $x = 50$ cm on a flat plate. $U_1 = 23$ cm/sec, $\delta = 1{\cdot}2$ cm at $x = 130$ cm.



(*Facing p.* 240)

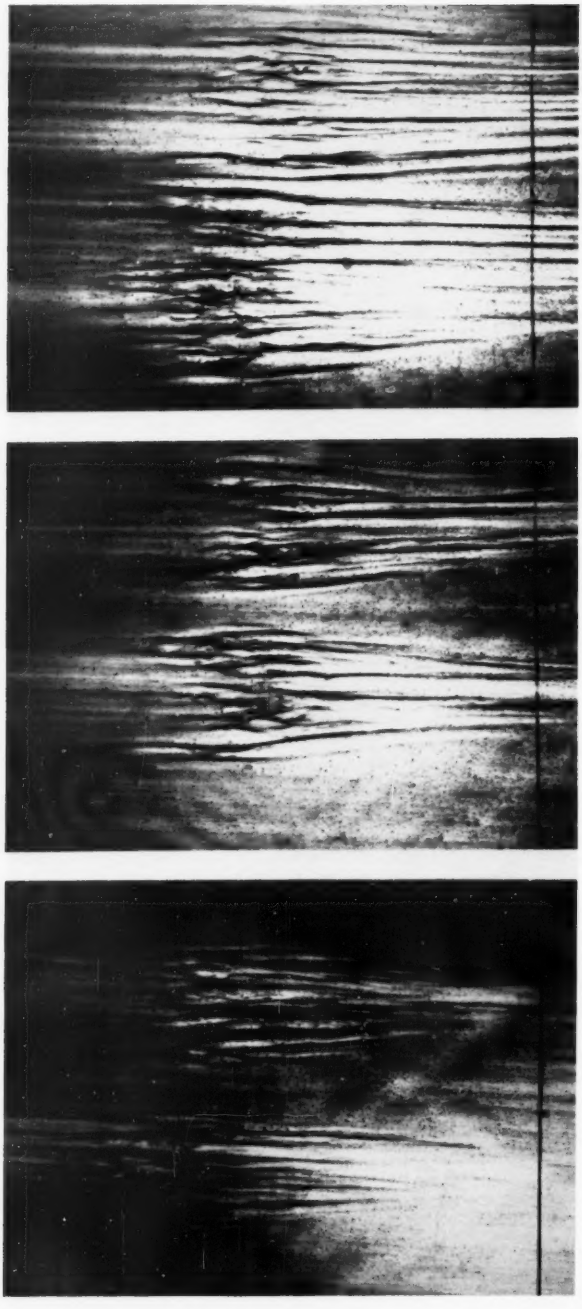

FIGURE 4. Photographs of two spots initiated 5 cm apart in a classroom demonstration channel. Water depth 5 mm, discharge velocity 32 cm/sec. The lines are spaced 20 cm apart. The photographs show an area approximately 15 × 10 cm.

disturbance is produced at some point, say the end of a rod momentarily poked into the boundary layer, the motion produced by the disturbance as it moves downstream is clearly revealed by breaks or clear patches occurring in the dye sheet. If the disturbance is large enough a turbulent spot will be initiated. Figure 2, plate 1, shows a photograph of the disturbed dye sheet produced by a turbulent spot, obtained by this method in the 14 in. water flume of the Engineering Laboratory, Cambridge. The photograph was taken 3·9 sec after a disturbance lasting 0·1 sec was produced 50 cm downstream of the plate leading edge with a free stream of velocity $U_1 = 23{\cdot}0$ cm/sec and $\delta = 1{\cdot}2$ cm at $x = 130$ cm.

The general features of a spot as revealed by figure 2 (plate 1), have already been obtained from hot-wire measurements by Schaubauer & Klebanoff (1955). To the right of the photograph is a V-shaped region of turbulent fluid lying 115–145 cm downstream of the leading edge and to the left the fluid returns to laminar flow as the spot passes downstream to the right. The striations in this laminar region are due to elements of dye which are rapidly extended in the flow direction by the high shear near the plate. The turbulent–laminar boundary is sharply defined, although distorted on a scale comparable with the boundary-layer thickness. This property of a sharp division between laminar and turbulent fluid appears to be one of the general characteristics of turbulent fluid. Within the spot itself a large portion of the fluctuating motion is surprisingly regular and periodic. The principal components of the fluctuating motion appear very similar to so-called horseshoe vortices; that is, regions of localized vorticity, the core of which is U-shaped and parallel to the plate but with the head of the U pointing downstream and moving away from the wall. They appear similar to structures identified by Grant (1958) in a turbulent boundary layer. As yet, however, no detailed investigation of the structure of spots has been reported.

### *Interaction*

It was mentioned that little attention has been given to Emmons's assumption which relates to the manner in which turbulent spots interact. This problem of the interaction of spots is also of interest in connexion with transition on a finite flat plate (to be published). It has been shown experimentally that transition occurs near the side edges of a finite plate much sooner than transition in the middle of the plate. Turbulent spots originate from a small volume on the edge of the plate and as they grow downstream sweep out a narrow tongue of disturbed fluid near the edge, while the bulk of the flow over the plate is still laminar. We then have the problem of the manner in which the edge regions combine with the normal transition zone, or if the plate is very narrow with one another. Both these problems are most simply investigated by studying the interaction of two equal but laterally displaced spots.

A thin aluminium flat plate was set parallel to the incident stream ($U_1 = 820$ cm/sec) in the 15 in. wind tunnel of the Cavendish Laboratory, Cambridge. Sparks were fired simultaneously at a rate of 2/sec across two 3 mm spark gaps placed 25 cm downstream of the leading edge and 5 cm apart so that two spots were simultaneously initiated 5 cm apart at the spark gaps. The subsequent interaction downstream of the spark gaps was studied with a hot-wire placed so that $y/\delta = 0{\cdot}4$

and connected to a triggered oscilloscope, the triggering signal for which was obtained from the spark generator. The proportion of time $\gamma$ that the flow at a point was turbulent was obtained directly from the pulse length observed on the oscilloscope. The results are shown in figure 3 as a series of curves of constant $\gamma$. (Notice that here $\gamma$ is proportional to the pulse rate.) Superimposed on the figure are two overlapping shaded areas representing the outline of each of the turbulent spots at a particular instant assuming each spot grows independently of the other. (The outline was traced from that of figure 2, plate 1.) Figure 3 shows that the assumption is correct. An isolated spot grows linearly in time as is verified here

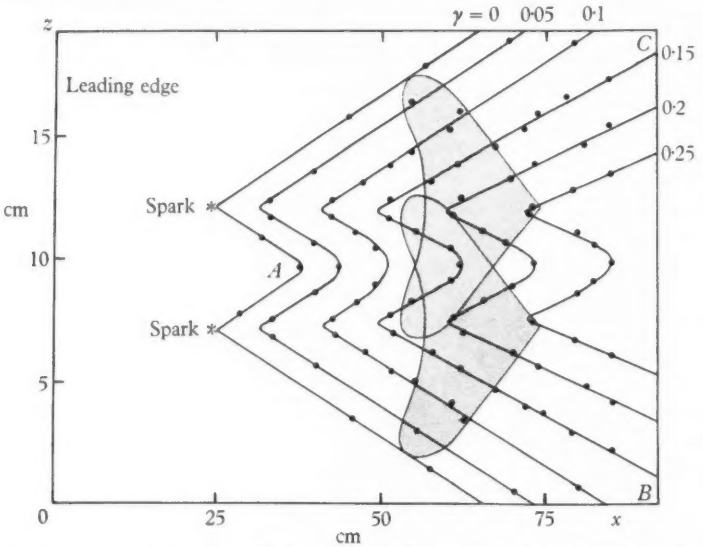


FIGURE 3. Interaction of two equal spots initiated 5 cm apart at $x = 25$ cm. Curves of constant intermittency $\gamma$ for a fixed repetition rate of 2 pulses/sec. The overlapping shaded areas represent the outline of the two spots at a particular instant. The outline was copied from figure 2 (plate 1). Scale 1:4.

where the lines of constant $\delta$ are largely made up of straight lines. But this is also the case within the possible interaction zone, the triangular area $BAC$. A small interaction zone does exist on the line of symmetry through $A$, but its width is only of order $\delta$ as might be expected, since the edge of a spot is contorted with a scale of order $\delta$. A simple demonstration of the independent growth rate was given by noting that $\gamma$ was unaltered in $BAC$ (except for the narrow strip of width $\delta$ through $A$) if either spark was switched off and also unaltered below $AB$ if the upper spark was switched off. Thus the curve dividing turbulent from laminar fluid is the envelope of the superimposed curves from independent individual spots.

The interaction of spots can also be studied qualitatively in the same manner as that used to obtain figure 2 (plate 1). Figure 4 (plate 2), shows a series of photographs of two spots initiated 5 cm apart in a shallow flume used for classroom demonstrations. The flume was 30 cm wide and water was supplied up to

10 gal./min from a laboratory tap. The difference in the shape of the spots in figures 2 and 4 is due to the fact that in figure 4 the undisturbed flow is independent of $x$. A visual study of the interaction of spots in the water flume confirmed that there was no noticeable alteration in the growth rate of one spot due to the presence of another.

## 4. Turbulent breakdown, experimental results

We wish to know the conditions under which an isolated and localized pulse will initiate a turbulent spot. The main difficulty in determining these conditions accurately is in producing a regular sequence of pulses as near similar as possible. The first method tried was that of a small circular cylinder momentarily introduced into the boundary layer through a hole in the plate. (The alternatives of a cylinder introduced from the free stream or a puff of air through a hole in the plate were not tried.) The cylinder was mounted on the armature of an electric

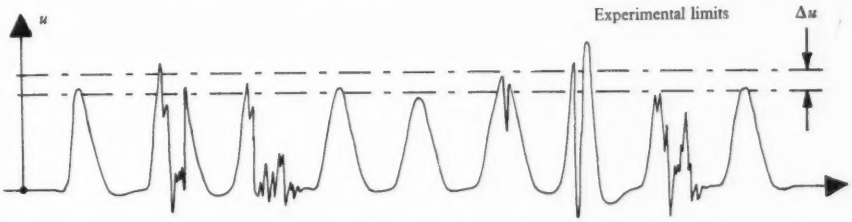


FIGURE 5. Oscillograph trace downstream of a regular sequence of spark pulses.

relay with a variable stop to the motion of the armature, so that the distance the cylinder penetrated the flow could be easily varied. Pulses of a few cycles/sec to operate the relay were obtained from a scale of 64 counter fed by a Beat Frequency Oscillator. This method was only moderately successful. The motion of the pulse was obscured by the presence of quasi-periodic oscillations and there was great variation in the pulse amplitude from pulse to pulse. The second method was that of a spark driven by discharging a condenser across the primary of a 1:100 transformer. Control over the pulse amplitude was obtained by varying the condensor charging voltage. It was found that even when no spark occurred that a velocity pulse was formed from the motion of the partially ionized air in the vicinity of the spark gap. No consideration was given to possible non-isothermal effects after a spark, since the ionization level was seen by visual observation with the laboratory blacked out to be negligible less than 1 cm (1 msec) downstream of the spark gap. Figure 5 shows a schematic oscillograph trace obtained from the hot-wire probe although in practice the signal was observed on a triggered oscilloscope. The voltage pulse was gradually increased until some of the pulses were turbulent. The critical velocity fluctuation $u_m$ and the experimental limit $\Delta u$ was determined such that (1) all pulses of amplitude greater than $u_m + \frac{1}{2}\Delta u$ had broken down, (2) no pulse of amplitude less than $u_m - \frac{1}{2}\Delta u$ had broken down. This procedure is complicated by the occasional extra-strong pulse for which turbulence is fully spread through the pulse, since the maximum values of $u$ in the spot generally drop off rapidly as the eddies of smaller size appear

in the spot. Successive pulses were sufficiently similar to allow $u^*$ to be determined to $\pm 10\,\%$. Pulses were produced over the following ranges: $x = 15$–$100$ cm and $U_1 = 200$–$1500$ cm/sec, or $R = 2 \times 10^4$ to $10^6$ and $X/\delta = 0{\cdot}5$–$30$.

It should be emphasized that the hot-wire probe was always downstream of the spark, the spark and the probe were separated by varying distances and that the critical pulse intensity was that which caused breakdown just ahead of the probe, rather than at the spark.

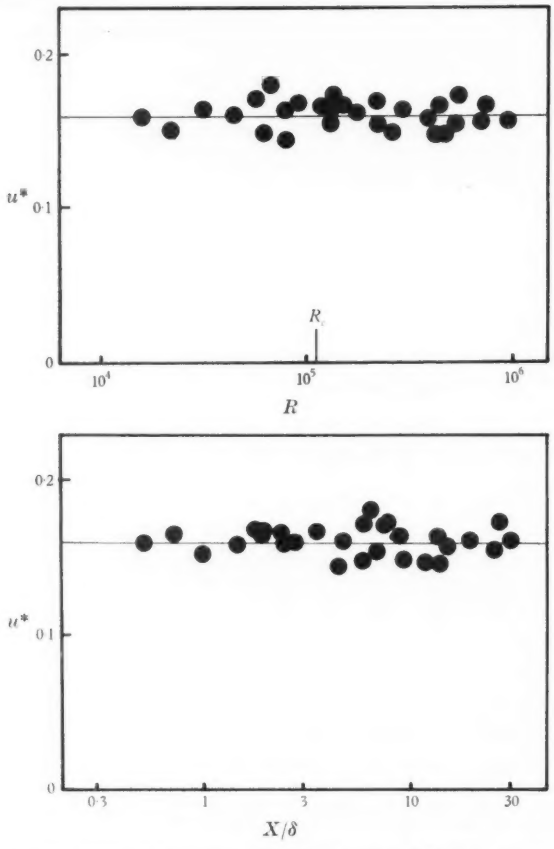


FIGURE 6. Critical intensity $u^*$ at fixed $y/\delta = 0{\cdot}6$ as a function of $R = U_1 x/\nu$ and $X/\delta$.

Figure 6 presents the main result of the paper $u^*$ as a function of $R$ and $X/\delta$, obtained at $y/\delta = 0{\cdot}6$. It was not possible, however, to vary $R$ and $X/\delta$ completely independently, but in the data of figure 6 for each value of $R$ values of $X/\delta$ were possible covering a range of about 10:1. Thus it is simplest to regard figure 6 as presenting the same data in two different ways. This method is preferable to a three-dimensional diagram with axes $u^*$, $R$ and $X/\delta$, since $R$ and $X/\delta$ are only slightly correlated.

The breakdown condition is independent of the Reynolds number over the 50:1 range $2 \times 10^4$ to $10^6$. This remarkable result confirms the idea that breakdown is determined by local factors alone. It is also important to notice that breakdown is possible at Reynolds numbers much lower than $R_c = 1{\cdot}12 \times 10^5$, the critical value below which the layer is stable to all small disturbances (Schlichting 1955). It is also surprising that $u^*$ is independent of $X/\delta$. (The lateral extent of the pulses $Z/\delta$ was in the range 0·5–10 but was not controlled or generally measured.)

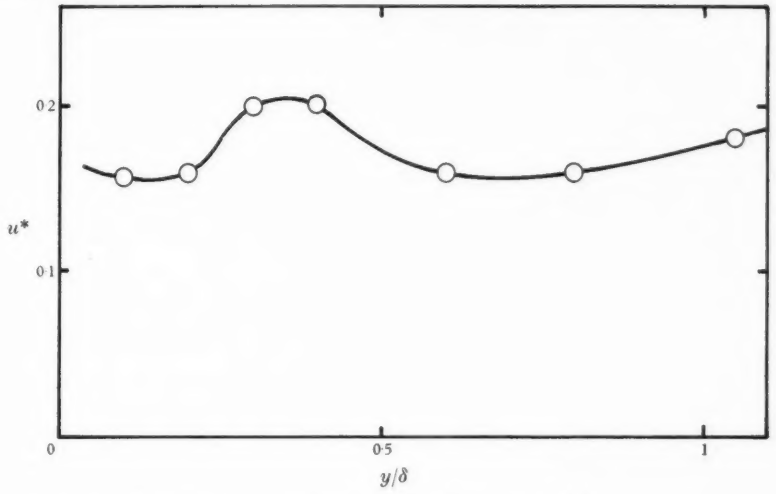


FIGURE 7. Critical intensity as a function of $y/\delta$.

The critical intensity $u^*$ is therefore a function only of $y/\delta$ and this relation is shown in figure 7. Over most of the layer $u^* \doteqdot 0{\cdot}18$.

It is now clear that transition to turbulence is largely independent of the particular way in which disturbances arise in a layer and that the Reynolds number which has hitherto been considered as an important parameter, directly affecting transition, is important merely in the processes responsible for the growth of the disturbances.

I gratefully acknowledge that my period of research at Cambridge was made possible by my employers, the New Zealand Defence Scientific Corps.

## REFERENCES

DHAWAN, S. & NARASIMHA, R. 1958 *J. Fluid Mech.* **3**, 418.
DRYDEN, H. L. 1953 *J. Aero. Sci.* **20**, 477.
EMMONS, H. W. 1951 *J. Aero Sci.* **18**, 490.
GRANT, H. 1958 *J. Fluid Mech.* **3**, 149.
HAMA, F. R., LONG, J. D. & HEGARTY, J. C. 1956 *J. Appl. Phys.* **28**, 388.
KLEBANOFF, P. S. & TIDSTROM, K. D. 1959 *N.A.S.A. Tech. Note* D-195.
LANDAU, L. 1944 *C.R. Acad. Sci., U.R.S.S.*, **44**, 311.

Schlichting, H. 1955 *Boundary Layer Theory*. London: Pergamon Press.
Schlichting, H. 1959 *Handbuch der Physik*, **8**, 1. Springer-Verlag, Berlin.
Schubauer, G. B. & Klebanoff, P. S. 1955 *NACA Rep.* 909.
Schubauer, G. B. & Skramstad, H. K. 1948 *NACA Tech. Note* 348.
Shen, S. F. 1954 *J. Aero Sci.* **21**, 62.
Stuart, J. T. 1956 *J. Aero Sci.* **23**, 86 and 894.
Stuart, J. T. 1958 *J. Fluid Mech.* **4**, 1.
Webb, W. H. & Harrington, R. P. 1956 *J. Aero. Sci.* **23**, 792.

# On the movement of ships in restricted waterways

By T. CONSTANTINE
Department of Civil Engineering, Manchester University

(Received 4 May 1960)

In this paper some simple theoretical considerations concerning the movement of ships in restricted waterways are discussed, and it is shown that for a ship towed from the bank, or by any external force, there are three distinct speed ranges: subcritical, critical and supercritical. In the subcritical and supercritical ranges, Bernoulli's equation and the continuity equation are satisfied everywhere by a state of steady motion relative to the ship, but in the critical range these laws require that a quantity of fluid is piled up continuously ahead of the ship in the form of a bore. Experimental confirmation is given by means of photographs of model tests.

## 1. Introduction

When a ship passes along a canal or other restricted waterway, it has been observed that the distance between the keel of the ship and the canal bottom decreases as the speed increases, and in fact on occasions the ship has been known to strike the bottom. This phenomenon is known as 'squatting'. In response to a request from the Manchester Ship Canal Company, the author undertook an investigation into the problem of squatting. In addition to a theoretical consideration of the problem many model tests were carried out in the Whitworth Laboratories at Manchester University.

One of the main outcomes of the investigation was the elucidation of a distinctive yet little-known general property concerning the movement of floating bodies along canals. This is that there are three types of flow régime according to different speed ranges. The principal aim of the present paper is to explain this property and to show, for each of the three cases, the relationships between the salient parameters of the problem, such as the dimensionless ship speed (i.e. a Froude number) and a dimensionless parameter measuring the degree of squatting. The theoretical model considered is severely simplified, but photographs of an experimental demonstration are presented which confirm the essential distinctions between the three possible régimes.

## 2. Theoretical treatment

To reduce the problem to its simplest form, the following assumptions are made:

(1) The ship moves with a constant velocity $V_1$ along a canal of uniform rectangular cross-section breadth $b$ and undisturbed depth $y_1$.

(2) The canal extends rectilinearly to infinity in both directions.

(3) The cross-section of the ship is uniform over its whole length and the end effects are ignored.

(4) The velocities of the water particles in any cross-section are constant over that cross-section.

(5) The loss of head due to friction is neglected.

(6) The effects of the secondary wave system are ignored.

(7) Any force necessary to move the ship is provided externally—not by means of a propeller which causes a reaction on the water.

Let us choose a frame of reference moving with the ship, so that the problem is reduced to one of steady flow. The sides and bottom of the canal must of course be considered to be moving past the ship with a velocity $V_1$; but since we are in effect dealing with an ideal fluid, this motion of the wetted boundary will not influence the flow.

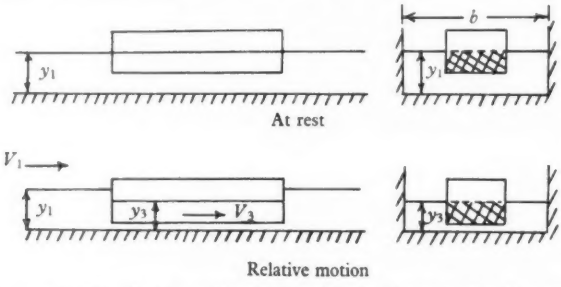


FIGURE 1. Idealized motion of the ship in the subcritical range.

With reference to figure 1, we have as the equation continuity

$$V_1 b y_1 = V_3(b y_3 - A), \tag{1}$$

where $A$ is the underwater cross-sectional area of the ship, $y_3$ the depth of the water alongside the ship, and $V_3$ the velocity of the water alongside the ship. Bernoulli's equation takes the form

$$\frac{V_1^2}{2g} + y_1 = \frac{V_3^2}{2g} + y_3. \tag{2}$$

Combining equations (1) and (2), we get

$$V_1 b y_1 = V_3\left\{b y_1 - \frac{(V_3^2 - V_1^2)\,b}{2g} - A\right\}. \tag{3}$$

Introducing the dimensionless parameters

$$S = \text{blockage factor} = \frac{A}{b y_1},$$

$$d = \frac{y_1 - y_3}{y_1}, \quad F_1 = \frac{V_1}{(g y_1)^{\frac{1}{2}}}$$

it can be shown that (3) reduces to

$$F_1 = \left[\frac{2d(1-d-S)^2}{1-(1-d-S)^2}\right]^{\frac{1}{2}}. \tag{4}$$

If the relationship between $F_1$ and $d$ for various values of the blockage factor $S$ is plotted, a remarkable property comes to light (see figure 2). It would appear that

for a given blockage factor there is a certain speed beyond which it is impossible for the ship to go. At this 'maximum' speed the ship will have squatted by a certain amount shown by the value of $d$ corresponding to the maximum value of $F_1$. If the value of $x/y_1$ (where $x$ is the clearance between the bottom of the ship and the bottom of the canal when stationary) is less than this limiting value of $d$, then the ship will strike the canal bottom at a speed corresponding to $d = x/y_1$.

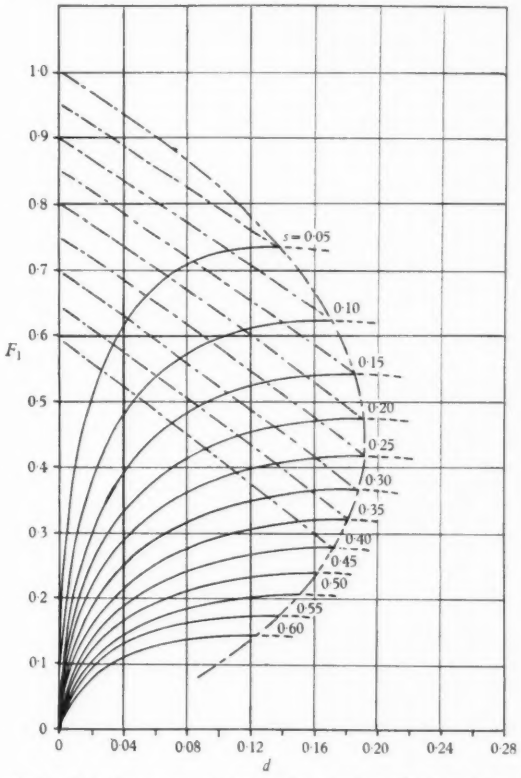


FIGURE 2. The relationship between the Froude number $F_1$ (based on the speed of the ship and the undisturbed depth of the canal) and the dimensionless 'squat' $d$ of the ship for various values of the blockage factor $S$.

This speed of course will be less than the maximum for that one blockage factor. If, however, the value of $x/y_1$ is greater than the limiting value of $d$, it is necessary to ask what happens to the ship if it attempts to exceed the 'maximum' speed?

## 3. Conditions at higher speeds

At first sight a possible solution to this problem is that the ship would catastrophically sink if the velocity was increased by a fraction; but a more likely solution follows from an idea given in a publication by Lap (1950) in which he considers the work of Krietner (1934).

From equation (3) we can derive

$$\frac{V_1}{(gy_1)^{\frac{1}{2}}} = \frac{V_3}{(gy_1)^{\frac{1}{2}}}\left[1 - S - \frac{1}{2}\left(\frac{V_3^2}{gy_1} - \frac{V_1^2}{gy_1}\right)\right].$$

If now $V_3/(gy_1)^{\frac{1}{2}}$ is plotted against $V_1/(gy_1)^{\frac{1}{2}}$ for a range of values of $S$, figure 3 is obtained. Here it can be seen that, as $V_1$ increases, so does $V_3$ up to a certain maximum value beyond which once again there is apparently no real solution.

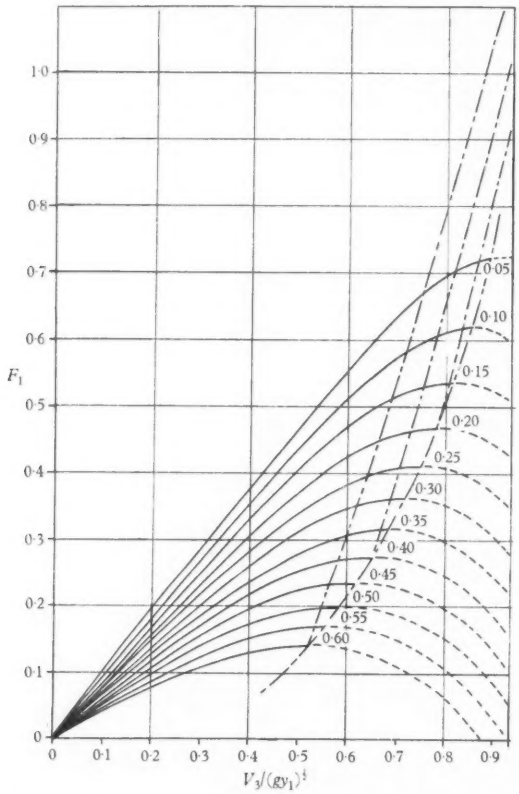


FIGURE 3. The relationship between the Froude numbers based on the speed of the ship and the relative velocity alongside the ship for various values of the blockage factor $S$.

In other words, up to this maximum value of $V_3$ the quantity of water flowing past the sides of the ship is capable of adjusting itself to take all the water presented by the corresponding value of $V_1$. Beyond the maximum, however, $V_3$ is no longer capable of keeping pace with $V_1$, and the excess water must be piled up in front of the ship.

Before this problem can be considered further, it is necessary to investigate what happens fore and aft of the ship as the water is piled up.

## 4. Idealized 'piston' motion in a canal

Consider a canal of uniform rectangular cross-section (see figure 4) extending rectilinearly to infinity in both directions. The canal is filled with a perfect liquid to a depth of $y_1$. Across the cross-section, and completely blocking it, is a flat plate capable of being moved along the length of the canal at a constant speed. If in

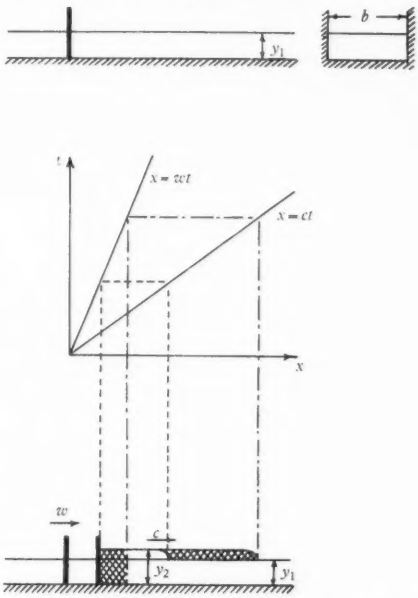


FIGURE 4. Idealized piston motion in a canal.

fact the plate is moved with a constant velocity $w$, the resulting motion ahead of the plate will be as shown and the speed of the bore front will be given by

$$c = \left[ g \frac{y_2}{y_1} \left( \frac{y_1 + y_2}{2} \right) \right]^{\frac{1}{2}}$$

(cf. Stoker 1957, p. 328).

To investigate the motion at the rear of the plate it is convenient to consider first the motion of a simple wave in shallow water (Stoker 1957, Ch. 10). If $u$ the horizontal velocity component and $c$ the propagation speed are both functions of $x$, the horizontal distance travelled, and of time $t$, it can be shown that in the $(x, t)$-plane we have two sets of characteristics $C_1$ and $C_2$ which are the solution curves of the ordinary differential equations

$$C_1: \frac{dx}{dt} = u + c,$$

$$C_2: \frac{dx}{dt} = u - c.$$

Also

$u + 2c = k_1$ a constant along $C_1$,

$u - 2c = k_2$ a constant along $C_2$.

This can now be used to determine the form of a disturbance behind a plate which is completely blocking the canal, and which is moving at a constant velocity $w$ in still fluid of constant depth $y_1$. The acceleration of the plate to the velocity $w$ may be either gradual or instantaneous but provided the position of the plate is known for all $t$, solutions are possible.

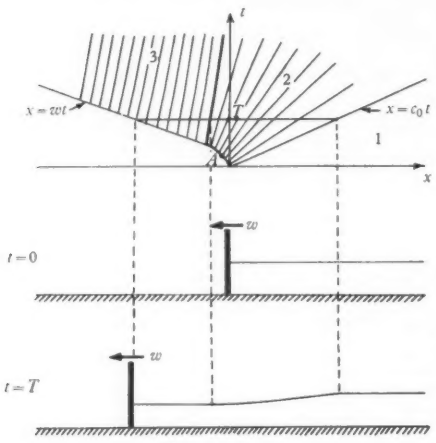


FIGURE 5

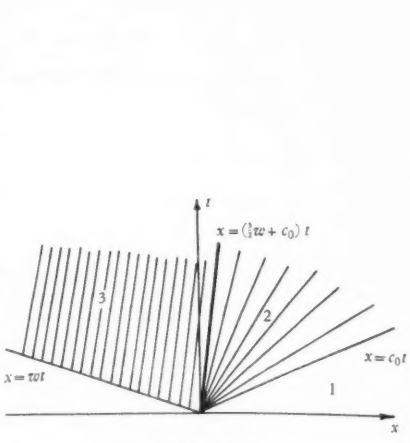


FIGURE 6

FIGURE 5. The $(x, t)$-relationship describing the disturbance to the rear of a plate which completely blocks the canal cross-section and accelerates gradually from rest to a constant velocity $w$.

FIGURE 6. The $(x, t)$-relationship describing the disturbance to the rear of a plate which completely blocks the canal cross-section and accelerates instantaneously to a constant velocity $w$.

The situation when the acceleration of the plate is not instantaneous is given in figure 5. Zone 1 represents the quiet area where the disturbance has not reached, and zone 2 represents a region of variable depth joining zone 1 to zone 3 which is another zone of constant depth. The two equations which define the straight characteristics in zone 2 are determined as follows:

$$u_0 - 2c_0 = u_a - 2c_a = -2c_0, \quad c_a = \tfrac{1}{2}u_a + c_0,$$

$$\frac{dx}{dt} = u_a + c_a = \tfrac{3}{2}u_a + c_0.$$

Since $c_a = [g(y_1 + \eta_a)]^{\frac{1}{2}}$, the surface elevation $\eta_a$ can be determined anywhere in zone 2 at any time $t$.

Similarly the equation for zone 2 when the acceleration of the plate is assumed to be infinite (figure 6) is derived as follows:

$$\frac{dx}{dt} = \frac{x}{t} = \tfrac{3}{2}u + c_0, \quad u = \frac{2}{3}\left(\frac{x}{t} - c_0\right),$$

$$c = \tfrac{1}{2}u + c_0 = \tfrac{1}{3}(\tfrac{1}{2}x + 2c_0).$$

Again knowing $c = [g(\eta + y_1)]^{\frac{1}{2}}$, the surface elevation $\eta$ can be determined anywhere in zone 2 at any time $t$.

Thus for the given condition we can accurately describe the motion fore and aft of the plate when it moves with a uniform velocity $w$.

## 5. The critical and supercritical ranges

Whilst on the face of it there seems to be little connexion between a plate which completely blocks the canal and a ship which is floating and in addition only blocking a fraction of the canal cross-section, the information just derived can in fact be used. The water piled up in front of the ship will cause, as in the case of the plate, a surge or bore to travel ahead and consequently a negative disturbance aft of the ship. This is illustrated in figure 7. It should be noted that we are still assuming that there are no end effects and the ship therefore retains an even keel.

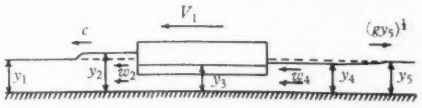


FIGURE 7. Idealized motion of the ship in the critical range.

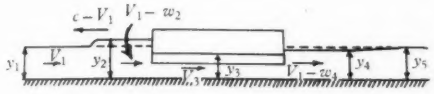


FIGURE 8. Idealized motion of the ship in the critical range, the frame of reference moving with the ship.

It is easily seen that the expression for $c$ has the same form as before. Considering now the motion to the aft of the ship, we have, for the total quantity passing the ship,

$$b(V_1 - w_2)\, y_2 = b(V_1 - w_4)\, y_4.$$

But we know that

$$c = (gy_4)^{\frac{1}{2}} = (gy_5)^{\frac{1}{2}} - \tfrac{1}{2}w_4 = (gy_1)^{\frac{1}{2}} - \tfrac{1}{2}w_4,$$

$$w_4 = 2[(gy_1)^{\frac{1}{2}} - (gy_4)^{\frac{1}{2}}],$$

$$(V_1 - w_2)\, y_2 = [V_1 - 2\{(gy_1)^{\frac{1}{2}} - (gy_4)^{\frac{1}{2}}\}]\, y_4.$$

Thus, given $y_2$, we have sufficient information to determine $y_4$ and $w_4$. If, therefore, a relationship between $y_2$ and $V_1$ can be determined, we have a complete picture of the behaviour of the ship under the ideal conditions assumed.

When the ship does start to push forward a quantity of water, the depth and velocity immediately in front of the ship will alter and $V_3$ (see figure 8) will adjust itself to pass the maximum under the new conditions. With sufficient computational labour it is possible to work out the values of $V_3/(gy_1)^{\frac{1}{2}}$ and $d$ for values of $V_1/(gy_1)^{\frac{1}{2}}$ in excess of the critical, i.e. when the steady state ceases to exist. These results are shown as chain lines in the graphical representation in figures 2 and 3. As $V_1/(gy_1)^{\frac{1}{2}}$ increases, $V_3/(gy_1)^{\frac{1}{2}}$ continues to increase but at a much slower rate than before. At the same time $d$ decreases in value, i.e. the ship begins to rise.

But what happens as $V_1/(gy_1)^{\frac{1}{2}}$ becomes equal to and exceeds unity? If equations (1) and (2) are re-examined it will be seen that in addition to the solution already plotted for the subcritical range there are solutions for $F_1 > 1$. These additional solutions are shown for a range of blockage factors in figures (9) and (10).

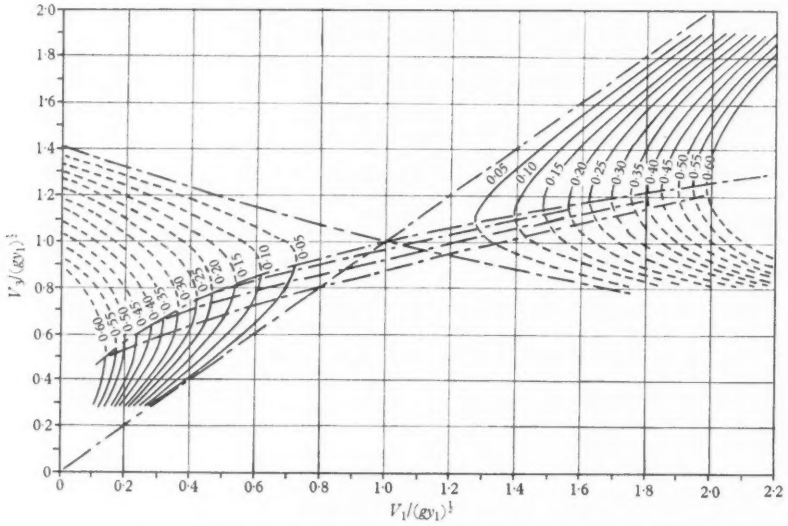


FIGURE 9. The relationship between the Froude numbers based on the speed of the ship and the relative velocity alongside the ship for various values of the blockage factor $S$.

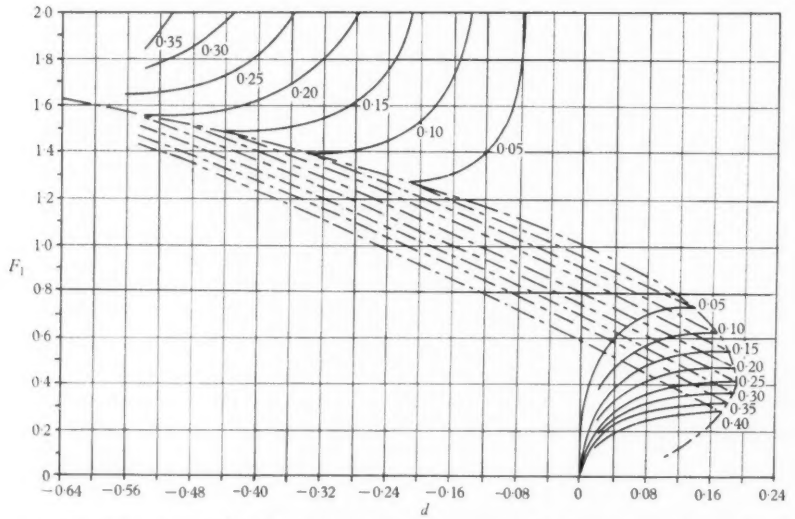


FIGURE 10. The relationship between the Froude number $F_1$ (based on the speed of the ship and the undisturbed depth of the canal) and the dimensionless 'squat' of the ship for various values of the blockage factor $S$.

It is clear from a study of these graphs that for a ship moving in a restricted passage of fluid (or indeed for any floating body which is moving in a restricted passage of fluid, or which is stationary in a moving body of fluid), there are three distinct speed ranges: subcritical, critical and supercritical. In the subcritical range the Bernoulli and continuity equations are satisfied by a steady state everywhere, the excess velocity alongside the ship causing a decrease in the depth of fluid and consequently the squatting of the ship. In the supercritical range the 'steady-state' Bernoulli and continuity equations are again satisfied everywhere, but, contrary to the subcritical range, there is a reduced velocity alongside the

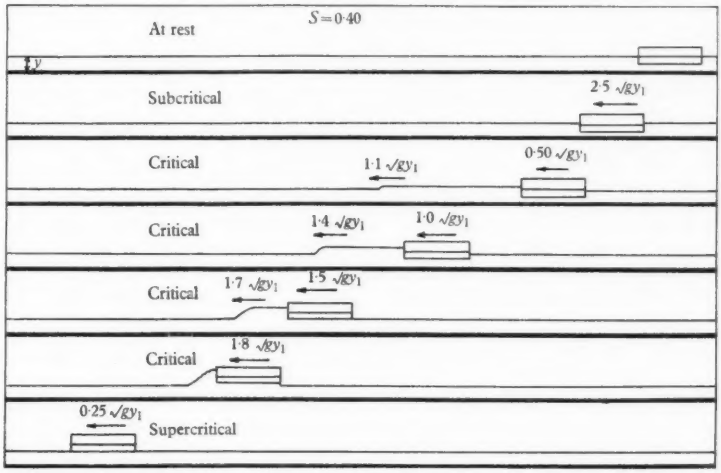


FIGURE 11. The idealized behaviour of a ship as it moves at speeds in the subcritical, critical and supercritical range. For ease of comparison the diagrams give the position of the ship and bore at one fixed time after starting instantaneously from rest.

ship and hence an increase in the depth of fluid causing the ship to rise above its original static position. Connecting the subcritical and the supercritical is the critical range where the Bernoulli and continuity equations can only be satisfied in the vicinity of the ship if a quantity of fluid is piled up ahead of it. This causes a bore to advance ahead and a negative disturbance to move aft and away from the ship. Contrary to the other two ranges in which the motion is steady, the motion in this case is unsteady.

It can be shown that as $F_1$ increases above the lower critical speed the height of the bore increases. At the same time the absolute speed of the bore front increases but its speed relative to the ship decreases, i.e. the ship tries to catch up the bore front. At the upper critical speed the bore height is a maximum and the ship is travelling at a speed only slightly less than that of the bore front, a small quantity of fluid still being pushed ahead. Immediately the upper critical speed is exceeded however the ship 'jumps' on the bore and the bore as such disappears, the ship no longer pushing ahead any fluid. Figure 11 shows quite clearly the effect as $F_1$ increases through the subcritical and supercritical range for the ideal case considered.

Clearly the shape of the ship and the viscous effects of the fluid will affect the results just derived. These effects along with the case of self-propulsion are to be dealt with in a separate paper.

This phenomenon was conclusively demonstrated in the laboratory by towing a small ship (8 in. long) along a small Perspex channel filled with water. The photographs given in figures 12(*a*), (*b*) and (*c*) (plate 1) show the ship in the subcritical, critical and supercritical ranges, respectively. It will be noticed that in contrast to the ideal case considered the ship takes on a considerable trim in the critical range.

The author would like to thank Professor J. A. L. Matheson for his guidance and encouragement throughout the whole project and Professor M. J. Lighthill for his valuable help on the theoretical treatment.

## REFERENCES

KRIETNER, J. 1934 Über den Schiffswiderstand auf beschranktem Wasser. *Werft Reederei Hafen.*

LAP, A. J. W. 1950 *Fundamentals of Ship Resistance and Propulsion, Part A, Resistance.* Netherlands Ship Model Basin.

STOKER, J. J. 1957 *Water Waves.* New York: Interscience.

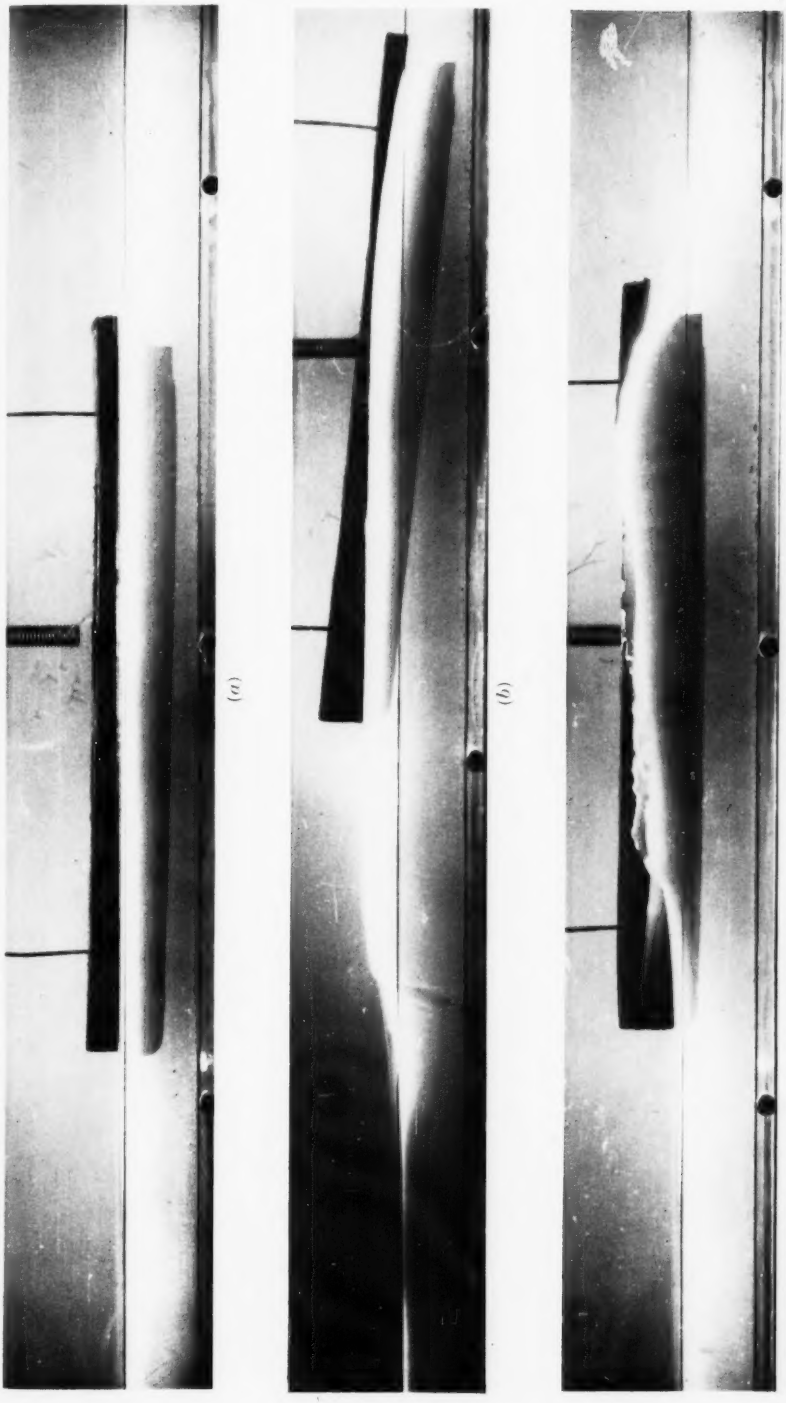


FIGURE 12. (*a*) Subcritical range. (*b*) Critical range. The ship has only just started to move and therefore the distance between the bow of the ship and the bore front is small. (*c*) Supercritical range.



(*Facing p.* 256)

# Stability and transition of a supersonic laminar boundary layer on an insulated flat plate

By JOHN LAUFER AND THOMAS VREBALOVICH
Jet Propulsion Laboratory, California Institute of Technology, Pasadena, California

(Received 9 May 1960)

Self-excited oscillations have been discovered experimentally in a supersonic laminar boundary layer along a flat plate. By the use of appropriate measuring techniques, the damping and amplification of the oscillations are studied and the stability limits determined at free-stream Mach numbers 1·6 and 2·2. The wave-like nature of the oscillations is demonstrated and their wave velocities are measured using a specially designed 'disturbance generator'. It is shown empirically that the stability limits expressed in terms of the boundary-layer-thickness Reynolds number are independent of the Mach number and dependent only on the oscillation frequency. The main effect of compressibility is an increase in wave velocity with Mach number. This has the consequence that the disturbances, although possessing the same dimensionless amplification coefficient as in the incompressible case, have less time (per unit distance) to grow in amplitude. Thus, the adiabatic compressible boundary layer is shown to be more stable than the incompressible one. In general, the experiments confirm the basic assumptions and predictions of the existing stability theory and also suggest the desirability of improvement in the theory in certain phases of the problem. Finally, on the basis of these results a rough estimate of the transition Reynolds number is made in the compressible flow range.

## 1. Introduction

The transition of a boundary layer from a laminar to a turbulent state is one of the outstanding unsolved problems in fluid mechanics. Its practical importance is especially recognized in supersonic flows, where the accompanying aerodynamic heating effects become an essential design consideration.

Today it is a well-accepted fact that in incompressible flows transition is the result of not one but of several instability mechanisms (Dryden 1955; Morkovin 1958). The first stage of the process is the so-called instability with respect to small disturbances (provided the free steam is void of large disturbances). This instability provides the triggering mechanism for the whole transition process and therefore must be considered very important. There are many indications that in compressible flows the transition phenomenon is basically the same. The present investigation was therefore undertaken with the belief that the study of the first stage of transition in the compressible boundary layer, the instability with respect to small disturbances, should result in valuable information.

When the historical development of the stability problem in the incompressible

laminar boundary layer is considered, it is surprising to note that despite the great interest of theoretical researchers and the great practical importance of the problem, very few basic stability experiments were carried out. The comparatively slow progress and the strong controversies in the 1930's were mainly the result of this lack of basic experimental work. After all, fourteen years elapsed between 1929, when Tollmien (1929) first published his small-disturbance theory for the boundary layer, and 1943, when the experiments of Schubauer & Skramstad (1948) fully confirmed the theory. During this period the theory was exposed to strong criticism, not only because of its lack of mathematical rigour, but also because of its underlying physical model for the transition process. Specifically, the theory was attacked because the connexion between the small-disturbance instability and transition was not understood at that time, and the linearized two-dimensional theory was considered too great an oversimplification to describe adequately the strongly non-linear transition process. Furthermore, the self-excited boundary-layer oscillations, the most striking prediction of the theory, had not yet been observed. Obviously, only direct experiments could and did satisfy such criticism. The measurements of Schubauer & Skramstad demonstrated not only the existence of the instability waves, but also the fact that the behaviour of these waves agrees quantitatively with the theoretical predictions. These experiments were followed by a few similarly basic ones: Liepmann (1943) applied the technique to boundary layers on curved walls; Bennett (1953) considered the effect of increased free-stream turbulence level on stability; and, finally, Wortmann (1955) studied the stability problem using a completely different experimental method. It is believed that as a result of these experiments and of the theoretical studies, especially those of Lin (1945), who answered the remaining mathematical questions, the first stage of transition in the incompressible boundary layer is well understood.

If attention is turned now to the stability problem in the compressible boundary layer, the lack of basic experimental work again becomes evident. After 1946, when the pioneering theoretical work of Lees & Lin (1946) extended the small-disturbance stability theory to flows at low supersonic Mach numbers, no pertinent experiments were reported in the literature for more than ten years. In contrast to the incompressible theory, however, the theoretical work gained ready acceptance; in fact, it was even applied to problems outside the immediate scope of the theory. Lees & Lin have clearly indicated that their work is restricted to flows at low Mach numbers (below approximately 1·5), where the wave velocities are small compared with the free-stream velocity and where the temperature fluctuations can be neglected in the relation for the characteristic values of the problem. These limitations were partially removed by Dunn & Lin (1955), who also included three-dimensional disturbances in their theory. Any further extension of the theory to high Mach numbers, however, would become exceedingly difficult because of some of the inherent assumptions in the formulation of the theory. Neglect of disturbances that are supersonic relative to the free stream, for instance, would have to be justified. Undoubtedly, measurements examining such questions would be of great value.

The available experiments, however, do not deal with this basic problem, but

with the study of the transition 'point' of a compressible boundary layer in the light of the stability theories. Although, in principle, strong objections may be raised against such direct comparisons, some qualitative results have been obtained. It has been shown in several instances that surface cooling increases the transition Reynolds number, which is consistent with Lees's prediction of increased stability with cooling (e.g. Lees 1947). Furthermore, various investigators have reported that with increasing Mach number it becomes more difficult to trip the boundary layer, indicating in a loose sense that the layer becomes more stable at larger Mach numbers, which is again consistent with Lees's (1952) calculations of decreasing amplification rates.

At the time the present work was initiated, no experiments which directly concerned the first stage of transition (experiments analogous to those of Schubauer & Skramsted in incompressible flows) existed. This situation derived from several serious difficulties. It is well known from experience in incompressible flows that a suitable experimental environment is of vital importance. Not only the mean velocity and pressure gradients in the wind tunnel, but the tunnel turbulence level, as well, must be minimized. Supersonic free-stream turbulence is not yet well understood. Also, mechanical and electronic instrumentation can present a major difficulty. In the measurement of small-amplitude flow fluctuations, it is obvious that mechanical vibrations in the traversing mechanisms, probes, and flat plates must be largely eliminated. Finally, the hot-wire technique must be developed and adapted so that measurements up to 100,000 c/s can be carried out and interpreted correctly.

The experiments presented here succeeded to a large extent in overcoming these difficulties. By a careful and detailed examination of the free-stream fluctuations in the wind tunnel, a Mach number range in which the stability measurements could be accepted with confidence was chosen. The mechanical instrumentation was designed in such a way that any vibration or flow disturbance induced by the system could be immediately detected and corrected. Finally, the hot-wire technique and accompanying instrumentation were developed to the extent that they were not the major limiting factors in determining the scope of the experiments.

Under these circumstances the investigation at the Jet Propulsion Laboratory succeeded in accomplishing the following:

(1) The existence of self-excited oscillations in a supersonic boundary layer was shown experimentally.

(2) A detailed study of the behaviour of these oscillations was made, and the results were compared with theoretical predictions.

(3) Some of the differences between the stability of the incompressible boundary layer and the stability of the supersonic boundary layer were further brought to focus.

Some early results of this work are described elsewhere (Laufer 1956; Laufer & Vrebalovich 1957). Also, parallel with the present investigation, Demetriades (1958, 1960) obtained some interesting results on the stability problem in the hypersonic tunnel of the California Institute of Technology at Mach number 5·8 using techniques similar to those described here.

## 2. Experimental equipment

### 2.1. *Wind tunnel*

Most of the measurements were carried out in the Jet Propulsion Laboratory $18 \times 20$ in. supersonic wind tunnel; some of the initial data were obtained in the $12 \times 12$ in. wind tunnel. The Mach number in the working section of the larger tunnel was continuously variable from 1·3 to 5·0. The distribution of the static pressure in the test section was uniform to within 2 % along the centre-line and 5 % six inches below and above the centre-line in the whole Mach number range. Such a uniform mean flow field served to great advantage in these experiments.

Considerable time and effort were spent to reduce the turbulence level in the supply section. Figure 1 shows a portion of the tunnel circuit. The first two screens shown in the short entrance diffuser were installed in order to prevent local flow separation. At the entrance of the 8 ft. diameter stagnation chamber, an Airmat paper filter* was stretched across the section to protect the hot wires from fine dust particles. The subsequent six damping screens served to reduce the turbulence level.

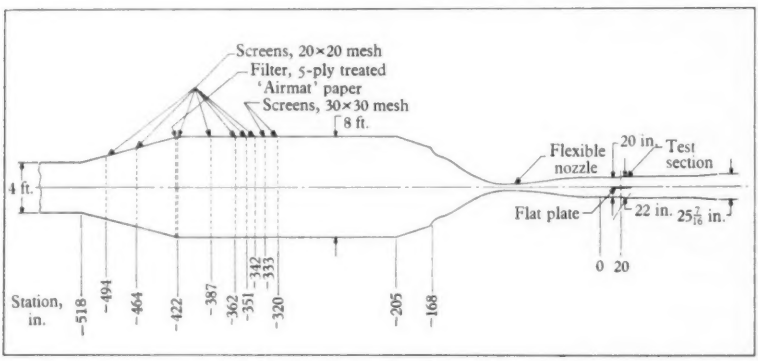


FIGURE 1. Supply section and test section of $18 \times 20$ in. wind tunnel.

Turbulence-level measurements in the supply section were made approximately $2\frac{1}{2}$ ft. downstream of the last damping screen. The results indicated that the temperature fluctuations were negligibly small and the velocity fluctuations were 1 % of the local mean velocity for all the tunnel pressures and free-stream Mach numbers except for $M_1 \geqslant 4{\cdot}5$, where the level dropped to $\frac{1}{2}$ %. When it is considered that even for the lowest Mach number flow the velocity ratio of the free-stream and supply-section flow is somewhat more than 40 : 1, a velocity fluctuation of less than 0·01 % in the free stream is calculated using Tucker's method (1953). Consequently, the 1 % turbulence level in the supply section was believed to be satisfactory.

Measurements in the supersonic free stream presented much more difficulty. By use of a method proposed by Kovasznay (1953) and Morkovin (1956), the

* Manufactured by American Air Filter, Louisville, Ky.

mass-flow (figure 2) and total-temperature fluctuations could be calculated and were found to increase very rapidly with Mach number. It is also seen in the figure that the fluctuations increase with decreasing tunnel pressure. The results of a detailed study of this problem will be published elsewhere (Laufer 1959) and will therefore not be described. Briefly, the fluctuations found in the free stream are shown to be due to a pure sound field produced by the thick turbulent boundary layers of the tunnel walls. Any reduction of the turbulence level at the higher Mach number flows would involve removing the boundary layers from the tunnel walls, an extremely elaborate and difficult task, or operating the wind tunnel at pressure levels low enough to sustain laminar boundary layers. Unfortunately, because of practical limitations, neither was possible.

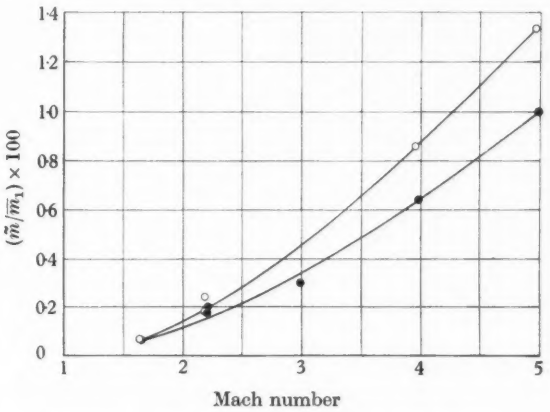


FIGURE 2. Mass-flow fluctuations in test section.
○, $Re$/in. ~ 90,000; ●, $Re$/in. ~ 330,000.

From the above considerations it is obvious that any boundary-layer-stability work, in which low free-stream turbulence level is a necessity, is possible only at the lower Mach number flows in this tunnel. The choice of the upper Mach number limit is described in § 5.3.

### 2.2. *Flat plates*

The experiments were carried out using two different flat plates. For the measurements at $M_1 = 1{\cdot}6$, a $\frac{1}{2}$ in. thick, 25 in. long, plate with a leading edge of 13 degrees was used. For the measurements at higher Mach numbers, a 1 in. thick, 33 in. long, plate with a leading-edge angle of 24 degrees was provided. Both plates were ground and lapped; the leading-edge radii were less than 0·001 in.

### 2.3. *Traversing mechanisms*

Most of the data were obtained with the hot-wire probe attached to a servo-controlled carriage and traversing mechanism (figures 3 and 4). The mechanical details are described elsewhere (Laufer & Vrebalovich 1958).

## 2. Experimental equipment

### 2.1. *Wind tunnel*

Most of the measurements were carried out in the Jet Propulsion Laboratory $18 \times 20$ in. supersonic wind tunnel; some of the initial data were obtained in the $12 \times 12$ in. wind tunnel. The Mach number in the working section of the larger tunnel was continuously variable from 1·3 to 5·0. The distribution of the static pressure in the test section was uniform to within 2 % along the centre-line and 5 % six inches below and above the centre-line in the whole Mach number range. Such a uniform mean flow field served to great advantage in these experiments.

Considerable time and effort were spent to reduce the turbulence level in the supply section. Figure 1 shows a portion of the tunnel circuit. The first two screens shown in the short entrance diffuser were installed in order to prevent local flow separation. At the entrance of the 8 ft. diameter stagnation chamber, an Airmat paper filter* was stretched across the section to protect the hot wires from fine dust particles. The subsequent six damping screens served to reduce the turbulence level.

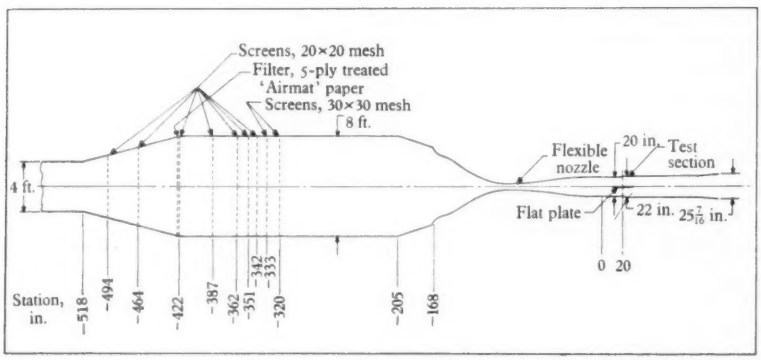


FIGURE 1. Supply section and test section of $18 \times 20$ in. wind tunnel.

Turbulence-level measurements in the supply section were made approximately $2\frac{1}{2}$ ft. downstream of the last damping screen. The results indicated that the temperature fluctuations were negligibly small and the velocity fluctuations were 1 % of the local mean velocity for all the tunnel pressures and free-stream Mach numbers except for $M_1 \geqslant 4{\cdot}5$, where the level dropped to $\frac{1}{2}$ %. When it is considered that even for the lowest Mach number flow the velocity ratio of the free-stream and supply-section flow is somewhat more than 40 : 1, a velocity fluctuation of less than 0·01 % in the free stream is calculated using Tucker's method (1953). Consequently, the 1 % turbulence level in the supply section was believed to be satisfactory.

Measurements in the supersonic free stream presented much more difficulty. By use of a method proposed by Kovasznay (1953) and Morkovin (1956), the

* Manufactured by American Air Filter, Louisville, Ky.

mass-flow (figure 2) and total-temperature fluctuations could be calculated and were found to increase very rapidly with Mach number. It is also seen in the figure that the fluctuations increase with decreasing tunnel pressure. The results of a detailed study of this problem will be published elsewhere (Laufer 1959) and will therefore not be described. Briefly, the fluctuations found in the free stream are shown to be due to a pure sound field produced by the thick turbulent boundary layers of the tunnel walls. Any reduction of the turbulence level at the higher Mach number flows would involve removing the boundary layers from the tunnel walls, an extremely elaborate and difficult task, or operating the wind tunnel at pressure levels low enough to sustain laminar boundary layers. Unfortunately, because of practical limitations, neither was possible.

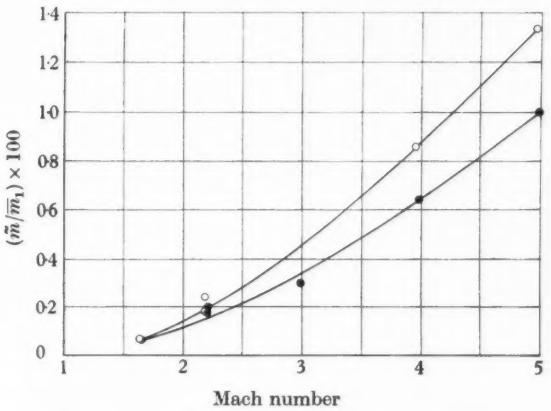


FIGURE 2. Mass-flow fluctuations in test section.
○, $Re$/in. ~ 90,000; ●, $Re$/in. ~ 330,000.

From the above considerations it is obvious that any boundary-layer-stability work, in which low free-stream turbulence level is a necessity, is possible only at the lower Mach number flows in this tunnel. The choice of the upper Mach number limit is described in § 5.3.

### 2.2. *Flat plates*

The experiments were carried out using two different flat plates. For the measurements at $M_1 = 1{\cdot}6$, a $\frac{1}{2}$ in. thick, 25 in. long, plate with a leading edge of 13 degrees was used. For the measurements at higher Mach numbers, a 1 in. thick, 33 in. long, plate with a leading-edge angle of 24 degrees was provided. Both plates were ground and lapped; the leading-edge radii were less than 0·001 in.

### 2.3. *Traversing mechanisms*

Most of the data were obtained with the hot-wire probe attached to a servo-controlled carriage and traversing mechanism (figures 3 and 4). The mechanical details are described elsewhere (Laufer & Vrebalovich 1958).

### 2.4. *Hot-wire probes*

In all of the experiments described, the hot wires were 90% platinum–10% rhodium and were 0·00005 or 0·0001 in. in diameter with nominal lengths of 0·015 or 0·020 in., respectively. The hot-wire probe (figure 5, plate 1) is mounted in the carriage as shown in figure 4.

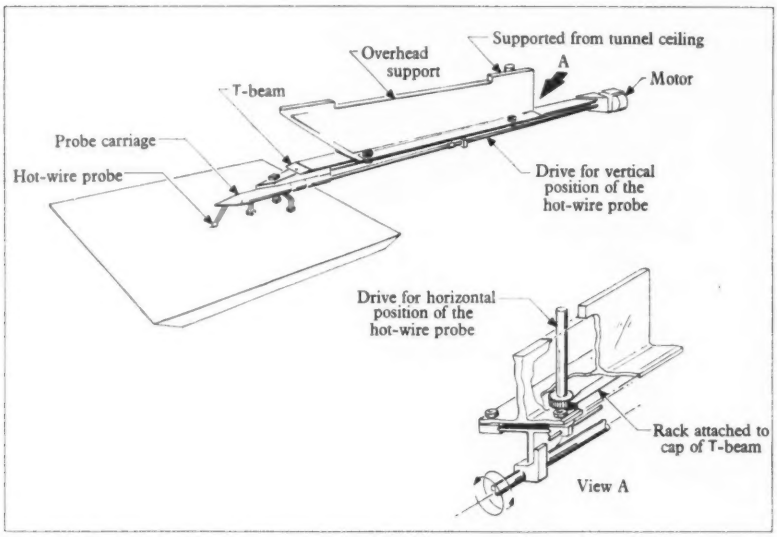


FIGURE 3. Diagram of $x$-traversing mechanism.

### 2.5. *Disturbance generator*

The basic problem was to generate the disturbances in the frequency range of 5000 to 50,000 c/s without affecting the normal boundary-layer growth and the flow field. Several different methods were attempted in order to produce single-frequency disturbances near the leading edge of the flat plate.

The disturbance generator finally adopted was essentially a high-speed valve. This opened and closed a narrow slit in the surface of the flat plate to allow periodic air pulses of any desired strength and frequency to disturb the boundary layer on the surface of the plate. The main part of this generator was a hollow cylinder (figure 6) 0·3 in. in diameter and 3·0 in. long (1·5 in. long for the 1 in. thick plate), with 40 slots, 0·01 in. wide, milled parallel to its axis (figure 7, plate 2). A slot (figure 6) 0·003 in. wide and 3 in. long was milled near the plate centre-line in the surface of the plate along the axis of the cylinder 1·7 in. (0·8 in. for the 1 in. thick plate) from the leading edge. The cylinder was connected to the variable-speed motor by means of gears, a long shaft in the plate, a high-speed grinder spindle, and a timing belt and pulleys. This arrangement can be seen in figure 8 (plate 3). The maximum rpm of the motor was 5000; this corresponded to the 90,000 rpm of the cylinder.

The chamber that surrounded the slotted cylinder was sealed by a cover plate and by a Van de Graaff type of seal around the shaft (Strong 1938). Air was allowed to enter the chamber through a porous plug in order to obtain uniform flow through the slit along its 3 in. length (figure 7, plate 2). The flow rate (i.e. the disturbance amplitude) was regulated by a needle valve. The generator frequency was monitored by the arrangement seen in figure 7 (plate 2). A light source and

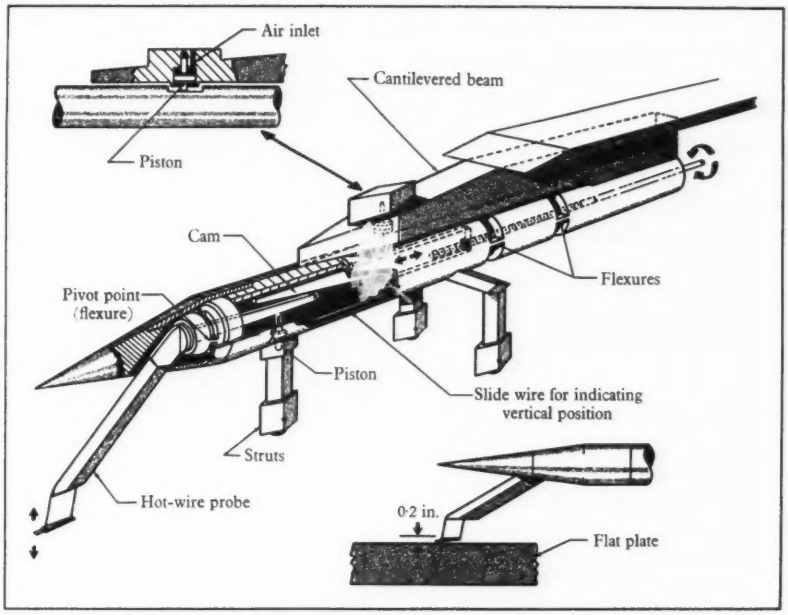


FIGURE 4. Hot-wire carriage and $y$-traversing mechanism.

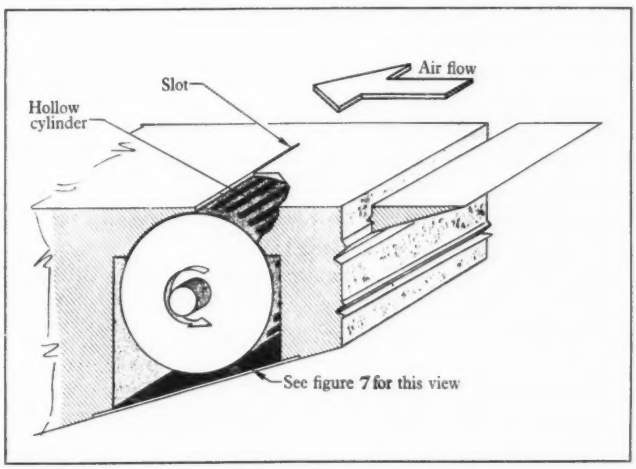


FIGURE 6. Schematic diagram of the disturbance generator.

photocell were placed so that the reflected light from the rotating cylinder struck the photocell. Each time one of the cylinder slats passed the light path a reflexion occurred which was recorded by the photocell. Thus, the output of the photocell gave the proper reference frequency.

### 2.6. *Hot-wire set, auxiliary equipment*

*Hot-wire amplifier.* The design requirements of the hot-wire equipment used for fluctuation measurements in supersonic flows have been described in detail by Kovasznay (1954). The high frequencies that are expected in supersonic flow fields necessitate an amplifier with a frequency response of several hundred kilocycles. Low-noise input circuitry is critical in such an amplifier, especially because of the greater frequency bandwidth and low level of the fluctuations expected. The commercially available Shapiro–Edwards Model 50 B constant-current hot-wire set (Shapiro and Edwards, South Pasadena, California) satisfies these requirements and was used throughout the experiment.

*Wave analysers.* Several different harmonic wave analysers were used to determine the power spectrum of the hot-wire signals. A Panoramic SB 7a ultrasonic harmonic wave analyser (Panoramic Radio Products, Inc., Mt Vernon, N.Y.), which exhibited the spectrum of the hot-wire signal from 1 to 300 kc on an internal oscilloscope, was very useful in quickly showing if there were extraneous oscillations in the signal. Sharp peaks in the spectrum distribution observed on the analyser indicated hot-wire or probe vibrations, possible flat-plate vibrations, or oscillations in electronic equipment; and remedial measures could be taken immediately.

Quantitative power-spectrum measurements were obtained with two different harmonic wave analysers. These instruments were also used as very narrow band-pass filters in order that the growth and decay of the energy in a narrow frequency band of the disturbance could be observed. The low-frequency range of the spectrum was covered by a Hewlett-Packard Model 300 A harmonic wave analyser (Hewlett-Packard Co., Palo Alto, California) with a frequency range of 30–16,000 c/s and a variable effective bandwith of 10 to 45 c/s. The high range of frequencies was detected by a Sierra Model 104 carrier-frequency voltmeter (Sierra Electronic Corp., Menlo Park, California) with a frequency range from 3 to 150 kc and a bandwith of 600 c/s.

The output circuitry of both analysers was modified to enable the installation of a vacuum thermocouple which would give an output thermocouple voltage proportional to the mean square of the output signal of the analyser. The method for plotting spectra will be described in detail in § 4.1.

*Plotting table.* Power spectra and the growth and decay of disturbances in the boundary layer were plotted on an Electronics Associates Variplotter (Electronic Associates, Inc., Long Branch, N.J.).

## 3. Theoretical considerations

It is outside the scope of this paper to discuss the theory of compressible-boundary-layer stability; that subject is adequately covered in the literature (Lees & Lin 1946; Dunn & Lin 1955). Instead, attention is focused on the under-

lying assumptions of the theory and on its predictions, so that they may be examined in the light of the experiments.

### 3.1. *Basic assumptions of the stability theory*

Under consideration are the general equations of motion of an ideal, viscous, heat-conducting, compressible fluid in which perturbations are introduced about a steady-state solution in the form

$$Q(x,y,z,t) = \bar{Q}(x,y,z) + Q'(x,y,z,t).$$

Thus, any quantity $Q$ is decomposed into two parts: a time-averaged mean value and a time-dependent perturbation.

*Assumption* 1. It is assumed now that

$$\frac{Q'}{\bar{Q}} \ll 1,$$

so that second-order interactions between perturbations can be neglected. As a result of this assumption the equations become linear and can be handled by conventional methods. The theory considers now the flow over a flat plate and makes additional assumptions.

*Assumption* 2. The usual boundary-layer approximations are introduced. Furthermore, from detailed considerations of orders of magnitude (Dunn & Lin 1955), it is concluded that certain viscous terms in the momentum equations and all the dissipation terms in the energy equation can be neglected provided the Mach number is not very high.

*Assumption* 3. It is also assumed that the mean flow in the boundary layer can be considered parallel when the boundary-layer stability at a given location is to be obtained. Here again, a high Mach number is the limiting factor for the validity of this assumption (Dunn & Lin 1955).

With these simplifications the structure of the equations allows the perturbations to have the form (see p. 296 for an explanation of the notation)

$$Q' = q\left(\frac{y}{\delta}\right) e^{\beta_i t} e^{ix(\alpha - c t)}, \tag{3.1}$$

where the amplitude function $q$ depends on $y/\delta$ only. The more general three-dimensional case is treated by Dunn & Lin (1955).

The simplified equations now take the following form.

Continuity equation:

$$\frac{\partial \rho'}{\partial t} + \bar{u}\frac{\partial \rho'}{\partial x} + v'\frac{\partial \bar{\rho}}{\partial y} + \bar{\rho}\left(\frac{\partial u'}{\partial x} + \frac{\partial v'}{\partial y}\right) = 0. \tag{3.2}$$

Momentum equations:

$$\bar{\rho}\left(\frac{\partial u'}{\partial t} + \bar{u}\frac{\partial u'}{\partial x} + v'\frac{\partial \bar{u}}{\partial y}\right) = -\frac{\partial p'}{\partial x} + \bar{\mu}\frac{\partial^2 u'}{\partial y^2}, \tag{3.3}$$

$$\bar{\rho}\left(\frac{\partial v'}{\partial t} + \bar{u}\frac{\partial v'}{\partial x}\right) = -\frac{\partial p'}{\partial y} + \bar{\mu}\frac{\partial^2 v'}{\partial y^2}. \tag{3.4}$$

Energy equation:

$$\bar{\rho}C_v\left(\frac{\partial T'}{\partial t}+\bar{u}\frac{\partial T'}{\partial x}+v'\frac{\partial \bar{T}}{\partial y}\right)=-\bar{p}\left(\frac{\partial u'}{\partial x}+\frac{\partial v'}{\partial y}\right)+\bar{k}\frac{\partial^2 T'}{\partial y^2}. \tag{3.5}$$

Equation of state:

$$\frac{p'}{\bar{p}}=\frac{\rho'}{\bar{\rho}}+\frac{T'}{\bar{T}}. \tag{3.6}$$

Or, if all the fluctuating quantities are written according to equation (3.1), where $f$, $\phi$, $\pi$, $r$ and $\theta$ are the amplitude functions of $u'$, $v'$, $p'$, $\rho'$ and $T'$, respectively:

$$i\alpha(\bar{u}-c)r+\phi\frac{\partial\bar{\rho}}{\partial y}+\bar{\rho}\left(i\alpha f+\frac{\partial\phi}{\partial y}\right)=0, \tag{3.7}$$

$$\bar{\rho}\left[i\alpha(\bar{u}-c)f+\phi\frac{\partial\bar{u}}{\partial y}\right]=-\pi i\alpha+\bar{\mu}\frac{\partial^2 f}{\partial y^2}, \tag{3.8}$$

$$\bar{\rho}[i\alpha(\bar{u}-c)\phi]=-\frac{\partial\pi}{\partial y}+\bar{\mu}\frac{\partial^2\phi}{\partial y^2}, \tag{3.9}$$

$$\bar{\rho}C_v\left[i\alpha(\bar{u}-c)\theta+\phi\frac{\partial\bar{T}}{\partial y}\right]=-\bar{p}\left(i\alpha f+\frac{\partial\phi}{\partial y}\right)+\bar{k}\frac{\partial^2\theta}{\partial y^2}, \tag{3.10}$$

$$\frac{\pi}{\bar{p}}=\frac{r}{\bar{\rho}}+\frac{\theta}{\bar{T}}. \tag{3.11}$$

The boundary conditions satisfied by the perturbations at the wall are

$$f(0)=\phi(0)=0,$$

$$a\frac{d\theta}{dy}(0)+b\theta(0)=0,$$

where $a$ and $b$ depend on the frequency of oscillation and the physical properties of the gas and the wall.

On the free-stream side the boundary conditions depend on the nature of the disturbance considered. Here the theory introduces the following assumption.

*Assumption* 4. Only disturbances that are propagating with subsonic speed with respect to the free stream are considered. It is conjectured that supersonic disturbances do not play an important role in the boundary-layer stability problem. This question has not yet been studied either theoretically or experimentally. From this assumption it follows that, for $y\to\infty$,

$$f,\quad \phi,\quad \text{and}\quad \theta\to 0.$$

With the above six boundary conditions and the sixth-order system of linear differential equations, a characteristic-value problem is defined. The equation relating the eigenvalues may be written formally

$$E(M_1^2,\alpha R_e,\alpha^2,c)=0.$$

The solution of the stability problem is now reduced to solving this relation. In their formulation, Lees & Lin used a method of approximation within

which the above relation and the boundary conditions become independent of the temperature fluctuations. The approximation is based on the following assumption.

*Assumption* 5. In essence it is required that the critical layer be near the wall. This is valid if the free-stream Mach number is subsonic or slightly supersonic. A consequence of this assumption is that the relation for the characteristic values becomes independent of the temperature fluctuations and the boundary conditions imposed on them. Later Dunn & Lin relaxed this assumption and showed that for higher Mach numbers the role of the temperature fluctuations does become important.

The solution of the above secular equation involves elaborate and complex mathematical arguments, some of which are still not completely settled. However, no new physical assumption is introduced.

### 3.2. *General results of the theory*

On the basis of these five assumptions the theory leads to the following general conclusions concerning the stability of a compressible boundary layer on an insulated flat plate:

(1) The basic mechanism of stability is the same as that found in the incompressible case.

(2) Three-dimensional disturbances become important at supersonic Mach numbers.

From the relatively few existing numerical calculations (Dunn & Lin 1955; Lees 1947) some interesting insight can also be obtained into the effect of Mach number on the quantitative behaviour of the stability parameters. It is found that with increasing Mach number:

(*a*) The propagation speed increases and the wave-number decreases.

(*b*) The minimum critical Reynolds number diminishes.

(*c*) The maximum amplification ratios also decrease rapidly.

## 4. Measuring techniques

### 4.1. *Disturbance amplitude*

In order to measure disturbance amplitudes along the flat plate in a continuous manner, it was of great advantage to maintain the hot wire at a constant sensitivity. It should be remembered that the hot wire is sensitive to a combination of velocity, density and temperature fluctuations and that the relative sensitivities to these fluctuations change if the mean flow field changes. It follows that these sensitivities remain constant as $x$ varies only if for each $x$-station the wire is placed at $y$-positions where the mean flow conditions are the same. Since the mean resistance of the hot wire is a sensitive indicator of the mean flow conditions, the voltage unbalance of the hot-wire bridge was used to place the wire automatically at the desired $y$-position. This was done in the following way. A Brown servo amplifier was connected parallel with the null galvanometer in the hot-wire resistance bridge (figure 9). If the resistance bridge became unbalanced (when, for instance, the wire moved to a slightly different $x$-position),

the servo amplifier energized a Brown servo motor which in turn caused the hot wire to move in the $y$-direction until the resistance bridge again was balanced. The $y$-position of the hot wire was obtained from the contact-point position on the $y$-slide wire (figure 4). This, together with the $Y$-axis scale-factor control, provided the $y$-position signal for one of the $Y$-axis plotting arms, as shown in figure 9.

The $x$-position of the hot wire was determined by a slide wire on the T-beam (figure 3). The system for plotting this position was identical with that for the $y$-position plotting. With this method the spatial position of the wire could be

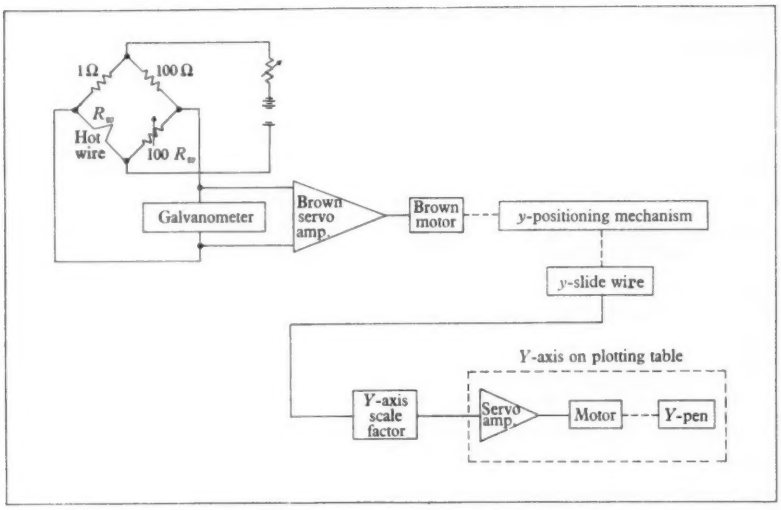


FIGURE 9. Constant $y/\delta$ servo system and $y$-position plotting.

easily followed visually. The wire signal was fed into a wave analyser, the output of which provided the signal $\overline{e_f^2}$ for the second plotting arm of the table. The $y$-positions of the hot wire and the mean-square output of the analyser were thus plotted simultaneously against the $x$-position of the hot wire.

It should be mentioned that the plots $\overline{e_f^2}$ *vs* $x$ obtained in this way could be used directly to calculate the logarithmic derivatives (or amplifications) of the velocity, density, or temperature perturbations. Experimentally, it was found that the mass-flow and total-temperature fluctuations were anticorrelated and that at a given $y/\delta$ the logarithmic derivative of $\overline{e_f^2}$ was independent of hot-wire temperature (i.e. sensitivity). Under these conditions it may be shown, using the hot-wire equation (5.1), that

$$\frac{1}{2\overline{e_f^2}}\frac{d\overline{e_f^2}}{dx} = \frac{1}{\tilde{Q}}\frac{d\tilde{Q}}{dx},$$

where $\tilde{Q}$ is the root mean square of velocity, density, or temperature perturbation.

### 4.2. *Wave velocity*

The wave velocity $c$ was obtained from phase measurements using the artificially introduced single-frequency disturbances. The technique is briefly described as follows. The signals from the reference source and from the hot wire located at $x$ have the form

$$e'_{\text{ref}} = a \sin \beta t,$$

$$e'_f = b(x) \sin \beta\left(t - \frac{x}{c}\right),$$

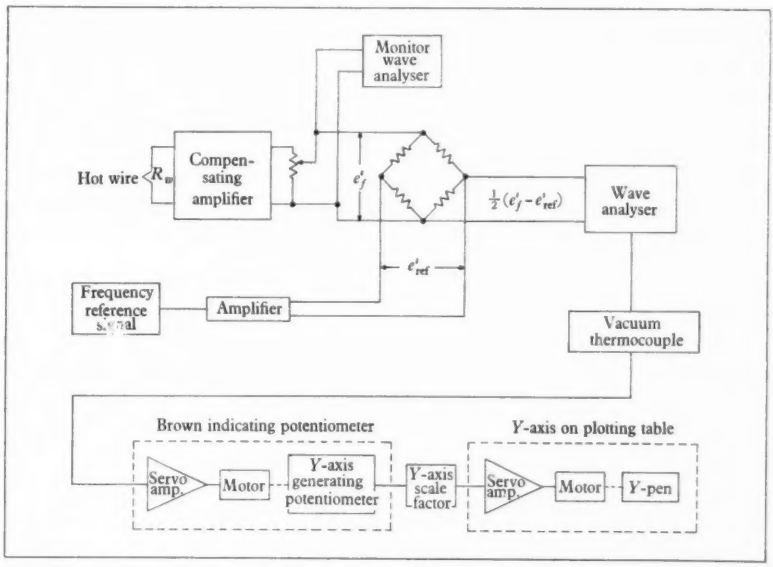


FIGURE 10. Wavelength measurements.

where $a$ is a constant and $\beta$ is the angular frequency. As the hot wire is moved along the plate the mean-square difference of these two signals can be recorded *vs* $x$, while $b(x)$ is kept constant. Thus,

$$\overline{(e'_{\text{ref}} - e'_f)^2} = \frac{a^2}{2} + \frac{b^2}{2} - 2ab\,\overline{\sin \beta t \sin \beta\left(t - \frac{x}{c}\right)}$$

$$= \frac{a^2 + b^2}{2} - ab \cos \beta \frac{x}{c}.$$

It is easily seen that if the mean-square difference goes through a full cycle from position $x_1$ to $x_2$, then

$$\frac{\beta}{c}(x_1 - x_2) = 2\pi,$$

or

$$c = \frac{\beta}{2\pi}(x_1 - x_2) = \frac{\beta}{2\pi}\lambda = \lambda f.$$

During the experiment the output of the hot-wire amplifier was fed across two terminals of a balanced bridge and the reference signal was placed across the opposite terminals of the bridge (figure 10). A wave analyser monitored the hot-wire signal in order to keep the amplitude $b(x)$ constant as the hot wire moved along the plate. The mean-square difference of the hot-wire and reference signals was then automatically plotted.

### 4.3. *Amplitude distribution across the boundary layer*

The hot-wire probe was fixed at a given $x$-position on the flat plate, and the output and current of the wire were plotted against its $y$-position. A Brown servo system kept the heated-wire resistance constant as the probe moved through the layer. The $y$-position of the wire was plotted as the abscissa of the plotting table, and the d.c. current in the wire was one of the two ordinates. The output of the hot-wire amplifier vacuum thermocouple or the wave-analyser vacuum thermocouple was used as the second ordinate on the table. The time constant and sensitivity of the wire changed, of course, as the wire was moved through the layer; these were calculated and the data corrected appropriately. Later, the correct precalibrated time constant was manually set during the measurements.

## 5. Results and discussion

### 5.1. *Establishment of a laminar boundary layer*

Before the study of the fluctuations in the boundary layer was undertaken, the mean flow field in the layer was examined. For this reason three types of mean measurements were made: (1) pressure distribution on the plate, (2) rate of boundary-layer growth, and (3) velocity distribution across the layer.

(1) Figure 11 shows the static-pressure distributions along the plate for $M_1 = 1{\cdot}6$ and $M_1 = 2{\cdot}2$ and at tunnel pressures most often used during this investigation. The dashed line indicates the pressure distribution on the centre-line of the empty tunnel. It is seen that in the region of interest the pressure is constant along the plate within 2%.

(2) The rate of growth of the boundary layer was examined using the method described in § 4.1. By tracing the position of the hot wire as it follows points of constant mean mass flow along the plate, the boundary-layer growth can be easily checked. From boundary-layer similarity considerations the trace, of course, has to be parabolic. This method provided an easy and sensitive means of checking whether or not the measurements were made under the desired conditions. For instance, the trace became non-parabolic if the hot-wire probe was too close to the plate surface and disturbed the flow locally or if a pressure gradient destroyed the similarity because of some exterior condition. All the measurements of disturbance amplitude variations along the plate were accompanied by such traces. A typical example is shown in figure 12. It is to be noted here that near the last inch the trace deviates from the parabola, indicating some irregularity in the flow (nearness of transition).

(3) Measurement of the mean velocity distribution at one station of the plate was also made. This was carried out while artificial disturbances were introduced

in the boundary layer in order to check whether or not the mean flow field had been disturbed by the slight bleeding of air through the slot of the disturbance generator. The accuracy of the mean measurements could have been improved by using a longer and thicker wire; however, fluctuation measurements, which

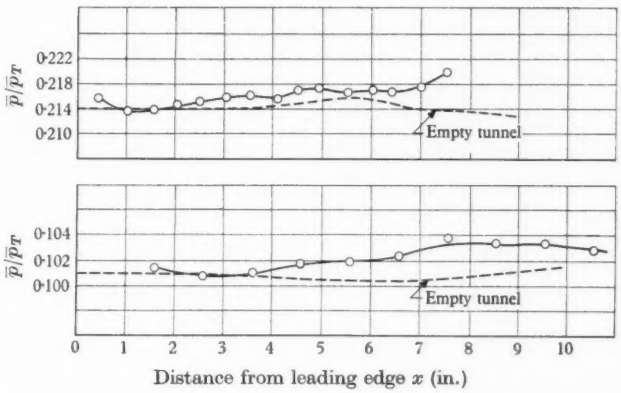


FIGURE 11. Static-pressure distributions along the flat plate and in empty tunnel. Upper figure: $M_1 = 1{\cdot}6$, $Re$/in. = 180,000. Lower figure: $M_1 = 2{\cdot}2$, $Re$/in. = 75,000.

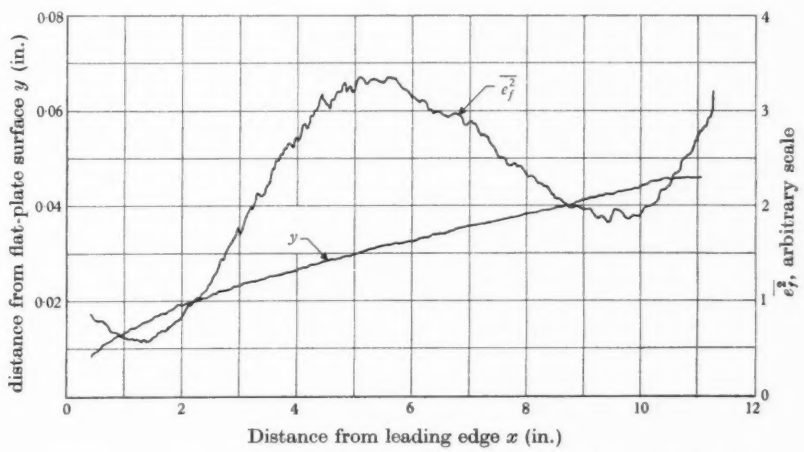


FIGURE 12. Growth of boundary layer and variation of disturbance amplitude along the flat plate. $M_1 = 2{\cdot}2$, $Re$/in. = 77,000, $f = 23$ kc.

were made simultaneously, limited the wire diameter to small sizes. Figure 13 shows the raw data for the unheated-wire-resistance change in the boundary layer from which the total temperature can be easily calculated. The typical maximum is clearly seen from the trace. Figure 13 also shows the current distribution for one particular temperature loading. From such traces the velocity distribution can be calculated using the method described by Laufer & McClellan

(1956). Also the data provide the necessary information for computing the hot-wire sensitivities. Using these and the mean-square hot-wire output $\overline{e_f^2}$ (figure 14) the various flow fluctuations may be calculated (see § 5.5).

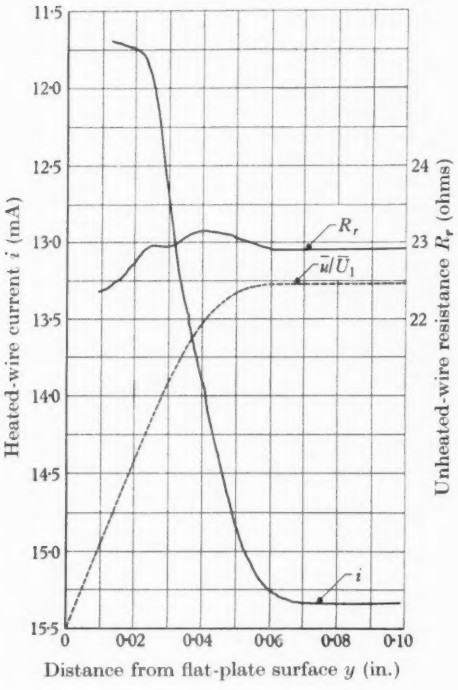


FIGURE 13

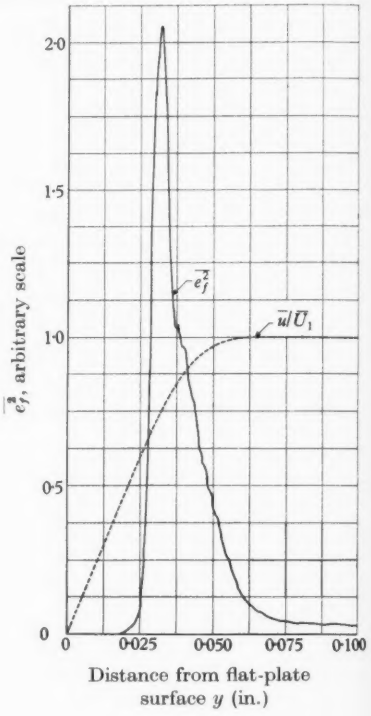


FIGURE 14

FIGURE 13. Unheated-wire resistance and current variation across the boundary layer. $M_1 = 2{\cdot}2$, $Re/\text{in.} = 77{,}000$, $x = 5$ in., $R_w = 33{\cdot}58\,\Omega$.

FIGURE 14. Mean-square hot-wire voltage across the boundary layer at a fixed frequency. $M_1 = 2{\cdot}2$, $Re/\text{in.} = 77{,}000$, $x = 5$ in., $f = 23{\cdot}2$ kc.

In figure 15 the solid line is the theoretical velocity distribution calculated by Mack (1958) using the Klunker–McLean method. The agreement between the experiments and theory is seen to be satisfactory. Near the wall (for $M < 1{\cdot}2$) the measurements were not reduced, since here the reduction is more complicated and not reliable. (The heat loss of the wire here is not only a function of the local Reynolds number, but also of the Mach number.) For later reference the calculated Mach number and temperature distribution are also given in figure 16.

### 5.2. *First indications of instability*

In the stability problem under study here, the existing low-speed experiments and the theory gave many helpful hints as to what to look for and what to observe. However, it was difficult to decide how and where to make the obser-

00

y
e
)
fl
l
.

s
o
r

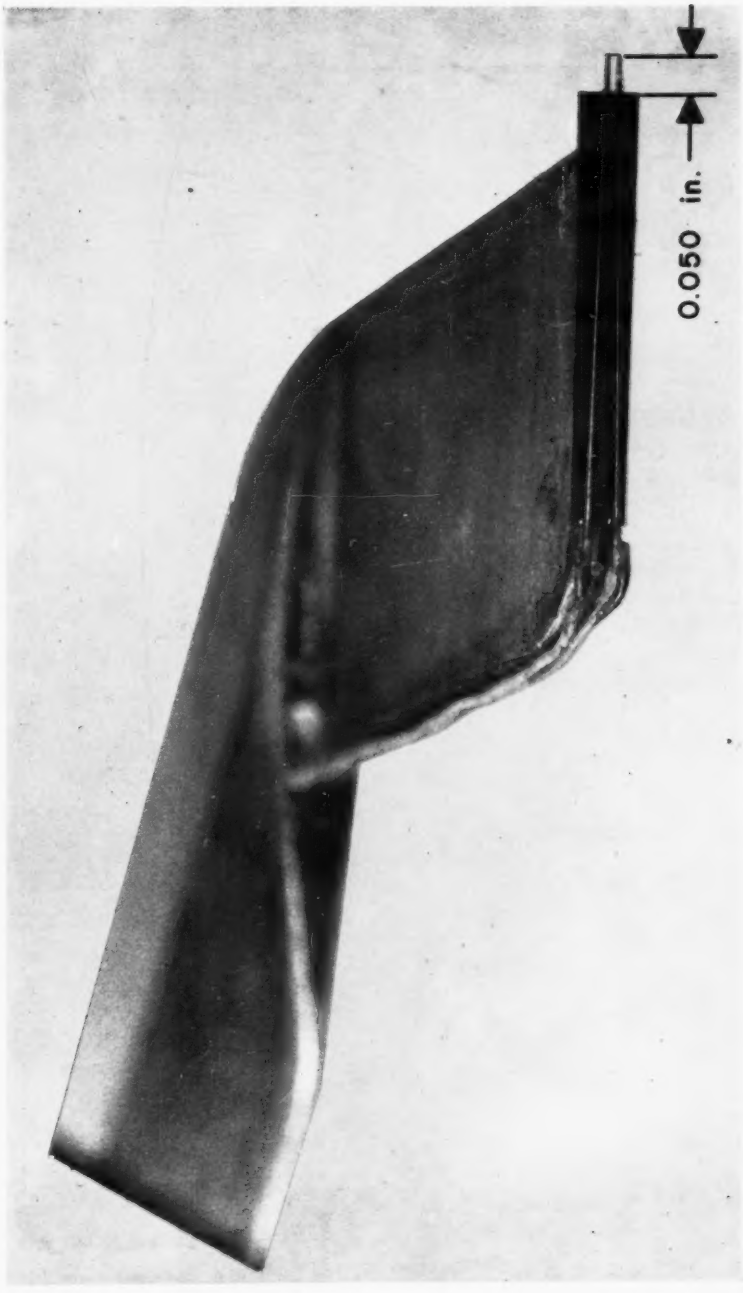


FIGURE 5. Hot-wire probe.



(*Facing p.* 272)

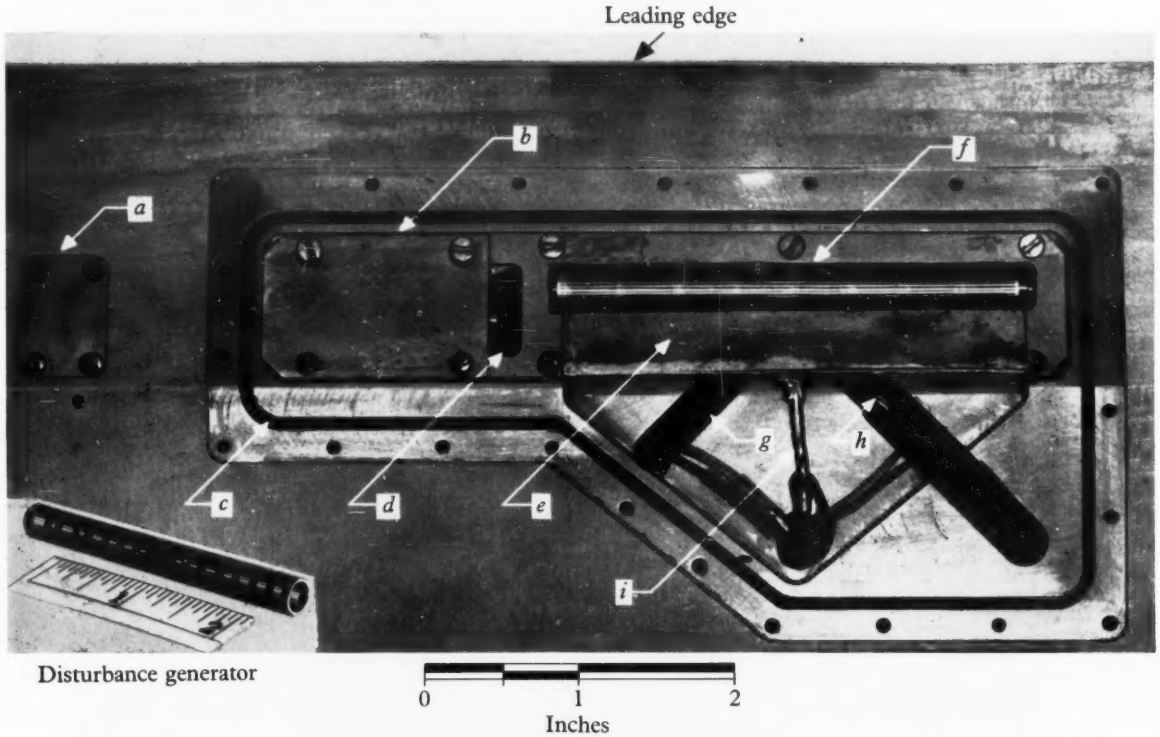


FIGURE 7. Disturbance generator installation in flat plate. *a*, bearing block; *b*, sealing block; *c*, O-ring; *d*, 2·5:1 gear; *e*, porous block; *f*, disturbance generator; *g*, light source; *h*, photo cell; *i*, air line.

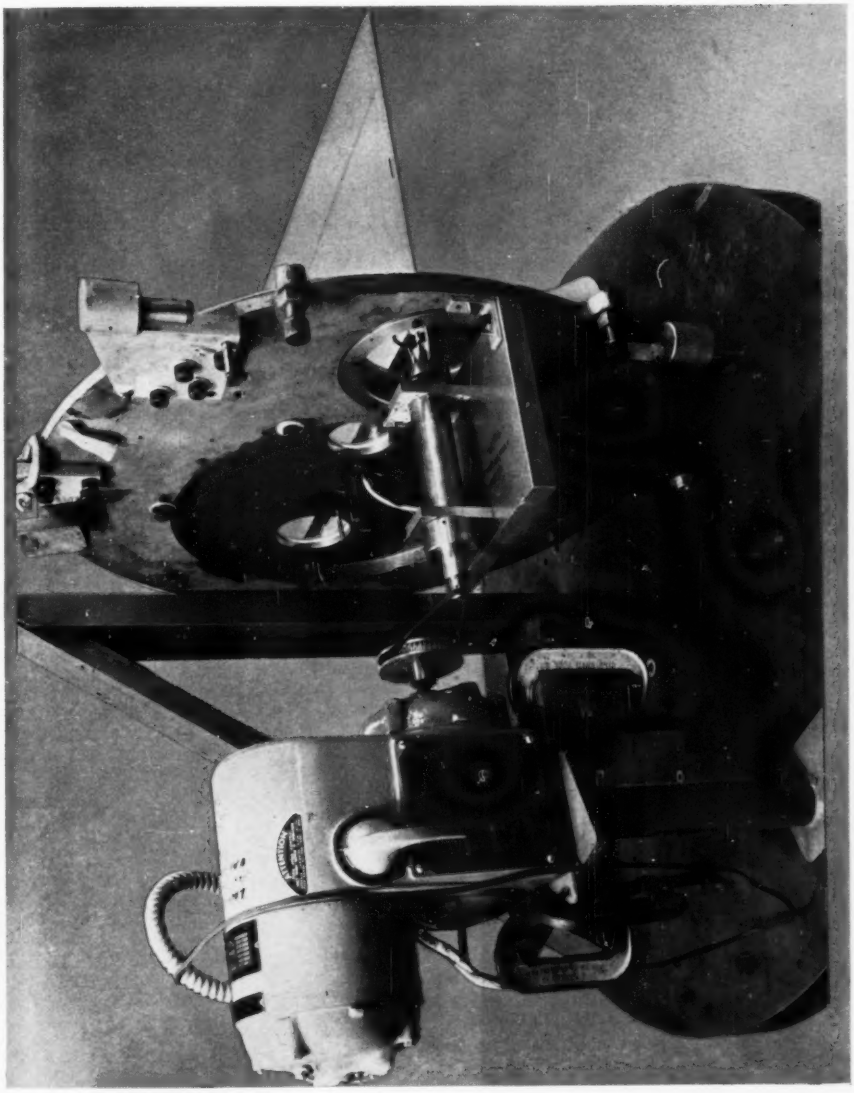

FIGURE 8. Varidrive motor and spindle installation for actuating disturbance generator.

vations, because of the great differences between the experimental environments, because of the magnitudes of the physical variables such as frequency and mean velocity in low speed and supersonic flow, and because of the more complicated flow field. Therefore, considerable time and effort were required before the existence of instability could be detected and the 'real' evidence isolated from

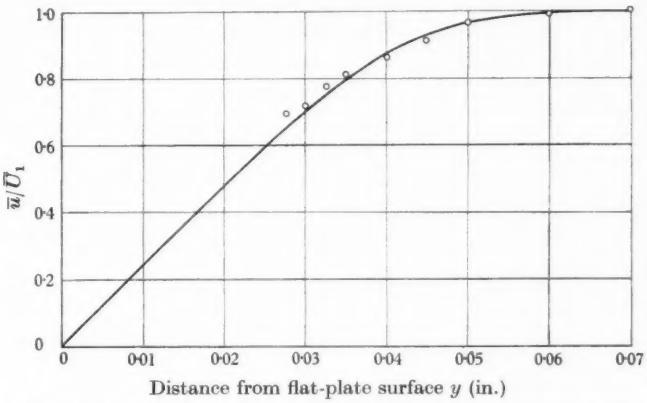


FIGURE 15. Mean velocity distribution across the boundary layer. $M_1 = 2{\cdot}2$, $Re$/in. = 77,000, $x = 5$ in.

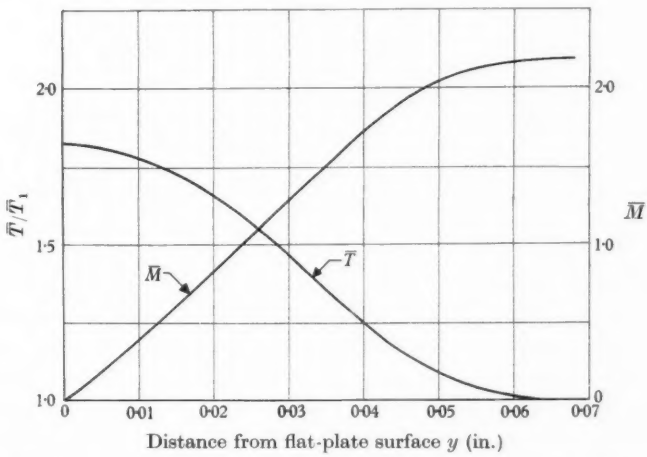


FIGURE 16. Mach number and temperature distribution across the boundary layer. $M_1 = 2{\cdot}2$, $Re$/in. = 77,000, $x = 5$ in.

the 'fictitious' evidence. A qualitative description of the observations identifying the instability will be given in § 5.2; a more critical and quantitative examination of the results will be made later.

*The critical layer.* It was noticed in the early phase of the experiments that even though the measurements of mean quantities had clearly demonstrated the laminar state of the boundary layer, the fluctuations within the layer were con-

siderably larger than those in the free stream. A detailed examination of their amplitude distribution across the layer indicated a remarkably sharp peak near the centre of the layer ($M_1 = 2{\cdot}2$), no matter at which $x$-station the measurement was carried out, including stations a few tenths of an inch ($R_\theta \approx 100$) from the leading edge. Figure 17 shows a typical distribution of the mean-square hot-wire output $\overline{e^2}$ across the layer, clearly exhibiting the peak. Incidentally, $\overline{e^2}$ corresponds approximately to the mean-square mass-flow fluctuations. It is well

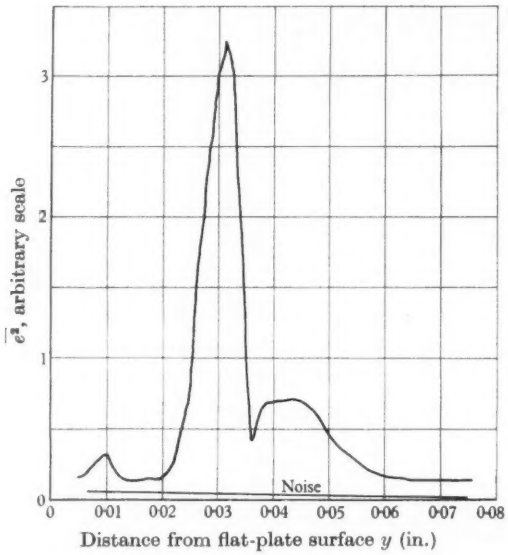


FIGURE 17. Distribution of the hot-wire output across the boundary layer. $M_1 = 2{\cdot}2$, $Re$/in. = 80,000, $x = 5{\cdot}0$ in.

known that such a peak is a characteristic feature of the self-excited instability oscillations in the incompressible laminar boundary layer (Schubauer & Skramstad 1948) and is the result of strong vorticity concentration at points where the local mean velocity is equal to the propagation velocity of the oscillations. Whereas in the incompressible case the peak was always located near the wall, in the present experiments for $M_1 = 2{\cdot}2$ the peak was found to be near the centre of the layer, indicating a higher ratio of wave velocity to free-stream velocity, as expected from theoretical calculations (Lees 1947).

*Maximum amplification curves.* Observation of the fluctuations on an oscilloscope did not reveal any periodic oscillations as reported by Schubauer & Skramstad. However, examination of the energy spectra indicated a characteristic maximum which shifted to lower frequencies as the distance from the leading edge $x$ was increased, and at the same time the peaks were seen to be sharper. Figure 18 shows several such spectra. The question that immediately arises is whether the peaks are the result of the boundary-layer instability process. If indeed they are, it should be expected that the dimensionless frequencies

corresponding to the maxima be unique functions of the boundary-layer Reynolds number. This was examined by varying the Reynolds number two ways during the spectrum measurements: (1) spectrum data were taken at various distances from the leading edge while the tunnel pressure was kept constant; (2) the tunnel pressure was changed for each spectrum distribution obtained at a constant

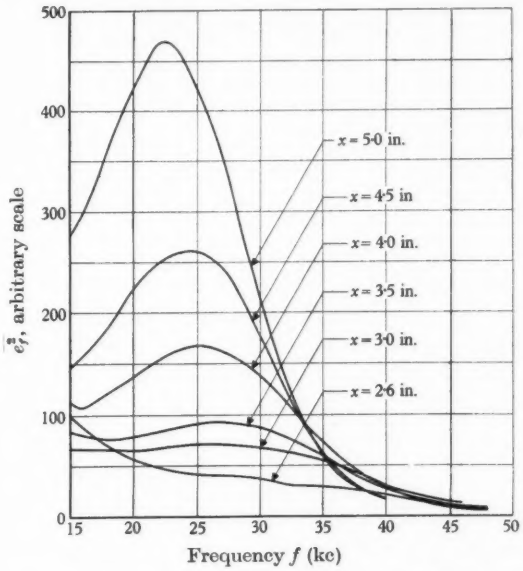


FIGURE 18. Energy spectra of the natural disturbances in the boundary layer at several $x$-positions. $M_1 = 2{\cdot}0$, $Re$/in. = 300,000.

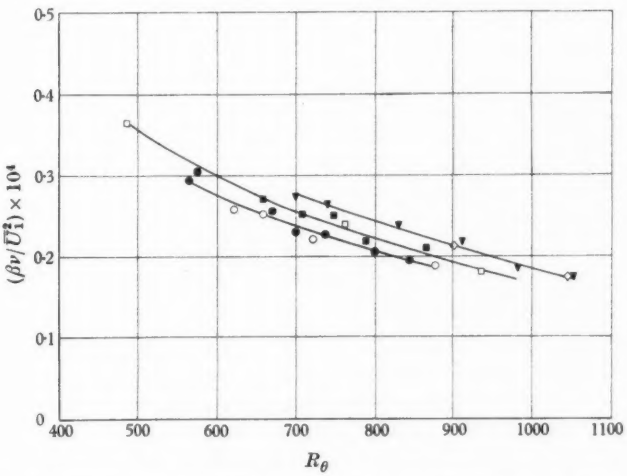


FIGURE 19. Maximum amplification curves. ◇, $M_1 = 1{\cdot}5$; ▽, $M_1 = 1{\cdot}6$; □, $M_1 = 2{\cdot}0$; ○, $M_1 = 2{\cdot}2$. Open symbols: stationary hot wire; solid symbols: moveable hot wire.

$x$-position. The results of the two sets of tests, indicated by open and solid symbols in figure 19, are seen to be consistent for each Mach number tested. It is further seen from figure 19 that the curves, usually referred to as the maximum-amplification curves, move to lower values of the non-dimensional frequencies as the Mach number increases. This tendency is expected from the stability calculations of Lees (1947). These measurements thus gave further clues that the observations must be related to the boundary-layer instability.

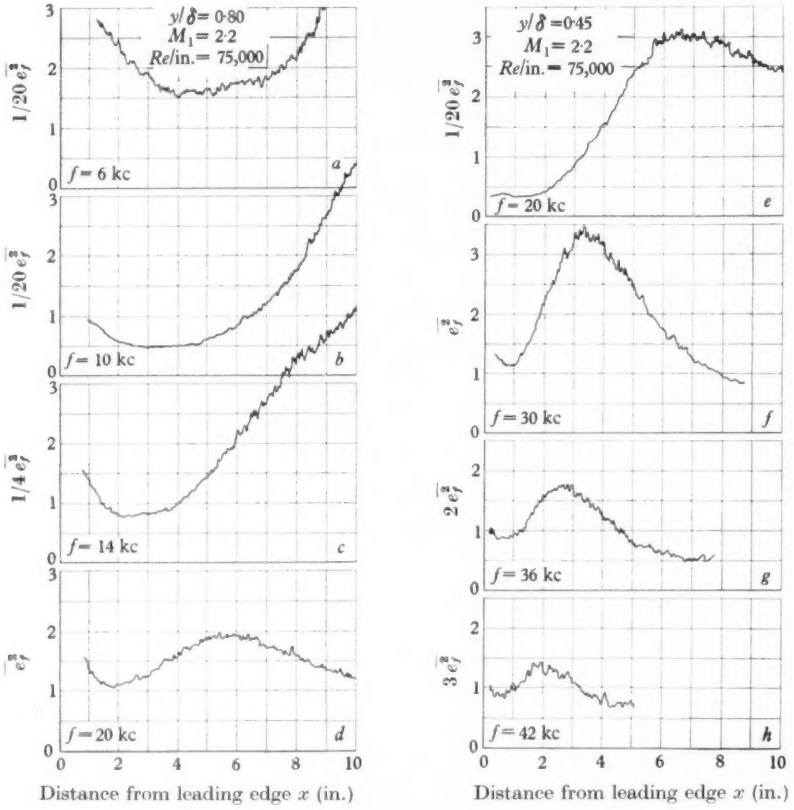


FIGURE 20. Variation of disturbance amplitudes along the flat plate at several frequencies.

*Amplitude variations along the plate.* The most direct and most positive evidence of the small-disturbance type of instability was obtained from the examination of the energy content of various narrow frequency bands at various distances from the leading edge. This kind of experiment was suggested by the well-known 'filtering action' of the boundary layer whereby it augments the energy in certain frequency bands of the disturbances and diminishes the energy in others, depending on the Reynolds number. Figure 20 shows such measurements carried out at Mach number 2·2 in the frequency range of 6 to 42 kc. These curves were

obtained by the method described in § 4.1; that is, the wire was moved along lines of constant $y/\delta$ and the signal was fed through a wave analyser. The ordinates of the various curves are comparable as indicated; the absolute scale, however, is arbitrary. It is seen in figure 20 that the curves exhibit a minimum or a maximum or both, demonstrating the amplifying and damping effect of the boundary layer. At the $x$-positions where the curves have negative slopes, the boundary layer is stable with respect to the disturbances and unstable where the slopes are positive.

### 5.3. *Disturbances present in the boundary layer*

The experiments that have been described gave strong evidence of the existence of self-excited oscillations in the boundary layer. However, before any quantitative conclusions are drawn from them, there are several points that should be further discussed.

*Extraneous effects.* Most of the experiments utilized the convenient (but not always desirable) free-stream disturbances as a means of studying the stability problem. The disturbances were found to be spatially homogeneous and to have a continuous energy spectrum, the energy decreasing with frequency. At the leading edge of the flat plate these disturbances are carried into the boundary layer and their energy spectra (corresponding to a constant $y/\delta$) undergo certain changes along the plate. For the purpose of the present investigation, it is essential to know that these changes are due primarily to the stabilizing (or destabilizing) action of the boundary layer, and that secondary effects that also may influence the energy spectrum are negligibly small. Causes of such extraneous effects might be: (1) disturbances convected into the boundary layer along its outer edge by the mean mass influx; (2) interaction between disturbance energies corresponding to different frequency bands (this effect would rule out the use of disturbances having wide, continuous energy spectra); (3) strong interaction between the disturbances and the mean flow field.

In order to examine the importance of (1) and (2) above, an artificial disturbance of controlled frequency and amplitude was introduced near the leading edge, and its amplitude variation along the plate was studied. The initial amplitudes were chosen to be much larger than those of the natural disturbances but not large enough to disturb the mean flow field of the boundary layer. A comparison of the neutral curves (to be shown and discussed later) that were obtained using natural and artificial disturbances shows complete agreement. It may thus be concluded that any influence of these effects on the location of the stable and unstable regions is negligibly small.

The optimum amplitude for the artificial disturbances, incidentally, could be conveniently determined by observing the traces of the boundary-layer growth (see § 4.1). In figure 21 a typical example of the effect of excessive injection rate is given. The figure also shows the extreme sensitivity of the boundary-layer stability mechanism (and, incidentally, of the instrumentation) to any change in the mean flow field. The boundary-layer growth curves (designated by $y$), obtained with and without injection through the slot, do not coincide, indicating a change in the mean flow field. It should be remembered that through the servo

system the hot wire automatically seeks points of constant mean mass flow. Thus, as the boundary layer thickens because of an excessive injection rate, the hot wire moves a certain distance away from the wall. At the same time it is to be noted in figure 21 that the amplitude curves (designated by $\overline{e_f^2}$) do not peak at the same $x$-position. However, if the increase in boundary-layer thickness is taken into account, the neutral points correspond closely to the same value of the Reynolds number.

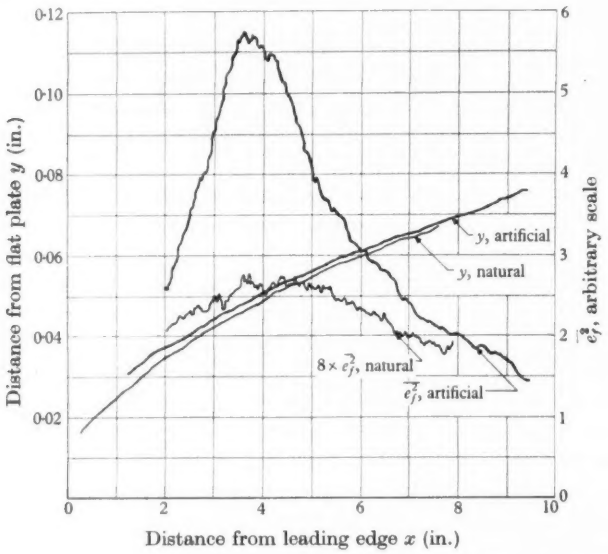


FIGURE 21. Variation of a natural and an artificial disturbance with corresponding boundary-layer growth curves. $M_1 = 2{\cdot}2$, $Re$/in. = 75,000, $f = 23$ kc.

Any further increase in the amplitude of the artificial disturbance resulted in a measurable change in the boundary-layer growth rate, indicating the presence of effect (3). If the non-linear interactions of the type listed under (3) are to be considered negligible, the amplitudes of the disturbances introduced in the boundary layer must be small in all the frequency bands. Of course, it is difficult to decide *a priori* what can be considered a small amplitude. One possibility would be by means of a comparison of stability results obtained using different initial disturbance amplitudes. Unfortunately, variation of the free-stream disturbance level for a given flow Mach number proved to be impractical. Instead, the stability measurements were repeated at various flow Mach numbers (1·6, 2·2, and 3·0) in which cases the free-stream mass-flow fluctuations were approximately 0·1, 0·2, and 0·4 %, respectively. It was established that the results at $M = 2{\cdot}2$ were consistent with those obtained at $M = 1{\cdot}6$; whereas at $M = 3{\cdot}0$ the detection of self-excited oscillations was much more difficult and less reliable. For this reason the experiments were limited to Mach numbers below 2·5.

*Repeatability of the measurements.* Once an acceptable upper limit to the free-stream disturbance amplitudes was decided on (that corresponding to $M = 2{\cdot}2$), it was not too difficult to ascertain that all subsequent measurements should be carried out within this amplitude limit. Since the position of transition from the laminar to the turbulent state is a sensitive indication of the disturbance amplitudes present in the boundary layer, an early transition immediately indicated excessive disturbances. The reason for this not too infrequent occurrence was traced to leaking nozzle seals or pressure holes or to damage on the flat-plate leading edge. However, once such a situation was remedied, all the measurements described here were well reproducible even if they were repeated after a considerable time interval (one year). The maximum shift in the neutral points seldom exceeded $\Delta R_\theta = 20$. The reliability of the measurements was further enhanced by the close agreement with the results obtained using artificial disturbances.

### 5.4. *Neutral stability curves and amplifications*

Examining the stability of the boundary layer with respect to a given disturbance, one is interested not in the absolute amplitudes of these perturbations but rather in their streamwise logarithmic derivatives (amplifications) along the plate. The boundary layer may then be considered stable at a given Reynolds number if

$$\frac{1}{\tilde{Q}}\frac{\partial \tilde{Q}}{\partial x} < 0,$$

and unstable if

$$\frac{1}{\tilde{Q}}\frac{\partial \tilde{Q}}{\partial x} > 0,$$

where $\tilde{Q}(x, y/\delta)$ is any quantity such as $\tilde{u}$, $\tilde{\rho}$, or $\tilde{T}$. The so-called neutral points where the logarithmic derivative vanishes correspond to the limits between the stable and unstable regions. Such a stability criterion, however, does not define a unique neutral curve as described below.

In figure 20 the hot-wire outputs $\overline{\tilde{e}_f^2}$ are plotted as a function of $x$. Since the logarithmic derivative of $\tilde{e}_f$ is equivalent to that of $\tilde{Q}$ (§ 4.1), the stability limits may therefore be determined from the curves of figure 20. According to the stability criterion given above, the extrema of the curves correspond to the neutral points; the $x$-location of a minimum indicates the beginning of the unstable region (lower-branch neutral point), and that of a maximum the end (upper-branch neutral point). In figure 22 the non-dimensional frequency is plotted against the positions of the corresponding neutral points expressed in terms of $R_\theta$. The figure includes not only the neutral points from figure 20, but also those obtained at other tunnel Reynolds numbers and those obtained using artificial disturbances.

Figure 22 clearly shows that the stability limits so obtained depend on the value of $y/\delta$ at which the observations were made. The difference in the neutral curves is definitely within the accuracy limits of the measurements. Subsequent observations at higher tunnel pressures (to check for possible probe interference) and using artificial disturbances gave the same result.

In figures 20*d* and 20*e* one may directly compare two amplitude distributions ($f = 20$ kc) made at $y/\delta = 0{\cdot}8$ and $y/\delta = 0{\cdot}45$. The $x$-positions of the maxima and minima are noticeably different; furthermore, the minimum obtained at $y/\delta = 0{\cdot}8$ is much better defined that at $y/\delta = 0{\cdot}45$. As a matter of fact, for lower frequencies the minimum could be detected only with difficulty or not at all at $y/\delta = 0{\cdot}45$ (not shown).

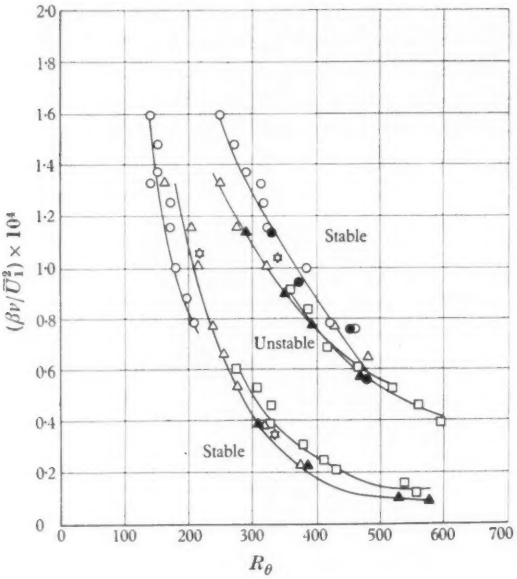


FIGURE 22. Neutral stability curve at $M_1 = 2{\cdot}2$.

| | Disturbance | |
|---|---|---|
| $y/\delta$ | Natural | Artificial |
| 0·34 | □ | |
| 0·45 | ○ | ● |
| 0·7–0·8 | △ | ▲ |
| Area method | ✡ | |

The differences become even more apparent if the logarithmic derivatives for the two cases are compared. Figure 23 shows these derivatives in a non-dimensional form computed at various values of the Reynolds number. It is seen that the amplifications always appear smaller in the outer edge of the layer and that the difference becomes less apparent with increasing Reynolds number.

In order to further examine this problem, the stability criterion will now be expressed somewhat differently. We define a mean amplitude $\Gamma$ averaged across the boundary layer (the use of a mean energy would lead to similar results),

$$\Gamma(x) = \int_0^1 \tilde{e}_f d\left(\frac{y}{\delta}\right);$$

and we propose to call the boundary layer stable where

$$\frac{1}{\Gamma}\frac{d\Gamma}{dx} < 0,$$

and unstable where

$$\frac{1}{\Gamma}\frac{d\Gamma}{dx} > 0.$$

This stability criterion is equivalent to the previous one if

$$\frac{1}{\Gamma}\frac{d\Gamma}{dx} = \frac{1}{\tilde{e}}\frac{d\tilde{e}}{dx} \quad \text{or} \quad \frac{\partial}{\partial x}\frac{\tilde{e}_f}{\Gamma} = 0$$

for all values of $y/\delta$, that is, if the distribution $\tilde{e}_f/\Gamma$ is a function of $y/\delta$ only and thus follows the boundary-layer similarity. This condition will now be experimentally investigated. For the calculations of $\Gamma$, amplitude distributions across

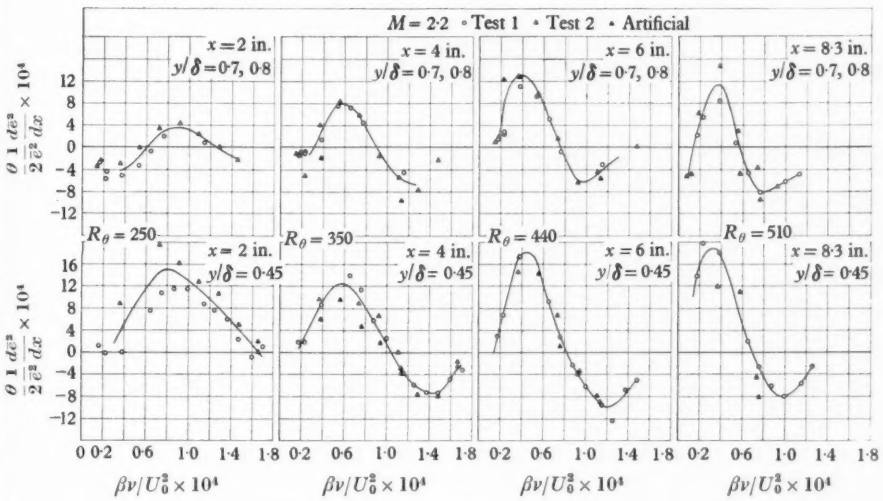
M = 2·2 ◦ Test 1 ▪ Test 2 ▪ Artificial
x = 2 in. y/δ = 0·7, 0·8
x = 4 in. y/δ = 0·7, 0·8
x = 6 in. y/δ = 0·7, 0·8
x = 8·3 in. y/δ = 0·7, 0·8
Rθ = 250
Rθ = 350
Rθ = 440
Rθ = 510
x = 2 in. y/δ = 0·45
x = 4 in. y/δ = 0·45
x = 6 in. y/δ = 0·45
x = 8·3 in. y/δ = 0·45
θ 1 dẽ² / 2 ẽ² dx × 10⁴
βν/U₀² × 10⁴

FIGURE 23. Amplification curves.

the layer were measured at various $x$-positions. A sample of such distributions corresponding to 30 kc frequency is shown in figure 24. (Incidentally, the typical maximum near the critical layer is already noticeable at $x = 0{\cdot}5$ in.; the curious secondary peaks will be discussed in § 5.5.)

In figure 25 the normalized amplitudes

$$\frac{\tilde{e}(x, y/\delta)}{\Gamma(x)}$$

are plotted against $y/\delta$ for various values of $R_\theta$. (For clarity, not all the distributions are shown.)

Clearly, the above condition is not satisfied. Near the critical layer $(\partial/\partial x)(\tilde{e}_f/\Gamma)$ is positive, and near the free-stream end it is mainly negative. This explains why the

amplifications obtained at $y/\delta = 0{\cdot}45$ are larger than those at $y/\delta = 0{\cdot}8$ (figure 23), or why the unstable region corresponding to $y/\delta = 0{\cdot}45$ in figure 22 is wider.

Deciding which stability limits to adopt is really an academic question. In a comparison of disturbance amplitudes corresponding to the same mean flow

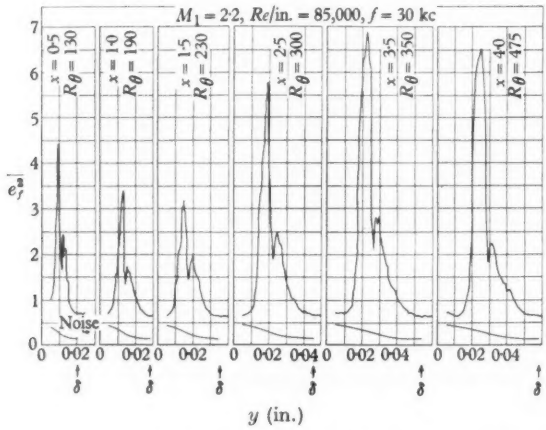
$M_1 = 2{\cdot}2$, $Re$/in. = 85,000, $f$ = 30 kc
$x$ = 0·5, $R_\theta$ = 130
$x$ = 1·0, $R_\theta$ = 190
$x$ = 1·5, $R_\theta$ = 230
$x$ = 2·5, $R_\theta$ = 300
$x$ = 3·5, $R_\theta$ = 350
$x$ = 4·0, $R_\theta$ = 475
$e_f^2$
Noise
0 0·02 0·04
$\delta$
$y$ (in.)

FIGURE 24. Amplitude distribution across the boundary layer of a fixed-frequency disturbance at several $x$-positions.

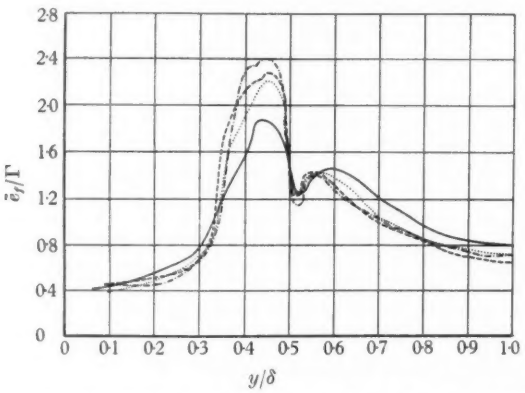


FIGURE 25. Normalized amplitude distributions. $M_1 = 2{\cdot}2$, $Re$/in. = 85,000, $f$ = 30 kc.

| | $x$ (in.) | $R_\theta$ |
|---|---|---|
| ———— | 1·5 | 230 |
| ..... | 2·5 | 300 |
| – – – – – – – | 3·5 | 350 |
| —·—·— | 4·5 | 400 |

conditions (constant $y/\delta$), the physical fact is that disturbances are amplified more near the critical layer than near the inner and outer edges of the boundary layer, especially for low Reynolds numbers. Should one want to talk about a unique neutral curve, the second stability criterion is preferable. Using this criterion, some calculated neutral points are shown as stars in figure 22.

### 5.5. *Amplitude distributions across the boundary layer*

In the previous section some distributions in terms of the hot-wire output $\overline{e_f^2}$ have been shown (figure 24). The behaviour of the velocity, temperature, and pressure fluctuations across the layer will now be examined.

An artificial disturbance having a frequency of 23 kc ($\beta\nu/U_1^2 = 0{\cdot}85 \times 10^{-4}$) was chosen for the experiment and was examined at a position $x = 5$ in. ($R_\theta = 400$). This approximately corresponded to a point on the upper branch of the neutral stability curve. In order to express the hot-wire output voltages in

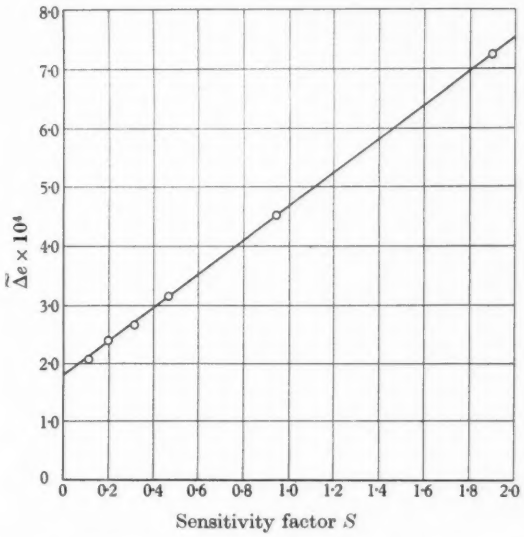


FIGURE 26. Fluctuation mode diagram in the free stream near the edge of the boundary layer. $M_1 = 2{\cdot}2$, $Re_1$/in. = 77,000.

terms of the flow quantities, the method suggested by Kovasznay (1953) was applied. As is well known, only two of the perturbations, mass-flow

$$[m'/\overline{m} = \rho'/\overline{\rho} + u'/\overline{u}]$$

and total temperature $\quad [T'_T/\overline{T}_T = \alpha(T'/\overline{T}) + \beta(u'/\overline{u})]$

fluctuations can be obtained (see equation (5.1)) in the range $M > 1{\cdot}2$. Typical raw data of the hot-wire output are shown in figure 17. The measurements resulted in mode diagrams similar to that shown in figure 26, indicating that inside the layer, just as outside, $\tilde{m}/\overline{m}$ and $\tilde{T}_T/\overline{T}_T$ appear to be perfectly anti-correlated (the points in the diagram define a straightline). From such diagrams the mass-flow and total-temperature fluctuations may be directly computed; the result is plotted in figure 27. The very pronounced peak near the critical layer ($y \approx 0{\cdot}28$ in.) is well illustrated.

Unfortunately, a result of this nature is not very instructive unless the three basic fluctuation quantities can be separated. In order to do this it is necessary

to make an assumption concerning the fluctuation field. Outside the boundary layer, in the potential field of the oscillation, this does not present a problem. Here isentropic relations between the temperature and density fluctuations exist and they can therefore be calculated separately (see § 5.6). Inside the boundary layer, however, the situation is different: the dominating action of viscosity near the wall and at the critical layer prevents the making of such an

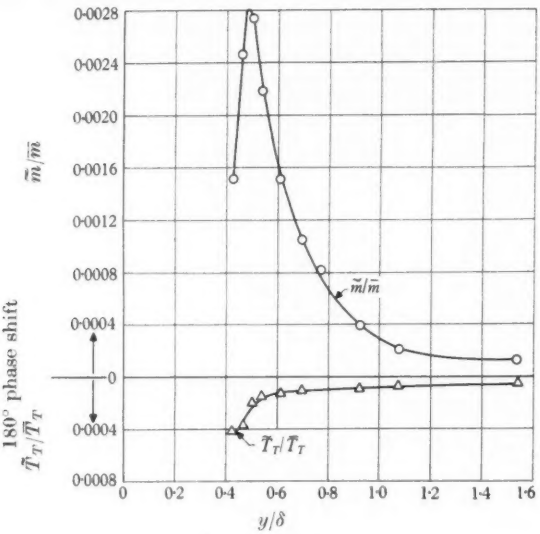


FIGURE 27. Mass-flow and total-temperature fluctuations in the boundary layer. $M_1 = 2{\cdot}2$, $Re/\text{in.} = 77{,}000$, $x = 5$ in.

assumption. Another simplification is used instead, based on the following qualitative argument. A wave motion superimposed on the boundary layer produces a pressure gradient $\partial\tilde{p}/\partial y$ that diminishes with decreasing wave amplitude and increasing wavelength. Since $v'/\overline{u}$ is small and the wavelength is large (approximately $10\delta$) in the present experiments, it will be assumed that $\partial\tilde{p}/\partial y$ is small and thus $\tilde{p}$ is constant across the layer. The magnitude of $\tilde{p}$ was calculated from the mass-flow fluctuation measurement near the edge of the boundary layer ($y/\delta = 1{\cdot}08$), using isentropic relations between the perturbations. Since the phase relation between the pressure and the velocity (or temperature) fluctuations is not known (except the fact that they are in phase or 180 degrees out of phase), two distributions of these quantities are obtained from the hot-wire equations. One set of roots, for instance, results near the critical layer in a positive pressure-temperature correlation if one chooses negative pressure-velocity correlation, and vice versa.

Without additional information it is not possible to choose which of the two sets of roots is the correct one. It was necessary to refer to the solution of the perturbation equations (3.1–3.11) to decide on this. For this purpose the inviscid equations of motion were integrated in the outer half of the boundary

layer using the theoretical eigenvalues,* and the results were compared with the corresponding distributions calculated from the measurements. The amplitude of the computed mass-flow fluctuations was matched to the measured value at $y = \delta$, and the theoretical results were plotted as thin solid lines in figure 28. It is seen that the theoretical pressure fluctuations indeed are fairly constant within about 15 %, at least in the outer half of the boundary layer.† Thus, the assumption of constant $\tilde{p}$ used in the reduction of the measured data is justified. The symbols in figure 28 correspond to the roots of the hot-wire equations nearest the

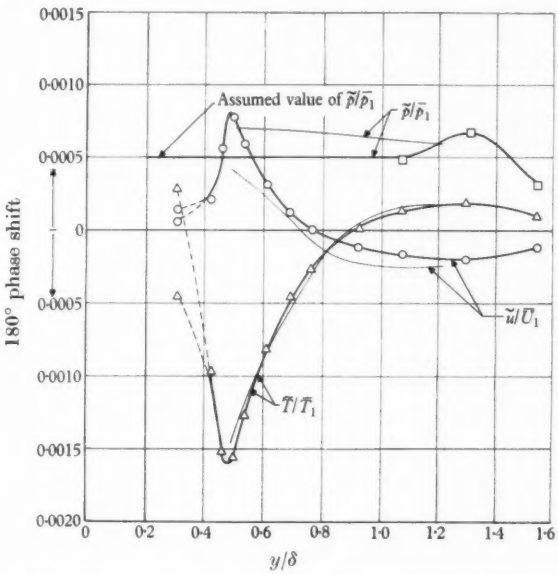


FIGURE 28. Velocity, temperature, and pressure fluctuations in the boundary layer. $M_1 = 2{\cdot}2$, $Re/\text{in.} = 77{,}000$, $R_\theta = 400$, $c/\bar{U}_1 = 0{\cdot}62$.
Experiment: ○, $\tilde{u}/\bar{U}_1$; △, $\tilde{T}/\bar{T}_1$; □, $\tilde{p}/\bar{p}_1$.
Theory ($R_\theta = 440$, $c/\bar{U}_1 = 0{\cdot}616$): ———.

theoretical curves. Since the second set of roots defines a completely different velocity and temperature distribution, it was not difficult to pick out the correct roots. The only exception was the point nearest the wall ($y/\delta = 0{\cdot}31$); in this case both roots are shown. Incidentally, this point corresponds to a position where $M = 0{\cdot}8$, and the more general hot-wire equations suggested by Morkovin (1956) were used in reducing the data. It should also be mentioned that since the hot-wire sensitivities at transonic flows are not well established, the measurements here are less reliable.

The root-mean-square values of the various fluctuations in figures 27 and 28 were plotted in a fashion that shows the phase relations between them. It was mentioned earlier that these fluctuations were always either in phase or 180

* The authors are grateful to Dr L. Mack for providing these calculations.

† Some recent calculations of Dr E. Reshotko show that this is true across the whole layer.

degrees out of phase with each other. In the figures the phase relations with respect to the pressure fluctuations are indicated: in-phase fluctuations are plotted in the positive sense, out-of-phase ones in the negative sense. For instance, outside of the boundary layer where the isentropic relations hold between pressure, density, and temperature fluctuation (they are all in phase), the temperature fluctuations are plotted in the positive sense. It is interesting to notice that inside the layer not only the velocity oscillations (as found in the incompressible case), but also the temperature oscillations undergo a 180-degree phase shift.

At this point a comment is in order on the secondary peaks clearly shown in the distributions figure 24. These peaks were almost always present (also with artificial disturbances) when measurements were made at high mean-wire temperatures; at low temperatures, only a small peak or no peak was observed. Thus, the secondary peaks are believed to be the result of a curious combination of the hot-wire response and the particular distribution of the velocity, temperature, and density fluctuations.

One of the most striking features of the fluctuation distributions shown in figure 28 is the large amplitude of the temperature (and density) distribution near the critical layer. Since the mean temperature gradient in the boundary layer increases rapidly with Mach number, such a result is not surprising. As a matter of fact, with increasing free-stream Mach number the temperature and density fluctuations will become more and more important. From the continuity and energy equations (3.7) and (3.10), one obtains, neglecting conductivity,

$$\left(1-\frac{c}{\bar{u}}\right)\left[\frac{\theta}{\bar{T}}-(\gamma-1)\frac{r}{\bar{\rho}}\right]=\frac{i\gamma}{\alpha\bar{T}}\frac{d\bar{T}}{dy}\frac{v'}{\bar{u}}.$$

In the region of our interest, near but just outside the critical layer where the non-viscous approximation is still valid, the temperature and density fluctuations are 180 degrees out of phase. Therefore, in terms of root-mean-square values, the above equation becomes

$$\frac{\frac{\tilde{\theta}}{\bar{T}}+(\gamma-1)\frac{\tilde{r}}{\bar{\rho}}}{\frac{1}{\alpha\delta}\frac{\tilde{v}}{\bar{u}}}=-\frac{1}{1-\frac{c}{\bar{u}}}\frac{\gamma}{\bar{T}}\frac{d\bar{T}}{d\frac{y}{\delta}}.$$

The right side of the equation increases rapidly with Mach number; thus, for a given disturbance, $(\tilde{v}/\bar{u})\,(1/\alpha\delta)$ constant, the temperature and density fluctuations become large indeed.

### 5.6. *The propagation velocity*

From theoretical considerations it is expected that once a disturbance is introduced locally into the boundary layer it will develop into a wave motion having a definite wave velocity and amplitude variation. The latter has already been discussed; it remains to be shown experimentally that the motion is wave-like. This was done by two different methods: (1) by measurement of the wavelength and (2) by a more indirect technique.

(1) The determination of the wavelength of an artificial disturbance of known frequency was described in § 4.2, and a typical result is shown in figure 29. The plot, which incidentally is raw data, indicates unquestionably the wave character of the disturbance and provides the wavelength directly. From the measured wavelength corresponding to the neutral point and from the known frequency, the velocity of a neutral wave can be obtained.

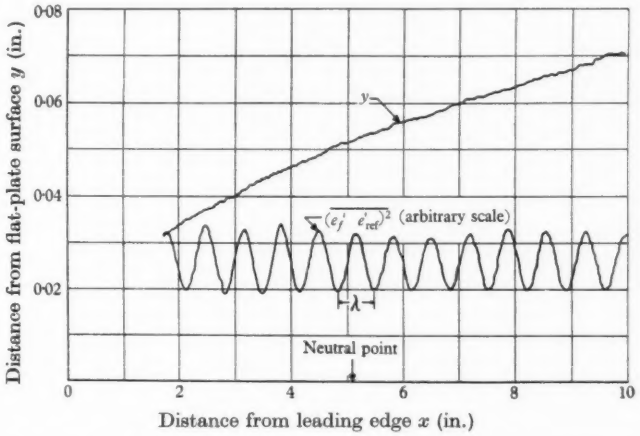


FIGURE 29. Wavelength measurements of an artificial disturbance. $M_1 = 2{\cdot}2$, $Re$/in. = 77,000, $f = 19{\cdot}6$ kc.

(2) The alternative method is based on the idea that if the artificial disturbance indeed develops into a wave motion, the boundary layer may be considered a moving wavy wall. From the measurements of the pressure and velocity fluctuations in the potential field just outside the layer, the velocity of the wavy wall can be calculated. Clearly, from such an indirect method it is not expected to obtain accurate values of $c$ (especially since $c$ is only approximately constant along $x$). Nevertheless, the method is described here in order to show that with the present hot-wire technique measurements of fluctuations in supersonic flows may be made with confidence.

The general hot-wire equation

$$\Delta e = \alpha \frac{T'}{\overline{T}} + \beta \frac{u'}{\overline{u}} - S\left(\frac{\rho'}{\overline{\rho}} + \frac{u'}{\overline{u}}\right) \tag{5.1}$$

may be put in a simpler form, since outside the boundary layer an isentropic relation between the fluctuations may be assumed:

$$\Delta e = \alpha(\gamma - 1)\left[\frac{\rho'}{\overline{\rho}_1} + M_1^2 \frac{u'}{\overline{U}_1}\right] - S\left[\frac{\rho'}{\overline{\rho}_1} + \frac{u'}{\overline{U}_1}\right],$$

where

$$\alpha = \left(1 + \frac{\gamma - 1}{2} M_1^2\right)^{-1}$$

and

$$\beta = (\gamma - 1)\alpha M_1^2.$$

Figure 26 shows that $\Delta\tilde{e}$ is a linear function of $S$, indicating that the total-temperature (first term) and mass-flow (second bracketed term) fluctuations are perfectly anticorrelated, consistent with the assumption of isentropy. From mode diagrams such as figure 26, the velocity and density fluctuations (also $\tilde{p}$ and $\tilde{T}$) may be obtained. From the potential solution of a moving wavy wall (Liepmann & Roshko 1957) and from the measured $\tilde{u}$ and $\tilde{\rho}$, the velocity of the wall may be calculated:

$$\frac{c}{\overline{U}_1} = 1 - \frac{\tilde{p}/\overline{p}_1}{\gamma M_1^2 \tilde{u}/\overline{U}_1}.$$

For the conditions represented in figure 26 the wave velocity was found to be $c/\overline{U}_1 = 0{\cdot}60$, which compares well with the value of 0·62 obtained from phase measurement.

### 5.7. *Comparison with theory*

The results that have been described confirm qualitatively the predictions of the stability theory: the existence of unstable oscillations in a supersonic boundary layer; the wave-like character of the oscillations; and the existence of an inner layer within the boundary layer where the amplitude of the oscillations is much larger than outside it. In this section a more quantitative comparison will be made in the light of the various assumptions of the theory.

*Amplitude of the perturbations.* In order to be able to compare the experimental results with the linear theory, it is necessary, of course, to ascertain that the disturbances studied in the experiments are small (assumption 1 of § 3.1). In the incompressible case it was shown recently by Schubauer (1958) that provided the velocity disturbances do not exceed an amplitude of 1–2 % of the free-stream velocity, the use of a linear theory for predicting their behaviour is justified. On the basis of the results described subsequently (§ 5.8), the same criterion may be used for the compressible case.

In the present experiments using artificial disturbances, it is estimated, based on the results of figure 28, that the fluctuation levels did not exceed the 0·5 % value. (The amplitudes of the natural disturbances were, of course, even smaller.) On this basis, therefore, a comparison of the experimental results with a linear theory is justified.

*Two- and three-dimensional disturbances.* The question arises whether a two- or three-dimensional theory should be used in the comparison. In the incompressible boundary layer this problem was not essential since, as pointed out recently by Lin (1958), the neutral curves for the two cases are almost identical.

In the present experiments the natural disturbances were certainly three-dimensional, while the artificial ones—although not purely two-dimensional—could be considered as containing predominantly two-dimensional disturbances. Nevertheless, the measurements made by both types of perturbations produced the same results concerning the stability limits and amplifications. On the basis of this evidence it may be assumed, therefore, that at least up to $M = 2{\cdot}2$ the stability of the boundary layer with respect to a two- and a three-dimensional disturbance does not change measurably. This is in agreement with the conclusion reached by Dunn & Lin (1955). Because of the approximations involved,

their result cannot be extended beyond a Mach number of approximately 1·8; but within this range they show that the three-dimensional disturbances are less important than the two-dimensional ones and become dominant only for the case of a cooled boundary layer.

On the basis of the above discussion the results of the two-dimensional theory will be used for the comparison with the experimental findings.

*Neutral curves.* Before making a quantitative comparison between the theoretical and experimental results, a fundamental difficulty has to be pointed out.

Let us first examine the problem considered by the theory: it is a non-stationary one in which the boundary layer of constant thickness (fixed $R_\theta$) is perturbed at time $t = t_0$. The amplitude of the disturbances, $Q'$, is then examined to determine how it changes for $t > t_0$. If the damping coefficient

$$\frac{1}{Q'}\frac{dQ'}{dt} \equiv \beta_i$$

is positive, the boundary layer is said to be unstable at $R_\theta$ with respect to the disturbance considered.

On the other hand, the experimenter faces a quasi-stationary problem: a disturbance introduced at the leading edge propagates along the layer, its amplitude changing in space and time. Thus, at a fixed $R_\theta$ one cannot measure a damping coefficient in the sense of the theory since the disturbance, the amplitude of which is observed at $t = t_0$, propagates into a region of increasing $R_\theta$ at $t > t_0$. What one can do is to measure at one fixed point in the layer the temporal mean value of $Q'$ and observe how this value changes with $x$; thus, one can calculate an amplification defined as $(1/\tilde{Q})\,(d\tilde{Q}/dx)$. The basic difficulty now is to interpret this quantity in terms of the damping coefficient $\beta_i$ of the theory. The general mathematical problem is a difficult one and no attempt is made here to discuss it; only one particular aspect will be considered.

It would be desirable to set up a simple criterion indicating the conditions under which comparison between the quantities $\beta_i$ and $(1/\tilde{Q})\,(d\tilde{Q}/dx)$ could be made directly. In the past the two quantities were compared directly as follows: the disturbance being propagated by its eigenvelocity, $c = dx/dt$, served as the required transformation between the space and time co-ordinates; consequently it was postulated that

$$\frac{1}{\tilde{Q}}\frac{d\tilde{Q}}{dx} = \frac{1}{Q'}\frac{dQ'}{dt}\frac{dt}{dx} = \frac{\beta_i}{c}.$$

This procedure, however, is not strictly correct. It should be remembered that the amplitude function $q$ as shown in equation (3.1) implicitly depends on the eigenvalues of the problem, thus in particular on the Reynolds number. Therefore, as the variation of $Q$ with $x$ is measured, keeping $y/\delta$ constant, $R_\theta$ changes (the boundary layer thickens) and, as mentioned above, $q$ changes also. Therefore, the above equation must contain a term that takes into account this change. Thus, one may formally write

$$\frac{1}{\tilde{Q}}\frac{d\tilde{Q}}{dx} = \frac{1}{q}\left(\frac{\partial q}{\partial x}\right)_{y/\delta} + \frac{\beta_i}{c}.$$

In principle, both quantities on the right-hand side could be calculated from the theory and then their sum compared with the measured amplification $(1/\tilde{Q})\,(d\tilde{Q}/dx)$. This, however, has not been done, mainly because of the extremely time-consuming calculations involved. Instead, one may set up the criterion that the experimental amplifications can be compared directly with the theoretical damping coefficients only if the condition

$$\frac{1}{q}\left(\frac{\partial q}{\partial x}\right)_{y/\delta} \ll \frac{1}{\tilde{Q}}\frac{d\tilde{Q}}{dx}$$

is satisfied.

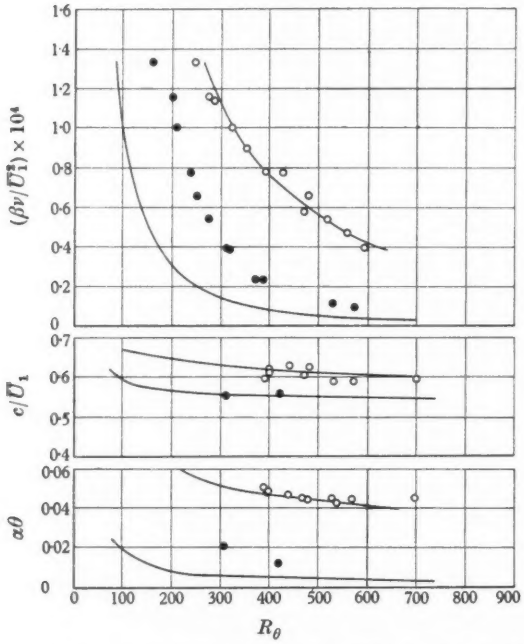


FIGURE 30. Theoretical and experimental neutral stability curves at $M_1 = 2{\cdot}2$. Experiment: ○, upper branch; ●, lower branch. Theory: ——.

This inequality can easily be checked from the plots shown in figure 25. The above condition implies that the amplification distributions with frequency be the same for all values of $y/\delta$ for a given Reynolds number. It is seen that on the outer edge of the boundary layer and for $R_\theta$ larger than approximately 300, this is approximately satisfied.

With the above limitation in mind we may proceed now to discuss the experimental results in the light of the theory. Accordingly, only the amplification measurements far from the critical layer are considered ($y/\delta \approx 0{\cdot}8$). In figures 30 and 31 the theoretical curves were calculated by Mack (1960), using the method proposed by Dunn & Lin (1955).

Considering first the velocity neutral curves of figures 30 and 31, one may easily verify that in all cases the propagation velocities of the self-excited oscilla-

tions are always subsonic with respect to the free stream. As discussed in § 3.1, this was an important assumption (assumption 4) of the theory that hereby finds complete verification. It is also seen that the absolute values of the velocities are in very good agreement with the theoretical predictions, with the possible exception of the lower branch points at $M = 1{\cdot}6$. (The measurements of the larger wavelengths, corresponding to the lower branches, were found to be more difficult.)

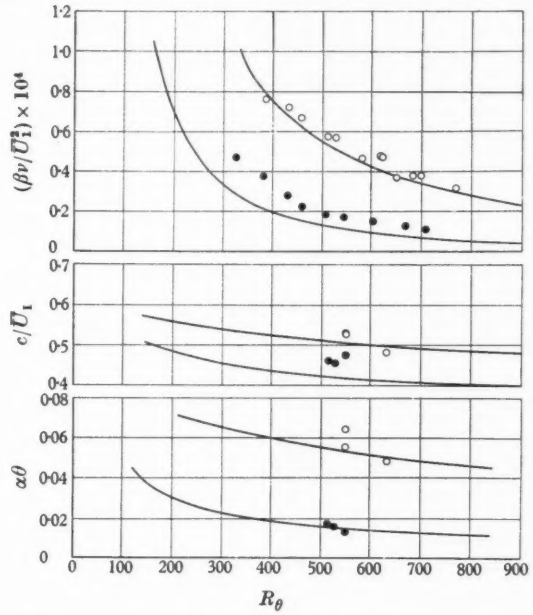


FIGURE 31. Theoretical and experimental neutral stability curves at $M_1 = 1{\cdot}6$. Experiment: ○, upper branch; ●, lower branch. Theory: ——.

Regarding the frequency neutral curves in these figures, the upper branches of the experimental and theoretical neutral curves agree satisfactorily. On the other hand, there is considerable discrepancy, especially at $M = 2{\cdot}2$, between the lower branches. Since the lower branches depend mainly on the viscous solutions of the stability problem, the source of the difficulty is believed to lie in these solutions.*

### 5.8. *Effect of compressibility on boundary-layer stability*

With the present formulation of the mathematical stability problem, it is not possible to answer easily the question of whether compressibility increases or decreases the stability of an adiabatic laminar boundary layer. As a matter of fact, one may arrive at a wrong conclusion by considering only certain phases

* In a recent work, Dr E. Reshotko critically examines the stability problem at supersonic Mach numbers and discusses this problem further.

of the problem. For instance, the supersonic inviscid boundary layer can be shown to be unstable, while the incompressible one is stable; also, from the expression of the minimum critical Reynolds number derived by Lees (1947), it is found that it decreases with increasing Mach number. From both of these results an erroneous conclusion could be drawn. Only the elaborate numerical calculations of Lees concerning the maximum amplification ratios of a disturbance give an indication of greater stability as the free-stream Mach number increases (Lees 1952). Under these circumstances it is most desirable if on the basis of the experimental findings some correlation could be found between the incompressible and compressible stability data from which the question posed above could be more readily answered. This problem will now be examined.

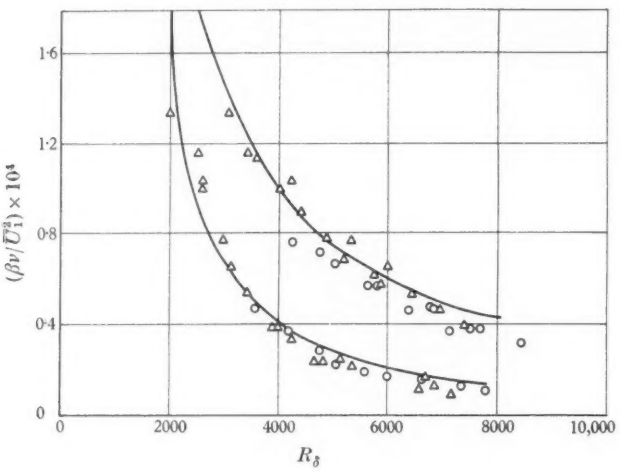


FIGURE 32. Experimental neutral stability curves.
——, $M = 0$ (Schubauer–Skramstad); ○, $M = 1{\cdot}6$; △, $M = 2{\cdot}2$.

The results of the theoretical eigenvalue calculations are usually presented in terms of the boundary-layer momentum thickness as the characteristic length. This is done mainly because, for a given $x$, the momentum thickness $\theta$ is practically constant over a wide range of Mach numbers. Considering now the frequency neutral curves as a function of $R_\theta$ for various Mach numbers (figures 30 and 31), it was noticed that the curves were similar but displaced in $R_\theta$. Next to be examined was the question of whether by stretching the characteristic length the neutral curves could be correlated. The fact that the well-known Howarth co-ordinate transforms (with some additional minor assumptions) the compressible velocity distribution into the incompressible one suggests the use of the velocity instead of the momentum thickness as the characteristic length. In figure 32 the frequency neutral curves obtained at $M = 0$ by Schubauer & Skramstad (1948) are compared with those measured at $M = 1{\cdot}6$ and $2{\cdot}2$ on the basis of the velocity thickness Reynolds number. The agreement is surprisingly good.

Indeed a correlation exists, not only for the neutral oscillation, but for the amplified oscillations also. Considering sufficiently high Reynolds numbers for reasons already discussed in § 5.7, we may write

$$\frac{1}{2\overline{e^2}}\frac{d\overline{e^2}}{dx} = \frac{1}{\tilde{Q}}\frac{d\tilde{Q}}{dx} = \frac{\beta_i}{c},$$

or, in non-dimensional form,

$$\frac{\delta}{2\overline{e^2}}\frac{d\overline{e^2}}{dx}\frac{c}{\overline{U}_1} = \frac{\beta_i \delta}{\overline{U}_1}.$$

The calculation of the amplification coefficient involves a differentiation of the amplitude measurements, resulting in some scatter. Nevertheless, within the accuracy of the results a satisfactory agreement between the incompressible

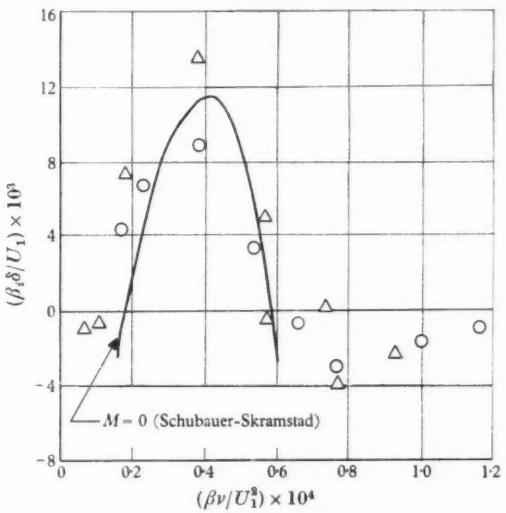


FIGURE 33. Amplification coefficients.
○, test 1; △, test 2; $M = 2{\cdot}2$; $y/\delta = 0{\cdot}7$, $0{\cdot}8$; $R_\delta = 6400$.

amplification coefficients and those at $M = 2{\cdot}2$ for approximately the same $R_\delta$ (figure 33) is obtained. For the propagation velocity the value $c = 0{\cdot}58$ was used, although it actually changed from $0{\cdot}55$ to $0{\cdot}61$ in the frequency range considered.

On the basis of the comparisons made, it is seen that in the Mach and Reynolds number ranges under consideration the stability limits of a disturbance of given frequency depend only on the local thickness $\delta$ and are independent of the Mach number. Furthermore, it is apparent that the non-dimensional amplification coefficient that is the temporal amplification rate $\beta_i\delta/\overline{U}_1$ corresponding to a given $R_\delta$ and frequency also is unaffected by the Mach number. On the other hand, the spatial amplification rate

$$\frac{\delta}{\tilde{Q}}\frac{d\tilde{Q}}{dx} = \frac{\beta_i \delta}{c}$$

decreases with increasing Mach number.

These conclusions are a consequence of the empirical results previously described. Unfortunately, the authors have been unsuccessful so far in finding a satisfactory explanation for this surprisingly simple correlation within the framework of the present theory. Only some rather general inferences may be drawn as follows. In the Mach number range considered, the boundary-layer stability is affected mainly by the change in the mean flow field (by the existence of mean density and temperature gradients), while the density and temperature fluctuations do not play an important role. (Roughly speaking, this implies the result of Lees & Lin (1946), who showed that the relation between the eigenvalues is independent of the temperature fluctuations.) Furthermore, as a result of this change in the mean flow field the disturbance of a given frequency acquires a larger wavelength; that is, the disturbance propagates faster downstream. As a consequence, the oscillations that have the same amplification coefficients have less time available to grow in amplitude over a given length of surface. Thus, a compressible boundary layer is more stable than the incompressible one.

### 5.9. *Effect of Mach number on transition*

Despite the great practical importance of the transition problem, as yet no reliable information, either experimental or theoretical, is available for the case of an adiabatic surface with zero pressure gradient. Specifically, it is not possible to make a definitive statement on the variation of transition Reynolds number with Mach number. Under the circumstances, therefore, it is worthwhile to examine the possibility of estimating, even in a crude fashion, the effect of compressibility on transition Reynolds number, using the present results.

As mentioned already in § 1, the Tollmien–Schlichting instability mechanism is only the initial stage of the transition process; therefore, at least in principle, it is not justifiable to use the linear theory for predicting the point of transition. However, in the incompressible case some favourable circumstances are known to exist which, at least for engineering purposes, permit the use of the linear theory. Some recent work of Schubauer (1958) and Klebanoff & Tidstrom (1959) indicates that the distance interval between the point of transition, $x_t$, and the point where the linear approximation becomes invalid, $x_e$, is small compared with $x_t$, and that the breakdown into turbulent spots occurs at approximately the same oscillation amplitude ($\tilde{u}/\overline{U}_1 \approx 7\,\%$). The fair success of the method proposed by Smith (1956) in predicting transition Reynolds numbers, using a linear theory, is believed to hinge on these experimental findings.

Unfortunately, in the compressible case very little is known at present about the non-linear region of transition. From the lower amplification rates obtained in the present work, it is expected that the estimation of the transition point will be less successful. Nevertheless, because of the lack of anything better, an attempt is made to obtain an approximate variation of transition Reynolds number with Mach number. The assumptions involved in the calculation are as follows: (1) the amplification ratio at breakdown is the same as in the incompressible case ($\log[\tilde{Q}/Q_0] = 6{\cdot}5$, which yields the transition Reynolds number $R_x = 3 \times 10^6$ observed by Schubauer & Skramstad); (2) the initial amplitude

$Q_0$ of the critical disturbances is independent of frequency and Mach number; (3) the ratio $c/c_{\text{inc}}$ is independent of $R_\delta$.

From the form of the disturbance (3.1) we may write

$$\log\frac{\tilde{Q}}{Q_0} = \int_{t(x_0)}^{t(x)} \beta_i\, dt = \int_{x_0}^{x} \frac{\beta_i}{c}\, dx$$

$$= \frac{2}{a^2}\int_{R_{\delta_0}}^{R_\delta} \frac{\overline{U}_1}{c}\frac{\beta_i\delta}{\overline{U}_1}\, dR_\delta \quad \text{since} \quad \frac{\delta}{x} = \frac{a}{\sqrt{R_x}},$$

where $a$ is constant.

In the incompressible case, Pretsch calculated and charted the value of this integral for all unstable frequencies. By means of his calculations,* it is easily verified that the minimum Reynolds number at which the disturbance reaches an amplification ratio $\log(\tilde{Q}/Q_0) = 6{\cdot}5$ turns out to be $R_\delta = 10{,}400$ or $R_x = 3\times10^6$. For the compressible case on the basis of assumption 3, one may rewrite the above equation

$$\log\frac{\tilde{Q}}{Q_0} = 6{\cdot}5 = \left[\frac{a_{\text{inc}}^2}{a^2}\frac{c_{\text{inc}}}{c}\right]\left[\frac{2}{a_{\text{inc}}^2}\int_{R_{\delta_0}}^{R_{\delta_{\text{tr}}}} \frac{\overline{U}_1}{c_{\text{inc}}}\frac{\beta_i\delta}{\overline{U}_1}\, dR_\delta\right].$$

Using the present experimental result that $\beta_i\delta/U_1$ is a function of $R_\delta$ only, independently of $M$, Pretsch's charts can be used for the evaluation of the second factor on the right-hand side of the above equation. The new 'fictitious' amplification ratio is

$$\frac{a^2}{a_{\text{inc}}^2}\frac{c}{c_{\text{inc}}}\,6{\cdot}5.$$

The table below shows the transition Reynolds number ratios for various Mach numbers and the approximate values of $c/c_{\text{inc}}$ used in the calculation:

| $M$ | 0 | 0·4 | 0·8 | 1·3 | 1·6 | 2·0 |
|---|---|---|---|---|---|---|
| $c/c_{\text{inc}}$ | 1·0 | 1·06 | 1·13 | 1·20 | 1·33 | 1·76 |
| $[R_x/R_{x,\text{inc}}]_{\text{tr}}$ | 1·0 | 1·1 | 1·2 | 1·4 | 1·6 | 2·3 |

The rapid increase in transition Reynolds number is quite apparent.

## 6. Conclusion

A detailed exploration has been made of small-amplitude disturbances in a laminar supersonic layer up to $M = 2{\cdot}2$, and the stability of the layer with respect to these perturbations was examined. The results may be summarized as follows.

(1) The experiments succeeded in detecting self-excited oscillations in the layer. Generally speaking, the basic features of these oscillations are the same as found in the incompressible layer and are in agreement with the existing theory. Specifically, the boundary layer acts as a frequency selective-amplifier with respect to the disturbances: depending on the local Reynolds number, it attenuates certain frequencies and amplifies others, thus causing detectable oscillations in a narrow bandwidth.

(2) Amplitude distributions of velocity, temperature, and density fluctuations have been calculated from the measurements. It was found that at $M = 2{\cdot}2$

* The authors are grateful to A. M. O. Smith, who extended and re-plotted Pretsch's calculations in a more convenient form and made his charts accessible.

the temperature and density fluctuations are several times that of the velocity, and this ratio is shown to increase further with increasing Mach number.

(3) Comparing the results with the stability theory of Lees, Lin, and Dunn, one may conclude that the theory predicts correctly the basic features of the compressible-boundary-layer stability. Quantitatively, the viscous solutions predict Reynolds numbers corresponding to the lower stability limits which are considerably below the measured values. On the other hand, the theoretical upper stability branch agrees very well with that obtained by the experiments.

(4) Within the accuracy of the measurements, results of the incompressible and compressible stability problem may be correlated; it is shown that up to $M = 2{\cdot}2$ the stability limits (two positions on the plate between which a disturbance is amplified) of a perturbation of a given frequency depend only on the Reynolds number based on the local boundary-layer thickness $\delta$, and are independent of the Mach number. Furthermore, the non-dimensional amplification coefficient $\delta\beta_i/\overline{U}_1$ depends only on the local eigenvalues (frequency, $R_\delta$) and not on the Mach number.

(5) The effect of compressibility manifests itself mainly in changing the wave velocity of the disturbances: they propagate faster with increasing Mach number. This has the important consequence that a disturbance propagating to a given $x$-position will not be amplified as much in a higher Mach number flow because its time available to grow is less, even though its amplification coefficient $(\delta\beta_i/\overline{U}_1)(R_\delta)$ is the same. Thus, the adiabatic compressible boundary layer is shown to be more stable with respect to small disturbances than the incompressible one.

(6) On the basis of the above results, a rough estimate of the transition Reynolds number is made; the calculations indicate a considerable increase in its value as the Mach number increases.

The authors wish to acknowledge the constant support and encouragement of Drs F. E. Goddard and P. P. Wegener of the Jet Propulsion Laboratory during the entire period of this investigation. The extremely valuable discussions with Prof. Lester Lees, Drs Leslie M. Mack, Alan Kistler, Eli Reshotko, and R. Betchov are also gratefully acknowledged. Mr Carl Thiele contributed many basic ideas in the design of the mechanical and electronic systems used, while Mr A. Irving and his group and Mr W. Simms carried out their construction expertly. Their valuable help contributed greatly to the results of the investigation.

This paper presents the results of one phase of research carried out at the Jet Propulsion Laboratory, California Institute of Technology, under joint sponsorship of the Department of the Army, Ordnance Corps (under Contract No. DA-04-495-Ord 18), and the Department of the Air Force.

## Notation

| | |
|---|---|
| $c$ | wave velocity |
| $C_v$ | specific heat at constant volume |
| $e$ | hot-wire voltage |
| $e_f$ | hot-wire voltage filtered by wave analyser |

| | |
|---|---|
| $\Delta e$ | a dimensionless hot-wire voltage fluctuation |
| $f$ | frequency |
| $i$ | heated-wire current |
| $k$ | thermal conductivity |
| $m$ | mass flow |
| $M$ | Mach number |
| $p$ | static pressure |
| $Re$ | Reynolds number |
| $R_r$ | unheated-wire resistance |
| $R_w$ | heated-wire resistance |
| $R_\theta$ | Reynolds number based on boundary-layer momentum thickness |
| $R_\delta$ | Reynolds number based on boundary-layer thickness at $u/\overline{U}_1 = 0{\cdot}999$ |
| $Q'$ | perturbation of any one of the flow quantities |
| $S$ | hot-wire sensitivity factor |
| $t$ | time |
| $T$ | static temperature |
| $u$ | velocity in the $x$-direction |
| $\overline{U}_1$ | mean velocity in free stream |
| $v'$ | velocity fluctuation perpendicular to plate |
| $x$ | co-ordinate along the free-stream direction; $x = 0$ corresponds to plate leading edge |
| $y$ | co-ordinate perpendicular to free-stream direction and the flat plate; $y = 0$ corresponds to plate surface |
| $X, Y$ | abscissa and ordinate on the plotting table |
| $\alpha$ | wave-number |
| $\beta$ | $2\pi f$, angular frequency |
| $\beta_i$ | damping coefficient |
| $\gamma$ | ratio of specific heats |
| $\Gamma =$ | $\int_0^1 \tilde{e}_f d\frac{y}{\delta}$ |
| $\delta$ | boundary-layer thickness |
| $\theta$ | boundary-layer momentum thickness |
| $\lambda$ | $2\pi/\alpha$, wavelength |
| $\mu$ | viscosity |
| $\nu$ | kinematic viscosity |
| $\rho$ | density |

*Superscripts and subscripts*

| | |
|---|---|
| $\overline{(\ )}$ | temporal mean |
| $\overline{(\ )}^2$ | mean-square value of a fluctuating quantity |
| $\tilde{(\ )}$ | root-mean-square value of a fluctuating quantity |
| $(\ )'$ | instantaneous value of a fluctuating quantity |
| $(\ )_1$ | free-stream condition |
| $(\ )_T$ | stagnation condition |

## REFERENCES


BENNET, H. W. 1953 *An Experimental Study of Boundary Layer Transition.* Neenah, Wisconsin: Kimberly-Clark.

DEMETRIADES, A. 1958 An experimental investigation of the stability of the hypersonic laminar boundary layer. *J. Aero./Space Sci.* **25**, 599.

DEMETRIADES, A. 1960 An experiment on the stability of the hypersonic laminar boundary layer. *J. Fluid Mech.* **7**, 385.

DRYDEN, H. L. 1955 Transition from laminar to turbulent flow at subsonic and supersonic speeds. *Proceedings of the Conference on High-Speed Aeronautics*, no. 41. Polytechnic Institute of Brooklyn.

DUNN, D. W. & LIN, C. C. 1955 On the stability of the laminar boundary layer in a compressible fluid. *J. Aero. Sci.* **22**, 455.

KLEBANOFF, P. S. & TIDSTROM, K. D. 1959 Evolution of amplified waves leading to transition in a boundary layer with zero pressure gradient. *N.A.S.A. Tech. Note*, no. D-195.

KOVASZNAY, L. S. G. 1953 Turbulence in supersonic flow. *J. Aero. Sci.* **20**, 657.

KOVASZNAY, L. S. G. 1954 Development of turbulence-measuring equipment. *N.A.S.A. Rep.* no. 1209.

LAUFER, J. 1956 Experimental observation of laminar boundary-layer oscillations in supersonic flow. *J. Aero. Sci.* **23**, 184.

LAUFER, J. 1959 Aerodynamic noise in supersonic wind tunnels. Jet Propulsion Laboratory, Pasadena, California, Progress Rep. no. 20–378.

LAUFER, J. & MCCLELLAN, R. 1956 Measurement of heat transfer from fine wires in supersonic flows. *J. Fluid Mech.* **1**, 276.

LAUFER, J. & VREBALOVICH, T. 1957 Experiments on the instability of a supersonic boundary layer. IX. Congrès International de Mécanique Appliquée, Université de Bruxelles.

LAUFER, J. & VREBALOVICH, T. 1958 Stability of a supersonic laminar boundary layer on a flat plate. Jet Propulsion Laboratory, Pasadena, California, Rep. no. 20–116.

LEES, L. 1947 The stability of the laminar boundary in a compressible fluid. *N.A.C.A. Rep.* no. 876.

LEES, L. 1952 Instability of laminar flows and transition to turbulence. Consolidated Vultee Aircraft Corporation, San Diego, California, Rep. no. ZA-7-006.

LEES, L. & LIN, C. C. 1946 Investigation of the stability of the laminar boundary layer in a compressible fluid. *N.A.C.A. Tech. Note*, no. 1115.

LIEPMANN, H. W. 1943 Investigations on laminar boundary-layer stability and transition on curved boundaries. *N.A.C.A. Rep.* no. W-107.

LIEPMANN, H. W. & ROSHKO, A. 1957 *Elements of Gasdynamics.* New York: John Wiley and Sons.

LIN, C. C. 1945 On the stability of two-dimensional parallel flows. *Quart. Appl. Math.* **2**, 117; **3**, 218; **4**, 277.

LIN, C. C. 1958 On the instability of laminar flow and its transition to turbulence. *IUTAM Symposium on Boundary Layer Research at Freiburg, 1957*, pp. 144–87. Springer.

MACK, L. M. 1958 Calculation of the laminary boundary layer on an insulated flat plate by the Klunker–McLean method. Jet Propulsion Laboratory, Pasadena, California, Progress Rep. no. 20–352.

MACK, L. M. 1960 Numerical calculation of the stability of the compressible laminar boundary layer. Jet Propulsion Laboratory, Pasadena, California, Rep. no. 20–122.

MORKOVIN, M. V. 1956 Fluctuations and hot-wire anemometry in compressible flows. North Atlantic Treaty Organization, Advisory Group for Aeronautical Research and Development, Paris, AGARDograph 24.

MORKOVIN, M. V. 1958 Transition from laminar to turbulent shear flow—a review of some recent advances in its understanding. *Trans. Amer. Soc. Mech. Engrs*, **80**, 1121.

SCHUBAUER, G. B. 1958 Mechanism of transition at subsonic speeds. *IUTAM Symposium on Boundary Layer Research at Freiburg, 1957*, pp. 85–107. Springer.

SCHUBAUER, G. B. & SKRAMSTAD, H. K. 1948 Laminary-boundary-layer oscillations and transition on a flat plate. *N.A.C.A. Rep.* no. 909.

SMITH, A. M. O. 1956 Transition, pressure gradient and stability theory. Douglas Aircraft Rep. no. ES 26388.

STRONG, J. 1938 *Procedures in Experimental Physics*, p. 134. Englewood Cliffs, New Jersey: Prentice-Hall.

TOLLMIEN, W. 1929 Über die Entstehung der Turbulenz. *Nachrichten der Gesellschaft der Wissenschaften zu Göttingen, Mathematisch-Physikalische Klasse*, pp. 21–44. (Translated as *N.A.C.A. Tech. Memo.* no. 609.)

TUCKER, M. 1953 Combined effect of damping screens and stream convergence on turbulence. *N.A.C.A. Tech. Note*, no. 2878.

WORTMANN, F. X. 1955 Untersuchung instabiler Grenzschichtschwingungen in einem Wasserkanal mit der Tellurmethode. *50 Jahre Grenzschichtforschung*, pp. 460–70. Braunschweig: Friedr. Vieweg und Sohn.

# On unsteady laminar boundary layers

By H. A. HASSAN
Virginia Polytechnic Institute, Blacksburg, Virginia

(Received 11 April 1960)

A transformation is introduced which, for a class of outer pressure distributions, reduces the unsteady incompressible laminar boundary-layer equations in two dimensions to an equation in which the time does not appear explicitly. A formally exact solution of the resulting equation is then presented in the form of a series and it is shown that the solution can be expressed in terms of universal functions.

## 1. Introduction

Early attempts to discuss unsteady laminar boundary-layer flows were mainly restricted to early phases of a motion starting from rest and to oscillatory motions without a mean flow. Very little attention was paid to the subject because it was felt that boundary-layer growth took place in such a short time that the flow may be considered steady. It is clear that such considerations do not apply if one considers the problem of a vehicle moving with variable speed over its entire trajectory, and a detailed investigation of unsteady flows is required if reliable information concerning skin friction and heat transfer is desired.

Recently Lighthill (1954) considered the influence of free-stream fluctuations on skin friction and heat transfer, and Yang (1958) studied the stagnation point flow. Moore (1951) analysed the problem of the laminar compressible boundary layer over an insulated flat plate moving with a time dependent velocity and, later, Ostrach (1955) extended Moore's results to the case of an isothermal flat plate.

This paper presents a solution of the problem of unsteady incompressible laminar boundary-layer flow for a certain class of outer pressure distributions. The method employed makes use of a transformation, a special case of which was given by the author in a recent note (Hassan 1960), which reduces the governing equation to an equation in which the time does not appear explicitly. In spite of the fact that such a scheme restricts to a great extent the free-stream velocity distributions that can be considered, yet the distribution considered includes, as special cases, a number of flows which are of interest.

It is assumed that the solution has a power series representation and it is shown that it can be recast in terms of universal functions. As an example of skin-friction calculations, the special case of the assumed flow where the free-stream velocity is a function of time is considered.

## 2. Basic equations and transformations

The differential equation for unsteady incompressible laminar boundary layer in two dimensions can be written as

$$\psi_{yt}+\psi_y\psi_{xy}-\psi_x\psi_{yy}=V_t+VV_x+\nu\psi_{yyy}, \tag{2.1}$$

where $\psi$ is the stream function, $V$ is the free-stream velocity and $\nu$ is the kinematic viscosity. The boundary conditions are

$$\psi(x,y,t)=\psi_y(x,y,t)=\psi_x(x,y,t)=0 \quad \text{at} \quad y=0,$$
$$\psi_y(x,y,t)\to V(x,t) \quad \text{as} \quad y\to\infty. \tag{2.2}$$

Letting
$$s=(x/l)\,(2\nu t/l^2)^{\frac{1}{2}(\lambda-1)}, \quad \sigma=y/\sqrt{(2\nu t)},$$
$$V=(\nu/l)\,(2\nu t/l^2)^{-\frac{1}{2}(1+\lambda)}h(s), \quad \psi=\nu(2\nu t/l^2)^{-\frac{1}{2}\lambda}\chi(s,\sigma), \tag{2.3}$$

where $l$ is a characteristic length, $\lambda$ is any real or complex number,

and
$$h(s)=s^\alpha\sum_0^\infty a_n s^n, \quad a_0\neq 0, \quad \alpha \text{ an integer}; \tag{2.4}$$

and substituting into (2.1) and (2.2) one finds that

$$\chi_{\sigma\sigma\sigma}+(1-\lambda)\,s[\chi_{s\sigma}-h']+(1+\lambda)\,[\chi_\sigma-h]$$
$$+\sigma\chi_{\sigma\sigma}+\chi_s\chi_{\sigma\sigma}-\chi_\sigma\chi_{s\sigma}+hh'=0, \tag{2.5}$$

and
$$\chi=\chi_\sigma=\chi_s=0 \quad \text{at} \quad \sigma=0; \quad \chi_\sigma\to h(s) \quad \text{as} \quad \sigma\to\infty. \tag{2.6}$$

It is seen from (2.3) and (2.4) that the assumed expression for the free-stream velocity represents a very special class of $V(x,t)$. The assumed expression for $V$ makes it necessary for $\psi$ to assume the form given in (2.3) because $V=\psi_y$ at infinity.

Equation (2.6) shows that the boundary conditions depend on $h(s)$. However, a substitution which renders the boundary conditions independent of the free-stream velocity and paves the way for expressing the solution in terms of universal functions can be written as (Hassan 1960)

$$\xi=s, \quad \eta=\sigma f(s), \quad \chi=(h/f)\,\phi(\xi,\eta), \tag{2.7}$$

where
$$f(\xi)=\xi^{\frac{1}{2}(\alpha-1)} \quad \text{for} \quad \alpha\leqslant 0; \quad f(\xi)=1 \quad \text{for} \quad \alpha>0. \tag{2.8}$$

Introducing (2.7) into (2.5) and (2.6), one obtains

$$\phi_{\eta\eta\eta}+(1/f^2)\,[1+\lambda+(1-\lambda)\,(\xi h'/h)]\,[\phi_\eta-1]$$
$$+(1/f^2)\,[1+(1-\lambda)\,(\xi f'/f)]\,\eta\phi_{\eta\eta}+(1-\lambda)\,(\xi/f^2)\,\phi_{\xi\eta}$$
$$+(1/f)\,(h/f)'\,\phi\phi_{\eta\eta}+(h/f^2)\,[\phi_\xi\phi_{\eta\eta}-\phi_\eta\phi_{\xi\eta}]$$
$$+(h'/f^2)\,(1-\phi_\eta^2)=0, \tag{2.9}$$

and
$$\phi=\phi_\eta=\phi_\xi=0 \quad \text{at} \quad \eta=0; \quad \phi_\eta\to 1 \quad \text{as} \quad \eta\to\infty. \tag{2.10}$$

## 3. Solution of equation (2.9)

The solution of (2.9) in the region of convergence of (2.4) will be assumed to be expressible as

$$\phi=\sum_{n=0}^\infty \phi_n(\eta)\,\xi^n. \tag{3.1}$$

Substituting (2.8) into (2.9) and letting

$$1+\lambda+(1-\lambda)(\xi h'/h)=\sum_{n=0}^{\infty}b_n\xi^n, \quad b_0=1+\alpha+\lambda(1-\alpha), \tag{3.2}$$

one obtains the following system of total differential equations for the functions $\phi_n$.

(1) $\alpha \leqslant 0$:

$$\phi_0'''+\tfrac{1}{2}a_0(1+\alpha)\phi_0\phi_0''+a_0\alpha(1-\phi_0'^2)=0, \tag{3.3}$$

and

$$\phi_n'''+\tfrac{1}{2}a_0(1+\alpha)\phi_0\phi_n''-a_0(n+2\alpha)\phi_0'\phi_n'+a_0[n+\tfrac{1}{2}(1+\alpha)]\phi_0''\phi_n=R_{n-1} \quad (n\geqslant 1), \tag{3.4}$$

where

$$\begin{aligned}R_{n-1}=Q_{n-1}\equiv a_n[(n+\alpha)(\phi_0'^2-1)-\{n+\tfrac{1}{2}(1+\alpha)\}\phi_0\phi_0'']\\ +a_0\sum_{k=1}^{n-1}[(k+\alpha)\phi_k'\phi_{n-k}'-\{k+\tfrac{1}{2}(1+\alpha)\}\phi_k\phi_{n-k}'']\\ -\phi_0\sum_{k=1}^{n-1}a_k[k+\tfrac{1}{2}(1+\alpha)]\phi_{n-k}''+\phi_0'\sum_{k=1}^{n-1}a_k(k+\alpha)\phi_{n-k}'\\ +\sum_{k=1}^{n-1}\sum_{m=1}^{n-k}a_k[(m+k+\alpha)\phi_m'\phi_{n-m-k}'-\{m+k+\tfrac{1}{2}(1+\alpha)\}\phi_m\phi_{n-m-k}''],\\ \text{for} \quad n\leqslant -\alpha; \quad (3.5a)\end{aligned}$$

and

$$\begin{aligned}R_{n-1}=Q_{n-1}+b_{n+\alpha-1}-\sum_{k=0}^{n+\alpha-1}b_k\phi_{n+\alpha-k-1}'-\tfrac{1}{2}b_0\eta\phi_{n+\alpha-1}''\\ -(1-\lambda)(n+\alpha-1)\phi_{n+\alpha-1}' \quad \text{for} \quad n>-\alpha. \quad (3.5b)\end{aligned}$$

It is to be understood that, in (3.5$a$), $Q_{n-1}$ is identical to the right-hand side of the equation for all $n$, while $R_{n-1}$ is equal to the right-hand side for restricted $n$ as indicated.

(2) $\alpha=1$:

$$\phi_0'''+2(\phi_0'-1)+\eta\phi_0''+a_0[1+\phi_0\phi_0''-\phi_0'^2]=0, \tag{3.6}$$

and

$$\phi_n'''+(\eta+a_0\phi_0)\phi_n''+[2+n(1-\lambda)-a_0(n+2)\phi_0']\phi_n'+a_0(n+1)\phi_0''\phi_n=R_{n-1} \quad (n\geqslant 1), \tag{3.7}$$

where

$$\begin{aligned}R_{n-1}=a_n(n+1)[\phi_0'^2-\phi_0\phi_0''-1]+a_0\sum_{k=1}^{n-1}(k+1)[\phi_k'\phi_{n-k}'-\phi_k\phi_{n-k}'']\\ -\phi_0\sum_{k=1}^{n-1}a_k(k+1)\phi_{n-k}''+\phi_0'\sum_{k=1}^{n-1}a_k(k+1)\phi_{n-k}'\\ +\sum_{k=1}^{n-1}\sum_{m=1}^{n-k}(m+k+1)a_k[\phi_m'\phi_{n-m-k}'-\phi_m\phi_{n-m-k}'']\\ -b_n(\phi_0'-1)-\sum_{k=1}^{n-1}b_k\phi_{n-k}'. \quad (3.8)\end{aligned}$$

(3) $\alpha>1$:

$$\phi_0'''+\eta\phi_0''+[1+\alpha+\lambda(1-\alpha)][\phi_0'-1]=0, \tag{3.9}$$

and

$$\phi_n'''+\eta\phi_n''+[1+\lambda+(n+\alpha)(1-\lambda)]\phi_n'=R_{n-1} \quad (n\geqslant 1), \tag{3.10}$$

where $$R_{n-1} = Q_{n-1} \equiv -b_n(\phi_0' - 1) - \sum_{k=1}^{n-1} b_k \phi_{n-k}' \quad (n \leqslant \alpha - 2), \tag{3.11a}$$

and

$$R_{n-1} = Q_{n-1} + \sum_{k=0}^{n+1-\alpha} \sum_{m=0}^{n+1-\alpha-k} a_k(k+\alpha+n)\,[\phi_m' \phi_{n-m-k-\alpha+1}' - \phi_m \phi_{n-m-k-\alpha+1}''] - (n+1)\,a_{n+1-\alpha} \quad (n > \alpha - 2). \tag{3.11b}$$

The boundary conditions are

$$\phi_0(0) = \phi_0'(0) = 0, \quad \phi_0'(\infty) = 1; \quad \phi_n(0) = \phi_n'(0) = \phi_n'(\infty) = 0 \quad (n \geqslant 1). \tag{3.12}$$

The equations governing the zeroth order term, i.e. (3.3), (3.6) and (3.9), will be discussed next. Equation (3.3) can be easily reduced to the well-known equation of Falkner and Skan, and its solution was given by Hartree (1937). Equation (3.6), which is identical to the equation for unsteady stagnation-point flow, has been solved by Yang (1958). Finally, equation (3.9) is a linear equation which has a known solution:

$$\phi_0' = 1 - \eta^{-\frac{1}{2}} \exp(-\tfrac{1}{4}\eta^2) W_{k,m}(\tfrac{1}{2}\eta^2), \tag{3.13}$$

where $W_{k,m}$ is the confluent hypergeometric function (Whittaker & Watson 1927) with

$$k = \tfrac{1}{2}b_0 - \tfrac{1}{4}, \quad m = \tfrac{1}{4}. \tag{3.14}$$

Applying the boundary conditions reduces (3.13) to

$$\phi_0' = 1 - \exp(-\tfrac{1}{2}\eta^2)\, {}_1F_1[\tfrac{1}{2}(1-b_0), \tfrac{1}{2}, \tfrac{1}{2}\eta^2], \tag{3.15}$$

where

$${}_1F_1(a,b,x) = 1 + \sum_{n=1}^{\infty} \frac{a(a+1)\dots(a+n-1)}{b(b+1)\dots(b+n-1)} \frac{x^n}{n!}. \tag{3.16}$$

The functions $\phi_n$ $(n \geqslant 1)$ are governed by linear equations and can be expressed as linear combinations of universal functions for a given $\alpha$, $\lambda$ and $a_0$. This can be accomplished by letting

$$\begin{aligned} \phi_1 &= \delta_1 f_1 + a_1 g_1 + \beta_1 h_1, \\ \phi_2 &= \delta_1^2 f_{11} + \delta_2 f_2 + a_1^2 g_{11} + a_2 g_2 + \beta_1^2 h_{11} + \beta_2 h_2 + \delta_1 a_1 p_{1,1} + a_1 \beta_1 q_{1,1} + \beta_1 \delta_1 r_{1,1}, \\ &\dots\dots\dots

and the governing equations are

$$\phi_0''' + \tfrac{1}{2}a_0\phi_0\phi_n'' = 0, \tag{4.5}$$

$$\phi_1''' + \tfrac{1}{2}a_0\phi_0\phi_1'' - a_0\phi_0'\phi_1' + \tfrac{3}{2}a_0\phi_0''\phi_1 = b_0[1 - \phi_0' - \tfrac{1}{2}\eta\phi_0''],$$

..... (4.6)

Letting $$\phi_0 = a_0^{-\frac{1}{2}}F, \quad \phi_1 = -b_0a_0^{-\frac{3}{2}}h_1, \quad \ldots, \quad \eta = 2a_0^{-\frac{1}{2}}\zeta, \tag{4.7}$$

we find that (4.5), (4.6) and (3.12) reduce to

$$F''' + FF'' = 0, \tag{4.8}$$

$$h_1''' + Fh_1'' - 2F'h_1' + 3F''h_1 = -4(2 - F') + 2\zeta F'', \tag{4.9}$$

$$F(0) = F'(0) = 0, \quad F'(\infty) = 2, \quad h_1(0) = h_1'(0) = h_1'(\infty) = 0, \quad \ldots. \tag{4.10}$$

Equation (4.8) is the well-known Blasius equation, and (4.9) has been solved by Moore (1951). Therefore, one may write

$$\begin{aligned} C_f &= [\tfrac{1}{2}a_0^{-\frac{1}{2}}\xi^{-\frac{1}{2}}](2\nu t/l^2)^{\frac{1}{2}\lambda}[F''(0) - (b_0/a_0)\,h_1''(0)\,\xi + \ldots] \\ &= [\tfrac{1}{2}a_0^{-\frac{1}{2}}\xi^{-\frac{1}{2}}](2\nu t/l^2)^{\frac{1}{2}\lambda}[1{\cdot}328 - 3{\cdot}394\{(1+\lambda)/a_0\}\xi + \ldots]. \end{aligned} \tag{4.11}$$

For accelerating flows $1 + \lambda < 0$ and (4.11) shows that positive acceleration causes an increase in skin friction above the 'quasi-steady' value.

Considering the case of complex $\lambda$ and letting

$$1 + \lambda = a + i\omega, \tag{4.12}$$

one obtains

$$V = a_0(\nu/l)\,(2\nu t/l^2)^{-\frac{1}{2}a}\exp[-\tfrac{1}{2}i\omega\log(2\nu t/l^2)] \tag{4.13}$$

and $$C_f = \tfrac{1}{2}a_0^{-\frac{1}{2}}(l/x)^{\frac{1}{2}}\,(2\nu t/l^2)^{\frac{1}{4}a}\exp[\tfrac{1}{4}i\omega\log(2\nu t/l^2)][1{\cdot}328 - \ldots]. \tag{4.14}$$

Equations (4.13) and (4.14) show that the maximum of skin friction is not in phase with the maximum of the free-stream velocity.

## 5. Concluding remarks

The transformation that has been introduced makes it possible to give the solution of a wide class of unsteady flow problems without resorting to approximate methods. The method of solution gives a unified presentation to a number of special cases discussed in the literature and reduces the actual solution for a given problem to a solution of a few linear differential equations.

It should be noted, however, that although the method is well suited to problems in which $V(x,t) \sim x^n t^m$, it fails if $V(x,t) \sim f(x)\,F(t)$, where $f$ and $F$ are arbitrary functions.

## REFERENCES


Hartree, D. R. 1937 *Proc. Camb. Phil. Soc.* **33**, 223.

Hassan, H. A. 1960 *J. Aero. Sci.* **27**, 474.

Lighthill, M. J. 1954 *Proc. Roy. Soc.* A, **224**, 1.

Moore, F. K. 1951 *Nat. Adv. Comm. Aero., Wash., Tech. Note*, no. 2471.

Ostrach, S. 1955 *Nat. Adv. Comm. Aero., Wash., Tech. Note*, no. 3569.

Whittaker, E. T. & Watson, G. N. 1927 *Modern Analysis*. Cambridge University Press.

Yang, K. T. 1958 *J. Appl. Mech.* **25**, 421.

# Note on the swimming of slender fish

By M. J. LIGHTHILL
Royal Aircraft Establishment, Farnborough, Hampshire

(Received 9 May 1960)

The paper seeks to determine what transverse oscillatory movements a slender fish can make which will give it a high Froude propulsive efficiency,

$$\frac{\text{(forward velocity)} \times \text{(thrust available to overcome frictional drag)}}{\text{(work done to produce both thrust and vortex wake)}}.$$

The recommended procedure is for the fish to pass a wave down its body at a speed of around $\frac{5}{4}$ of the desired swimming speed, the amplitude increasing from zero over the front portion to a maximum at the tail, whose span should exceed a certain critical value, and the waveform including both a positive and a negative phase so that angular recoil is minimized. The Appendix gives a review of slender-body theory for deformable bodies.

## 1. Introduction

It has frequently been noted that swimming speeds attained both by fish and by mammals (such as porpoises) are remarkably high in relation to their available muscle power. This has been held to indicate, first, that frictional drag is so low that a large fraction of the boundary layer must be laminar, and, secondly, that the movements generating the thrust to balance frictional drag must produce only a small fractional drag increase as a result of the vorticity they create. Such achievements should be regarded as a challenge to other species wishing to propel themselves economically through fluids.

The analysis of both these postulated achievements must be helped if the flow outside the boundary layer—that is, the inviscid-fluid flow around the swimming animal—can be determined. This provides the environment in which the boundary layer develops, and determines how and how much vorticity is shed.

Now this external flow is easy to evaluate approximately for what we shall call a 'slender fish'—namely, either a fish or a swimming mammal, whose dimensions and movements at right angles to its direction of locomotion are small compared with its length, while its cross-section varies along it only gradually. The 'slender-body' theory (which goes back to Munk's work (1924) on flow about airships; for a general review see Lighthill (1960)) can be applied to these.

In this note the theory is worked out for a slender fish which makes swimming movements only in a single direction at right angles to its direction of locomotion. Types of movement producing thrust with a small vortex-drag penalty are determined, and some remarks made on the boundary-layer development which they might induce.

## 2. Inviscid-flow theory of the forces produced by swimming movements

It is convenient to consider swimming movements which enable the fish to stay still in water flowing with velocity $U$ in the $x$-direction. We investigate the inviscid flow around the fish, remembering that, for the calculation to be relevant, it must yield a mean thrust on the fish sufficient to balance the mean frictional drag.

We describe the fish in the stream as 'stretched straight' when it is held stationary in a standard position such that no resultant normal force acts on any cross-section. When the fish is stretched straight the cross-section of its surface $S$ at a distance $x$ downstream from the nose will be denoted by $S_x$.

We suppose now that in swimming the cross-section $S_x$ receives a displacement $h(x,t)$ from the stretched straight position, in the $z$-direction, so that the displacement is at right angles to the direction of locomotion and varies both with position and time. Then on slender-body theory the flow can be regarded as compounded of

(i) the steady flow around the stretched straight body;
(ii) the flow due to the displacements $h(x,t)$.

To envisage the flow component (ii), we observe that a cross-section $S_x$ moves, relative to the fluid flowing past it with velocity $U$, at a velocity

$$V(x,t) = \frac{\partial h}{\partial t} + U\frac{\partial h}{\partial x}, \tag{1}$$

and that, locally, the body shape differs little from that of an infinite cylinder $C_x$ whose cross-section is $S_x$ all the way along. Accordingly, to the slender-body approximation, the flow component (ii) near $S_x$ is identical with the two-dimensional potential flow that would result from the motion of the cylinder $C_x$ through fluid at rest with velocity $V(x,t)$.

We suppose now that this flow has momentum

$$\rho V(x,t)\, A(x) \tag{2}$$

per unit length of cylinder, where $\rho$ is the density. In the usual terminology, $\rho A(x)$ is the 'virtual mass' of the cylinder $C_x$ per unit length for motions in the $z$-direction. Thus, the coefficient $A(x)$ has the dimensions of area; for example, it is equal to the area of the cross-section $S_x$ when the latter is circular, while for an ellipse with minor axis in the $z$-direction $A(x)$ is the area of its circumscribing circle.

To obtain the instantaneous lift per unit length of fish, $L(x,t)$, that is, the force in the $z$-direction on the cross-section $S_x$, we observe that this must be equal and opposite to the rate of change of momentum of the fluid passing $S_x$; that is,

$$L(x,t) = -\rho\left(\frac{\partial}{\partial t} + U\frac{\partial}{\partial x}\right)\{V(x,t)\, A(x)\}. \tag{3}$$

We next write down the rate, $W$, at which the fish does work by making displacements $h(x,t)$ in the direction in which these lift forces act; this is

$$\begin{aligned} W &= -\int_0^l \frac{\partial h}{\partial t} L(x,t)\,dx = \rho \int_0^l \frac{\partial h}{\partial t}\left(\frac{\partial}{\partial t}+U\frac{\partial}{\partial x}\right)\{V(x,t)\,A(x)\}\,dx \\ &= \rho\int_0^l \left(\frac{\partial}{\partial t}+U\frac{\partial}{\partial x}\right)\left\{\frac{\partial h}{\partial t}\,V(x,t)\,A(x)\right\}dx - \rho\int_0^l \frac{\partial V}{\partial t}\,VA(x)\,dx \\ &= \frac{\partial}{\partial t}\left\{\rho\int_0^l \frac{\partial h}{\partial t}\,VA(x)\,dx - \tfrac{1}{2}\rho\int_0^l V^2A(x)\,dx\right\} + \rho U\left[\frac{\partial h}{\partial t}\,VA(x)\right]_0^l. \end{aligned} \tag{4}$$

The mean over a long time of the time-derivative in this last expression is zero. As regards the final term, we have $A(0) = 0$, but because the fish has a tail $A(l)$ is non-zero—at least on the approximation of assuming a straight trailing edge, which makes $A(l)$ equal to the area of the circle with the trailing edge as diameter. Hence, (4) gives for the mean rate of working by the fish

$$\overline{W} = \rho U A(l)\left\{\overline{\frac{\partial h}{\partial t}\left(\frac{\partial h}{\partial t}+U\frac{\partial h}{\partial x}\right)}\right\}_{x=l}. \tag{5}$$

This value can be interpreted physically as the mean of the product of the lateral velocity $\partial h/\partial t$ of the tail trailing edge with the rate of shedding $(\rho VA)\,U$ of lateral momentum (2) behind the trailing edge, on the argument that rate of working equals velocity times rate of change of momentum.

On the other hand, the rate of shedding of kinetic energy of lateral fluid motions is $(\frac{1}{2}\rho V^2A)\,U$, with (again) the trailing edge values of $V$ and $A$. If, now, we subtract the mean value of this from the mean rate of working $\overline{W}$, we should obtain the rate of working available for producing the mean thrust, say, $\overline{P}$; this rate is $\overline{P}U$. If the result of this subtraction were negative, one would infer that there was a mean drag, more energy being shed in the wake than is put into the fluid by the swimming movements. In this case an external force would be needed to supply the extra work to push the fish through the fluid against this drag and the frictional drag together. *Positive* thrust, on the other hand, would produce motion at the speed at which it is exactly balanced by frictional drag.

To sum up,

$$\overline{W} - \tfrac{1}{2}\rho\overline{V^2}AU = \overline{P}U, \tag{6}$$

whence by (5) the mean thrust is

$$\overline{P} = \tfrac{1}{2}\rho A(l)\left\{\overline{\left(\frac{\partial h}{\partial t}\right)^2} - U^2\overline{\left(\frac{\partial h}{\partial x}\right)^2}\right\}_{x=l}. \tag{7}$$

The above arguments for determining $\overline{P}$ are attractively simple, but may not be overwhelmingly convincing. To put it beyond a doubt that the inviscid-flow slender-body pressure distributions do yield (7) as mean resultant thrust, the author has calculated them in the Appendix (which was in any case desirable) and demonstrated the point—and may as well admit that he thought of the above arguments only after getting the answer by the method of the Appendix.

## 3. Conditions for efficient thrust

The dynamic problem of obtaining efficient thrust, with the values of forces which were obtained in § 2, is as follows. We want a high value of the inviscid-flow efficiency of the swimming movements, which by (5) and (6) is

$$\eta_F = \frac{\overline{PU}}{\overline{W}} = 1 - \frac{1}{2}\left\{\left(\overline{\frac{\partial h}{\partial t} + U\frac{\partial h}{\partial x}}\right)^2\right\}_{x=l} \Big/ \left\{\overline{\frac{\partial h}{\partial t}\left(\frac{\partial h}{\partial t} + U\frac{\partial h}{\partial x}\right)}\right\}_{x=l}. \tag{8}$$

The suffix $F$ here is intended to suggest 'Froude efficiency', which similarly relates thrust to the total kinetic energy added to the fluid—including energy devoted to forming a vortex wake.

At the same time the displacements $h(x,t)$ which the fish can make are restricted by two considerations. First, the rate of change of lateral momentum which they produce must be equal to the resultant of the lift forces; this means that

$$\rho\int_0^l S(x)\frac{\partial^2 h}{\partial t^2}\,dx = -\rho\int_0^l \left(\frac{\partial}{\partial t} + U\frac{\partial}{\partial x}\right)\left\{A(x)\left(\frac{\partial h}{\partial t} + U\frac{\partial h}{\partial x}\right)\right\}dx, \tag{9}$$

where $S(x)$ is the area of the cross-section $S_x$ and the density of the fish has been taken equal to the density $\rho$ of the water. Secondly, the rate of change of angular momentum about the $y$-axis which they produce must be equal to the moment of the lift forces about that axis:

$$\rho\int_0^l xS(x)\frac{\partial^2 h}{\partial t^2}\,dx = -\rho\int_0^l x\left(\frac{\partial}{\partial t} + U\frac{\partial}{\partial x}\right)\left\{A(x)\left(\frac{\partial h}{\partial t} + U\frac{\partial h}{\partial x}\right)\right\}dx. \tag{10}$$

Any movements attempted by the fish which failed to satisfy (9) and (10) would automatically produce reactions, or 'recoils', in the form of rigid-body movements

$$F(t) + xG(t), \tag{11}$$

which when added to $h(x,t)$ would cause it to satisfy (9) and (10).

Now, from (8), we see that an efficiency $\eta_F$ only a little less than 1 will be obtained if at the trailing edge typical values of $V = \partial h/\partial t + U\,\partial h/\partial x$ are small compared with those of $\partial h/\partial t$, but positively correlated with them. The last point is essential; negative correlation would produce negative thrust. The first point, on the other hand, must not be overdone: although for given tail velocity $\partial h/\partial t$ the efficiency is increased by making $\partial h/\partial t + U\,\partial h/\partial x$ smaller, we see from (7) that the actual thrust is reduced, so that a compromise is required.

The condition that $\partial h/\partial t + U\,\partial h/\partial x$ must have values generally smaller than, but positively correlated with, $\partial h/\partial t$ is a somewhat restrictive one. For example, a standing-wave form $H(x)\cos\omega t$ for $h$, although it could always be made to satisfy (9) and (10) by incorporation of a linear 'recoil function' in $H(x)$, would give a Froude efficiency

$$\eta_F = 1 - \frac{1}{2}\frac{\omega^2 H^2(l) + U^2 H'^2(l)}{\omega^2 H^2(l)}, \tag{12}$$

which cannot exceed $\frac{1}{2}$. This is doubtless why fish do not normally attempt to swim by causing their bodies to execute the rather simple movements of a standing wave.

A more satisfactory form of $h(x,t)$, if only it could be made to satisfy (9) and (10), would be

$$h(x,t) = f(x)\,g\left(t-\frac{x}{c}\right), \tag{13}$$

where $g(t)$ is an oscillatory function such as $\cos\omega t$. Equation (13) represents a travelling wave, which moves down the fish's body with velocity $c$, and whose amplitude $f(x)$ may vary with position along the fish. Substitution in (8) gives

$$\eta_F = 1-\frac{1}{2}\frac{\overline{\left\{\left(1-\frac{U}{c}\right)f(l)\,g'\left(t-\frac{l}{c}\right)+Uf'(l)\,g\left(t-\frac{l}{c}\right)\right\}^2}}{f(l)\,g'\left(t-\frac{l}{c}\right)\left\{\left(1-\frac{U}{c}\right)f(l)\,g'\left(t-\frac{l}{c}\right)+Uf'(l)\,g\left(t-\frac{l}{c}\right)\right\}}$$

$$= 1-\frac{1}{2}\frac{\left(1-\frac{U}{c}\right)^2 f^2(l)\,\overline{g'^2}+U^2f'^2(l)\,\overline{g^2}}{\left(1-\frac{U}{c}\right)f^2(l)\,\overline{g'^2}}. \tag{14}$$

The rate of working is positive only if $c > U$. To make $\eta_F$ close to 1 it is desirable to have $f'(l)$ practically zero; indeed, a non-zero value of $f'(l)$ reduces the thrust without altering the rate of working. On the other hand, it is wasteful to keep $f(x)$ constant all along the length of the fish, since the thrust depends only on values at $x = l$; and it will be found desirable, also for other reasons, to let $f(x)$ increase gradually from zero at $x = 0$ to a maximum, with $f'(l) = 0$, at the trailing edge.

Under these circumstances, $\eta_F$ would be $\frac{1}{2}(1+U/c)$, and for example, $\eta_F = 0{\cdot}9$ for $c = 1{\cdot}25U$. Such a value of $c$ is sufficiently in excess of $U$ to give a substantial positive mean thrust

$$\overline{P} = \tfrac{1}{2}\rho A(l)\left(1-\frac{U^2}{c^2}\right)f^2(l)\,\overline{g'^2}. \tag{15}$$

To investigate whether the thrust (15) would be adequate with $c = 1{\cdot}25U$, note that in a real flow it would have to balance the frictional drag

$$D = \tfrac{1}{2}\rho U^2 C_D S, \tag{16}$$

where $C_D$ is a drag coefficient based on the total surface area $S$. In (15), $f^2(l)\,g'^2$ is the mean square lateral velocity of the trailing edge, which should not exceed $0{\cdot}05U^2$ if the assumptions which have been made in the theory are to hold—and, indeed, these restrictions to small disturbances are almost certainly beneficial in reducing drag. With this limitation, and with $c = 1{\cdot}25U$, the balance of thrust and drag can be achieved only if

$$A(l) > \frac{C_D S}{0{\cdot}018}. \tag{17}$$

Here $A(l) = \frac{1}{4}\pi s^2$, where $s$ is the span of the tail trailing edge, and equation (17) indicates the advantage for efficiency of having a tail of adequate span.

Such a conclusion would be too optimistic, however, as it does not take account of recoil. A precise solution of the problem of what efficiency can be obtained with adequate thrust, and within the limitations set by our assumptions, from a displacement function into which a recoil function (11) has been incorporated to make it satisfy (9) and (10), would necessitate an extensive computing programme. However, the following general remarks would probably be supported by such computations.

Any angular recoil (represented by the second term in (11)) tends to reduce thrust without affecting rate of working, for it produces extra terms in $(\partial h/\partial x)_{x=l}$ which, being dependent on displacement rather than velocity, do not correlate well with $(\partial h/\partial t)_{x=l}$, and therefore contribute (through their mean square) to the numerator of (8) but not to the denominator—just as did the terms in $f'^2(l)$ in (14).

By contrast, a small transverse recoil of the mass-centre without angular motion, if well correlated with the trailing-edge movement, would not alter the efficiency that can be obtained for given mean square trailing-edge velocity and mean thrust, although it would somewhat increase the value of the wave-velocity $c$ required to obtain that efficiency. (This is because the reduction of $\partial h/\partial t$ requires a corresponding reduction of $\partial h/\partial x$.)

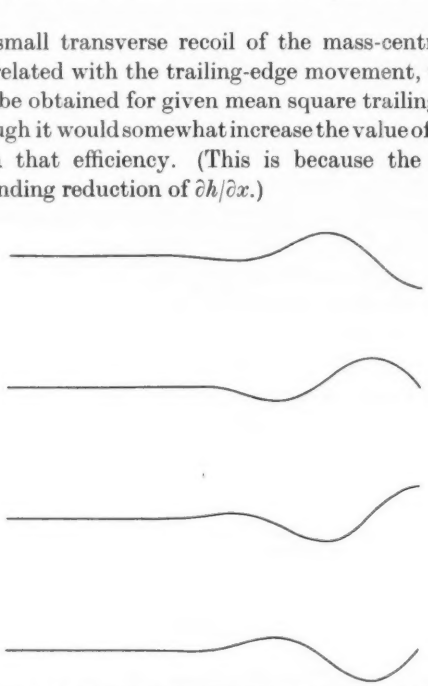

FIGURE 1. Suggested cycle of swimming movements. Successive shapes of fish centre-line are shown, with time increasing downwards. Motion is from right to left.

Accordingly, such travelling wave-forms as produce minimal angular recoil are desirable. A good solution appears to be as follows:

(i) confine motions to the rear part of the fish where fish mass is low;

(ii) keep $V$ low for given $\partial h/\partial t$ by having $c$ near to $U$, thus reducing water momentum in spite of the high virtual mass of the rear cross-sections;

(iii) most important of all, let the wave-form have a positive and a negative phase in the region of substantial amplitude (figure 1), so that the angular recoils produced by each tend to cancel out. (This, incidentally, will tend also to reduce

the transverse recoil of the mass centre and so keep down the value of $c$, and hence of $V$, thus assisting (ii).)

These arguments seem to confirm that the type of swimming action favoured by most fish has good efficiency.

## 4. Boundary-layer considerations

The inviscid flow around the swimming fish, which is calculated in detail in the Appendix and whose effects on its dynamics have been studied in §§ 2 and 3, provides (as remarked in § 1) the environment in which the boundary layer develops. We now consider briefly the possible effects of the boundary layer on the flow and on the dynamics, asking first whether separation occurs and if so to what effect, and secondly whether there is transition to turbulence.

Separation is most likely to occur in the cross-flows. Consider a thin slab of fluid with plane faces perpendicular to the $x$-direction, moving past the fish at velocity $U$ with only slight distortions from the plane shape. This slab of fluid is aware of the presence of a body of approximately cylindrical shape $C_x$ in its midst, but the cross-section $S_x$ of that body changes slowly with time and exhibits a movement through the fluid in the $z$-direction with velocity $V(x,t)$. If the flow produce by this movement has momentum $M$ and energy $E$ per unit width of slab, then in the absence of boundary-layer separation $M$ and $E$ have the potential-flow values $\rho VA$ and $\frac{1}{2}\rho V^2 A$, and the resultant forces are as calculated in § 2.

When, however, vorticity is released from the surface by boundary-layer separation in this transverse flow, $M$ and $E$ are altered by amounts equal to the momentum and energy of the vortex system in the presence of the boundary. But the physical arguments of § 2 indicate that we will still have

$$\overline{W} = U\overline{\left\{M\frac{\partial h}{\partial t}\right\}_{x=l}}; \tag{18}$$

that is, the mean rate of working of the fish will be equal to the mean product of the lateral velocity of the trailing edge with the rate of shedding of momentum from it; while the wasted part of this rate of working will be

$$\overline{W} - \overline{P}U = U\{\overline{E}\}_{x=l}, \tag{19}$$

that is, the rate of energy shedding from the trailing edge. The Froude efficiency is therefore

$$\eta_F = 1 - \frac{\{\overline{E}\}_{x=l}}{\{M\,\partial h/\partial t\}_{x=l}}. \tag{20}$$

Now, it follows from (20) that, for the efficient types of swimming motion discussed at the end of § 3, the effect of $\eta_F$ on vortex contributions to $E$ and $M$ is limited to a slight increase in the factor $\frac{1}{2}$ in equation (8). Note first that, even when the wave-form has a positive and a negative phase as in figure 1, the slab of fluid moving past it, at a velocity $U$ only a little less than the wave velocity, experiences cross-section movements essentially in a single direction, with

$V$ increasing to a maximum at the tail. Whatever vorticity is generated, the fluid energy per unit width of slab must increase during this process at a rate

$$\frac{dE}{dt} = V\frac{dM}{dt}. \tag{21}$$

The effect of vortex shedding as $V$ increases means that $M$ will increase more rapidly than in direct proportion to $V$, due to the vortex drag, and this with (21) makes $E/MV$ somewhat greater than $\frac{1}{2}$ (for example, if $M \propto V^3$, then $E/MV$ rises to $\frac{3}{4}$), although $M$ remains in phase with $V$ and $E$ with $V^2$. These considerations make a change in the factor $\frac{1}{2}$ in equation (8), but do not qualitatively alter the conclusions about efficiency; for example, 85 % is not much worse than 90 % in this context.

Physically, this is still because transverse velocities $V$ of fish relative to fluid are being kept small compared with absolute transverse velocities.

As to the boundary layer in the flow along the fish, the additional pressures due to the transverse motions (called $p_1+p_2$ in the Appendix) are too small, when $V$ is kept small relative to $\partial h/\partial t$, to affect substantially its development. The only problem, therefore, is the long-standing one of why the boundary layer should have any special tendency to laminar flow. Here one can only draw attention to the remarkable results achieved by Coleman-Kramer Inc. of Los Angeles with their 'Lamiflo' coating (Judge 1960), which consists of a thin rubber skin attached to the surface of a body by short rubber pillars between which a free-flowing viscous fluid is present. This has been found to halve turbulent boundary-layer drag of the body in water, presumably owing to reduction of turbulence level by damping of surface pressure fluctuations. It is possible that layers of blubber can have a similar effect.

The author expresses his gratitude to Sir James Gray for extremely interesting discussions of the problem.

REFERENCES

JUDGE, J. F. 1960 *Missiles and Rockets* (Feb. 1), pp. 42–3.
LIGHTHILL, M. J. 1960 *J. Roy. Aero. Soc.* **64**, 375–94.
MUNK, M. M. 1924 *Nat. Adv. Com. Aero., Washington, Rep.* no. 184.

## Appendix. The inviscid flow around a slender fish

To obtain the pressure distribution in this problem it is almost essential to make a transformation of co-ordinates, so that the body becomes a fixed surface—for, otherwise, there are severe difficulties due to applying boundary conditions at a surface whose position is displaced in a direction in which gradients are specially steep.

Accordingly we introduce new co-ordinates $X$, $Y$, $Z$ and $T$, where

$$X = x, \quad Y = y, \quad Z = z - h(x,t), \quad T = t \tag{A 1}$$

so that

$$\frac{\partial}{\partial x} = \frac{\partial}{\partial X} - \frac{\partial h}{\partial x}\frac{\partial}{\partial Z}, \quad \frac{\partial}{\partial y} = \frac{\partial}{\partial Y}, \quad \frac{\partial}{\partial z} = \frac{\partial}{\partial Z}, \quad \frac{\partial}{\partial t} = \frac{\partial}{\partial T} - \frac{\partial h}{\partial t}\frac{\partial}{\partial Z}. \tag{A 2}$$

Then Laplace's equation for the potential $\phi$ becomes

$$\left(\frac{\partial}{\partial X}-\frac{\partial h}{\partial X}\frac{\partial}{\partial Z}\right)\left(\frac{\partial \phi}{\partial X}-\frac{\partial h}{\partial X}\frac{\partial \phi}{\partial Z}\right)+\frac{\partial^2 \phi}{\partial Y^2}+\frac{\partial^2 \phi}{\partial Z^2}=0. \tag{A 3}$$

If now $\epsilon$ is a slenderness parameter (so that the fish's lateral dimensions do not exceed $\epsilon l$, nor its lateral velocities $\epsilon U$), then the first term in (A 3) is of order $\epsilon^2$ relative to the second and third, so that near the body we can use the two-dimensional Laplace equation

$$\frac{\partial^2 \phi}{\partial Y^2}+\frac{\partial^2 \phi}{\partial Z^2}=0. \tag{A 4}$$

If now the equation of the surface $S$ of the stretched straight fish is $F(x,y,z)=0$, then in these co-ordinates (A 1) the surface of the swimming fish has the equation $F(X,Y,Z)=0$, and the boundary condition on it is obtained by setting equal to zero the rate of change $DF/Dt$ of $F(X,Y,Z)$ following a particle of fluid. By (A 2), this gives

$$-\frac{\partial h}{\partial T}\frac{\partial F}{\partial Z}+\left(\frac{\partial \phi}{\partial X}-\frac{\partial h}{\partial X}\frac{\partial \phi}{\partial Z}\right)\left(\frac{\partial F}{\partial X}-\frac{\partial h}{\partial X}\frac{\partial F}{\partial Z}\right)+\frac{\partial \phi}{\partial Y}\frac{\partial F}{\partial Y}+\frac{\partial \phi}{\partial Z}\frac{\partial F}{\partial Z}=0. \tag{A 5}$$

We now put $$\phi = UX+\phi_0(X,Y,Z)+\phi_1(X,Y,Z,T), \tag{A 6}$$

where $UX+\phi_0$ is the potential of the flow when $h=0$ (that is, the steady flow when the fish is held stationary in the stream). For a slender fish $\partial F/\partial X$ is small compared with $\partial F/\partial Y$ and $\partial F/\partial Z$, and derivatives of $\phi_0$ and $\phi_1$ with respect to $X$, $Y$ and $Z$ are small compared with $U$. Also $\partial h/\partial X$ is small, and $\partial h/\partial T$ small compared with $U$. Hence, with products of small quantities neglected in (A 5), we obtain

$$-\frac{\partial h}{\partial T}\frac{\partial F}{\partial Z}+U\left(\frac{\partial F}{\partial X}-\frac{\partial h}{\partial X}\frac{\partial F}{\partial Z}\right)+\left(\frac{\partial \phi_0}{\partial Y}+\frac{\partial \phi_1}{\partial Y}\right)\frac{\partial F}{\partial Y}+\left(\frac{\partial \phi_0}{\partial Z}+\frac{\partial \phi_1}{\partial Z}\right)\frac{\partial F}{\partial Z}=0. \tag{A 7}$$

The special case $h=0$, $\phi_1=0$ gives us

$$\frac{\partial \phi_0}{\partial Y}\frac{\partial F}{\partial Y}+\frac{\partial \phi_0}{\partial Z}\frac{\partial F}{\partial Z}=-U\frac{\partial F}{\partial X} \tag{A 8}$$

as the boundary condition for $\phi_0$. Subtracting this from (A 7), we obtain

$$\frac{\partial \phi_1}{\partial Y}\frac{\partial F}{\partial Y}+\left(\frac{\partial \phi_1}{\partial Z}-\frac{\partial h}{\partial T}-U\frac{\partial h}{\partial X}\right)\frac{\partial F}{\partial Z}=0 \tag{A 9}$$

as the boundary condition for $\phi_1$.

We shall not discuss the method of calculating the steady-flow potential $\phi_0$, which is fairly well known, and leads to a pressure distribution with no resultant force or moment for a symmetrical shape like a fish. Passing therefore to $\phi_1$, we note that equation (A 4), with the boundary condition (A 9) and the condition that $\phi_1 \to 0$ at infinity, implies that, for each $X$, $\phi_1$ is the potential of the two-dimensional flow in the $Y$, $Z$ plane, resulting from the movement of an infinite cylinder $C_X$, whose cross-section is $S_X$, that is, the fish cross-section for the given value of $X$, and which moves in the $Z$-direction with velocity

$$V(X,T)=\frac{\partial h}{\partial T}+U\frac{\partial h}{\partial X}. \tag{A 10}$$

If, therefore, $\Phi(X, Y, Z)$ is the potential due to the said cylinder $C_X$ moving with unit velocity in the $Z$-direction through fluid at rest—note that it varies with $X$ only because the choice of cylinder cross-section does—then the solution to the equations for $\phi_1$ is

$$\phi_1(X, Y, Z, T) = V(X, T)\,\Phi(X, Y, Z). \tag{A 11}$$

We now calculate the associated pressure variations. Here we must remember that derivatives of $\phi_0$ and $\phi_1$ with respect to $X$ are of order $U\epsilon^2$ (more strictly, $U\epsilon^2 \log \epsilon^{-1}$),* but that derivatives with respect to $Y$ and $Z$ are of order $U\epsilon$. From Bernoulli's equation

$$p - p_\infty = -\rho\left(\frac{\partial \phi}{\partial T} - \frac{\partial h}{\partial T}\frac{\partial \phi}{\partial Z}\right) - \tfrac{1}{2}\rho\left(\frac{\partial \phi}{\partial X} - \frac{\partial h}{\partial X}\frac{\partial \phi}{\partial Z}\right)^2 - \tfrac{1}{2}\rho\left(\frac{\partial \phi}{\partial Y}\right)^2 - \tfrac{1}{2}\rho\left(\frac{\partial \phi}{\partial Z}\right)^2 + \tfrac{1}{2}U^2, \tag{A 12}$$

we must pick out the terms of order $\epsilon^2$, neglecting those of order $\epsilon^4$. This gives

$$\begin{aligned} p - p_\infty &= -\rho\frac{\partial \phi_1}{\partial T} + \rho\frac{\partial h}{\partial T}\left(\frac{\partial \phi_0}{\partial Z} + \frac{\partial \phi_1}{\partial Z}\right) - \rho U\left(\frac{\partial \phi_0}{\partial X} + \frac{\partial \phi_1}{\partial X}\right) \\ &\quad + \rho U\frac{\partial h}{\partial X}\left(\frac{\partial \phi_0}{\partial Z} + \frac{\partial \phi_1}{\partial Z}\right) - \tfrac{1}{2}\rho\left(\frac{\partial \phi_0}{\partial Y} + \frac{\partial \phi_1}{\partial Y}\right)^2 - \tfrac{1}{2}\rho\left(\frac{\partial \phi_0}{\partial Z} + \frac{\partial \phi_1}{\partial Z}\right)^2 \\ &= \rho\left\{-U\frac{\partial \phi_0}{\partial X} - \frac{1}{2}\left(\frac{\partial \phi_0}{\partial Y}\right)^2 - \frac{1}{2}\left(\frac{\partial \phi_0}{\partial Z}\right)^2\right\} + \rho\left\{-\frac{\partial \phi_1}{\partial T} - U\frac{\partial \phi_1}{\partial X}\right. \\ &\quad \left. + \left(V - \frac{\partial \phi_1}{\partial Z}\right)\frac{\partial \phi_0}{\partial Z} - \frac{\partial \phi_1}{\partial Y}\frac{\partial \phi_0}{\partial Y}\right\} + \rho\left\{V\frac{\partial \phi_1}{\partial Z} - \frac{1}{2}\left(\frac{\partial \phi_1}{\partial Y}\right)^2 - \frac{1}{2}\left(\frac{\partial \phi_1}{\partial Z}\right)^2\right\} \\ &= p_0 + p_1 + p_2, \end{aligned} \tag{A 13}$$

say, where $p_0$ is the pressure distribution in steady flow past the stretched straight fish, $p_2$ is the pressure distribution due to steady motion of the cylinder $C_X$ through fluid at rest with velocity $V$, and $p_1$ is the remainder of the pressure distribution. Thus, $p_0$ depends solely (and quadratically) on the shape of the stretched straight fish, $p_2$ solely (and quadratically) on its displacements, and $p_1$ linearly on both.

Now we are interested mainly in the distribution of the lift (that is, resultant force in the $z$-direction) per unit length, $L(X, T)$, and in the resultant thrust $P$. We obtain $L$ to order $\epsilon^3$, neglecting terms of order $\epsilon^5$.

There is no contribution to lift from $p_0$ or $p_2$; for $p_0$ has zero resultant in the $z$-direction over a cross-section by the definition of the stretched straight position, and $p_2$ has because the resistance to the motion of $C_X$ in steady potential flow is zero. Therefore, only $p_1$ produces any local normal force, and by (A 13)

$$L = -\rho\oint_{S_X}\left\{\frac{\partial \phi_1}{\partial T} + U\frac{\partial \phi_1}{\partial X} + \left(\frac{\partial \phi_1}{\partial Z} - V\right)\frac{\partial \phi_0}{\partial Z} + \frac{\partial \phi_1}{\partial Y}\frac{\partial \phi_0}{\partial Y}\right\} dY. \tag{A 14}$$

Now in (A 14) we can use the facts that $\phi_1 = V\Phi$, and that

$$\oint_{S_X} \Phi\, dY = A(X), \tag{A 15}$$

* For this reason the terms neglected in (A 7) were of order $\epsilon^2$ (more strictly $\epsilon^2 \log \epsilon^{-1}$) relative to those retained.

where $\rho A(X)$ is the virtual mass per unit length of the cylinder $C_X$, whose cross-section is $S_X$, when moving in the $z$-direction; thus, $A(X)$ has the dimensions of area. From (A 15) it follows that

$$\left(\frac{\partial}{\partial T}+U\frac{\partial}{\partial X}\right)\{VA(X)\}$$
$$=\oint_{S_X}\left(\frac{\partial}{\partial T}+U\frac{\partial}{\partial X}\right)(V\Phi)\,dY+U\oint_{S_X}V\frac{\partial\Phi}{\partial Z}\left(\frac{\partial Z}{\partial X}\right)_{Y\text{ const.}}dY, \quad \text{(A 16)}$$

where the last term results from the variation of the cross-section $S_X$ with $X$, which causes the value of $Z$ for given $Y$ to vary along the surface.

On the right-hand side of (A 16), the first term can be identified with the first part of the integral in (A 14). Also, the second term can be identified with the second part, for it is

$$-U\oint_{S_X}\frac{\partial\phi_1}{\partial Z}\frac{\partial F/\partial X}{\partial F/\partial Z}\,dY, \quad \text{(A 17)}$$

which by (A 8) is

$$\oint_{S_X}\frac{\partial\phi_1}{\partial Z}\left(\frac{\partial\phi_0}{\partial Z}+\frac{\partial\phi_0}{\partial Y}\frac{\partial F/\partial Y}{\partial F/\partial Z}\right)dY=\oint_{S_X}\frac{\partial\phi_1}{\partial Z}\left(\frac{\partial\phi_0}{\partial Z}dY-\frac{\partial\phi_0}{\partial Y}dZ\right)$$
$$=\iint_{E_X}\left\{\frac{\partial}{\partial Z}\left(\frac{\partial\phi_1}{\partial Z}\frac{\partial\phi_0}{\partial Z}\right)+\frac{\partial}{\partial Y}\left(\frac{\partial\phi_1}{\partial Z}\frac{\partial\phi_0}{\partial Y}\right)\right\}dY\,dZ, \quad \text{(A 18)}$$

where $E_X$ is the area external to $S_X$. Using Laplace's equation in two dimensions for $\phi_0$ and then for $\phi_1$, we can write (A 18) as

$$\iint_{E_X}\left\{-\frac{\partial^2\phi_1}{\partial Y^2}\frac{\partial\phi_0}{\partial Z}+\frac{\partial^2\phi_1}{\partial Y\partial Z}\frac{\partial\phi_0}{\partial Y}\right\}dY\,dZ=\oint_{S_X}\left(\frac{\partial\phi_1}{\partial Y}\frac{\partial\phi_0}{\partial Z}dZ+\frac{\partial\phi_1}{\partial Y}\frac{\partial\phi_0}{\partial Y}dY\right)$$
$$=\oint_{S_X}\left\{\left(\frac{\partial\phi_1}{\partial Z}-V\right)\frac{\partial\phi_0}{\partial Z}+\frac{\partial\phi_1}{\partial Y}\frac{\partial\phi_0}{\partial Y}\right\}dY, \quad \text{(A 19)}$$

where the boundary condition (A 9) has been used to throw (A 17) into the form shown in the second part of (A 14).

This equation now shows, as stated in § 2, and there interpreted physically, that the lift per unit length is

$$L(X,T)=-\rho\left(\frac{\partial}{\partial T}+U\frac{\partial}{\partial X}\right)\{VA(X)\}, \quad \text{(A 20)}$$

where $V$ is given by (A 10).

The mean value of the thrust $P$ is now obtained to order $\epsilon^4$, neglecting terms of order $\epsilon^6$. Writing $P$ as an integral over the surface of the swimming fish, and then using the co-ordinates (A 1) to express it as an integral over $S$, we obtain

$$P=\iint(p_0+p_1+p_2)\,dy\,dz=\iint_S(p_0+p_1+p_2)\,dY\left(\frac{\partial h}{\partial X}dX+dZ\right)$$
$$=\int_0^l L(X,T)\frac{\partial h}{\partial X}dX+\iint_S(p_0+p_1+p_2)\,dY\,dZ=P_1+P_2, \quad \text{(A 21)}$$

where $P_1$ is to be interpreted as the resultant in the forward direction of the lift forces $L(X, T)$, and we have simply

$$P_2 = \iint_S p_2 dY dZ, \tag{A 22}$$

since the pressures $p_0$ have zero resultant, and for a symmetrical fish $\iint p_1 dY dZ$ is zero (while even for an unsymmetrical fish the mean of this oscillatory force would be zero).

In (A 22), the $dY dZ$ is an elementary area of the surface $S$ of the stretched straight fish, projected in the negative $X$-direction (or thrust direction). Such an area lying between cross-sections $S_X$ and $S_{X+\delta X}$ can be written $-(\delta n)\, ds$, where $ds$ is an element of length around $S_X$, and $\delta n$ is the normal distance between the curves $S_X$ and $S_{X+\delta X}$ when projected on to the same plane (figure 2). Accordingly, that part of $P_2$ which arises from between the cross-sections $S_X$ and $S_{X+\delta X}$ can be written

$$-\oint_{S_X} (\delta n)\, p_2 ds. \tag{A 23}$$

Now, $p_2$ is the pressure distribution in potential flow due to the motion of the cylinder $C_X$ through fluid with constant velocity $V$ in the $z$-direction. In this

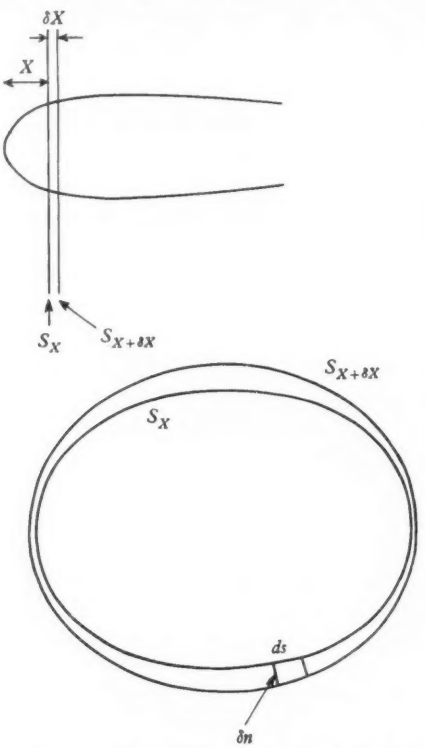


FIGURE 2. Neighbouring shapes of fish cross-section, viewed at right angles to the direction of locomotion in the upper diagram and along it (on a larger scale) in the lower.

motion the kinetic energy of the fluid per unit length of cylinder is $\frac{1}{2}\rho V^2 A(X)$ and the momentum $\rho V A(X)$. If now, during this motion, the cylinder $C_X$ performed gradually a small change of cross-section from $S_X$ to $S_{X+\delta X}$, the fluid momentum would change by

$$\rho V \delta A = \rho V\{A(X+\delta X) - A(X)\} = \rho V \frac{dA}{dX}\delta X, \tag{A 24}$$

and the cylinder, moving at constant speed $V$, must do work $\rho V^2 \delta A$ to produce this change of momentum.

But the motion of the cylinder is not simply rectilinear; in addition, each element $ds$ of the surface moves outwards a distance $\delta n$ (figure 2) against a pressure $p_2$. This means that the cylinder must also do a quantity of work given by the integral in (A 23), per unit length. But the total work done must equal the change in the kinetic energy $\frac{1}{2}\rho V^2 A$ of the fluid, giving*

$$\rho V^2 \delta A + \oint (\delta n)\, p_2 ds = \tfrac{1}{2}\rho V^2 \delta A. \tag{A 25}$$

This evaluates (A 23), the part of $P_2$ which arises from between the cross-sections $S_X$ and $S_{X+\delta X}$, and enables us to write

$$P_2 = \int_0^l \tfrac{1}{2}\rho V^2 dA(X). \tag{A 26}$$

We now throw the mean value of the part $P_1$ of the thrust, which arises from forward-directed lift, into a similar form. By (A 20) and (A 21), it is

$$\begin{aligned} P_1 &= -\rho \int_0^l \frac{\partial h}{\partial X}\left(\frac{\partial}{\partial T} + U\frac{\partial}{\partial X}\right)\{VA(X)\}\, dX \\ &= -\rho \int_0^l \left(\frac{\partial}{\partial T} + U\frac{\partial}{\partial X}\right)\left\{\frac{\partial h}{\partial X} VA(X)\right\} dX + \rho \int_0^l \frac{\partial V}{\partial X} VA(X)\, dX. \end{aligned} \tag{A 27}$$

The mean over a long time of the time-derivative in this last expression is zero. Hence the mean value $\overline{P_1}$ is

$$\overline{P_1} = -\rho U\left[\overline{\frac{\partial h}{\partial X} VA}\right]_0^l + \rho[\tfrac{1}{2}\overline{V^2}A]_0^l - \tfrac{1}{2}\rho \int_0^l \overline{V^2} dA(X). \tag{A 28}$$

Adding this to the averaged form of (A 26), we obtain, for the total mean thrust $\overline{P} = \overline{P_1} + \overline{P_2}$, the simple equation

$$\overline{P} = \tfrac{1}{2}\rho A(l)\left\{\overline{\left(\frac{\partial h}{\partial T}\right)^2} - U^2\overline{\left(\frac{\partial h}{\partial X}\right)^2}\right\}, \tag{A 29}$$

which was stated in § 2 as equation (7).

* The correctness of this formula is easily checked for a circle or an ellipse. When the cross-section is increasing, the integral in (A 23) comes out negative, which physically is because the regions of suction outweigh the regions of pressure around the surface.

# REVIEWS

**Plasma Physics.** By J. G. LINHART. Amsterdam: North Holland Publishing Co., 1960. 278 pp. 50*s*.

It is curious that the Greek idea of the Universe being built of four elements, earth, water, air and fire, has an interpretation in modern physics. These four 'elements' may be compared with the four states of matter in which most of the matter in the Universe exists, namely, solid, liquid, gaseous and plasma, the last being the state in which matter is ionized and consists of free electrons and ions. Although it is probable that more than 99·9 % of the Universe is in the plasma state, the study of plasmas has until the last decade been comparatively neglected and has been one of the backwaters of physics, perhaps because the plasma state occurs rarely in nature on the surface of the earth and then only briefly, for example in lightning and other electrical discharges, and is not easily produced in the laboratory. However, the prospect of unlimited power from thermonuclear fusion and the first steps into outer space, together with a growing realization by astrophysicists of the importance of plasma physics in their field, have given an enormous impetus to the subject. To produce fusion in a power station will require exceedingly high temperatures and low densities in which the hydrogen and its isotopes will be changed from the gaseous to the plasma state. Away from the neighbourhood of the earth's surface, man, or rather his rockets and satellites, is moving through a medium which is naturally in the plasma state. As a result, a flood of papers is coming from an apparently exponentially growing number of research workers, and the subject is now one of the most fashionable.

It might be thought that fluid dynamicists, who have so far been concerned with the liquid and gaseous states, would naturally take up plasma physics but few seem to have gone past the half-way house of magnetohydrodynamics or, as the plasma physicists prefer to call it, hydromagnetics. A reason may be the lack of introductory texts on the subject combined with the fact that a study of plasma physics requires knowledge from a variety of fields including electrodynamics, statistical mechanics, special relativity, and quantum theory, which the fluid dynamicist is not likely to have met since his undergraduate days, if then; whereas for much of magnetohydrodynamics the standard methods and techniques of fluid dynamics will suffice. Any introductory monograph is therefore to be welcomed as likely to help the fluid dynamicist find his feet instead of drowning in the literature and the unfamiliar ideas. The book under review serves this purpose reasonably well. It does not start from first principles, but the basic knowledge required by the reader can be found in degree course textbooks. It is basically on the same lines as the brief monograph by L. Spitzer, *The Physics of Fully Ionized Gases*, but is somewhat fuller and more detailed. In particular, the list of references is excellent and remarkably up-to-date, and includes the Russian literature. On the other hand, it lacks the clarity, elegance and insight of Spitzer's book, which the newcomer to the field would be well advised to read first.

An important difference between the mechanics of a plasma and that of a fluid is the existence of long-range Coulomb forces between the particles. Close collisions may in many cases be relatively unimportant and the motion of the plasma can then be described in terms of the motion of a single charged particle in the electromagnetic field generated by the plasma motion and by external means. This is called the single-particle picture, and is considered in the first chapter where the motion of a charged particle in the electromagnetic fields most likely to be encountered in practice is calculated. The treatment tends to be unduly complicated, but it has the virtue of being complete. An account of the various types of radiation emitted by a moving charged particle, bremsstrahlung, cyclotron radiation and Cerenkov radiation, is also included.

The study of individual particles, although often throwing light on the behaviour of a plasma, is not usually a convenient method for obtaining quantitative information, and the next two chapters are devoted to the more appropriate macroscopic approach which essentially regards the plasma as a mixture of two fluids, the electron gas and the ion gas. Moreover, it is necessary to investigate the distribution of particle velocities in the neighbourhood of a point in space, so that in fact a plasma is represented as a fluid in phase space and the basic equation is the Boltzmann equation. Continuum-type equations for macroscopic variables are then obtained by taking the first two integral moments in phase space of the Boltzmann equation and by making some assumption, appropriate to the circumstances, about the collision term and the momentum transfer or stress terms. Here the account is far from satisfactory, for these terms are simply supposed equivalent to an isotropic pressure and the reader is given little clue about the circumstances under which this is valid or about the difficulties which abound here. Various solutions of these equations are obtained corresponding with steady-state or equilibrium configurations of the plasma and the associated electromagnetic field, the best known being the Bennett pinch.

Waves and instabilities in plasmas are the topic of the next chapter. The whole gamut of linear oscillations is run, from hydromagnetic waves to electrostatic plasma oscillations. It is useful to have the whole variety described together in reasonably compact form, and the author can perhaps be excused for his cursory treatment of Landau damping of the electrostatic oscillations. This particular topic has been the cause of many headaches, and a full investigation may possibly be out of place in an introductory text, especially since there is a tendency for its importance to be inflated owing to it being a new phenomenon with no obvious analogue in fluid mechanics. The chapter ends with an introductory discussion of the main types of instability found in plasma motions, and is followed by a brief one on shock waves in plasmas and on plasmoids, the name given to an isolated cloud of plasma. The main features of the phenomena are described and enough is said to make the reader realize that this is a part of the field where theory is still a matter for conjecture.

The next chapter provides an introduction to the difficult and involved question of collision-dominated transport and relaxation processes in a plasma. The dynamics of binary collisions are studied and also the cumulative effects of

many distant collisions which, because of the long-range effect of the Coulomb forces, are particularly important in a plasma; this is followed by the derivation of the Fokker-Planck equation which describes the diffusion in velocity space, owing to collisions between particles, of a non-equilibrium velocity distribution function. Calculations of the transport coefficients for heat, electricity and momentum are also given.

The remaining two chapters are devoted to the applications of plasma physics to problems of practical importance, and it is a welcome feature of the book that these are included. It is all to the good that the more or less academic theoretician should be aware of the engineering problems which need to be overcome. One chapter discusses the problems of controlled fusion, the outstanding difficulties, and possible methods of overcoming them. Of value to the fluid dynamicist is a review of the sources of nuclear energy and the way in which nuclear energy is released. The other chapter deals with the problems involved in the use of plasmas to convert chemical energy directly into electrical energy and for energy storage, with plasma oscillators and accelerators, and (what is almost science fiction) the plasma rocket motor which, combined with a nuclear power source, may be the eventual means of propulsion of interplanetary space ships.

This book shows signs of having been hastily put together, and sometimes presents an oversimplified picture which will irritate the expert. But on the whole it serves its purpose of providing an introduction to and an up-to-date summary of a rapidly developing field.

P. G. Saffman

JOURNAL OF FLUID MECHANICS

Volume 9, Part 2 October 1960

CONTENTS

Exact solutions for steady two-dimensional flow of a stratified fluid
by CHIA-SHUN YIH *page* 161

On the disintegration of water drops in an air stream
by K. N. DODD 175

Rayleigh instability of a thermal boundary layer in flow through a porous medium
by R. A. WOODING 183

On the dynamics of unsteady gravity waves of finite amplitude. Part 1. The elementary interactions
by O. M. PHILLIPS 193

Deposition of a viscous fluid on a plane surface
by G. I. TAYLOR 218

Experiments on the effect of suction on the flow due to a rotating disk
by N. GREGORY and W. S. WALKER 225

An experimental investigation of turbulent spots and breakdown to turbulence
by J. W. ELDER 235

On the movement of ships in restricted waterways
by T. CONSTANTINE 247

Stability and transition of a supersonic laminar boundary layer on an insulated flat plate
by JOHN LAUFER and THOMAS VREBALOVICH 257

On unsteady laminar boundary layers
by H. A. HASSAN 300

Note on the swimming of slender fish
by M. J. LIGHTHILL 305

REVIEWS
*Plasma Physics* 318

*Printed in Great Britain at the University Press, Cambridge*
*(Brooke Crutchley, University Printer)*